

Assessment and Prediction of Biostabilization of Polycyclic Aromatic Hydrocarbons in Sediments

**Dr. Jeffrey W. Talley, Samuel Tucker
Environmental Laboratory, U. S. Army Engineer Research and
Development Center (ERDC), Vicksburg, MS 39180**

**John S. Furey
Dyncorp, Vicksburg, MS**

**Deborah R. Felt
Applied Research Associates, Vicksburg, MS**

**Dr. Upal Ghosh, Dr. Richard G. Luthy
Department of Civil and Environmental Engineering,
Stanford University
Stanford, CA 94305-4020**

**Dr. Seb Gillette, Dr. Richard N. Zare
Department of Chemistry, Stanford University, Stanford, CA 94305-4020**

**A Composite Report Submitted to the Strategic Environmental Research
and Development Office (SERDP) in Fulfillment of the Requirement for
Work Unit CU 1095**

**ASSESSMENT AND PREDICTION OF BIOSTABILIZATION OF
POLYCYCLIC AROMATIC HYDROCARBONS (PAHs)
IN SEDIMENTS**

**Dr. Jeffrey W. Talley, Samuel Tucker
Environmental Laboratory, U. S. Army Engineer Research and Development Center
(ERDC), Vicksburg, MS 39180**

**John S. Furey
Dyncorp, Vicksburg, MS**

**Deborah R. Felt
Applied Research Associates, Vicksburg, MS**

**Dr. Upal Ghosh, Dr. Richard G. Luthy
Department of Civil and Environmental Engineering, Stanford University
Stanford, CA 94305-4020**

**Dr. Seb Gillette, Dr. Richard N. Zare
Department of Chemistry, Stanford University, Stanford, CA 94305-4020**

**A Composite Report Submitted to the Strategic Environmental Research and
Development Office (SERDP) in Fulfillment of the Requirement for
Work Unit CU 1095**

January 2001

ABSTRACT

This work applied new investigative techniques to assess the locations, distributions, and associations of polycyclic aromatic hydrocarbons (PAHs) in dredged harbor sediment. Dredged materials from the Milwaukee Confined Disposal Facility were collected and homogenized to provide sufficient sample for four month bioslurry treatment testing and for PAH analyses on various size and density fractions before and after biotreatment. Sediment PAH analyses included both whole-sample measurements and, most importantly, the determination of PAH distribution by sediment particle size and type. Microprobe two-step laser desorption/laser ionization mass spectrometry was used to identify and characterize PAHs on the subparticle scale and scanning electron microscopy with wavelength dispersive X-ray spectroscopy was used for elemental microanalysis. Physicochemical analyses included room temperature Tenax bead aqueous desorption experiments and thermal program desorption-MS studies to assess PAH binding energies on sediment particle types. Thermal programmed desorption-MS experimental protocols and data reduction techniques were developed to evaluate apparent PAH binding activation energies on sediment particles. Microbial ecology testing used phospholipid fatty acid (PLFA) and DNA procedures and radiolabeled microcosm studies. Earthworm bioassays studied the acute toxicity effects and PAH bioaccumulation from untreated and biotreated PAH-impacted dredged materials. Overall, the results were used to synthesize and correlate data to assess the availability and treatability of PAHs in dredged sediments.

The significant findings of this work were: the release of PAHs is dependent both on PAH molecular weight and the character of the sediment sorbent material; two principle sediment

particle classes dominated the distribution and release of PAHs - clay/silt and coal-derived; PAHs were found preferentially on coal-derived particles; clay/silt particles released PAHs more readily than coal-derived particles; bioslurry treatment reduced PAHs on the clay/silt fraction but not the coal-derived fraction; PAH reduction in clay/silt fractions by biotreatment resulted in significant reduction in earthworm PAH bioaccumulation; PAHs on coal-derived particles were associated with high binding activation energies; and changes in the phenotype and genetic potentials of the extant microbiota can be used to assess intrinsic biodegradative potential. The benefits of this work include: improved assessment of toxicity and risk for PAH contaminants in sediments by use of particle-scale techniques to assess PAH distribution and behavior; improved assessment for the potential success of biotreatment through understanding of factors contributing to available and unavailable PAH fractions; improved decision making regarding sediment quality criteria for PAHs and the biotreatment of PAH-impacted sediments; and reduced treatment costs and greater likelihood for reuse of dredged sediments through knowledge of the underlying processes affecting PAH locations, availability, treatability, and toxicity.

TABLE OF CONTENTS

Abstract

Table of Contents

Section 1. Overview

Introduction
Relevance
Biodegradation and Bioavailability
The Sequestration of PAHs
Previous Thermal Desorption Work
Thermal Programmed Desorption MS
Experimental Approach
Report Outline
References

Section 2. Direct Observation of Polycyclic Aromatic Hydrocarbons on Geosorbents at the Subparticle Scale.

Section 3. Microscale Location, Characterization, and Association of Polycyclic Aromatic Hydrocarbons on Harbor Sediment Particle

Section 4. Thermal Program Desorption of PAHs from Mineral and Organic Surfaces

Section 5. Kinetics and Thermodynamics of PAH Desorption Process from Sediment Particles

Section 6. Succession of Phenotypic, Genotypic and Metabolic Community Characteristics During Bioslurry Treatment of PAH-Contaminated Sediments

Section 7. Availability and Bioslurry Treatment of PAHs in Contaminated Dredged Materials

Section 8. Summary and Conclusions

Appendix A. Measurements of Microbial Activity on Sediment Particle Surfaces and Correlation with Distribution of Sorbed PAHs

Appendix B. Data Reduction Methodology and Techniques

Appendix C. Data Tables For Section 4

Appendix D. Data Tables For Section 5

Appendix E. Data Tables For Section 6

Appendix F. Data Tables For Section 7

Section 1

Overview

Introduction

In-situ bioremediation is defined by the U.S. Environmental Protection Agency (EPA) as a managed or spontaneous process in which microbiological processes are used to degrade or transform contaminants to less toxic or nontoxic forms, thereby remedying or eliminating environmental contamination (1). These microbiological processes may reduce hydrocarbon concentrations in various types of soils and sediments to levels that no longer pose an unacceptable risk to the environment or human health (2). However, hydrocarbons that remain in treated soils and sediments still might not meet stringent regulatory levels, even if they represent site specific, environmentally acceptable endpoints (3). This unresolved issue of the availability of residual hydrocarbon contaminants was the focus of this work.

There is a great need to understand contaminant-soil/sediment interactions and their effect on bioavailability and toxicity (3). This is especially true for polycyclic aromatic hydrocarbons (PAHs). The adherence and slow release of PAHs from soils and sediments is an obstacle to remediation (4, 5) and is challenging our concepts about cleanup standards and risks (6). This is particularly the case for biological treatment of PAHs where one of the most important of the site-specific factors is the availability of the compounds held within solids and how this affects treatment rates and acceptable toxicological endpoints.

Biostabilization is a newly developed concept that could significantly benefit the remediation process for soils and sediments contaminated with PAHs. Biostabilization is the biodegradation of accessible pollutant fractions in a soil or sediment matrix, leaving a bound residue that is much more biologically unavailable and immobile (7). The concept, however, is still in a developmental stage and endpoints and appropriate measures of endpoints have not been defined. Very little research has been conducted on the applicability of

biostabilization principles. It has been hypothesized that residual hydrocarbons remaining after biotreatment may represent an acceptable treatment endpoint. This is an important concept, but for wide acceptance, better understanding of PAH release rates and mechanisms that bind or sequester PAHs within contaminated material is required.

Relevance

PAHs present one of the most pressing problems for biotreatment of contaminated soils or sediments. These compounds comprise a broad class of chemicals that appear as persistent contaminants in soils and sediments (3,4), including petroleum and fuel residues, tars, and creosotes. Such compounds have low solubility, low volatility, low intrinsic reactivity and typically exhibit very slow release rates from soil or sediment (8, 9). These characteristics make biotreatment difficult in any geologic setting, necessitating extensive, site-specific testing. These characteristics also confound risk assessment, wherein the availability of PAHs to organisms or the environment is unknown.

In theory, soils and sediments contaminated with PAHs may be treated utilizing various clean-up strategies. However, many proposed strategies have significant economic and feasibility problems. What is needed is an effective technology that supports the economics of disposal, eliminates adverse contaminant impacts, and supports the reuse of treated contaminated soils and sediments. In-place (in-situ) biotreatment combined with biostabilization offers a strong possibility to achieve these goals. Regardless if the biotreatment system is passive (natural attenuation) or engineered (in-place treatment), a pragmatic solution is to focus active biotreatment on the available contaminant fraction and confirm that if residuals are released, the rate is sufficiently slow to allow consumption by the microbial community, i.e., the contaminant is biostabilized. Thus, an alternative environmental endpoint (clean-up level) may be appropriate, rather than basing decisions solely on total concentration of contaminant in the soil or sediment.

It is also necessary to improve assessment of the toxicity and risk from residual hydrocarbons. Mechanisms that affect release rates and exposure need to be better defined. The potential benefits of such work could include: reduced treatment costs, improved

evaluation and design for clean-up technologies, greater regulatory and public acceptance of biotechnology, increase in the reuse/recovery opportunities for treated contaminated sediments, and potential application for in-situ capping of contaminated soils and sediments.

Biodegradation and Bioavailability

PAHs in soils and sediments may be biodegraded by microorganisms to a residual concentration that no longer decreases with time, or which decreases slowly over years with continued treatment (10, 11, 12). Further reductions are believed to be limited by the availability of the PAHs to microorganisms (13,14). Attempts have been made to increase this availability through the use of surfactants, but results have been varied (15, 16, 17, 18, 19). Additionally, as contaminants age they become less available compared to freshly contaminated material. As a consequence of binding with soils and sediments and subsequent slow release rates, residual PAHs may be significantly less leachable by water and less toxic as measured by uptake tests (20, 6, 21).

Generally, contaminants can only be degraded when they exist in the aqueous phase and come in contact with the cell membrane of a microorganism (22). In this way the contaminant serves as a substrate for the microorganism and is incorporated through membrane transport into the cell and utilized as an energy source in the cell's principal metabolic pathways. However, physical or chemical phenomena can limit the bulk solution concentration of the contaminant and thus significantly reduce the ability of the microorganisms to assimilate the contaminant. Therefore, the *bioavailability* of the contaminant can control the overall biodegradation of these compounds.

Another important factor relevant to biodegradation and bioavailability is the location and density of microorganisms. The majority of bacteria in the environment are attached to surfaces and their distribution in and on soils/sediments is very patchy. The majority of these bacteria range in size from 0.5 to 1.0 μm while micropores present in soils and sediments are far less than 1 μm . It is generally believed that bacteria are attached predominantly to the surface of soils and sediments and not to the interior surfaces of the micropores. It has been estimated that over 90% of the microorganisms present in geologic matrices accumulate on

the surfaces of soil/ sediment (23). Therefore, the majority of contaminant-microbial interactions occur in the biofilm that develop within macropores on the surfaces of soils/sediments.

This suggests that partitioning of an organic contaminant from the solid phase of the soil/ sediment to the aqueous phase in the larger pore spaces controls soil/sediment bioavailability. These partitioning mechanisms may include chemical bonding, surface complex formations, electrostatic interactions, and hydrophobic effects (24, 25). For hydrophobic contaminants like PAHs, sorption increases with the content of the organic matter in the soil/sediment and the degree of hydrophobicity of the specific PAH. Typically, the rate of desorption can be attributed to the mass transfer of the sorbate molecules from sorption sites on and in the soil/sediment. Active bacteria should correspond to the higher available PAH concentrations, which occurs where desorption is the most intense.

The Sequestration of PAHs

As already discussed, the partitioning of PAHs represents a significant part of the mass transfer process. However, describing this process is complicated by a combination of diffusion, dissolution, encapsulation, and adsorption phenomena. The combined effect of these factors can generally be defined as sequestration (7). The complexities of sequestration can best be understood in terms of examining the different scales of observation associated with the heterogeneity of soils and sediments. Shown in Figure 1 (7) are mineral surfaces in meso- and micropores; natural sorbent organic matter (SOM), both amorphous and condensed; and anthropogenic organic phase matter. The circled letters refer to different sorption mechanisms associated with specific domains within soil and sediments: Case A represents absorption into amorphous or "soft" natural organic matter (e.g., within an organic phase akin to solvent partitioning); Case B represents absorption into condensed or "hard" organic polymeric matter or combustion residue (e.g., into solid-like organic matter); Case C represents adsorption onto water-wet organic surfaces (e.g., soot); Case D represents adsorption to exposed water-wet mineral surfaces (e.g., quartz); and Case E represents adsorption into microvoids or microporous minerals (e.g., zeolites) with porous surfaces at water saturation <100% (7).

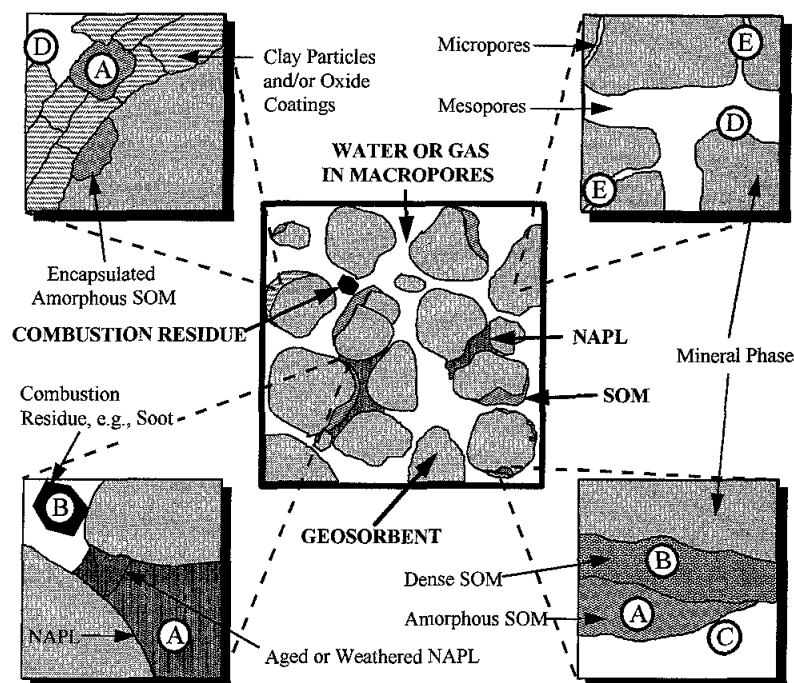


Figure 1: Conceptual model of where PAHs may reside in soils/sediments (Luthy et al., 1997)

These different domains within soils/sediments illustrate how structural and chemical heterogeneity can significantly affect how PAHs behave. Excluding entrapment due to weathering at interfaces (e.g., NAPL/water), case A presumably would exhibit fast kinetics with low desorption energy and high extractability, while case B would show slow kinetics, high desorption energy, and low extractability. Case C is characterized by fast kinetics with low desorption energy and high extractability. Case D would exhibit fast kinetics, low desorption energy, and high extractability, with case E showing slow kinetics, high desorption energy, and low extractability. Assuming all other environmental parameters are consistent among the five different cases, a qualitative ranking of bioavailability is as follows: $B_A, B_C, B_D > B_B, B_E$; where $B_A, B_B, B_C, B_D,$ and B_E is the bioavailability for cases A, B, C, D and E.

Although some correlation may be hypothesized with respect to bioavailability, it is difficult to specify the exact role each sorbent domain may have. For example, adherent or entrapped anthropogenic organic matter can also function as a sorbent, e.g., surfactants, soot,

or non-aqueous phase liquids (NAPLs) such as oils and tars (18, 26, 27). Also, there is a growing awareness that the affinity of nonpolar organics for SOM depends on the SOM's origin and geologic history. Grathwohl (28) showed that organic matter in unweathered shales and high-grade coals enhanced sorption by more than an order of magnitude when compared to more oxidized organic matter found in recent geologically young material, and highly weathered SOM. Huang and Weber (29) have suggested that changes in SOM oxygen-containing functional groups, e.g., changes in SOM O/C atomic ratios, can lead to a greater affinity of SOM for PAHs. Gustafsson et al. (30) differentiated two forms of SOM, i.e., humic acid and soot, for sediment by thermal treatment.

Presently there are very few direct observational data revealing the micro-scale location or locations in which PAHs accumulate when they associate with soils and sediments (43, 44). As a result, researchers must rely on inferences from macroscopic experimental observations that capture overall behavior and provide empirical evidence for deducing sorbent/sorbate mechanistic models (31, 32, 33, 30, 34, 29, 26). There is no reason to presume that only one sorption mechanism dominates in any particular case. Indeed, in real systems, more than one process likely contributes to rate-limited sorption behavior.

Current methods for assessing sorption and sequestration of PAHs on soils and sediments do not provide basic understanding of what is attainable by biostabilization or the bioavailability of recalcitrant PAHs, nor provide information to aid interpretation of results of ecotoxicological testing of residuals after biotreatment. Whether residual PAHs remaining after biotreatment represent an acceptable endpoint level requires understanding of the mechanisms that bind contaminant PAHs within soil or sediment. Research is needed that will assess the fundamental character of the binding of PAHs at the microscale level in parallel with the development of bioslurry treatment and ecotoxicological testing, to show how the nature of PAH association with soils and sediments relates to biostabilization and achievable treatment endpoints.

Research is needed to identify those factors affecting the bioavailability of PAHs on soils and sediments and the development of the technical basis for enhancing natural

recovery processes involved in the in-situ biotreatment of soils and sediments contaminated with PAHs. A special focus is needed on improving the mechanistic understanding of sequestration and bioavailability of PAHs in soils and sediments. Such research could result in providing guidelines for the assessment and prediction of the bioavailability of PAHs for in-situ biotreatment.

As envisaged in the research reported in this investigation the key questions that need to be addressed are:

- What is the distribution of desorption energies for PAHs from contaminated sediment, and how does this correlate with information on PAH association with sorbent carbon type?
- How does the effectiveness of bioslurry treatment of contaminated sediment with respect to removal of specific compounds, the fraction of labile and resistant PAHs, and the toxicity of residual material depend on the associations of PAHs with sorbent organic matter and distributions of desorption energies?
- How does toxicity depend on the association and binding of PAHs with sorbent organic matter (SOM)?
- How may knowledge of the association of PAHs with SOM and distribution of desorption energies be used to assess and predict the overall performance of bioslurry treatment processes for PAHs in sediments?

The research approach used in this work was to address these questions by integrating a series of physical, chemical, and biological measurements for sediment before and after bioslurry treatment. This included tests to determine PAH distribution by particle size and type, PAH desorption rate to the aqueous phase, PAH binding by thermal programmed desorption (TPD) mass spectrometry (MS), sediment particle-SOM characterization, and, toxicity testing on contaminated sediment before and after active biotreatment. The physical, chemical, and biological tests were designed to relate PAH-sediment interaction with biotreatment and toxicity. It is hypothesized that PAHs that exhibit slow desorption kinetics and high binding energies are also less biotreatable and relatively less toxic. It is proposed

that cases where interactions with SOM are dominant that there may be a correlation between desorption rate, distribution of desorption energies, and the association of PAHs with carbon type. It may be expected that the affinity of PAHs for SOM should relate to whether the SOM is relatively more or less aromatic or polar. The relative rates of desorption and the distribution of desorption energies exhibited by different sediment particle types may reveal whether it is possible to ascribe compound release to classes of SOM.

Previous Thermal Desorption Work

Various adaptations of thermal program desorption (TPD) techniques have been used in the past to study: desorption of gases from solid surfaces (35,36), desorption of toluene from kaolin pellets (37), pyrolysis of hydrocarbons from coal (38), estimation of PAH vapor pressures (39,40), and desorption activation energies of trichloroethylene from silica gel (41). Thermal desorption techniques have also been explored for their utility in detecting and quantifying organic contaminants in soil samples (42). Unlike other techniques for soil analysis, TPD requires no solvent extraction, little sample preparation, and is relatively quick. Samples are heated inside an oven or thermal desorption probe, and as the temperature increases the volatilized compounds are collected and detected using a mass spectrometer. The use of a direct insertion probe, which does not require transfer lines, with a mass spectrometer (MS) allows measurement of the release of trace organics from very small samples. Direct probes have been used for the analysis of coal pyrolysis products by Yun and Meuzelaar (38). To date, thermal desorption mass spectrometry with direct probes has been used for study of pyrolysis and as a means for inserting a sample into a mass spectrometer for compound identification. The technique has not been used previously to study desorption of organic substrates from solids

Thermal Programmed Desorption MS

As already described, previous TPD-MS efforts utilized the combination of GCs with thermal ovens or probes. These configurations entail some disadvantages that lower the quality of the TPD data. Specifically, heating samples in an oven or probe attached to a GC requires a transfer line, which can become coated with the desorbed species as it passes to the MS. This reduces the sensitivity of the MS. In addition, this increases the time required for

a desorbed species to show up in the MS data. If the heating ramp is too rapid, the MS data for a certain molecular ion at a specific time could be inaccurate. Therefore, a modification to TPD-MS analysis is required to improve the quality of the data. Thermal programmed desorption MS analysis with direct probe insertion should offer an improved method.

The challenge was to evaluate the release and binding characteristics of PAHs to determine if there is a correlation with different forms of SOM by comparing data on the energetics of PAH desorption with complementary information on the location and character of SOM. This was performed by assessing the desorption responses of several signature homolog masses from various field samples along with other spectroscopic characterizations of these samples to assess the character of the SOM, the locations of the PAHs on and within sediment particles, and the association of PAHs in the sediment. Termed direct probe MS, as the temperature is increased at a constant rate, the species with the lowest desorption activation energy should desorb first, followed by species with higher desorption energies.

Thermal programmed desorption mass spectrometer (TPD-MS) analyses was used to provide useful information on the distribution of desorption energies for several important PAH mass ions, to test the hypothesis that the greater the proportion of contaminants associated with more aromatic or nonpolar carbon, the greater the desorption energies, and to evaluate whether greater desorption energy corresponds to less bioavailability thus higher residual concentrations left bound in the SOM.

Experimental Approach

The approach taken in this study is to investigate how particle-scale phenomena affecting the binding and release of PAHs impacts PAH availability, extractability, and toxicity. The focus is on dredged sediment with material from Milwaukee Harbor serving as a case study. In this work, a combination of bioslurry tests, TPD-MS measurements, SOM characterization, and toxicity bioassays were employed to assess and characterize bioavailability and toxicity. Thermal program desorption mass spectrometry with a direct insertion probe was used to study the release characteristics of PAHs sorbed on different mineral and organic surfaces: glass, sand, kaolin, alumina, XAD-4 resin beads, coal,

pulverized activated carbon. Due to the high sensitivity of the instrument setup, measurements were possible at the milligram sample size. Once the TPD approach was validated, it was used to characterize untreated and biotreated PAH-impacted sediments from the Milwaukee Confined Disposal Facility (MCDF). These sediments underwent rigorous physical, chemical, and biological analyses for characterization before and after active bioslurry treatment. Earthworm bioaccumulation assays were conducted before and after treatment. Results from TPD-MS analyses, bioslurry tests, and the toxicity bioassays were correlated. These data helped to test the concept of biostabilization and improve the understanding and assessment of how PAHs that are susceptible or resistant to degradation depend on specific locations in the sediment, the association with SOM, and the distribution of desorption energies. Currently, no work has been done to assess how specific PAH locations and binding in sediment affects bioavailability or toxicity.

Report Outline

This report is presented in eight sections. A brief overview has been presented in this section. Sections 2 through 7 are stand-alone discourses and are organized as follows. Section 2, "Direct Observation of Polycyclic Aromatic Hydrocarbons on Geosorbents at the Sub-Particle Scale" has been published in *Environmental Science and Technology* (ES&T) in Volume 33 (8), 1999. This section describes the analytical technique of microprobe two-step laser desorption/laser ionization mass spectrometry to identify and characterize trace hydrophobic organic compounds found as contaminants on geosorbents. Section 3, "Microscale Location, Characterization, and Association of Polycyclic Aromatic Hydrocarbons on Harbor Sediment Particles", has also been published in ES&T, Volume 34(9), 2000. Complementary mass spectrometric and spectroscopic techniques employed to provide direct information at the microscale on the sequestration of PAH contamination in Milwaukee Harbor sediment particles were discussed in this section. Section 4 is entitled "Thermal Program Desorption of PAHs From Mineral and Organic Surfaces" and has been submitted to ES&T. This paper focuses on the development of TPD-MS as a new tool for characterization of environmental samples, and demonstrates its application on PAH-spiked glass, sand, kaolin, alumina, XAD-4 resin beads, coal, and pulverized activated carbon. This section assesses TPD data reduction techniques. Section 5, "Kinetics and Thermodynamics

of PAH Desorption Process From Sediment Particles,” will be submitted to ES&T as well. This paper examines the application of TPD-MS on untreated PAH-impacted Milwaukee Harbor dredged sediment. This work integrates the use of room temperature Tenax bead desorption experiments, TPD data, and modeling to determine desorption activation energies. Section 6, “Defining In-Situ PAH Biodegradation Activity In Terms of Microbial Phenotype and Genetic Potential,” provides a detailed description and interpretation of the microbial ecology of the bioslurry systems. This work will be submitted to *Applied and Environmental Microbiology* (AEM). Section 7, “Availability and Bioslurry Treatment of PAHs In Contaminated Dredged Materials,” is a section that puts together in concise fashion the overall work and will be submitted to ES&T. This section correlates sediment characterization, particle analyses, PAH desorption tests, TPD-MS measurements, bioslurry tests, and toxicity results for biotreated sediments. Section 8 summarizes conclusions from all of the work and suggests future research considerations Appendix A entitled “Measurements of Microbial Activity on Sediment Particle Surfaces and Correlation with Distribution on Sorbed PAHs” was written by Dr. Hap Pritchard at the Naval Research Laboratory, Washington, D.C. This appendix describes the work Dr. Pritchard did with SERDP funding on CU 1095. The data reduction associated with the TPD work was exhaustive in size and is therefore provided only in example form in Appendix B. Appendices C through F provide the raw data generated or modified at the ERDC for each of the sections. Each appendix lists the specific data files associated with that section. Each of the complete data files is recorded on the CD-ROM provided in the inner pocket located immediately after Appendix B.

References

1. EPA. *Assessment and Remediation of Contaminate Sediments (ARCS) Program, Final Summary Report*. EPA-905-S-94-001. Chicago: EPA **1994**.
2. Nalkes, D. V.; Linz, D. G; eds. *Environmentally Acceptable Endpoints in Soil*. Annapolis, MD: American Academy of Environmental Engineers, **1997**.
3. NRC, *Contaminated Sediments in Ports and Waterways, Cleanup Strategies and Technologies*, National Research Council Report, National Academy Press, Washington D.C., **1997**.

4. NRC, *Alternatives for Groundwater Cleanup*, National Research Council Report, National Academy Press, Washington, D.C., **1994**.
5. Moore, J.N.; Brook, E.J.; Johns, C.; "Grain Size Partitioning of Metals in Contaminated Coarse-Grained River Flood Plain Sediment", *Environmental Geology and Water Science*, **1989**, 14(2): 107-115.
6. Alexander, M. *Environ. Sci. Technol.* **1995**, 29, 2713-2717.
7. Luthy, R.G.; Aiken, G.R.; Brusseau, M.L.; Cunningham, S.D.; Gschwend, P.M.; Pignatello, J.J.; Reinhard, M.; Traina, S.; Weber, W.W., Jr.; Westall, J.C. "Sequestration of Hydrophobic Organic Compounds by Geosorbents", *Environ. Sci. Technol.* **1997**, 31, 3341-3347.
8. Steinberg, S.M.; Pignatello, J.J.; Sawhney, B.L. *Environ. Sci. Technol.* **1987**, 21, 1201-1208.
9. Pignatello, J. J.; Xing, B. *Environ. Sci. Technol.* **1996**, 30, 1-11.
10. Thoma, G. *Summary of the Workshop on Contaminated Sediment Handling, Treatment Technologies, and Associated Costs* held April 21-22, **1994**. Background paper prepared for the Committee on Contaminated Sediments, Marine Board, National Research Council, Washington D.C.
11. Luthy, R.G.; Dzombak, D.A.; Peters, C.A.; Roy, S. B.; Ramaswami, A.; Nakles, D.V.; Nott, B.R. *Environ. Sci. Technol.* **1994**, 28, 266A-277A.
12. Loehr, R.C.; Webster, M. T., "Effects of Treatment on Contaminant Availability, Mobility, and Toxicity", Chapter 2 in *Environmentally Acceptable Endpoints in Soil*, Linz, D.G.; Nakles, D.V., Eds., American Academy of Environmental Engineers, Annapolis, MD. **1997**.
13. Bosma, R.M.P.; Middeldorp, P.J.M.; Schraa, G.; Zehnder, A.J.B. *Environ. Sci. Technol.* **1997**, 31, 248-252.
14. Erickson, D.C.; Loehr, R.C.; Neuhauser, E.F. *Water Res.* **1993**, 27, 911-919.
15. Putcha, R. V.; Domach, M. M. *Environ. Prog.* **1993**, 12(2), 81-85.
16. Bury, S.J.; Miller, C.A. *Environ. Sci. Technol.* **1993**, 27, 104-110.
17. Chung, G.Y.; McCoy, B.J.; Scow, K.M. *Biotechnol. Bioeng.* **1993**, 41, 625-632.
18. Edwards, D.A.; Liu, Z.; Luthy, R.G. *J. Environ. Eng.* **1994**, 120, 5-22.
19. Auger, R.L.; Jacobson, A.M.; Domach, M. M. *Environ. Sci. Technol.* **1995**, 29, 1273-

- 1278.
20. GRI, Environmentally Acceptable Endpoints in Soil: Risked-Based Approaches to Contaminated Site Management Based on the Availability of Chemicals in Soil, Draft Report of Workshop Proceedings, Gas Research Institute, Chicago, IL **1995**.
 21. Kelsey, J.W.; Kottler, B. D.; Alexander, M. *Environ. Sci. Technol.* **1997**, 31,214-217.
 22. Fletcher,M. *Advances in Microbiology.* **1991**, 32, 53-85.
 23. Costerton, J.W.; Cheng, K.J.; Geesey, G.G.; Ladd, T.J.; Nickel, J.C.; Dasgupta, M.; Marrie, T. *Annual Review of Microbiology*, **1987**, 41, 435-464.
 24. Schwarzenbach, R .P.; Gschwend, P.M., and Imboden, D. M., *Environmental Organic Chemistry*, John Wiley & Sons, Inc., New York, **1993**.
 25. Stumm, W., "Adsorption", Chapter 4 in *Chemistry of the Solid-Water Interface*, **1992**, John Wiley & Sons, Inc., New York.
 26. Gustafsson, O.; Haghseta, F.; Chan, C.; MacFarlane, J.; Gschwend, P.M. *Environ. Sci. Technol.* **1997**, 31, 203-209.
 27. Boyd, S.A.; Sun, S. *Environ. Sci. Technol.* **1990**, 24, 142-144.
 28. Grathwohl, P. *Environ. Sci. Technol.* **1990**, 24, 1687-1693.
 29. Huang, W., Weber, W.J., Jr. *Environ. Sci. Technol.* **1997**, 31, 2562-2569 and 31, 3238-3243.
 30. Grathwohl, P.; Reinhard, M. *Environ. Sci. Technol.* **1993**, 27,2360-2366.
 31. Wu, S.; Gschwend, P.M. *Water Resour. Res.* **1988**, 24, 1373-1383.
 32. Nkedi-Kizza, P.; Brusseau, M.L.; Rao, P.S.C.; Homsby, A.G. *Environ. Sci. Technol.* **1989**, 23, 814-820.
 33. Brusseau, M.C.; Jessup, R.E.; Rao, P.S.C. *Environ. Sci. Technol.* **1991**, 25, 134-142.
 34. Werth, C.J.; Reinhard, M. *Environ. Sci. Technol.* **1997**, 31, 697-703.
 35. King, D.A. *Surface Science.* **1975**, 47, 384-402.
 36. Falconer, J.L., Madix, R.J. *Surface Science.* **1975**, 48, 393-405.
 37. Keys, B.R., Silcox, G.D. *Environ. Sci. Technol.* **1994**, 28, 840-849.
 38. Yun, Y.; Meuzelaar H.L.C. *Energy & Fuels.* **1991**, 5, 22-29.
 39. Tesconi, M. Yalkowski, S.H. *J. of Pharmaceutical Science*, **1998**, 87, 1512-1520
 40. Oja, V., Suuberg, E.M. *Anal. Chem.* **1997**, 69, 4619-4626.
 41. Farrell, J., Grassian, D., Jones, M. *Environ. Sci. Technol.* **1999**, 33, 1237-1243.

42. Robbat, A., Jr.; Liu, T.; Abraham, B.M. *Anal. Chem.* **1992**, *64*, 358-364.
43. Gillette, J.S.; Luthy, R.G.; Clemett, S.J.; Zare, R.N. *Environ. Sci. Technol.* **1999**, *33*, 1185-1192.
44. Ghosh, U.; Luthy, R.G.; Gillette, J.S.; Zare, R.N. *Environ. Sci. Technol.* **2000**, *34*, 1729-1736.

Section 2

Direct Observation of Polycyclic Aromatic Hydrocarbons on Geosorbents at the Sub-Particle Scale

Abstract

We use the new analytical technique of microprobe two-step laser desorption/laser ionization mass spectrometry ($\mu\text{L}^2\text{MS}$) to identify and characterize trace hydrophobic organic compounds found as contaminants on geosorbents. Specifically, we examine one laboratory prepared sample and three aged field samples for the presence of polycyclic aromatic hydrocarbons (PAHs). The resolution of the present $\mu\text{L}^2\text{MS}$ instrument is a circular spot size 40 μm in diameter, with the potential to be much less. We report PAH distributions across individual particles as well as from particle to particle. Our data show lateral variations in the extent of sorption at the sub-particle scale, which indicates that sorption phenomena are heterogeneous at sub-particle dimensions.

Introduction

The sorption interactions of hydrophobic organic compounds (HOCs) with geosorbents, i.e., soils, sediments, or aquifer media, often result in strong binding that may influence subsequent release rates. This behavior diminishes the bioavailability of HOCs to microorganisms and thus impacts the rate and overall removal of HOCs during bioremediation of contaminated geosorbents (1, 2). This behavior also impacts environmental exposure and toxicity (3).

Despite much recent research on sorption of HOCs on geosorbents, great uncertainty exists in fundamental knowledge of where HOCs reside on geosorbents and what are the underlying chemical mechanisms accounting for HOC sequestration and slow release (4). This paper introduces a new instrumental technique that may provide more direct information at the sub-particle scale on the locations of HOCs on geosorbents.

J. Seb Gillette, Richard G. Luthy, Simon J. Clementt, and Richard N. Zare
Department of Chemistry, Stanford University, Stanford, CA 94305-5080

Data are presented for the case of aged soils and sediments contaminated with polycyclic aromatic hydrocarbons (PAHs).

Binding of PAHs on Geosorbents. PAHs comprise a broad class of hydrophobic compounds that appear as persistent contaminants (5-7) introduced through sources such as petroleum and fuel residues, tars and creosotes, and combustion processes. Such compounds have low aqueous solubility, low volatility, and low intrinsic reactivity. They typically exhibit very slow release rates from soil or sediments (8), becoming less available with aging compared to freshly added material. However, residual PAHs may be significantly less leachable by water and less toxic as measured by uptake tests (9, 10). All of these factors combine to confound risk assessment.

While the underlying, fundamental phenomena governing the strong sorption of PAHs on geosorbents are unknown, prevailing hypotheses attribute such sequestration to interactions with different types of sorbent organic matter (11-14). As discussed in Luthy et al. (4), these organic matter components may take different forms, both amorphous and ordered, which makes differentiation of the specific roles of sorbent components extremely difficult and *a priori* predictions virtually impossible. Grathwohl (11) showed that organic matter in unweathered shales and high-grade coals enhanced sorption by more than an order of magnitude when compared to more oxidized organic matter found in recent soils, geologically young material, or highly weathered organic matter. Huang (14) examined differences in organic matter oxygen/carbon atomic ratios to correlate sorption affinity and nonlinearity, and to describe desorption hysteresis. Gustafsson et al. (15) hypothesized that the sorption of PAHs on harbor sediments is governed by a partitioning between two classes of sorbent organic matter; humic acid-type organic matter and soot. They suggest that soot possesses an especially strong affinity for PAHs, similar to that reported for activated carbon (16).

Presently no direct observational data exist revealing the microscale locations in which nonpolar organic compounds accumulate when they associate with natural geosorbents. Consequently, researchers must rely on inferences from macroscopic experimental observations (4). Answers to questions regarding the fate and toxicity of sorbed PAHs would be aided by information on where exactly the PAHs reside on aged sediments, how their concentrations correlate with organic matter location and type, and how biotreatment affects these associations.

Instrument Methods for PAHs on Geosorbents. The elemental analysis of heterogeneous surfaces on a microscopic scale has achieved a high level of development, and is consistently improving in both sensitivity and resolution. Unfortunately, the organic molecular analysis of the same samples presents a far greater challenge because of the thermal fragility associated with organic molecules. Additionally, the smaller the sample size or the finer the heterogeneity of a sample, the greater the need for highly localized heating to take advantage of sensitive gas-phase detection techniques such as mass spectrometry.

During recent years, several techniques have emerged to address the problem of microscale organic analysis. The two most successful have been secondary ionization mass spectrometry (17-19) and laser microprobe mass analysis (20-23). Both of these techniques combine desorption and ionization into a single step. In general, for a given wavelength, the energy required to volatilize material from a sample surface is less than that necessary for its ionization. The consequence is that such “one-step” desorption-ionization techniques often result in fragmentation of the constituent molecules. Although fragmentation can be useful for structural elucidation, it is a severe liability in the interpretation of spectra from samples containing a complex mixture of compounds. Combining the desorption and ionization processes in one step can lead to matrix ionization effects in which the efficiency of ionization and the release of charged species depends critically on the nature of the surface from which desorption is occurring. These drawbacks make quantitative comparisons between different sample matrices impossible without appropriate standards. Also, a 1,000-10,000 fold excess of neutral over ionized compounds is typically produced during desorption (24, 25), which dramatically reduces the sensitivity of one-step instruments. Finally, because the ionization process is not selective, interference signals from inorganic species can complicate spectral assignments (26). One way to avoid these problems is to decouple the desorption and ionization processes.

$\mu\text{L}^2\text{MS}$ Technique. Microprobe two-step laser desorption / laser ionization mass spectrometry ($\mu\text{L}^2\text{MS}$) is a new, powerful, microanalytical technique capable of analyzing some types of trace organic molecules with microscopic spatial resolution (27). In this technique a focused desorption laser is used to volatilize intact neutral molecules from a solid sample. The instrument incorporates the molecular selectivity and sensitivity of resonance-enhanced

multiphoton ionization and detection by reflectron time-of-flight mass spectrometry. To date, the most notable use of the $\mu\text{L}^2\text{MS}$ technique is the analysis of meteoritic samples (28, 29), including those believed to have originated from Mars (30). The instrument has also been used to analyze PAHs in meteoritic acid residues, interplanetary dust particles, and graphite grains that are believed to be interstellar in origin (31, 32). Other two step laser mass spectrometry applications include the screening of contaminated soils (33) and the spatial analysis of additives in polymers (34). In this paper we report on the use of the technique for measuring PAH distributions on contaminated geosorbents.

$\mu\text{L}^2\text{MS}$ is an ideal instrument for microscale characterization of PAHs on geosorbents for several reasons:

1. It employs in situ analysis, which minimizes the possibility of contamination and chemical alteration from more commonly used extraction techniques.
2. Sampling occurs from a 40 μm diameter spot, which is visualized through a microscope objective connected to a video monitor. Because a complete mass spectrum can be obtained from a single analysis spot, spatial distribution maps for various molecules can be produced.
3. Pulsed laser desorption can, in a very short time span, deposit large quantities of energy into a highly localized area. Such processes provide a remarkably versatile method for introducing intact into the gas phase thermally labile and high molecular weight species. Desorption with minimal decomposition and ionization with minimal fragmentation result in spectra consisting primarily of parent ion peaks.
4. Ionization of analyte molecules occurs through resonance enhanced multiphoton ionization. Because the ionization efficiency of a resonant mechanism is greater by many orders of magnitude than nonresonant multiphoton processes (35), only those molecules with a transition in resonance with the laser frequency will be appreciably ionized. It is by virtue of this effect that we can achieve species-selective ionization. The real elegance of this ionization scheme lies not only in its selectivity, but also because it provides a very efficient “soft ionization” route (36, 37); that is, ions are formed with very little internal excitation and consequently do not undergo any appreciable fragmentation. The fact that molecules are detected intact is what makes the analysis of complex mixtures possible.

5. Separate desorption and ionization steps largely eliminate matrix effects because the chemical matrix has much less influence on the release of neutral than charged species. Under our infrared irradiation conditions, laser desorption is consistent with a simple thermal desorption model, based on rapid bulk heating of the irradiated spot. The laser power is kept low enough so that only neutral species are desorbed, thus eliminating the complex matrix effects associated with one-step laser desorption mass spectrometric techniques. The instrument's response to analytes with similar binding strengths becomes solely dependent on the heating of the sample area, a process directly related to absorption of the matrix at the desorbing infrared wavelength, 10.6 μm . If various matrices have similar 10.6 μm absorptions, matrix effects can largely be ignored and quantitative comparisons can be made between similar compounds.
6. Finally, $\mu\text{L}^2\text{MS}$ is a gentle and relatively nondestructive technique that removes only monolayers of material at a time, making subsequent spectroscopic measurements possible. Scanning electron microscopy and electron microprobe are two techniques that have been used to examine samples previously analyzed by $\mu\text{L}^2\text{MS}$.

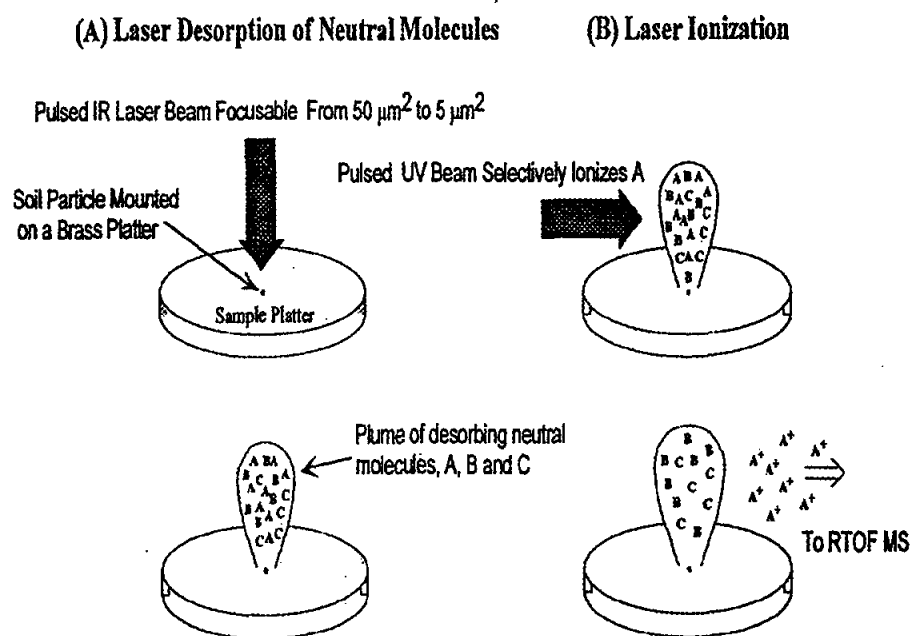
Objectives. The objectives of this work are to: 1) assess the utility of $\mu\text{L}^2\text{MS}$ for spatial characterization of PAHs on heterogeneous, natural soil and sediment particle surfaces; 2) assess possible matrix effects from natural organic matter or other organic contaminants as may be present in aged field samples; 3) evaluate whether the $\mu\text{L}^2\text{MS}$ technique is capable of measuring the lateral distributions of PAHs on contaminated field samples of both soils and sediments; and 4) use the results from the investigation to set directions for further work on microscale characterization for environmental assessment of PAHs and other HOCs on geosorbents. The experiments included work with humic acids, one spiked soil sample, and three aged field samples, one of which had been subjected to large pilot-scale bioslurry treatment. The humic acids and spiked sample were employed as controls to ensure that the instrument was capable of investigating the surface distribution of PAHs without introducing artifacts through the spurious formation of PAHs from organic matter. The field samples provided information on whether the lateral distribution of PAHs could be characterized successfully among a suite of contaminants subjected to long-term aging over many years.

Experimental Section

Soil or sediment particles, as received, are placed on a brass sample platter 7 mm in diameter and introduced into the instrument through a vacuum interlock. The instrument is maintained under vacuum at pressures between 1×10^{-7} and 5×10^{-8} torr. The sample platter is then positioned just below the extraction region of a reflectron time-of-flight mass spectrometer and brought into the focus of a Cassigrainian microscope objective using an X-Y-Z micrometer manipulator. For sample viewing, a macro zoom lens is used in a telescope mode, so that an image of each soil particle can be projected onto a CCD video camera. The sample is illuminated from the exterior of the vacuum chamber, through a side viewport, with a focused quartz halogen lamp. A sample may be analyzed across its surface or section by X-Y adjustments of the micrometer manipulator while the video camera gives a visual record of the regions being sampled.

Figure 1 presents a schematic drawing of the desorption/ionization technique. In the first step of analysis, constituent molecules on the sample's surface are desorbed with a pulsed infrared laser beam (Alltec AL 851, λ 10.6 μm) focused to a 40 μm diameter spot using the Cassigrainian microscope objective. The IR laser power is kept low, $\sim 2.5 \times 10^6 \text{ W} / \text{cm}^2$, to minimize decomposition and assure that only neutral species are desorbed. Sampling depth is dependent on laser power and less so on the sample matrix and sorbate. Laser radiation can cause ablation of the surface, but at the laser power used in this study no physical change of the sample is microscopically observable. However, ion signal corresponding to the removal of sorbate layers is seen. In light of these two results, sampling depth is estimated to be in the range of tens of nm. In the second step, the desorbed molecules are ionized with a pulsed ultraviolet laser beam (Spectra Physics DCR 11, λ 266 nm) using a (1+1) resonance enhanced multi-photon scheme, and the resulting ions are extracted into a reflectron time-of-flight mass spectrometer. The laser pulse energy, $\sim 1.25 \times 10^6 \text{ W} / \text{cm}^2$, is chosen to maximize parent ion signal from the ionization scheme. The ions produced by the UV laser are extracted from the source and injected into the reflectron mass spectrometer. A 20 cm^2 active area dual microchannel plate detector with an oversized anode is used in a chevron configuration to detect the ions. The output of the detector passes through a fast preamplifier (LeCroy VV100BTB) and a timing filter (Ortec 474) and is displayed on a digital oscilloscope (LeCroy 9450). The resulting signal can be summed or averaged in the

Figure 1: Schematic of the $\mu\text{L}^2\text{MS}$ method.



oscilloscope with subsequent laser shots or the data can be transferred to a computer and examined at a later time. As an internal reference, a metered leak valve can be used to introduce a constant background of perdeuterotoluene to aid in both optimization of the ion optics and mass calibration.

Samples. Humic acid was obtained from Aldrich (catalog number H1,675-2) and used as received. Another humic, Laurentian humic acid extracted from a forest podzol in an area controlled by Laval University (Quebec, Canada), was received from the University of Calgary, Alberta and is well characterized (38-40).

Hydrocarbon-added Sassafras soil was obtained from DuPont Central Research and Development (Dr. Scott Cunningham, DuPont Environmental Biotechnology). Clean soil (10% clay, 2.2% organic matter) was sterilized by gamma-ray radiation and a synthetic blend of 17 hydrocarbons, including naphthalene, phenanthrene, pyrene, and benzo(a)pyrene, in ethylbenzene was mixed in the soil resulting in hydrocarbon concentrations of 0.5 mmol/kg each. The sample was then allowed to volatilize for two hours before water was added to bring the moisture content to 70% of field capacity and the sample was aged eight months prior to use.

A coal-tar impacted aquatic sediment was obtained from the Gas Research Institute/Niagara Mohawk Power Corporation bioslurry technology demonstration project at Harbor Point in Utica, NY (41). Dredged material comprising about 34% sand, 52% silt, and 14% clay was processed in batch, aerobic, bioslurry treatment operations conducted for 69 days using 7,300 gallon-slurry volume, complete-mix reactors. PAH concentrations were reduced from 651 mg/kg to 203 mg/kg, but most reduction occurred in the first three to four weeks. A treated sediment sample from a drummed composite having moisture content of about 24% was provided for testing. Table 1 shows the concentration of selected PAHs in the sediment as determined by gas chromatography/mass spectrometry (GC/MS) single ion monitoring analysis of a soxhlet extraction using methylene chloride and acetone (50:50).

A field sediment sample was obtained from the confined disposal facility at Jones Island, Milwaukee, WI operated by the US Army Corps of Engineers and serving the Milwaukee Harbor. Coal tar, coal tar air emissions, gasoline engine exhaust tar, and runoff

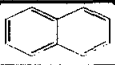
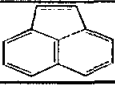
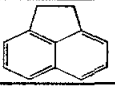
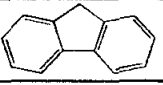
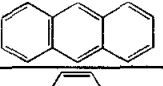
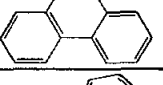
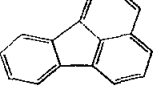
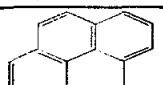
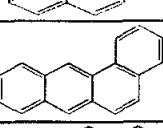
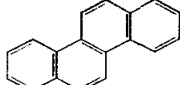
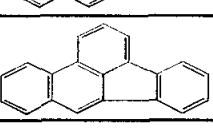
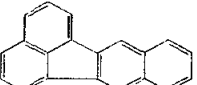
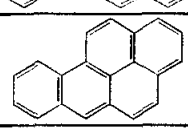
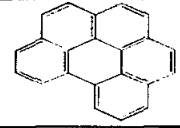
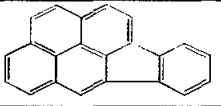
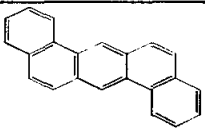
Analyte	Molecular		GRI Sediment (mg/kg)	Milwaukee Sediment (mg/kg)	Popile Soil (mg/kg)
	Weight (amu)	Structure			
Naphthalene	128		3.0	0.4	1.4
Acenaphthylene	152		5.6	1.4	18.0
Acenaphthene	154		2.4	1.1	22.2
Fluorene	166		1.4	1.2	45.3
Anthracene	178		4.0	2.1	153.5
Phenanthrene	178		9.6	10.5	157.5
Fluoranthene	202		21.0	1.7	73.5
Pyrene	202		25.0	14.0	71.4
Benzo(a)anthracene	228		18.0	5.7	12.6
Chrysene	228		20.0	6.9	16.3
Benzo(b)fluoranthene	252		15.0	4.8	5.7
Benzo(k)fluoranthene	252		18.0	4.2	5.4
Benzo(a)pyrene	252		26.0	5.5	4.3
Benzo(g,h,i)perylene	276		13.0	3.6	1.0
Indeno(1,2,3-c,d)pyrene	276		12.0	3.5	1.2
Dibenzo(a,h)anthracene	278		5.4	0.5	18.0

Table 1: PAH molecular weights, structures and concentrations (mg/kg) for the aged soil and sediment samples used in this study, as determined by GC/MS.

were major contributors to the harbor's PAH burden (42). Average PAH concentrations in the facility range from about 50-275 mg/kg depending on depth (43). The sediment sample used in this study was air-dried for seven days and then sieved. Table 1 shows the concentration of selected PAHs for the 0.25-1.0 mm size fraction used in this study based on the average of two replicate analyses by EPA method 8270 with hexane/acetone soxhlet extraction and GC/MS.

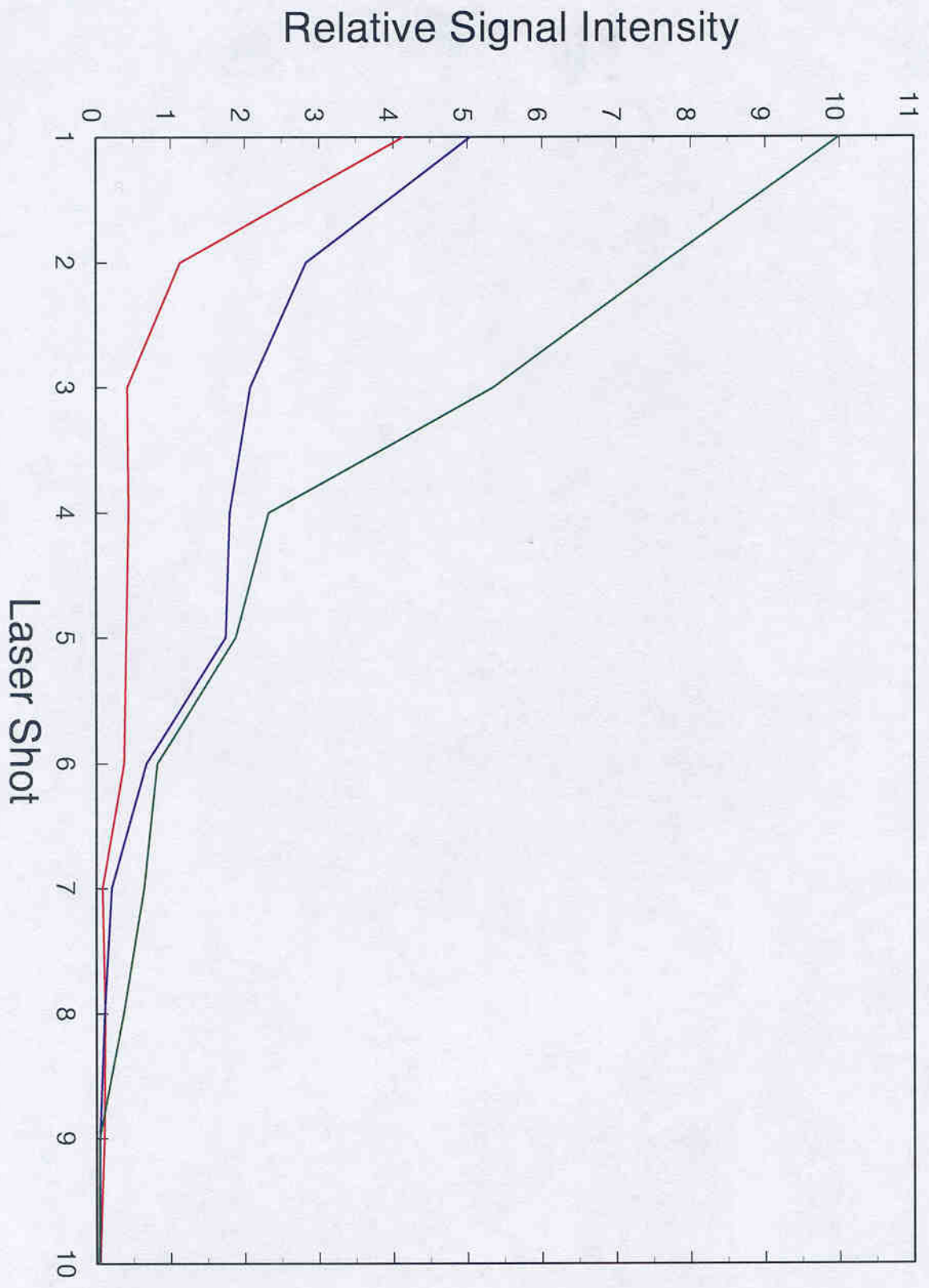
A soil sample was obtained from the Popile, Inc. Superfund Site, El Dorado, AK, which is an inactive wood preserving site that utilized creosotes, pentachlorophenol, and petroleum distillates (44). The sample was air-dried for seven days and then sieved. Table 1 shows the concentration of selected PAHs for the 0.25-1.0 mm size fraction used in this study based on the average of two replicate analyses by EPA method 8270 with hexane/acetone soxhlet extraction and GC/MS.

Results

Table 1 presents the molecular weight and structure of selected parent PAH compounds identified in this study. Molecular weight species 14 atomic mass units (amu) heavier than the parent compounds generally correspond to the addition of a methyl group to the basic PAH structure.

As discussed earlier, determining relative concentrations using the $\mu\text{L}^2\text{MS}$ method is especially reliable if the matrices have similar absorptions at 10.6 μm , the desorbing laser wavelength. Therefore, IR spectra of the soils and sediments, ground in to a KBr pellet, were taken. All of the materials had a similar absorption at 10.6 μm . Consequentially, we believe that concentration differences seen are not the result of varying CO_2 laser light absorption at different sites and that matrix effects caused by differential heating can largely be ignored and quantitative comparisons made. However, the Sassafras soil and the GRI sediment exhibit heterogeneity at the sub-particle scale and the IR spectra represent an analysis of the whole particle. Therefore, when relative quantification was performed for the Sassafras and GRI samples, the PAHs were totally desorbed from each analysis spot and the resulting signal was summed. Figure 2 illustrates the removal of PAHs from the GRI sediment at three separate 40 μm diameter spots, each with differing amounts of PAHs. By the tenth desorption laser shot, the signal from each site approached zero indicating that all of the PAHs had been removed.

PAH Signal vs Desorption Laser Shots



Because the Milwaukee and Popple samples are relatively homogeneous at the particle scale and the particles had a similar 10.6 μm absorbance, particle to particle comparisons were possible.

Humic Acid. One concern when volatilizing matter from a surface for subsequent mass spectrometry analysis is the possible production of PAHs through the desorption process. $\mu\text{L}^2\text{MS}$ spectra of two humic acids, Aldrich and Laurentian, were examined to assess whether PAHs are a pyrolysis byproduct of our laser desorption process. Humic acids were thought to be the most likely candidates for producing PAH end products owing to their abundant and varied carbon content. Various spectra were taken at normal operating IR power and also at 10 times the normal operating power. Each of the spectra comprised an average of 100 laser shots to enhance the overall signal-to-noise ratio. The resulting signal-to-noise ratio in the masses generally associated with PAHs ranged from 2-4. In comparison, the signal-to-noise ratio seen in the spiked Sassafras soil spectra ranged from 900-2500 in those same masses. It was therefore concluded that PAHs are not formed at any detectable level from these carbonaceous components of soil under the conditions used in this study. Furthermore, at laser powers ten times greater than are experimentally used, PAHs also are not produced.

Spiked Soil. $\mu\text{L}^2\text{MS}$ analysis of the laboratory-prepared Sassafras soil (Figure 3) demonstrates that our method is quite capable of detecting PAHs with no interference or spurious results from the soil matrix. The spectrum, a 100 laser shot average of an individual particle's surface, is dominated by three distinct peaks at 178, 202, and 252 amu corresponding to the added compounds phenanthrene, pyrene, and benzo(a)pyrene. There are small fragmentation peaks corresponding to the loss of H_2 , but no other fragmentation of the parent compounds is seen. The peak corresponding to naphthalene, 128 amu, is orders of magnitude smaller because most was evaporated off either during soil preparation, or storage, and was therefore not present in the soil at the time of analysis. The Sassafras soil was further investigated for lateral distributions of PAHs across individual soil particles approximately 400-500 μm in diameter. A 10-shot average was taken from one 40 μm diameter spot and then the sample was translated 50 μm and another 10-shot average was recorded from that 40 μm spot. At each location, signal from the PAHs had dropped to near zero by the time the final shot was taken indicating the depletion of all PAHs in the $\mu\text{L}^2\text{MS}$ sampling area. The data were then quantified using normalized peak areas. Figure 4 displays the results plotted on a x-y

Figure 3: $\mu\text{L}^2\text{MS}$ spectrum of a Sassafras soil particle spiked with PAHs and aged eight months.

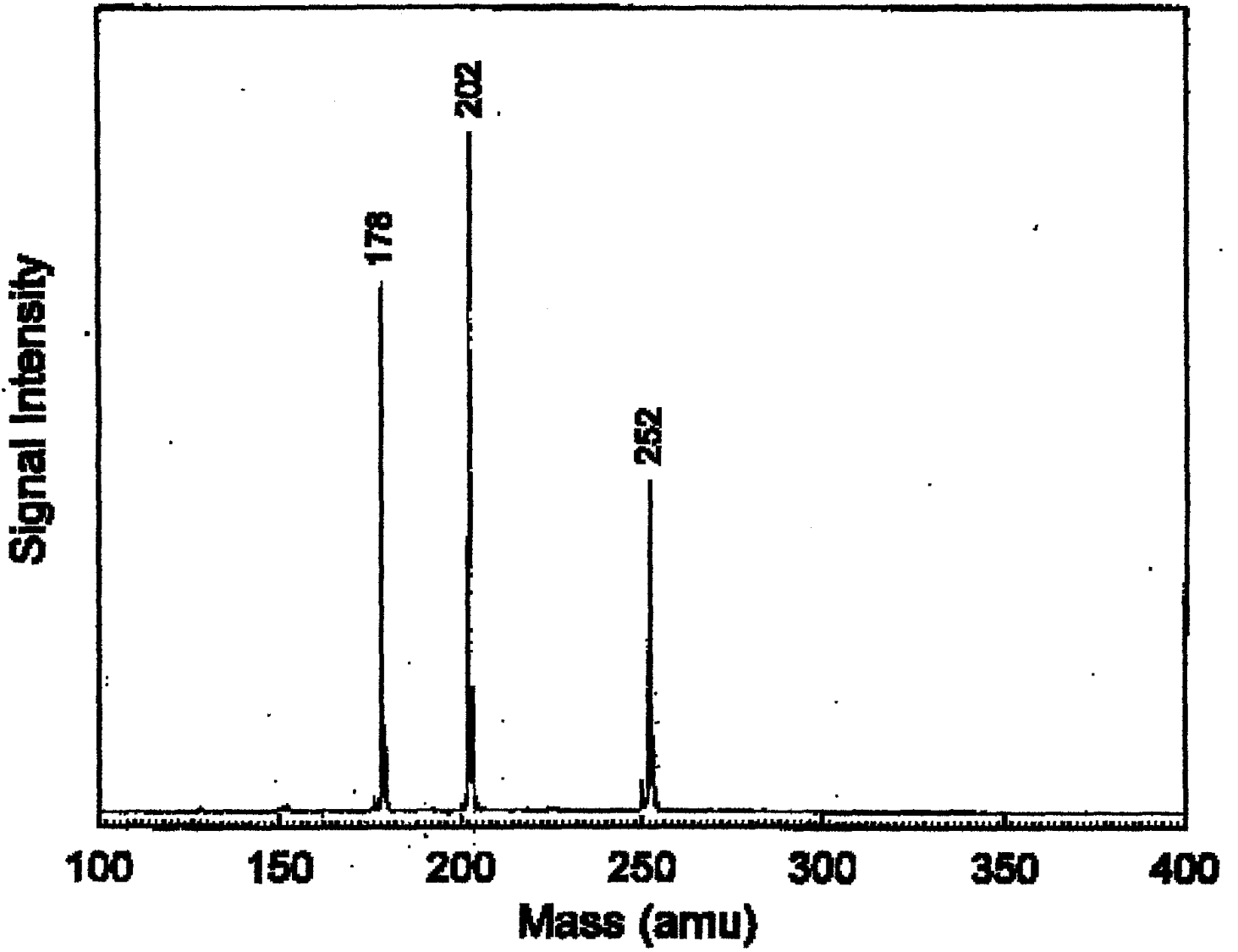
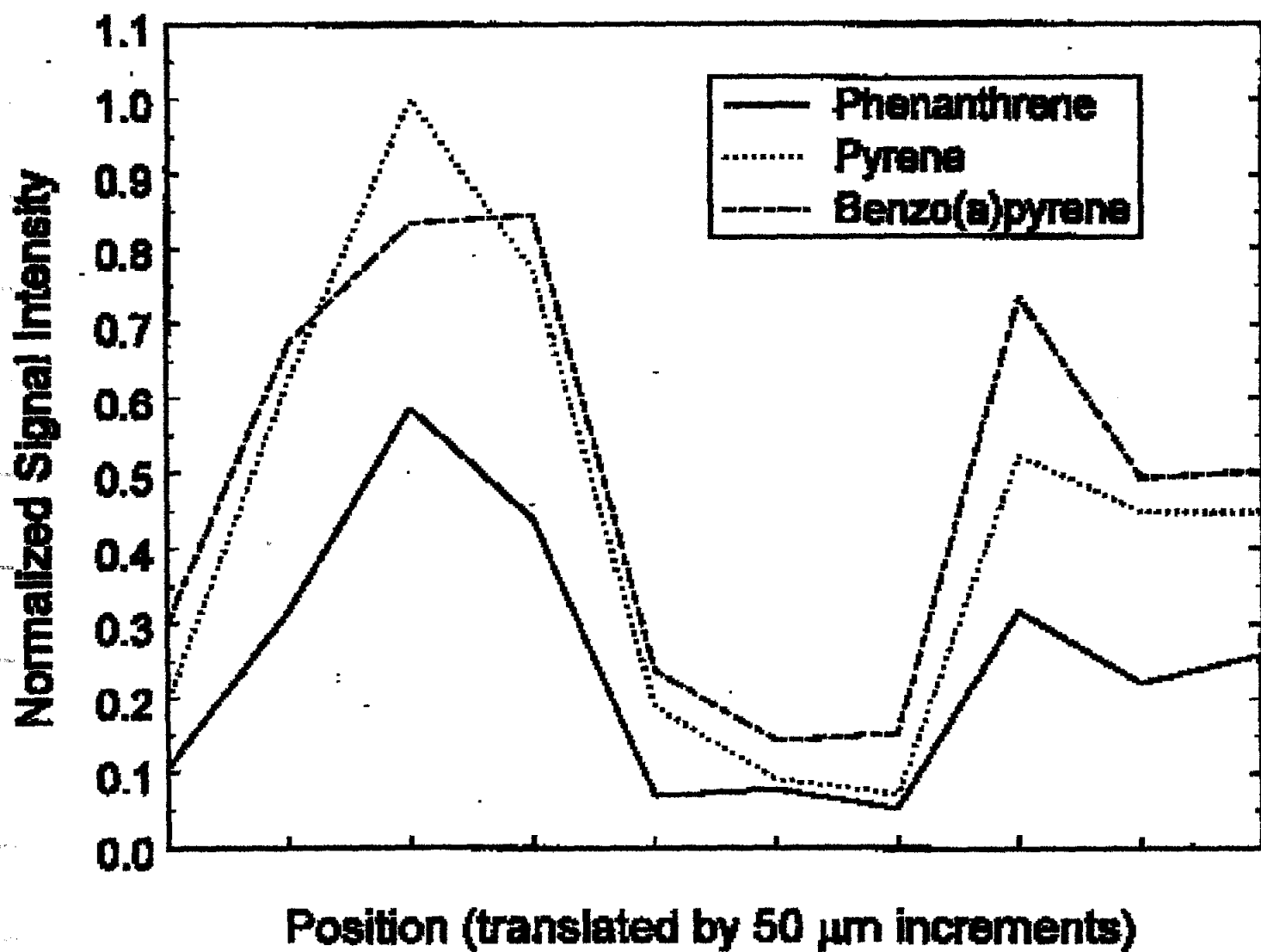


Figure 4: Plot of three PAH concentrations as a function of position across a Sassafras soil particle.



graph. It is seen that the PAH concentrations vary up to a factor of 14 across this 500 μm soil particle. Other Sassafras soil particles showed variability ranging from a factor of 13 up to 29 across the surface. It is also seen that the PAHs with different masses follow similar distribution patterns across the soil particle.

Bioslurry Treated Sediment. Analysis of the biotreated GRI sediment slurry indicates a more complex array of PAHs than the laboratory-prepared Sassafras sample. Figure 5 presents the average spectrum of 100 laser shots across a GRI sediment particle's surface. It shows an expansive mixture of PAHs with the major peaks corresponding to the parent PAHs displayed in Table 1. Additionally, a series of peaks at +14 amu increments from the parent peaks are representative of homologous methyl alkylations of the parent PAHs. Examples of this are a methylnaphthalene peak at 142 amu and peaks at 192, 206, and 220 amu resulting from the alkylation of anthracene or phenanthrene (178 amu). The predominant compounds detected by $\mu\text{L}^2\text{MS}$ are the same as those detected by GC/MS as discussed later. As with the Sassafras soil, lateral PAH concentrations were determined by removing PAHs from a 40 μm diameter spot, recording a spectrum, then translating the sample 50 μm , and repeating the process. Figure 6 displays the recorded signals plotted as a function of position for six representative PAH molecular masses. A total PAH variation factor of 7 and concentration variations for individual PAHs ranging from a factor of 5 to 8 are seen from this particular tract. In other analyses concentration variations from 5 to 11 were calculated. As in the Sassafras soil, the individual PAH concentrations follow similar distribution patterns across the GRI sediment particle. Here, the relative concentrations of lower molecular weight compounds follow a similar pattern of varying amounts, as do the higher molecular weight compounds.

Abundances of the same PAH compound in different soil samples can be directly estimated from the peak intensity but the peak intensity for each different PAH is dependent not only on the concentration of each compound, but also on the ionization efficiency or absorption cross-section at the laser wavelength employed. Nonetheless, the relative concentrations obtained by $\mu\text{L}^2\text{MS}$ are similar to those found by GC/MS. To illustrate this, a comparison of relative concentrations measured by the $\mu\text{L}^2\text{MS}$ system and a GC/MS system is shown in Figure 7. Although differences may be expected between surface and whole sample analyses, the two methods do give similar results with the exception of the 152 and 278 amu

Figure 5: $\mu\text{L}^2\text{MS}$ spectrum of a GRI sediment identifying parent PAH compounds (mass numbered) and their alkylated derivatives.

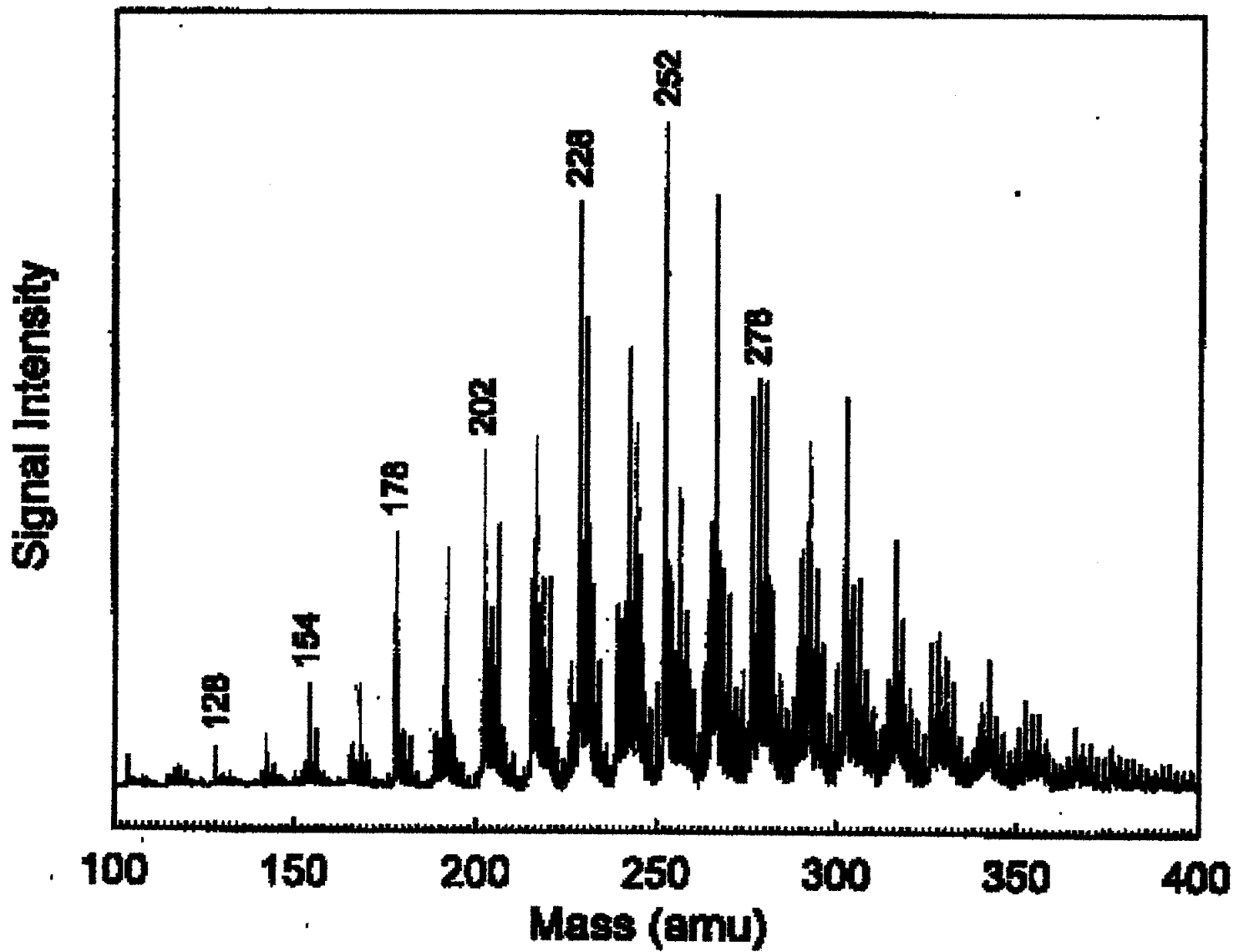


Figure 6: Plot of six representative parent PAH mass concentrations as a function of position across a GRI sediment particle.

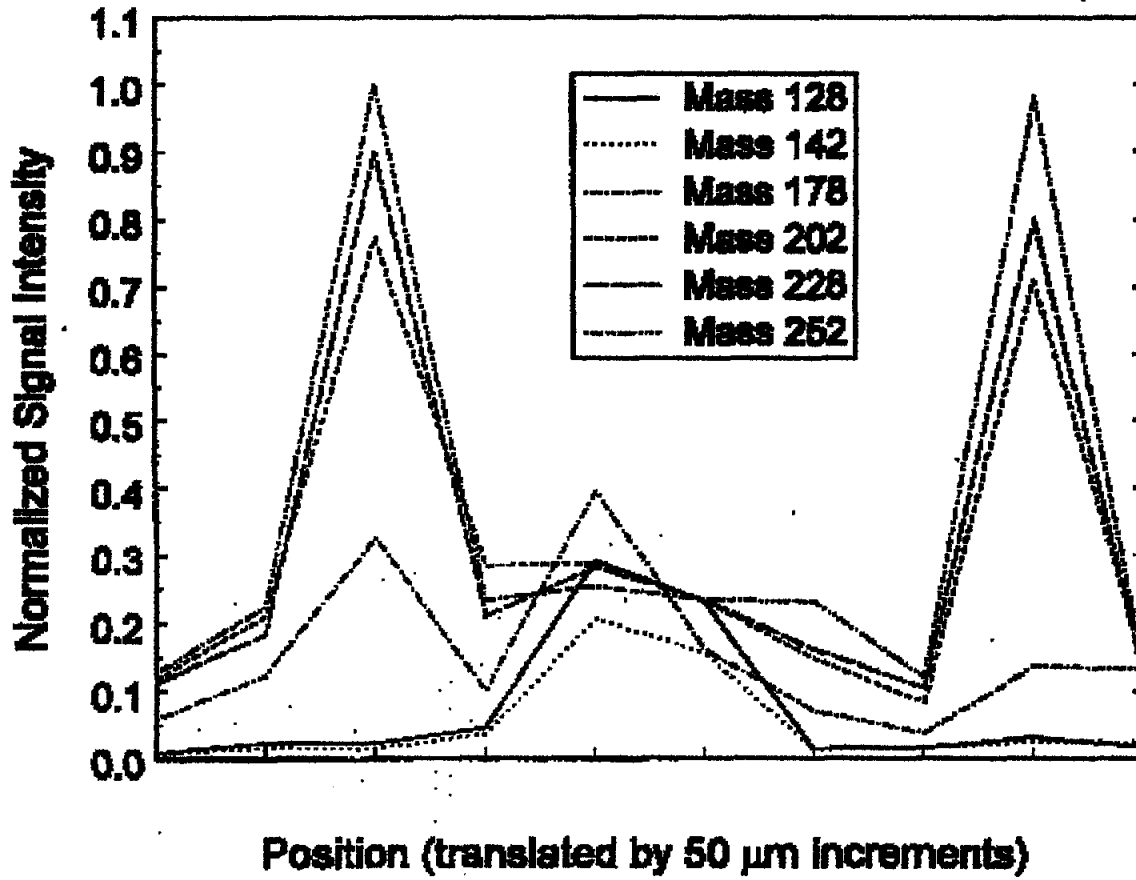
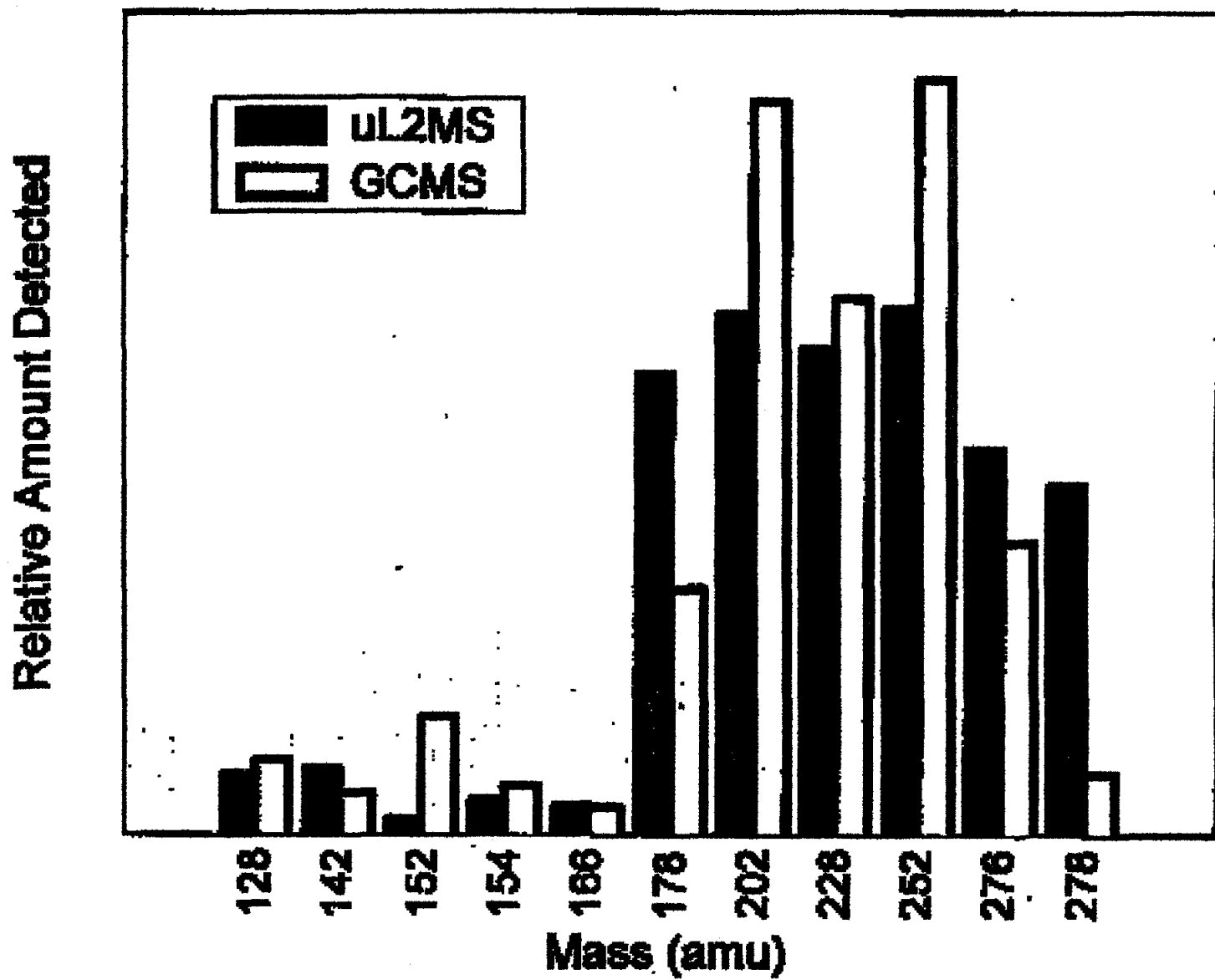


Figure 7: Comparison of $\mu\text{L}^2\text{MS}$ and GC/MS data for PAHs identified on GRI sediment.



compounds. Discrepancies in the relative concentrations determined by the two methods may be caused by the differing ionization efficiencies of each PAH. Additionally, the $\mu\text{L}^2\text{MS}$ data represents the average of over 10,000 laser shots on several sediment particles, which corresponds to only a very small sample compared to the 22.8 g used in the GC/MS analysis.

Both the Sassafras soil and the GRI sediment particles showed fluctuations in PAH concentration across their surfaces. Similar results were seen for all particles analyzed. These data show for the first time that soil or sediment particles actually comprise sub-particle size regions having different affinities for the PAHs. Although this idea has been inferred from macroscopic observations, the $\mu\text{L}^2\text{MS}$ instrument provides a technique whereby the variation in HOC location may be directly ascertained.

Milwaukee Sediment and Popile Soil. Both the Sassafras soil and the GRI sediment samples are more heterogeneous at the sub-particle scale in composition than the Milwaukee sediment or Popile soil. The latter samples contain particles ranging in appearance from glass-like crystal to totally opaque black. Thus for purposes of $\mu\text{L}^2\text{MS}$ characterization, the most homogeneous particles were separated into two categories, glassy or black. Both types of particles have a similar IR absorption at 10.6 μm allowing quantitative comparison of the particles by $\mu\text{L}^2\text{MS}$. The sediment particles were separated first by the naked eye and then by a stereo microscope. The particle spectra comprise 100-shot averages from various locations across the surface under identical conditions to allow direct comparison of signal intensities. Although desorption occurred across all of the sample, it was noted that if laser shots were taken on one 40 μm diameter spot the signal intensity was reduced to zero after multiple shots. A marked difference in PAH concentration was noted between the glassy and black particles with the moderate colored particles ranging in between. In these cases the $\mu\text{L}^2\text{MS}$ method clearly could differentiate particle-to-particle variations.

Electron microprobe analysis was used to characterize the glassy and black particles. This elemental analysis technique is based upon striking a sample with a focused beam of electrons to induce emission of characteristic X-rays. The method is highly sensitive, spatially resolved, and essentially nondestructive. For both the Milwaukee sediment and the Popile soil the electron microprobe work identified the glassy particles as primarily silicate, with occasional inclusions of feldspar and mica. The black particles are carbonaceous with patches

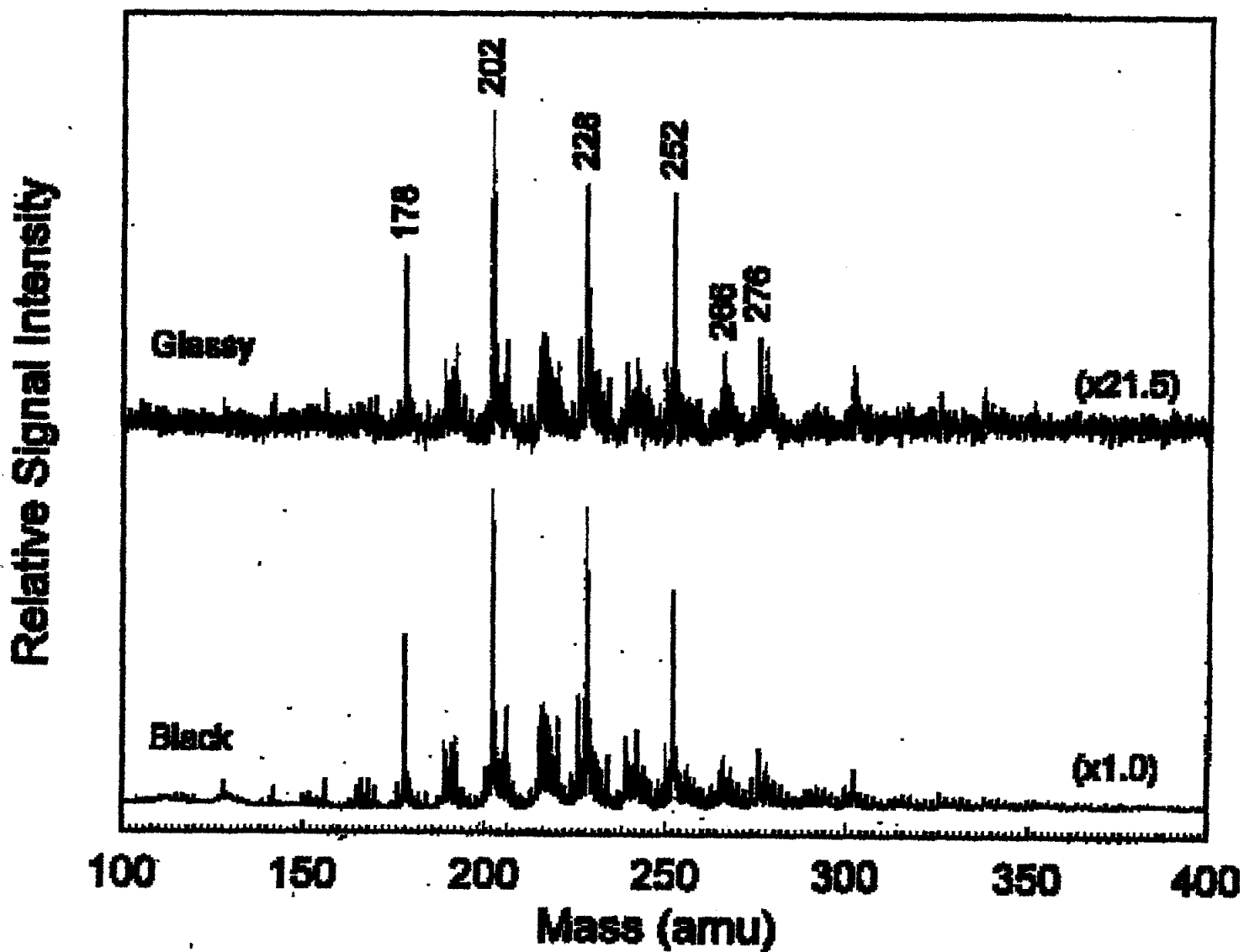
of silicate, pyrite, and calcium in the form of carbonate and also tiny amounts of feldspar and mica. Particles of both the glassy and black sediments from the 0.25-1.0 mm size fraction of the Milwaukee sediment were analyzed and representative spectra from each particle type are shown in Figure 8. In these spectra the black particle contains over twenty times the amount of PAHs on its surface than the glassy one does. Similar differences were seen in comparisons between other particles. Despite the differences in PAH concentration on these particles, the distribution of PAH species show the same relative patterns regardless of particle type. Both particle types exhibited less variability in PAH amount across their surface than was observed in the Sassafras and GRI samples.

The Popile soil sample also contained easily distinguishable particles so a similar course of analysis was followed as with the Milwaukee sediment samples. Representative spectra of each particle type, glassy and black, were taken, and again almost a factor of twenty difference between the two PAH concentrations was seen on the different particles. Here too, the same suite of PAHs was evident in both particle types. However, unlike the Milwaukee sediment the distribution was not the same between the two particle types. The black particle's major peak was mass 228 followed by compounds weighing 178, 202 and 252 amu. The glassy particle's major peak was at 178 amu with other large peaks at 166, 202, and 228 amu. It is unclear what causes this variation, but it was a trend seen in other analyses of various Popile soil particles.

Discussion

Our $\mu\text{L}^2\text{MS}$ instrument has proven useful in previous analyses of extraterrestrial materials and we report here the extension of its capabilities to terrestrial soil and sediment samples. The results of this study with laboratory-prepared and aged field samples demonstrate that this method can give important insight on the location and distribution of PAHs on a microscopic scale. $\mu\text{L}^2\text{MS}$ analysis of two soils and two sediments indicates a heterogeneous binding pattern of PAHs to geosorbents at a lateral resolution of 40 μm and also from particle to particle. These clear variations in the surface distribution of PAHs provide motivation to assess how the sorption of PAHs relates to geosorbent characteristics and the distribution of sorbent organic matter. Sorbed concentrations of PAHs to a geosorbent change at this 40 μm level and these binding characteristics should be considered at the sub-particle level. With the

Figure 8: $\mu\text{L}^2\text{MS}$ spectra of Milwaukee sediment showing the PAH concentrations for two particle classes.



exception of the Popile soil, the average spectra from particle to particle looked similar, with the only difference being in PAH concentration. In general, the suite of PAHs identified at the sub-particle scale was also similar. These results indicate there are consistent patterns in the mass distributions on the microscale throughout the whole sub-sample wherein the relative concentrations of varying ring size PAHs track together, regardless of the sample. Preliminary electron microprobe analyses of contaminated sediment and soil particles indicate that PAHs may preferentially bind to a higher carbon content matrix. Future work will attempt to correlate PAH location with geosorbent type through the combined use of $\mu\text{L}^2\text{MS}$, electron microprobe analysis, wavelength dispersive x-ray analysis, and infrared microspectroscopy.

Acknowledgments

Support for this work was provided by the Strategic Environmental Research and Development Program, the Department of Civil and Environmental Engineering Shimizu Visiting Professorship at Stanford University, and the Gas Research Institute. We thank Bob Jones at the Stanford Center for Materials Research for electron microprobe work.

References

1. Ramaswami, A.; Luthy, R. G.; *Manual of Environmental Microbiology* Hurst, C. J., Ed.; ASM Press: Washington DC, 1997, pp 712.
2. Zhang, W.; Bouwer, E. J.; Cunningham, A. B.; Lewandowski, G. L.; Hincsee, R. E., Brockman, F. L., Vogel, C. M., Eds.; *Proceedings Third International In-Situ and On-Site Bioreclamation Symposium*; Battelle Press: Columbus, OH, 1995; Vol. 3(8), p315.
3. Linz, D. G.; Nakles, D. V. *Environmentally Acceptable Endpoints in Soil*; American Academy of Environmental Engineers: Annapolis, MD, 1997.
4. Luthy, R. G.; Aiken, G. R.; Brusseau, M. L.; Cunningham, S. D.; Gschwend, P. M.; Pignatello, J. J.; Reinhard, M.; Traina, S.; Jr., W. J. W.; Westall, J. C. *Environ. Sci. Technol* 1997, 31, 3341.
5. NRC *Alternatives for Groundwater Cleanup*; National Research Council: Washington DC, 1994.

6. NRC *Contaminated Sediments in Ports and Waterways, Cleanup Strategies and Technologies*; National Research Council: Washington DC, 1997a.
7. NRC *Innovations in Groundwater and Soil Cleanup*; National Research Council: Washington DC, 1997b.
8. Xing, B.; Pignatello, J. J. *Environ. Sci. Technol.* 1996, 30, 2432.
9. Alexander, M. *Environ. Sci. Technol.* 1995, 29, 2713.
10. Kelsey, J. W.; Kottler, B. D.; Alexander, M. *Environ. Sci. Technol.* 1997, 31, 214.
11. Gratwohl, P. *Environ. Sci. Technol.* 1990, 24, 1687.
12. McGinley, P. M.; Katz, L. E.; Weber, W. J. *Environ. Sci. Technol.* 1993, 27, 1524.
13. Pignatello, J. J. *Environ. Sci. Technol.* 1996, 30, 1.
14. Huang, W. Ph.D. Dissertation, University of Michigan, Ann Arbor, 1997.
15. Gustafsson, O.; Haghseta, F.; Chan, C.; Macfarlane, J.; Gschwend, P. M. *Environ. Sci. Technol.* 1997, 31, 203.
16. Walters, R. W.; Luthy, R. G. *Environ. Sci. Technol.* 1984, 18, 395.
17. Briggs, D. *Surf. Interface Anal.* 1983, 5, 113.
18. Benninghoven, A.; Ruedenauer, F. G.; Werner, H. W. *Secondary Mass Spectrometry: Basic Concepts, Instrumental Aspects, Applications, and Trends*; Wiley: New York, 1987.
19. Gillen, G.; Simons, D. S.; Williams, P. *Anal. Chem.* 1990, 62, 2122.
20. Cotter, R. J. *Anal. Chim. Acta.* 1987, 195, 45.
21. Postumus, M. A.; Kistemaker, P. G.; Meuzelaar, H. W.; TeNoeverdeBrauw, M. C. *Anal. Chem.* 1978, 50, 985.
22. Novak, F. M.; Wilk, Z. A.; Hercules, D. M. J. *Trace Microprobe Tech.* 1985, 3, 149.
23. Wilk, Z. A.; Hercules, H. *Anal. Chem.* 1987, 59, 1819.
24. Sundqvist, B. U. R. *Int. J. Mass Spectrom. Ion Phys.* 1992, 118/119, 265.
25. Ens, W.; Mao, Y.; Mayer, F.; Standing, K. G. *Rap. Comm. Mass Spectr.* 1991, 5, 117.
26. Kimock, F. M.; Baxter, J. P.; Winograd, D. *Nucl. Instrum. Methods Phys. Res.* 1983, 218, 287.
27. Clemett, S. J.; Zare, R. N. In *Molecules in Astrophysics: Probes and Processes*; Dishoeck, E. F. v., Ed.: Netherlands, 1997, pp 305.

28. Hahn, J. H.; Zenobi, R.; Bada, J. F.; Zare, R. N. *Science* 1988, 239, 1523.
29. Zenobi, R.; Phillipoz, J.-M.; Buseck, P. R.; Zare, R. N. *Science* 1989, 246, 1026.
30. McKay, D. S.; Gibson, E. K.; Thomas-Keprta, K. L.; Vali, H.; Romanek, C. S.; Clemett, S. J.; Chillier, X. D. F.; Maechling, C. R.; Zare, R. N. *Science* 1996, 273, 924.
31. Clemett, S. J.; Maechling, C. R.; Zare, R. N.; Swan, P. D.; Walker, R. M. *Science* 1993, 262, 721.
32. Clemett, S. J.; Messenger, S.; Chillier, X. D. F.; Gao, X.; Walker, R. M.; Zare, R. N. *Lunar Planet. Sci. Conf.* 1996, XXVII, 229.
33. Dale, M. J.; Jones, A. C.; Pollard, S. J. T.; Langridge-Smith, P. R. R.; Rowley, A. G. *Environ. Sci. Technol.* 1993, 27, 1693.
34. Zhan, Q.; Zenobi, R.; Wright, S. J.; Langridge-Smith, P. R. R. *Macromolecules* 1996, 29, 7865.
35. Pappas, D. L.; Hrubowchak, D. M.; Ervin, M. H.; Winograd, N. *Science* 1989, 243, 64.
36. Shibanov, A. N. *Laser Analytical Spectrochemistry*; Adam Hilger: Bristol, 1985.
37. Winograd, N.; Baxter, J. P.; Kimock, F. M. *Chem. Phys. Lett.* 1982, 82, 581.
38. Bruccoleri, A.; Pant, B. C.; Sharma, D. K.; Langford, C. H. *Environ. Sci. Technol.* 1993, 27, 889.
39. Wang, Z. D.; Pant, B. C.; Langford, C. H. *Anal. Chim. Acta* 1990, 232, 43.
40. Wang, Z. D.; Gamble, D. S.; Langford, C. H. *Environ. Sci. Technol.* 1992, 26, 560.
41. *ReTeC Pilot-Scale Demonstration of Bioslurry Technology for Treating Manufactured Gas Plant Impacted Sediments*; Remediation Technologies Inc.: Ithaca, NY, 1996.
42. Li, A.; Razaak, I. A. A.; Christensen, E. R. *Toxic Organic Contaminants in the Sediments of the Milwaukee Harbor Estuary. Phase III. Kinnickinnic River Sediments*, 1995.
43. Bowman, D. W.; Brannon, J. M.; Batterman, S. A. *Proceedings of the 11th US Army Corps of Engineers Waterways Experiment Station Seminar*, 1996.
44. *CEC Field Sampling Plan for Bioremediation and Treatability Study, Remedial Action at Popile, Inc. Site, Eldorado, AK*; US Army Corps of Engineers: New Orleans, 1996.

Section 3

Microscale Location, Characterization, and Association of Polycyclic Aromatic Hydrocarbons on Harbor Sediment Particles

Abstract

Complementary mass spectrometric and spectroscopic techniques were employed to provide direct information at the microscale on the sequestration of polycyclic aromatic hydrocarbon (PAH) contaminants in Milwaukee Harbor sediment particles. Microprobe two-step laser desorption laser ionization mass spectrometry was used for PAH measurements, infrared microspectroscopy was used for organic carbon measurement, and scanning electron microscopy with wavelength dispersive X-ray spectroscopy was used for elemental microanalysis. PAH concentrations on coal- and wood-derived particles were found to be several orders of magnitude higher than on silica particles. A cryomicrotome sectioning procedure was employed for particle cross-sectional investigations and it was found that most PAHs are concentrated on external surface regions indicating near surface sorption mechanisms. The coal/wood-derived particles constitute only 5% of the sediment by weight, but contain 62% of the total PAHs. The remaining 38% are mainly in a clay and silt fraction. PAH desorption kinetic studies on these separated fractions revealed a relatively low availability of PAHs from the coal/wood fractions and a high availability from the clay/silt fraction. Additionally, these PAH-bearing coal and wood particles may be removed by density separation from heavier clay, silt, and sand.

Upal Ghosh¹ and Richard G. Luthy¹, J. Seb Gillette² and Richard N. Zare²

¹Department of Civil and Environmental Engineering, Carnegie Mellon University, Pittsburgh, PA 15213

²Department of Chemistry, Stanford University, Stanford, CA 94305-5080

Introduction

Owing to the abundance of polycyclic aromatic hydrocarbons (PAHs) in sediments and to the toxic, mutagenic, and carcinogenic effects attributed to these compounds, the clean up of PAH-contaminated sediment has drawn increasing attention (1). Though bioremediation is a potentially cost-effective treatment for PAH-contaminated sediments, a fundamental long-term issue confronting sediment bioremediation is the lack of understanding of contaminant-sediment interactions and the impacts of such interactions on the failure to achieve treatment goals (1-4). Little is known about the mechanisms of PAH and other hydrophobic organic compound (HOC) sequestration and aging in sediments and the resulting effects on chemical and biological availability (5). A major factor influencing successful sediment bioremediation is the availability of contaminants to microorganisms for degradation. However, contaminants that are strongly sorbed and not available to microorganisms, may also not be available for a toxic response (6, 7). Thus, knowledge of how and where PAHs are bound to sediment material is necessary to assess the efficacy of sediment bioremediation and to correlate this knowledge with reductions in availability, mobility, and toxicity.

Three fundamentally different mechanisms that may describe sorption of PAHs on sediments are: (1) surface sorption processes near the external regions of organic or inorganic particles; (2) diffusion processes leading to penetration within the interior regions of porous particles; and (3) diffusion within different types of organic matter (5, 8-13). Many diffusion-based models (14-17) assume a particle-scale diffusion process, although direct physical evidence is lacking on typical depths of penetration for contaminants in field sediments. Organic-matter diffusion models with shallow

penetration depths on the order of sub-micron to tens of nanometers have also been proposed (12,13,18). However, particle-scale pore diffusion and organic matter diffusion are similar mathematically and difficult to distinguish from model fitting of desorption kinetics data (5). The problem with these conceptualizations lies in their inability to independently measure both a diffusion coefficient and a diffusional distance in field contaminated sediments. Direct measurement of HOC contaminant location on sediments at the microscale has not been possible thus far. Hence, current methods that employ macroscopic techniques for assessing sorption and sequestration of HOCs, like PAHs, on geosorbents do not provide information about where toxic contaminants are located, how they are associated, and what fundamental mechanisms govern their sorption. These deficiencies point to the need for improved understanding of PAH-geosorbent interactions and sequestration processes, and the effect of such processes on bioavailability and toxicity of PAHs in geosorbents (1,5). Furthermore, an increased understanding is needed about the location and nature of PAH association in sediment that leads to their unavailability. Such knowledge could impact policy decisions for setting sediment quality criteria, defining cleanup goals, selecting appropriate treatment technologies, and establishing priorities among various environmental problems.

In this research we employed complementary microscale analytic techniques to investigate where PAHs reside in sediment and to determine the material with which they are associated. A primary technique employed in this study was microprobe laser desorption/laser ionization mass spectrometry ($\mu\text{L}^2\text{MS}$), which measures PAH concentrations from a 40 μm diameter spot (19). This technique was supplemented with fourier transform infrared (FTIR) microspectroscopy and scanning electron microscopy

with wavelength dispersive X-ray spectroscopy (SEM/WDX) to evaluate the organic and elemental components in the sediment with which PAHs are associated. A method for particle sectioning was developed that allowed the investigation of PAHs through the interior of sediment particles. The use of these novel instruments and techniques made it possible to describe the character of sorption mechanisms directly at a sub-particle level. Desorption kinetic tests were used to evaluate PAH affinity for the different sediment fractions identified in this study.

Materials and methods

The sediment used in this study was obtained from the Milwaukee Harbor Confined Disposal Facility (CDF) operated by the Milwaukee Harbor Port Authority. These sediments originated from the Milwaukee harbor during the process of dredging to maintain waterway navigability. Concerns have been raised about the potential for release of contaminants from such CDF sites and about closure requirements, as discussed by Bowman *et al.* (20).

Microscale PAH measurements. $\mu\text{L}^2\text{MS}$, as described in Gillette *et al.* (19), was used to identify and characterize the trace distribution of PAHs on sediment particles. The first step in the $\mu\text{L}^2\text{MS}$ analysis involves desorption of constituent molecules on a particle with a pulsed IR laser beam focused to a 40 μm spot or less using a cassegrainian microscope objective. In the second step, the desorbed molecules are selectively ionized with a pulsed ultraviolet laser (266 nm), and the resulting ions are extracted into a reflectron time-of-flight mass spectrometer.

Elemental analysis. Elemental analysis of the particle surfaces was conducted and correlated with PAH location and abundance. Measurement of the microscale elemental composition of sediment particles was performed using an SEM/WDX (Phillips XL-FEG40). The WDX analysis uses similar principles as energy dispersive X-ray (EDX) analysis, which collects and analyzes X-rays produced when an electron beam from a SEM strikes the specimen. The WDX employs an electromechanical system that uses crystals and gas-ionization detectors to collect and analyze the X-rays, however, giving it higher spectral resolution and sensitivity than the traditional EDX, as well as the ability to detect soft X-rays emanating from low molecular weight elements such as boron and carbon.

Microscale organic carbon measurements. FTIR micro-spectroscopy was used to discern the predominant types of sorbent carbon. FTIR microspectroscopy combines the spatial resolution of a microscope with FTIR spectral analysis making it possible to analyze IR absorbances down to a diffraction-limited spatial resolution of approximately 10 μm . Use of synchrotron radiation provides a nearly two-orders of magnitude brightness advantage over standard laboratory global IR sources. This work was carried out at the National Synchrotron Light Source, Brookhaven National Laboratory, using a Spectra Tech IR μs microspectrometer connected to infrared beamline U10B. The detector used was a mercury-cadmium-telluride element with a low energy spectral sensitivity limit of 600 cm^{-1} , and was cooled with liquid nitrogen. A gold mirror was used for background correction. Further details of the performance of the microspectrometer are available in Carr *et al.* (21) and Carr and Williams (22). These measurements were repeated at the Advanced Light Source, Lawrence Berkeley National

Laboratory (IR-beamline 1.4). Transmission FTIR using bulk material formed into KBr pellets was performed using a Mattson ATI FTIR-NIR spectrometer.

Particle sectioning. Sediment particles were sectioned by cryomicrotomy (Leica UltracutR) to expose the internal surface for microanalysis. Sectioning using cryomicrotomy was selected because it does not involve any contact of the specimen with organic materials or solvents, which may adversely affect the integrity of the sample. Particles were attached to the cryomicrotome stub using a small bead of water that was then frozen by immersion in liquid nitrogen. The frozen stub was then transferred to the cryomicrotome holder and maintained at -150°C during cutting. A 2.1 mm cryo-dry, 45° diamond knife (Diatome US, Fort Washington, PA) was used to section the particles at a cutting speed of 1-2 mm/sec with a cutting thickness of $0.2\ \mu\text{m}$. A clean-cut section on the particle was obtained after approximately 300-1000 sections were shaved off the particle. After sectioning, the particles were thawed in a dessicator and mounted on brass stubs for further analysis.

PAH analysis by gas chromatography-flame ionization detection (GC-FID). PAH extraction from whole sediment was performed by three successive ultrasonic extractions (15 seconds on and 15 seconds off pulsing for a total of 3 minutes) with a 50:50 mixture of hexane and acetone following EPA method 3550B. The extracts were combined and cleaned using a silica gel column as outlined in EPA method 3630C. A Hewlett Packard gas chromatograph (Model 6890) with a fused silica capillary column (HP-5, 30 m x 0.25 mm I.D.) and a flame ionization detector was used for analysis based on EPA method 8100 for PAHs. A standard EPA mixture of 16 PAH compounds obtained from Ultra Scientific was used for calibration.

PAH desorption study. PAH desorption kinetic studies were conducted using the original sediment and also separated fractions. Desorption tests followed procedures used previously by Pignatello (23) and Cornelissen *et al.* (24). Contaminated sediment (2.0 g) and Tenax beads (0.5g, 40-60 mesh, Suppelco, PA) were added to a 15 ml glass vial containing 10 ml of water and continuously mixed in a rotator. Mercuric chloride (1.0 mg) was added to the mixture to prevent any biological growth. These studies were conducted in duplicate. At sampling times, the Tenax beads were harvested by allowing the sediment to settle and the Tenax beads to float up. The Tenax beads were scooped out of the test tube and fresh Tenax beads were added. PAHs were extracted from the Tenax beads by agitating the beads in 10 ml of hexane and acetone (50:50 mixture) for 12 hours and repeating two more times. The extracts were then combined and concentrated, cleaned using silica gel, and analyzed by GC-FID.

Results and discussion

Sediment PAH concentration. PAH extraction and analysis of the original sediment showed a total PAH concentration (EPA 16 priority pollutant PAHs) of 96 mg/kg. Figure 1 shows the distribution of the 16 measured PAH compounds. Fluoranthene and pyrene were the most abundant PAHs. The ratio of phenanthrene/anthracene (7.6) and fluorene/pyrene (1.2) indicates pyrogenic sources of the PAHs as opposed to petroleum-based sources (25) i.e. phenanthrene/anthracene ratio < 10 and fluorene/pyrene ratio > 1.0. Coal burning and processing including gasification and coking are among the possible sources of PAHs in this sediment as indicated by Christensen and Zhang (26).

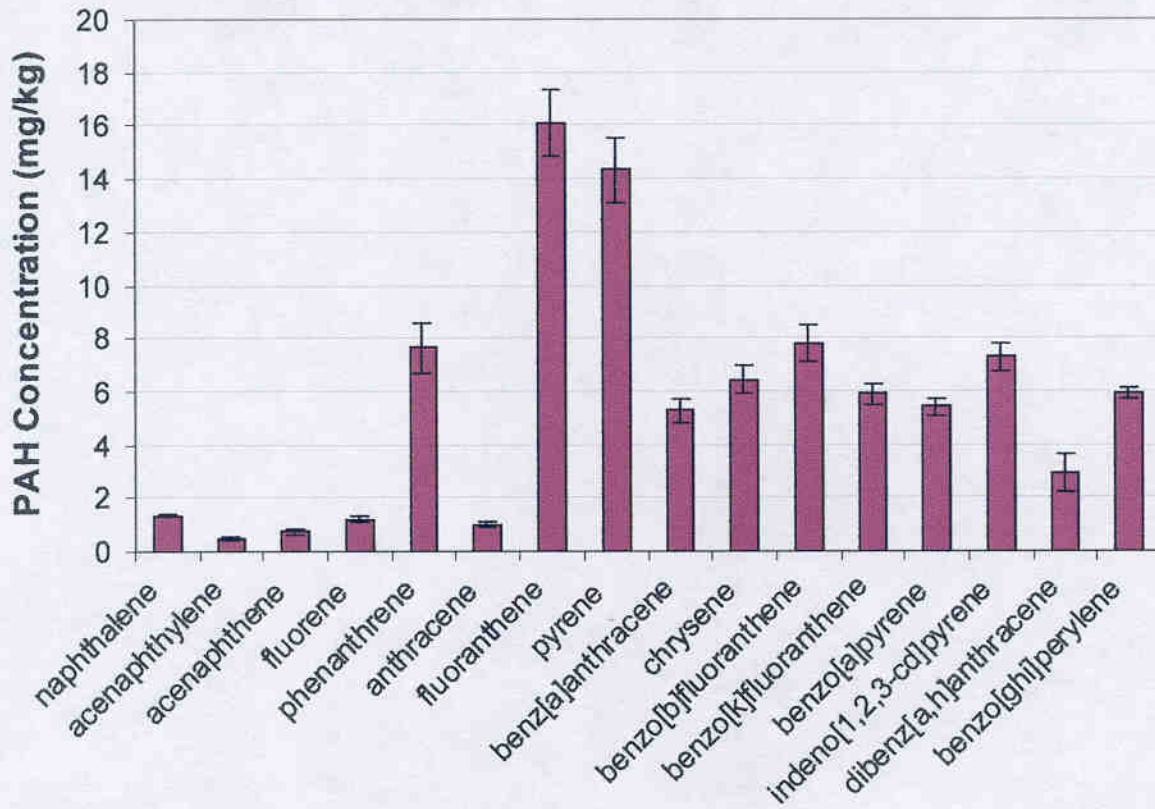


Figure 1. PAH distribution in whole Milwaukee CDF sediment

Identification of major particle classes in sediment. Composite sediment samples obtained from the CDF were separated into four size fractions ($>1000\ \mu\text{m}$, $1000\text{--}250\ \mu\text{m}$, $250\text{--}63\ \mu\text{m}$, and $<63\ \mu\text{m}$) by wet sieving prior to analysis. Figure 2 is a light microscope image of the sediment particles in the $63\text{--}250\ \mu\text{m}$ size fraction. The composition of these particles was determined by elemental analysis using SEM/WDX. The most abundant class of particles in the $>63\ \mu\text{m}$ size fractions is comprised of mainly silicon and oxygen and is designated as silica. The $<63\ \mu\text{m}$ size fraction was dominated by clay particles. The second most abundant particle class within all size fractions is comprised of black particles containing high carbon content. These black particles were identified through petrographic analysis as coal and coal-derived matter having undergone various stages of thermal treatment (using ASTM standard methods for coal analysis: D2797, D2798, and D2799). Microanalysis under reflected light of polished black particles showed optically distinct coal macerals such as vitrinite, fusinite, exinite, and cutinite as indicated in Figure 3. These coal-derived particles were observed in all size fractions of the sediment down to the limit of optical resolution. Historic coal coking and gasification units located near the Milwaukee Harbor and coal shipping operations in the harbor are thought to be sources of coal in the sediment at this site (27). Particles of wood and vegetative debris, which may have originated from wood burning and the natural decay and attrition of vegetative materials, also were found in all size ranges.

These observations agree with findings reported by Griffen and Goldberg (28) that the majority of carbonaceous particles in the top 30 cm of Lake Michigan sediment are coal-based particles. Karls and Christensen (27) also reported an abundance of coal- and wood-derived particles in sediments from Lake Michigan and neighboring areas.



Figure 2. Milwaukee CDF sediment particles: 63-250 μm size fraction.

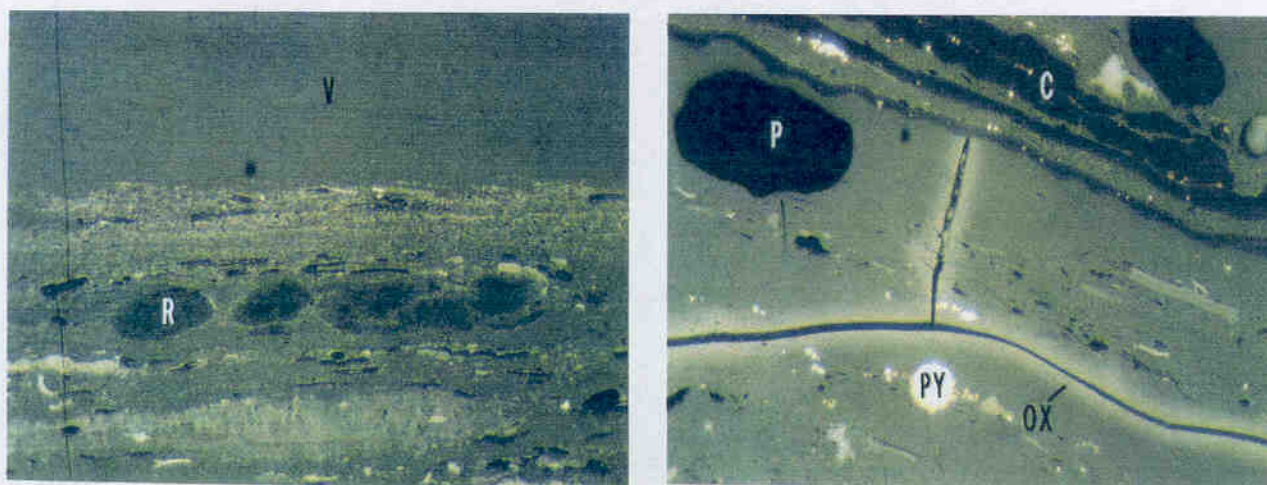
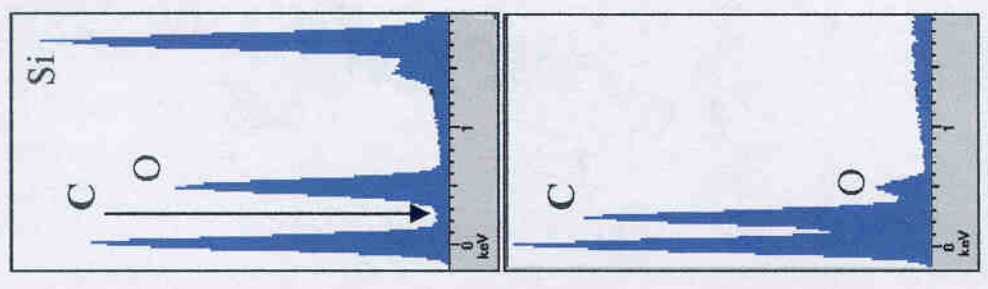


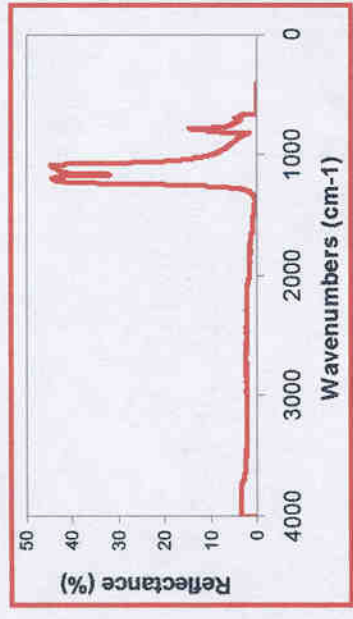
Figure 3. Coal petrography analysis of black particles in Milwaukee CDF sediment. (V: vitrinite, R: resinite, C: cutinite, P: pore, PY: pyrite, OX: oxidized layer) (525x magnification)

Although several studies have investigated the nature of sediment particles and proposed coal processing and wood burning as possible sources of PAHs in sediments, none have directly investigated the abundance of PAHs among the different sediment components.

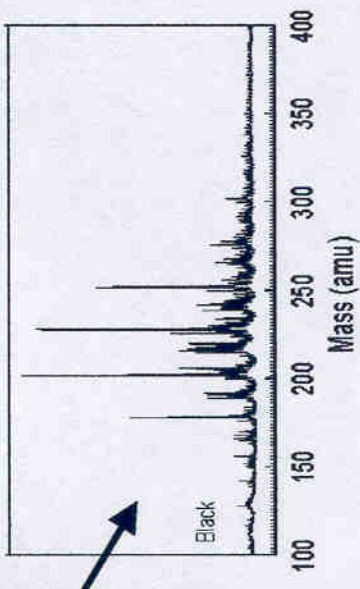
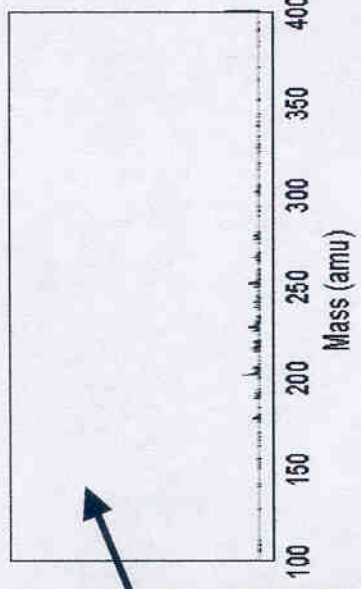
PAH association with different sediment components. $\mu\text{L}^2\text{MS}$ analysis of Milwaukee CDF sediments revealed a high inter-particle heterogeneity in the mass of sorbed PAHs. In a previous study, we have shown that the sediment has distinct particle types for which the surface of black particles contained much more PAHs than the surface of the silica particles (19). In this study we have characterized the black particles as coal-derived and performed parallel analyses of the location and relative abundance of PAHs, organic carbon, and elemental composition on more than one hundred particles ranging in size from 20-3000 μm . Figure 4 presents an example of coincident analysis of two sediment particles in the 63-250 μm size range. The black carbonaceous particles are found to have much greater abundance of PAHs. These black particles are also high in organic carbon, which is indicated by the high IR-absorbance signal for the C-H stretching mode at 2800-3000 cm^{-1} . SEM-WDX spot analysis also indicates a high concentration of elemental carbon. In comparison, the silica particles contain few PAHs and show no IR-absorbance at 2800-3000 cm^{-1} , but are high in silicon and oxygen as measured by SEM-WDX. When comparing a coal particle to a silica particle that has little or no attached organic matter, the coal particles were found to contain two to three orders of magnitude more PAHs on the surface. Wood-derived particles also were found to contain PAHs, but the abundance was one order of magnitude less, on average, than the coal-derived particles. The results of all these tests indicate that contaminating PAHs reside



Elemental Comp.



IR Reflectance



PAH Mass Signal



Figure 4. Coincident microscale analysis of PAH abundance, organic carbon, and elemental composition of Milwaukee CDF sediment particles showing high PAH abundance on organic-carbon rich particles compared to silica particles.

preferentially on the coal/wood particles. We confirmed this conclusion by particle separation and PAH analysis, which is discussed later.

Patchy location of PAHs on silica particles. Individual sediment silica particles were found to contain heterogeneous surface distributions of clayey deposits as identified by SEM/WDX. These patchy surface deposits were high in organic carbon content as measured by IR microspectroscopy. These organic carbon locations were also relatively high in PAH concentrations based on $\mu\text{L}^2\text{MS}$ analysis. Figure 5 displays an electron microscope image of a silica particle with a small depression on the mineral surface. IR microspectroscopy analysis of the particle revealed that this region contains organic material, as identified by the C-H stretching mode at $2800\text{-}3000\text{ cm}^{-1}$. The intensity of the C-H absorbance peak was mapped across the surface of the particle in the $200\text{ }\mu\text{m} \times 200\text{ }\mu\text{m}$ square region shown in Figure 5 and is illustrated as a grayscale image on the right. The white regions indicate high organic carbon content. IR microspectroscopy of the carbon patches on silica show an aliphatic C-H abundance ($2800\text{-}3000\text{ cm}^{-1}$), whereas IR spectra of the coal-derived particles also indicate a significant aromatic C-H component ($3000\text{-}3100\text{ cm}^{-1}$). This result suggests that the carbon patches on silica are comprised of a different carbon environment than coal-derived particles.

Figure 6 presents the subsequent $\mu\text{L}^2\text{MS}$ spot analyses of both the organic-rich region and the surrounding silica matrix. Inspection of this figure indicates that the PAHs on the silica particle lie mainly within the organic matter. Four spots on this particular particle were chosen for PAH analysis. Spots 1 and 2 were in the organic-rich region and spots 3 and 4 were on the bare silica region. Spots 1 and 2 each contain over 100 times more

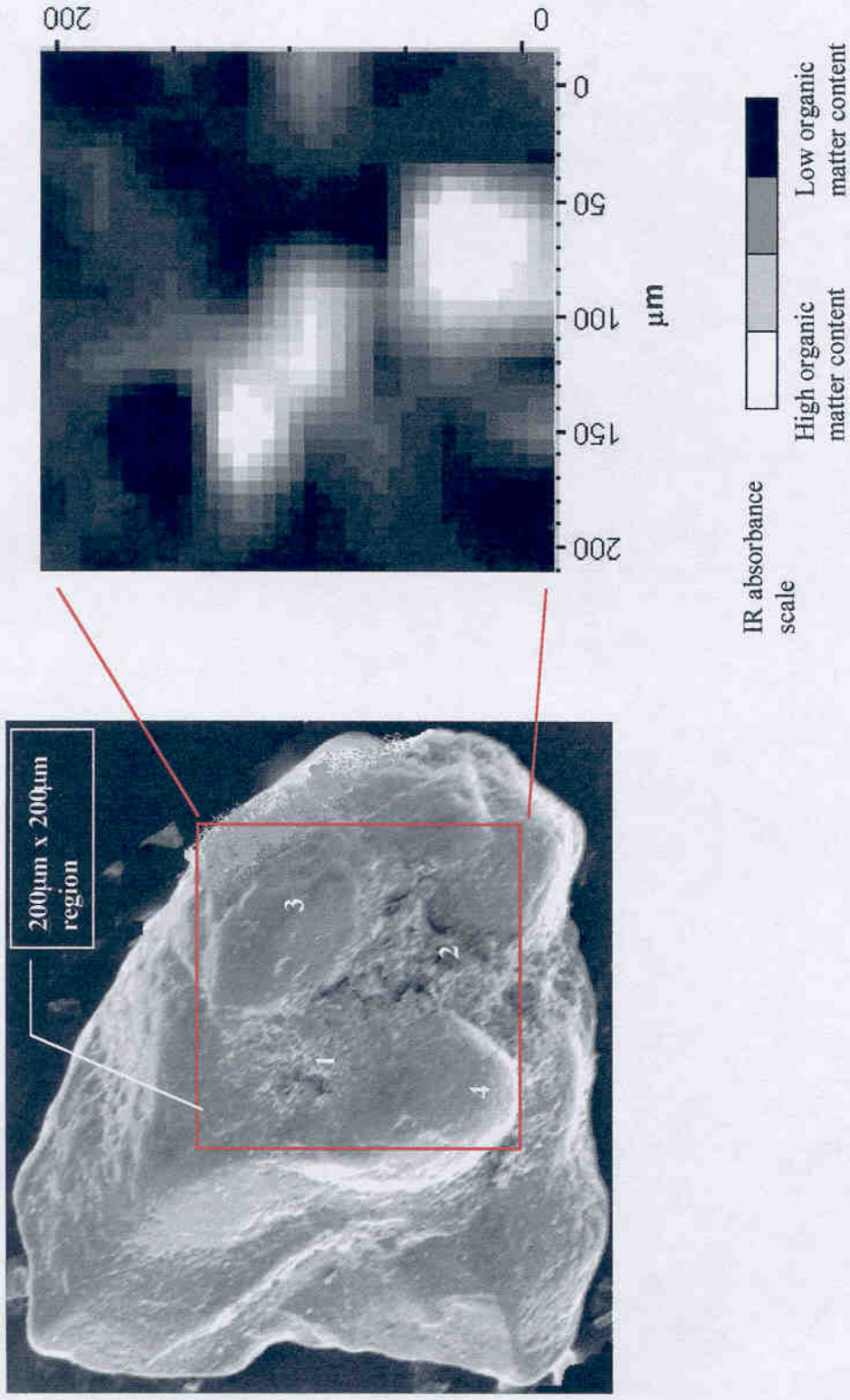


Figure 5. SEM image of a silica particle having patches of organic matter as indicated by the white regions in the IR mapping of C-H stretching absorbance shown in the right panel. Regions 1 and 2 also showed higher abundance of aluminum and magnesium compared to spots 3 and 4 as determined by SEM-WDX.

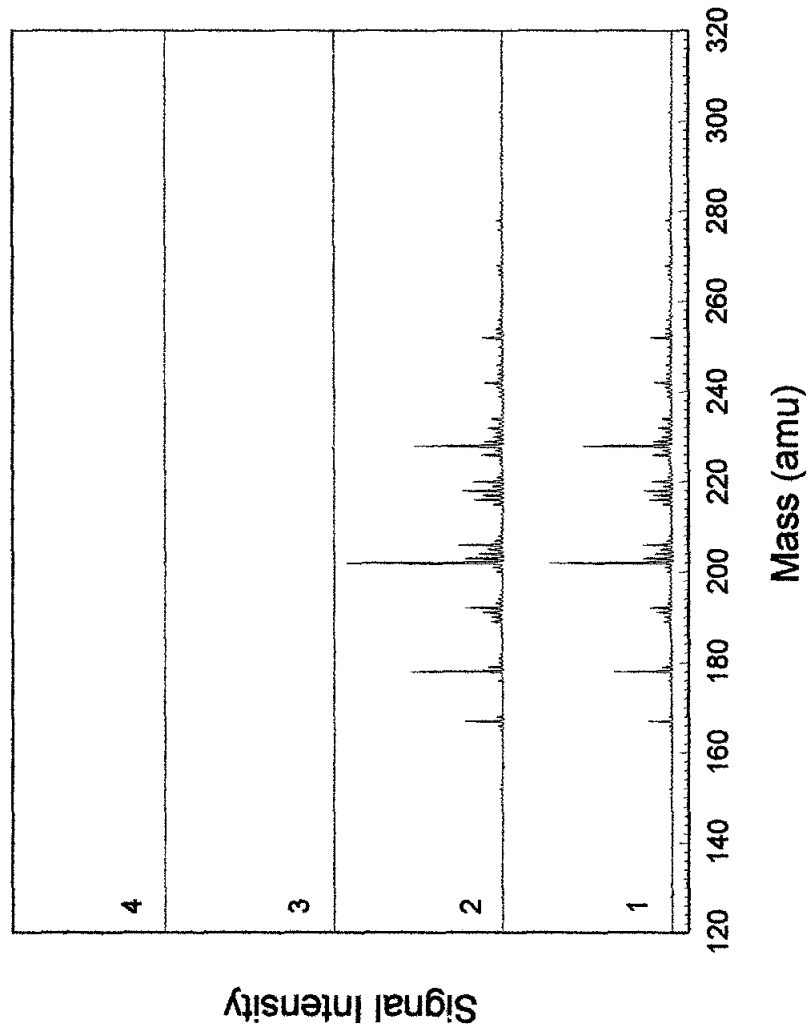


Figure 6. Spectra 1 and 2, resulting from $\mu\text{L}^2\text{MS}$ analysis of PAH concentration within organic matter patches on the silica particle (spots 1 and 2 in Figure 5), show a high PAH abundance. In contrast, spectra 3 and 4, resulting from analysis of PAH concentration on bare silica region (spots 3 and 4 in Figure 5), show no detectable PAHs.

PAHs than spots 3 and 4. It is apparent that PAHs on silica particles are associated with organic carbon deposits on the particles and not bare silica regions. Additional $\mu\text{L}^2\text{MS}$ analyses of various silica particles confirmed this characteristic pattern of PAH sorption wherein organic matter and PAHs exhibit patchy, co-located distributions.

It has been suggested previously that HOCs are partitioned into organic carbon on soils and sediments as a process of aging (29, 30). However, organic carbon can be present in soils and sediments in various forms such as humic matter particles, humic matter sorbed on mineral surfaces, detrital debris, vegetative debris, and products of coal and wood use and combustion. Little is known about the relative importance of these different forms of organic carbon in the sequestration of PAHs in sediments. Data in Figures 4 and 6 present direct evidence of the relative abundance of PAHs associated with these different forms of sediment organic carbon.

PAH distribution on particle interior regions. To date, no evidence exists in the literature on direct observation of PAHs, or any other sorbed organic contaminants, on the interior of natural particles. Hence, cross-sectional analysis of the Milwaukee sediment particles was performed to understand better what role diffusion or incorporation of PAHs into the interior regions of particles might play in sequestering PAHs.

A dozen samples each of the coal-derived and silica sediment particles, approximately 300 to 600 μm in diameter, were sectioned by cryomicrotomy and analyzed. Figure 7 shows a light microscope image of a typical coal-derived Milwaukee sediment particle after sectioning. SEM/WDX analysis revealed that the sectioned surface was abundant in

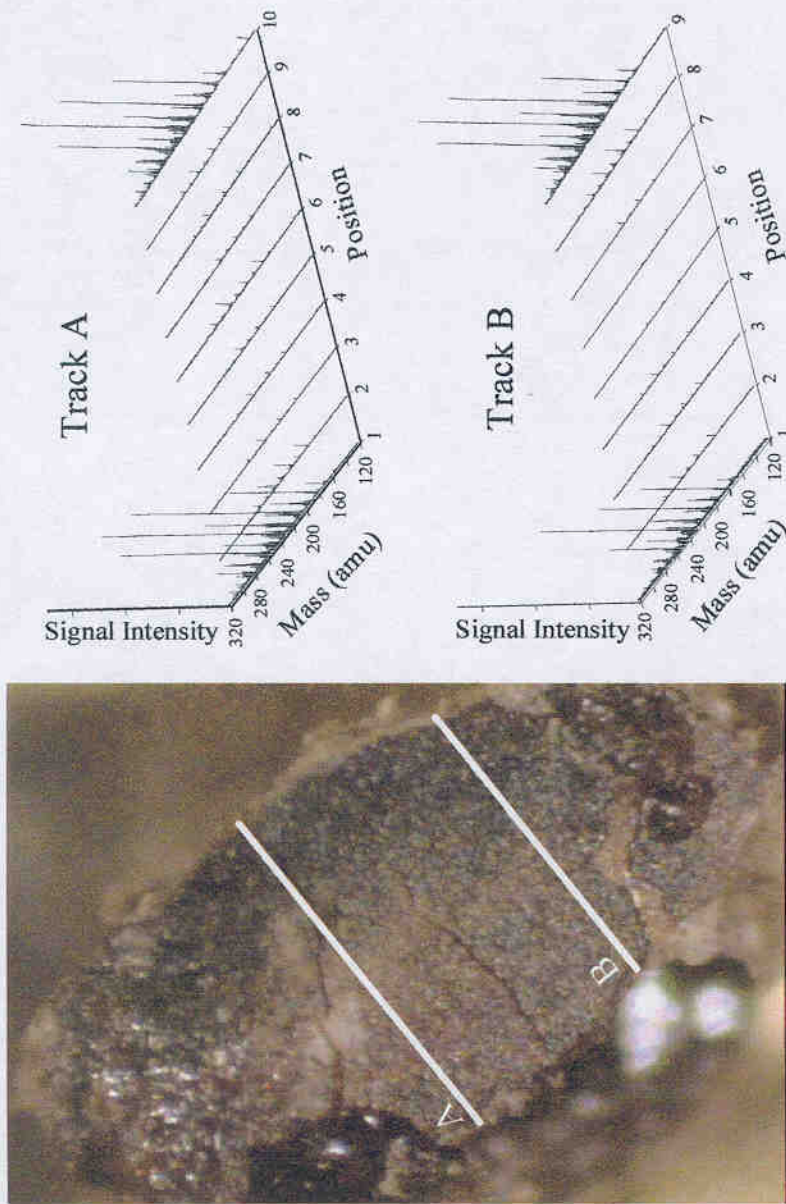


Figure 7. The left panel shows a sectioned surface of a coal-derived particle illustrating two linear tracks on which measurements of PAH concentrations by $\mu\text{L}^2\text{MS}$ were performed. PAH concentration profiles measured by $\mu\text{L}^2\text{MS}$ along tracks A and B, shown in the two plots on the right, indicate an abundance of PAHs on the near-surface regions compared to the interior regions.

elemental carbon throughout the interior. Mapping of organic carbon using IR microspectroscopy also revealed strong C-H stretching bands throughout the particle interior, indicating a more or less homogeneous substrate composed of organic matter. $\mu\text{L}^2\text{MS}$ spot analysis was performed on exterior portions of the particle surface and compared to the results from interior regions. The plots in Figure 7 result from analysis of PAH concentration at different locations across the particle transects at approximately 50- μm intervals. It is seen that the exterior surface locations (positions 1 and 10 in Track A and 1 and 9 in Track B) contain over 30 times more PAHs than adjacent interior locations (positions 2 and 9 in Track A and 2 and 8 in Track B). For PAH analysis of the adjacent interior locations, the periphery of the desorption spot was only 3 to 5 μm from the particle section edge. By translating the desorption spot an additional 45 μm toward the interior of the particle, it was observed that the total PAH concentration diminished by two orders of magnitude compared to the exterior regions. Analysis of various coal-derived Milwaukee sediment particles showed a consistent pattern of dramatic decrease in PAH concentration toward the interior. Milwaukee sediment silica particles also were sectioned and analyzed for PAHs and organic carbon. As described earlier, the surface of silica particles contain relatively few PAHs, all of which are associated with attached organic matter. Several silica particles were sectioned and no detectable PAHs were seen in interior regions.

These direct observations suggest that a particle-scale pore diffusion conceptual model is not appropriate to describe the association of PAHs with these sediment particles, whether coal-derived or silica. It is evident that a dominant sequestration mechanism for these particular sediment particles entails near-surface sorption processes, perhaps with

shallow penetration ($<5 \mu\text{m}$), as compared to incorporation throughout a porous substrate or within organic matter interior regions. Although this work is the first report of the direct observation of organic contaminant concentrations within sediment particles, some indirect evidence exists supporting shallow penetration depths of contaminants. Previous work by Pignatello *et al.* (18) and Brusseau *et al.* (12) on desorption rates of field-aged pesticides from soil showed little particle-size dependence down to the clay-size fraction, which suggested that diffusion lengths were on the order of $1 \mu\text{m}$ or less. Similarly, Carroll *et al.* (13) reported no particle size effects on PCB desorption from river sediments and suggested diffusion length scales on the order of 30 nm , which was estimated from theoretical calculations of diffusion coefficients of PCBs in humic polymers.

The complementary microscale analytical methodologies presented in this work provide direct evidence of PAH sorption on sediments at the sub-particle scale and may thereby help resolve some of the contentious issues in understanding sequestration processes. This study provides direct physical evidence of preferential PAH binding to coal-derived particle surfaces, which may reduce availability and toxicity and thereby reduce contaminant risk. These results may be useful in explaining differences in availability and toxicity of PAHs in sediment particles. These issues are explored in the following measurements of PAH distribution and desorption by particle size and type.

Separation of PAH-bearing coal and wood-derived particles in sediment. PAH-bearing coal and wood particles were separated from sand and clay to perform PAH extraction and analysis by particle size and type and for the purpose of measuring PAH

availability from these components. Previous work in isolating the carbonaceous particles in sediments has involved acid digestion of mineral matter followed by chemical or thermal oxidation of organic matter (27,31). In this work we desired to separate bulk quantities of coal/wood-derived particles without sacrificing the particle integrity or affecting the PAHs associated with such particles. Therefore, the difference in density of the coal/wood-derived particles and sand and clays was utilized to perform the separation.

Wet sieving was performed to separate the sediment into four size fractions ($>1000\ \mu\text{m}$, $1000\text{--}250\ \mu\text{m}$, $250\text{--}63\ \mu\text{m}$, and $<63\ \mu\text{m}$). The larger size fractions ($>63\ \mu\text{m}$) were composed primarily of sandy grains, coal-derived particles, and woody material as shown in Figure 2. It was possible to wash off the lighter fractions (coal and wood) from the heavier sand by swirling with water in a beaker and draining off the entrained lighter particles. This process was repeated several times until most of the lighter material was removed. Materials in the fine fraction ($<63\ \mu\text{m}$) were density separated using a cesium chloride solution having a specific gravity of 1.8. Five grams of wet sediment and 40 ml of cesium chloride solution were centrifuged at 2000 rpm for 10 minutes in 50 ml glass centrifuge tubes. The fine coal and wood particles floated to the top and were decanted off and collected in filter paper and washed with water several times. The heavy clay and silt were similarly washed several times to remove cesium chloride. Each of these size and density separated fractions were then analyzed for PAHs.

Figure 8a presents the sediment mass in each fraction. The heavy, $<63\mu\text{m}$ size fraction is comprised of clays and silt and is the most abundant component in the sediment at about 60% by weight. The sum of all heavy fractions in the sediment, which includes clays,

Figure 8

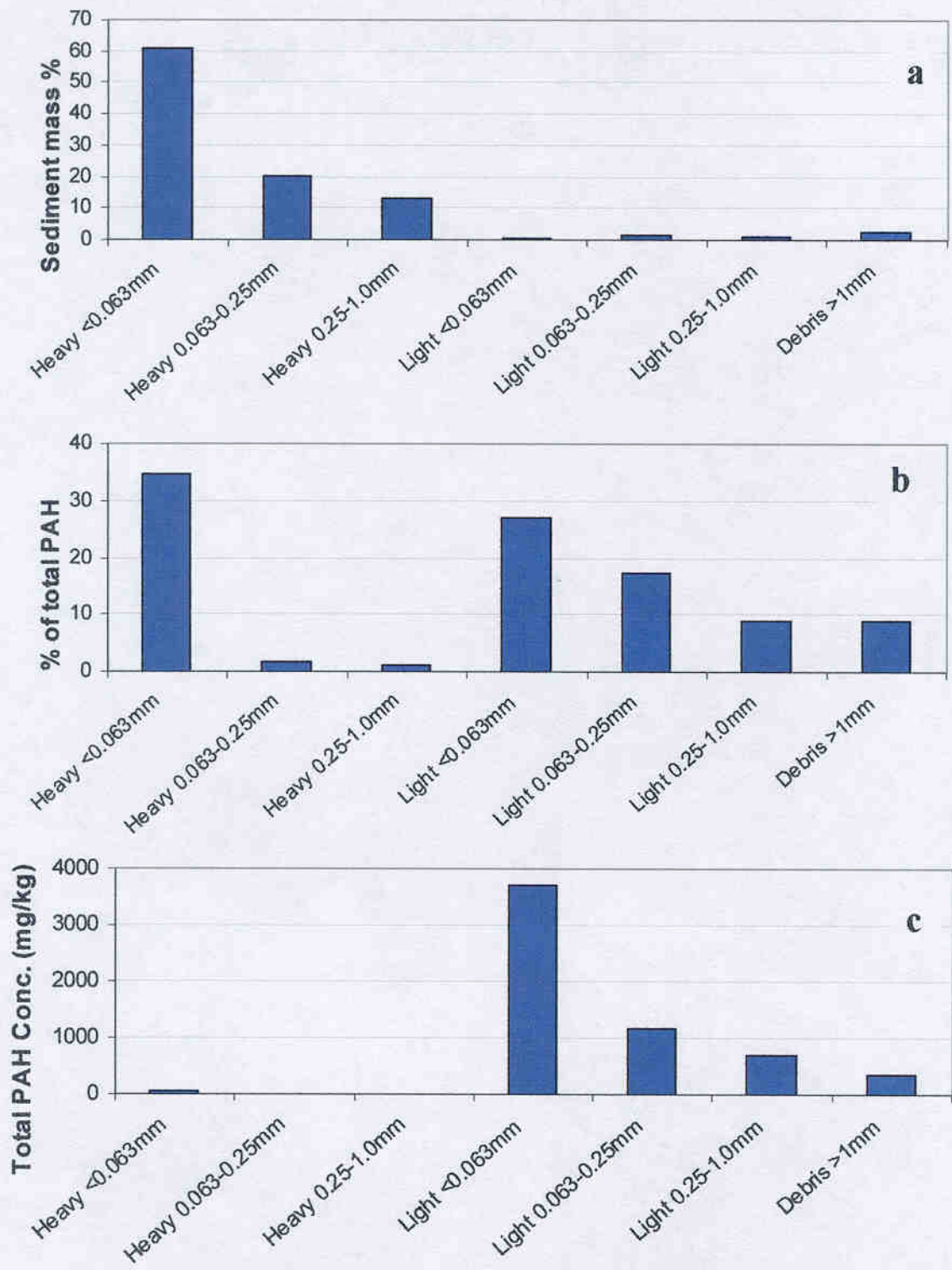


Figure 8. (a) Mass distribution of sediment by size and density fractions. (b) Total PAH distribution in sediment by size and density fractions (c) PAH concentration in sediment fractions by size and density

silt, and sand, constitutes about 95% of the sediment. The light fractions and debris constitute the remaining 5% of the sediment weight, but as shown in Figure 8b, 62% of the PAHs are associated with the lighter coal/wood-derived material and debris. Only 38% of the total PAHs are associated with the heavy sediment fraction (sand, silt, and clays), with clays & silt (<63 μm) contributing nearly all the PAHs for the heavy sediment fractions. Thus, 5% of the sediment, the coal/wood-derived material and debris, contains more than three-fifths of the total PAHs. Figure 8c shows the PAH concentration by dry mass within each fraction. The light fractions have two orders of magnitude higher PAH concentration than the heavier fractions. These bulk PAH measurements support our earlier microscale observation of 2-3 orders of magnitude higher PAH concentration on coal-derived particles compared to silica. Also, the PAH concentration in the light fraction increases with decreasing size range as shown in Figure 8c. PAH concentration in the light fractions was plotted against the inverse of the average radius of the size class to assess the effect of surface area to volume ratio on bulk concentration. An approximate linear relationship between PAH concentration and $(1/r)$ indicated a sorption mechanism possibly related to surface area. These observations support the $\mu\text{L}^2\text{MS}$ measurements of figures 4 and 7 showing a preponderance of PAHs on the outer surfaces of coal-derived particles.

There are several significant implications of the finding that majority of the PAHs are associated with coal derived particles. Gustafsson *et al.* (31) reported for Boston Harbor sediments that PAH sorption coefficients for carbonaceous residues from pyrogenic sources like soot may be two to three orders of magnitude greater than that for biogenic organic matter. Similarly, Grathwohl (32) has shown that partition coefficients for HOCs

on bituminous coals are approximately two orders of magnitude higher than that for HOCs on organic matter such as humic acids. Thus, an important implication of preferential sorption of PAHs onto coal and coal-derived materials is possible stronger affinity for PAHs and thus much less availability than for PAHs on organic matter associated with sand, silt, and clays.

Previous studies have shown the existence of an available and a relatively unavailable fraction of PAHs in aged sediments (7,23,24). Our findings indicate that 62% of the total PAHs are associated with coal and wood, and this fraction may be strongly sorbed and constitute a large proportion of the unavailable PAHs. The PAHs associated with clays or organic matter on clays, silt, and sand may be less strongly sorbed and constitute a large proportion of the readily available PAH fraction.

Desorption kinetics studies with density separated sediment fractions. Desorption experiments were conducted with the various fractions to evaluate whether PAHs desorb from the different components of the sediment at different rates. Unseparated Milwaukee sediment was subjected to desorption experiments with successive Tenax additions as the PAH extractant to study the overall desorption behavior of the PAHs in the sediment. Similar desorption experiments were performed with the lighter coal and wood fraction (63-250 μm) and the clay fraction ($< 63\mu\text{m}$) from which the lighter particles had been removed by density separation.

Figure 9 illustrates the results of these desorption experiments. The desorption study with the unseparated sediment was conducted in steps for a period of more than 100 days. This test shows that approximately 40% of the PAHs were released quickly and

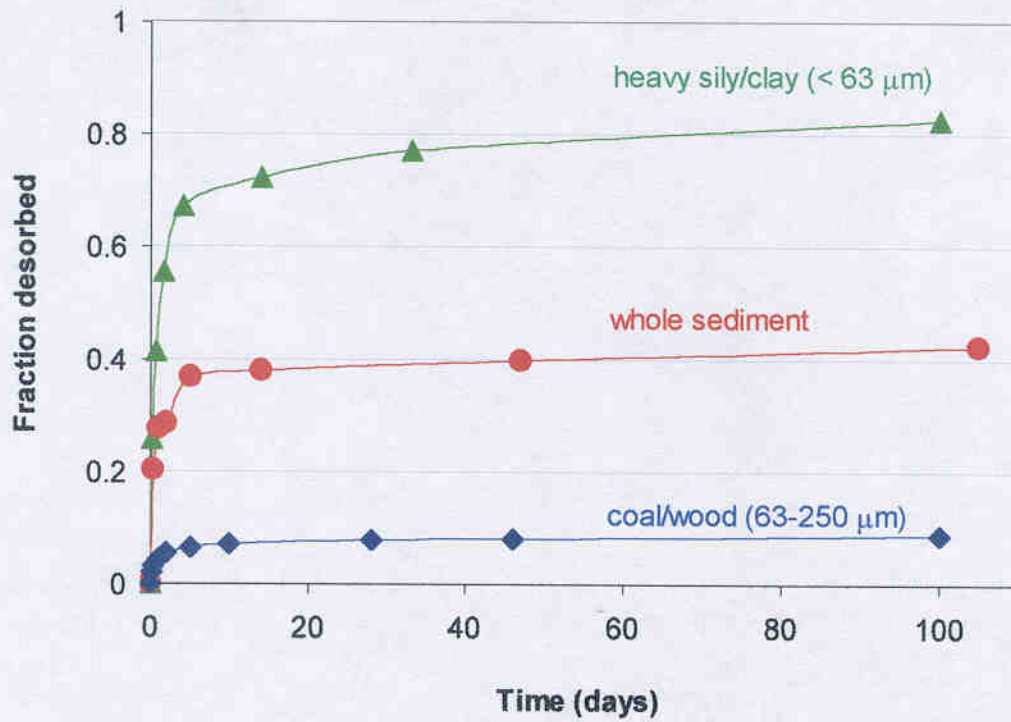


Figure 9. Total PAH desorption response from whole Milwaukee CDF sediment and from light (coal and wood) and heavy clay/silt fractions.

approximately 60% were strongly bound. Thus, approximately 40% of the PAHs in the whole sediment may constitute the available fraction. The PAHs associated with the light coal and wood fractions appear to be bound very strongly, as only about 8% of the PAHs in this fraction were released in one month. The majority of the PAHs associated with this coal and wood fraction may not be bioavailable for degradation nor exhibit a highly toxic response. In contrast, desorption data from the heavier clay/silt fraction indicate a higher availability with nearly 80% of the initial PAHs in this fraction readily desorbing in one month.

The unavailable fraction of PAHs in sediments has for a long time hindered remediation efforts. Our findings from microscale analyses of PAH locations and characterization of particle types followed by physical separation of the PAH-laden particles have provided a better understanding of sediment-contaminant behavior that may lead to low PAH availability. For Milwaukee Harbor dredged sediment, an important finding is that unavailable, strongly sorbed PAHs may largely be associated with the coal and wood fraction, while the available, less strongly sorbed PAHs may largely be associated with the clay/silt fraction. The finding that the majority of unavailable PAHs are associated with a small fraction of the sediment mass that appears to be easily separated should have significant implications for sediment management and remediation. The unavailable PAH fraction in these sediments may pose less risk and therefore be present only as a contaminant and not a pollutant.

The EPA has recently announced that there are too many site-specific variations in sediment composition that affect the bioavailability of contaminants in sediments to justify a national set of standards. Instead of numerical standards being used as legal

requirements, sediment quality guidelines are being proposed by the EPA and the US Army Corps of Engineers that will be used as guidance in conjunction with site-specific biological tests (33,34). Therefore, complementary microscale measurement techniques presented in this work and others under development can provide better understanding of physico-chemical mechanisms controlling site-specific bioavailability of contaminants and provide a stronger scientific basis for determining sediment quality guidelines.

Acknowledgements. We acknowledge funding for this research from the Department of Defense through the Strategic Environmental Research and Development Program and the US Army Waterways Experiment Station. We especially thank Mr. Jeffrey W. Talley and the Environmental Laboratory of the Waterways Experiment Station for providing sediment samples and the technical collaboration, which made this research possible. Additionally, we acknowledge the Brookhaven National Laboratory, National Synchrotron Light Source and Lawrence Berkeley National Laboratory, Advanced Light Source for providing access to FTIR microspectroscopy facilities. We specially thank Dr. Larry Carr from NSLS for his guidance in the FTIR analysis. We also thank Mr. Joseph Suhan from Carnegie Mellon University for his help with developing methods for particle sectioning.

REFERENCES

1. NRC, *Contaminated Sediments in Ports and Waterways, Cleanup Strategies and Technologies*. National Research Council, Washington DC, 1997.
2. NRC, *Innovations in Groundwater and Soil Cleanup*. National Research Council, Washington DC, 1997.
3. NRC, *Alternatives for Groundwater Cleanup*. National Research Council, Washington DC, 1994.
4. Wilson, S. C.; K. C. Jones, *Environ. Pollut.* **81**, 229-249 (1993).
5. Luthy, R.G.; Aiken, G.R.; Brusseau, M.L.; Cunningham, S.D.; Gschwend, P.M.; Pignatello, J.J.; Reinhard, M.; Traina, S.J.; Weber, W.J., Jr.; Westall, J.C. *Environ. Sci. Technol.*, **31**, 1997, 3341-3347.
6. Tang, J.; M. J. Carroquino, B. K. Robertson, M. Alexander, *Environ. Sci. Technol.* **32**, 3586-3590 (1998).
7. Linz, D. G.; D. V. Nakles, *Environmentally Acceptable Endpoints in Soil* (American Academy of Environmental Engineers, Anapolis, MD, 1997).
8. Pignatello, J. J.; *Environ. Sci. Technol.* **30**, 1-11 (1996).
9. Hatzinger, P. B.; M. Alexander, *Environ. Sci. Technol.* **29**, 537-545 (1995).
10. Steinberg, S. M.; J. J. Pignatello, B. L. Sawhney, *Environ. Sci. Technol.* **21**, 1201-1208 (1987).
11. Weber, W.J.Jr.; W. Huang, *Environ. Sci. Technol.* **30**, 881-888 (1996).
12. Brusseau, M.L.; Jessup, R.E.; Rao, P.S.C. *Environ. Sci. Technol.* **25**, 134-142 (1991a).
13. Carroll, K. M.; M. R. Harkness, A. A. Bracco, R. R. Balcarcel, *Environ. Sci. Technol.* **28**, 253-258 (1994).
14. Ball, W.P.; Roberts, P.V. *Environ. Sci. Technol.* **25**, 1237-1249 (1991).
15. Pedit, J.A.; C.T. Miller. *Environ. Sci. Technol.* **29**, 1766-1772 (1995).
16. Wu, S.; Gschwend, P.M. *Water Resources Research.* **24**, 1373-1383. 1988.
17. Gong, Y.; Depinto, J.V. *Water Research*, **32**, 2518-2532. (1998).

18. Pignatello, J.J.; Ferrandino, F.J.; Huang, L.Q. *Environ. Sci. Technol.* **27**, 1263-1571 (1993).
19. Gillette, J. S.; R. G. Luthy, S. J. Clemett, R. N. Zare, *Environ. Sci. Tech.* **33**, 1185-1192 (1999).
20. Bowman, D. W.; J. M. Brannon, S. A. Batterman, *Proceedings of the 11th US Army Corps of Engineers Waterways Experiment Station Seminar* (1996).
21. Carr, G.L.; J.A. Reffner, and G.P. Williams. Performance of an Infrared Microspectrometer at the NSLS. American Institute of Physics. 1995. 66, 1490-1492.
22. Carr, G.L.; G.P. Williams. Infrared Microspectroscopy with Synchrotron radiation. SPIE Conf. Proc. 3153. Accelerator Based Source of IR and Applications. 1997.
23. Pignatello, J.J. *Environ. Toxicol. Chem.* **1990**, 9, 1107-1126.
24. Cornelissen, G.; Van Noort, P.C.M.; Govers, A.J. *Environ. Toxicol. Chem.* **1997**, 16, 1351-1357.
25. Budzinski, H.; Jones, I.; Bellocq, J.; Piérard, C.; Garrigues, P. *Marine Chemistry*. 58, 85-97 (1997).
26. Christensen, E.R.; X. Zhang. *Environ. Sci. Technol.* **27**, 139-146 (1993).
27. Karls, J. F.; E. R. Christensen, *Environ. Sci. Technol.* **32**, 225-231 (1998).
28. Griffen, J. J.; E. D. Goldberg, *Science* **206**, 563-565 (1979).
29. Chiou, C. T. In *Reactions and Movement of Organic Chemicals in Soils* B. L. Sawhney, K. Brown, Eds. (Soil Science Society of America, Madison, WI, (1989) pp. 1-29.
30. Karickhoff, S.W. (1980) In *Contaminants and Sediments*; Baker, R.A., Ed.; Ann Arbor Science Pub. Inc. Ann Arbor, MI, 193-205.
31. Gustafsson, O.; F. Haghseta, C. Chan, J. MacFarlane, P. M. Gschwend, *Environ. Sci. Technol.* **31**, 203-209 (1997).
32. Gratwohl, P. *Environ. Sci. Technol.* **24**, 1687-1693 (1990).
33. EPA watch: Corps, EPA agree on sediment quality criteria. *Environ. Sci. Technol.* **33**, 192A-193A (1999).
34. Renner, R. *Environ. Sci. Technol.* **32**, 306A (1998).

Section 4

Thermal Program Desorption of PAHs From Mineral and Organic Surfaces*

Abstract

This research investigated the release of polycyclic aromatic hydrocarbons (PAHs) from solid surfaces using thermal desorption mass spectrometry. An experimental protocol was developed to obtain real-time PAH desorption data through use of a temperature programmed desorption probe that places the sample directly in the ion volume of a mass spectrometer then gradually heats the sample at a predetermined rate. Thermal desorption profiles of milligram-size samples were analyzed in order to explore the release of PAHs from mineral and organic surfaces and to compare the release of PAHs with increasing molecular weight. We show that the release of PAHs is dependent both on PAH molecular weight and the character of the sorbent material. Glass and sand exhibited much weaker binding than the other materials. The release of PAHs from glass and sand may be explained largely on the basis of the vapor pressure of the pure PAH compounds. Thermal desorption profiles for kaolin, alumina, XAD-4 resin beads, coal, and pulverized activated carbon demonstrated greater binding, resulting in lower vapor pressures and higher peak desorption temperatures. A nonlinear curve fitting technique based on activated first order desorption kinetics provided a good fit to the experimental data. It is demonstrated that thermal program desorption measurement in itself is insufficient to determine PAH binding activation energies owing to the data reduction techniques (peak temperature, Chan-Aris-Weinberg, leading edge, or nonlinear curve fitting methods) being dependent on two highly correlated parameters. We present the first real-time measurement of thermal program desorption spectra for release of PAHs and we suggest that such data may help infer availability and binding energy when used in combination with other measurement techniques.

Introduction

*Jeffrey W. Talley¹, Upal Ghosh², Samuel G. Tucker¹, John S. Furey¹, Richard G. Luthy²

¹Environmental Laboratory, U.S. Army Engineer Research and Development Center, Vicksburg, MS 39180

²Department of Civil and Environmental Engineering, Stanford University, Stanford, CA 94305-4020

Polycyclic aromatic hydrocarbons (PAHs) preferentially bind to various components of soil and sediment depending on organic matter content and type (1,2). The degree of PAH binding with geosorbents strongly influences PAH availability and environmental effects. For example, a major factor influencing successful sediment bioremediation is the availability of contaminants to microorganisms for degradation, whereas, contaminants that are strongly sorbed and not available to microorganisms may also not be available for a toxic response. Thus, an understanding of how binding to a solid substrate changes the availability of PAHs is important for evaluating the environmental fate and effects of these compounds. The processes affecting the availability of PAHs sequestered in soil and sediment are complex due to the large heterogeneity in soil/sediment particle types and sorbent organic matter typically present (3).

The availability of a compound sorbed on a solid surface can be described by the escaping tendency as quantified by fugacity. For a pure compound with equilibrated phases, the fugacity is the same as the vapor pressure. However, when a compound sorbs on a surface, the binding with the substrate results in a reduction of the vapor pressure. Thus, the vapor pressure of a compound sorbed to a solid material can provide an indication of the binding and relative availability of the compound. For many environmentally significant hydrophobic organic compounds (HOCs) like PAHs the vapor pressure at ambient temperatures are very low and difficult to measure directly. Because vapor pressure increases rapidly with temperature, many methods invoke higher temperatures for measuring vapor pressure or release of high molecular weight organic compounds from surfaces.

Various adaptations of thermal program desorption (TPD) techniques have been used in the past to study: desorption of gases from solid surfaces (4,5), desorption of toluene from kaolin pellets (6), pyrolysis of hydrocarbons from coal (7), estimation of PAH vapor pressures (8,9), and desorption activation energies of trichloroethylene from silica gel (10). Thermal desorption techniques have also been explored for their utility in detecting and quantifying organic contaminants in soil samples (11). Unlike other techniques for soil analysis, TPD requires no solvent extraction, little sample preparation, and is relatively quick. Samples are heated inside an oven or thermal desorption probe, and as the

temperature increases the volatilized compounds are collected and detected using a mass spectrometer. The use of a direct insertion probe, which does not require transfer lines, with a mass spectrometer (MS) allows measurement of the release of trace organics from very small samples. Direct probes have been used for the analysis of coal pyrolysis products by Yun and Meuzelaar (7). To date, thermal desorption mass spectrometry with direct probes has been used for study of pyrolysis and as a means for inserting a sample into a mass spectrometer for compound identification. The technique has not been used previously to study desorption of PAH homologs from mineral and organic surfaces.

In this work we use thermal program desorption mass spectrometry with a direct insertion probe to study the release characteristics of PAHs sorbed on different mineral and organic surfaces: glass, sand, kaolin, alumina, XAD-4 resin beads, coal, and pulverized activated carbon. Due to the high sensitivity of the instrument setup, measurements were possible at the milligram sample size. The TPD profiles of sixteen EPA priority pollutant PAHs spiked on these solids were studied.

Materials and Methods

Instrumentation. A schematic of the TPD-MS used in this work is shown in Figure 1. The probe used was a Thermoquest GCQ *Plus* Direct Insertion Probe with a glass sample vial as shown in Figure 2. This instrument configuration was selected so that a sample could be inserted directly into the ion volume of the MS. This allowed for better transfer of desorbed compounds as well as increased sensitivity. The sample is emplaced in an open sample vial and weighed. The sample vials are cylindrical with an inside diameter of 1.0 mm by 10 mm length. The probe holding the vial is inserted into the MS and heated linearly. The ion trap in the TPD-MS is a chamber consisting of an ion source, injection optics, mass analyzer, multiplier, and detector. The system is filled with helium damping gas and is regulated so that pressure in the system is approximately 10^{-7} atm. Excitation voltage is applied within the ion source and the excited ions produced by electron impact are then projected sequentially through a series of lenses to the mass analyzer. The cycle time for the entire process is in the range of milliseconds.

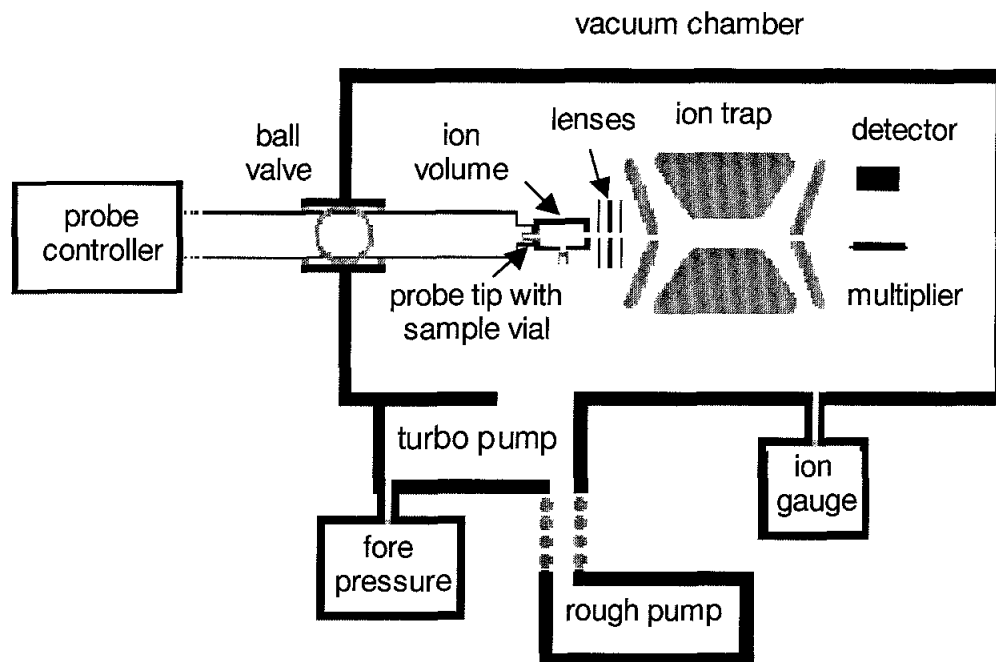


Figure 1. Schematic of the thermal program desorption mass spectrometer with a direct insertion probe.

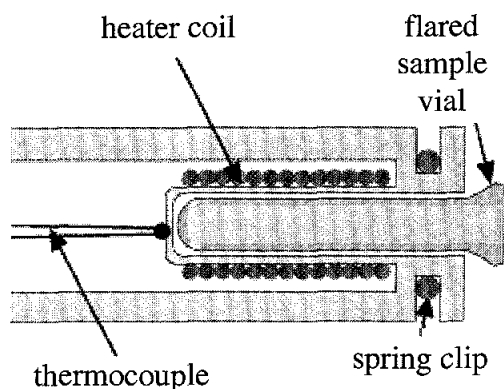


Figure 2. Schematic of the direct insertion probe tip with a sample vial placed inside.

Within each TPD run, the raw ion count is proportional to the molecular flux in the ion volume. Thus the ion count measured at any time is proportional to the rate of release of PAHs from the sample vial. PAHs typically produce molecular ions with little fragmentation, allowing multiple compounds to be analyzed simultaneously provided they have different molecular weights. The PAH mass homologs used in this work are shown in

Table 1. The sensitivity of the instrument with the direct insertion probe accommodates very small samples and in our work down to the single particle scale for granular material (0.1 mm diameter).

Table 1. PAH compounds in the spike standard mixture.

Mass homolog	Compound	Mass homolog	Compound
128	naphthalene	228	benzo(a)anthracene, chrysene
152	acenaphthylene	252	benzo(b)fluoranthene, benzo(k)fluoranthene,
154	acenaphthene		benzo(a)pyrene
166	fluorene	276	benzo(g,h,i)perylene, indeno(1,2,3-c,d)pyrene
178	phenanthrene, anthracene	278	dibenzo(a,h)anthracene
202	fluoranthene, pyrene		

Methods development. A primary task in this research was to provide an efficient and concise protocol for TPD-MS operation. The variables tested included sample vial configuration, sample volume, temperature ramp rates of 10°C, 20°C, or 30°C per minute, and final temperatures. A heating ramp rate of 10°C/min, final temperature of 400°C, and no hold time were selected. The temperature ramp rate of 10°C/min was chosen because of consistency and the ability to distinguish the different PAH homologs. A higher temperature ramp rate did not allow time for the PAH molecular weight 178 (phenanthrene and anthracene) to show a desorption curve on a consistent basis with some of the materials tested. A shift toward higher peak temperatures for desorption response with increased heating rate has been described by Yun and Meuzelaar (7). In that case the PAH could be released at a slightly elevated temperature because there maybe insufficient time for temperature equilibration. We observed that many organic samples exhibited pyrolysis starting at approximately 400°C, except for coal, which showed pyrolysis beginning at around 250°C. Thus, to make the desorption as complete as possible with uniformity, a maximum temperature of 400°C was chosen for all runs reported here. Stopping a run at a lower temperature would prevent the heavier molecular weight PAHs (276 and 278) from desorbing completely for some materials. Full scan mass spectrometry was performed to assess for any interferences.

The effect of the volume of solid material in the vial was investigated to assess the concomitant effects of packing on TPD response. All powdery samples exhibited a volume-dependent TPD response that was attributed to interparticle diffusion, such as illustrated in Figure 3. In these runs Ottawa sand was spiked with 40 ppm of MW 228 homolog (benzo(a)anthracene and chrysene) and 1.8 mg sand (3 grains) were placed in the vial. The sand grains were then covered with 0, 3, or 6 mm of kaolin. The results show that mass diffusion through the kaolin delayed the TPD-MS response. No similar effect was seen for any coarse mineral samples, which points to an interparticle diffusion delay for fine grained material packed in the sample vial.

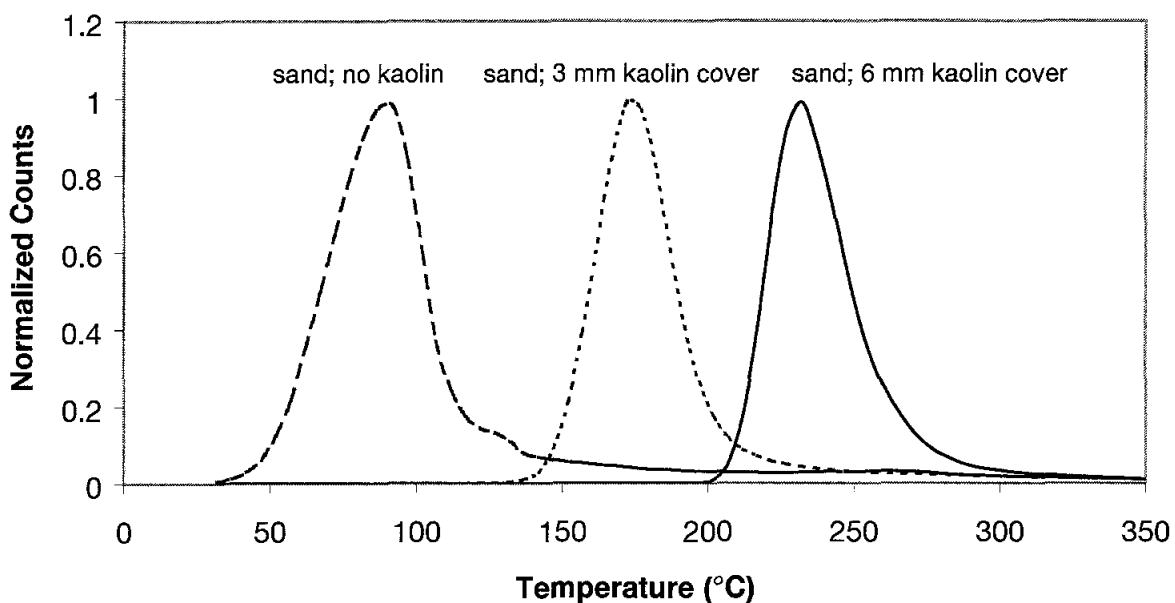


Figure 3. A thermal program desorption mass spectrometry response for PAH mass 228 homolog for PAH spiked sand covered by clean kaolin. The left curve is with no kaolin, the middle curve is with 3 mm of kaolin covering the sand, and the right curve is with 6 mm of kaolin covering the sand.

Tests were run with kaolin spiked with PAHs to assess the extent to which diffusion mass transport may restrict the release of PAHs from kaolin. In these tests the sample vial was filled with kaolin at various levels to assess the conditions for which the release of the PAH was independent of the amount of kaolin in the sample vial. It was demonstrated that

the smaller sample sizes of 1/8 and 1/16 filled sample vials were optimum, especially for powdery samples. For sample vials filled with powdery material at levels above 1/8 capacity, interparticle-diffusional influences appeared to retard the movement of PAHs out of the sample vial. Therefore, all TPD analysis presented here used a 1/8 filled sample vial.

Materials. Various mineral and organic surfaces were studied during method development and results for seven are reported in this work: kaolin, pulverized activated carbon, coal, glass beads, XAD-4 resin, alumina, and sand. The kaolin was bulk powder (Aldrich Chemical Co., Inc. cat. # 228834), the pulverized activated carbon was BL pulverized from Calgon Carbon Corporation, the coal was pulverized IBC 105 (Illinois Basin Coal Sample Program, 200 mesh <74 μm dia.), the sand was washed Ottawa sand, 20-30 mesh with typical dimension of about 400 μm (Fisher cat. # S23-3), the glass beads (Biospec Products, Inc. cat. # 11079-105) had a nominal diameter of 0.5 mm, XAD-4 was resin resin beads (Aldrich Chemical Co., Inc. cat. #37380-42-0), and alumina was 600 grit (Scientific Instrument Services, Inc. cat. #ALX6004). PAH standards were prepared from a PAH mixture (Sigma cat # 4-7930) of sixteen PAHs (listed in Table 1) in dichloromethane (Sigma cat # AH 300-4). The dichloromethane used was HPLC grade, methanol was GC grade, and the water was distilled deionized.

Spiking Procedure. An initial series of tests were conducted with individual PAH compounds spiked directly into the TPD sample vial followed by tests with the mixture of sixteen EPA priority pollutant PAHs spiked either into the TPD sample vial or onto various solids. The PAH molecular weights in the mixture are shown in Table 1 and PAH compounds within a homolog were not analyzed separately. Clean sample surfaces were prepared by washing first in water and then methanol, with thorough drying in ambient room air. Homogenization was achieved by manual stirring. The solid surfaces were spiked at several concentrations, with 20 ppm concentration each per PAH reported for most tests in this work, which for the sixteen compounds corresponded to 320 ppm total PAHs. One gram of solid sample was saturated with dichloromethane to produce a slurry. For the 20 ppm PAH mixture, 50 μL of a 1 to 5 dilution of the 2000 mg/L PAH standard in dichloromethane was spiked into the slurry, and stirred continuously for 15 minutes, followed by 5 minute

stirring every hour for 4 hours. Between the stirs, the material was allowed to dry in ambient air. Samples were stored in glass containers with foil-lined tops in a dark cooler at 4°C. Results reported in this work are average of triplicate runs measured the same day as spiking.

Results and Discussion

TPD response of PAHs from glass. In tests with individual PAHs, 1 μL 100 $\text{ng}/\mu\text{L}$ of a PAH in dichloromethane was added into the empty glass TPD sample vial and allowed to evaporate for fifteen minutes before the start of the run. A visible residue after evaporation indicated crystallization of PAH compounds within the vial. Results of TPD-MS analysis of a PAH-spiked sample vial is shown in Figure 4 for tests with six PAHs. These data show the release of phenanthrene and fluoranthene at 30°C at the start of the run owing to the low pressure in the instrument. The other four PAHs show release at peak temperatures of 102, 106, 130, and 143 °C, increasing with the molecular weight of the PAH compounds. To visually compare the TPD responses, the data were normalized by dividing by the total area under the peak of the TPD response curve (for Figures 4, 5, and 6).

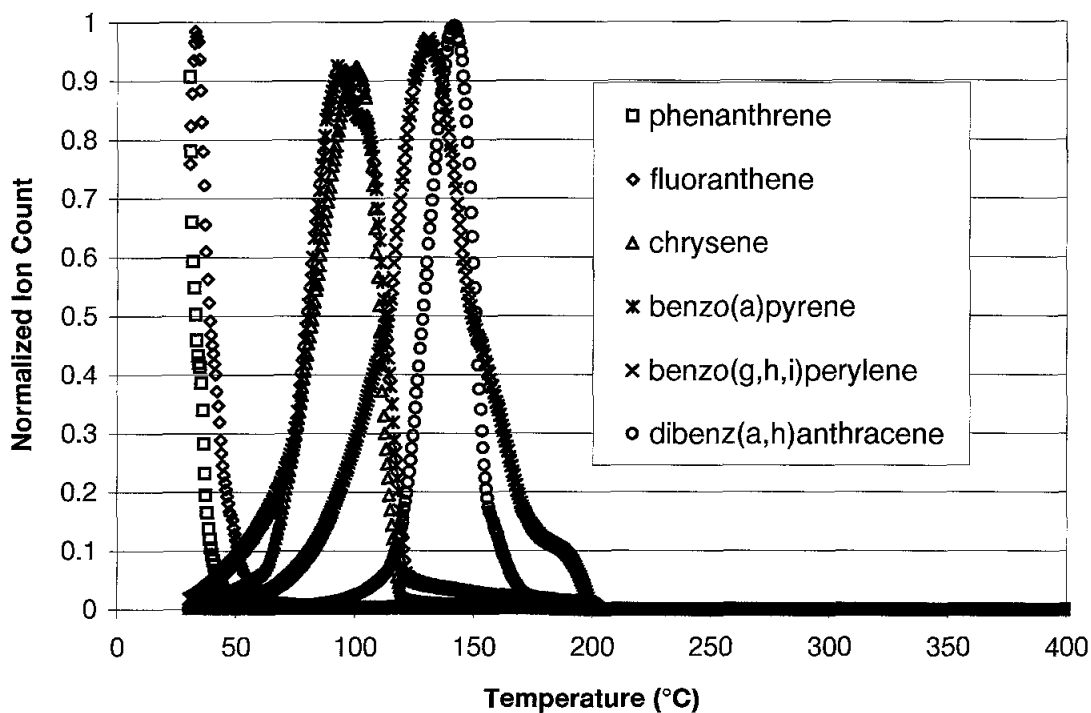


Figure 4. Thermal program desorption mass spectrometry profiles for individual PAHs spiked separately into an empty sample vial.

Data in Figure 5 show results for release of PAHs from the mixture of sixteen compounds spiked into an empty sample vial. One microliter of the mixture of sixteen PAHs each at 500 ng/ μ L was transferred into the empty glass TPD sample vial and allowed to evaporate for 15 minutes before the start of the run. Comparison of the results of the TPD-MS data in Figures 4 and 5 shows broader peaks for the mixtures but otherwise little difference in the appearance of the PAH peaks when added to the vial as individual PAHs or added as a mixture of sixteen PAHs. Thus the TPD response of a solid PAH is not affected significantly by the presence of other PAHs as a solid mixture.

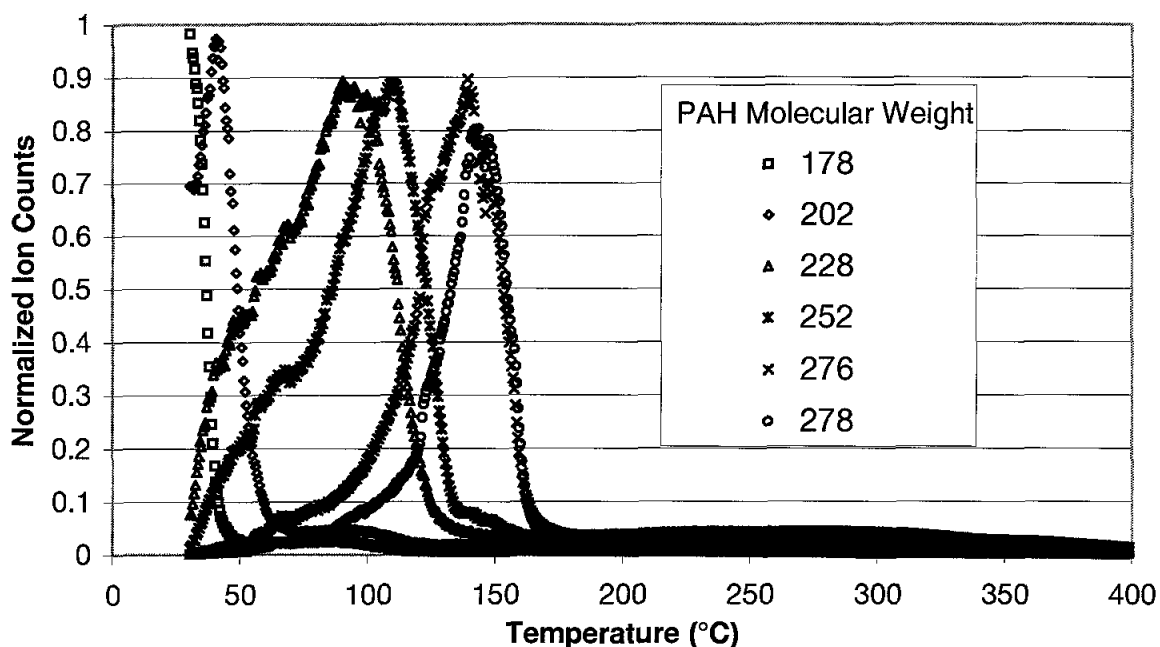


Figure 5. Thermal program desorption mass spectrometry profile for a mixture of sixteen PAHs spiked into an empty sample vial.

Results in Figure 6 show the release of PAHs from glass beads. As in the case of PAHs spiked directly in the glass sample vial, the release of PAHs from glass beads coated with PAHs shows a similar increase in peak temperature with increasing molecular weight. Molecular weights 276 for the sample vial, and 178 and 202 for glass beads show a split peak, which may be indicative of different desorption responses for the two PAH compounds comprising the mass homologs. The release of PAHs from the spiked sample vial and PAH-

coated glass beads are expected to be characteristic of volatilization of solid PAHs from a non-interacting surface, which may be described semi-quantitatively by the increase in vapor pressure with temperature of these compounds.

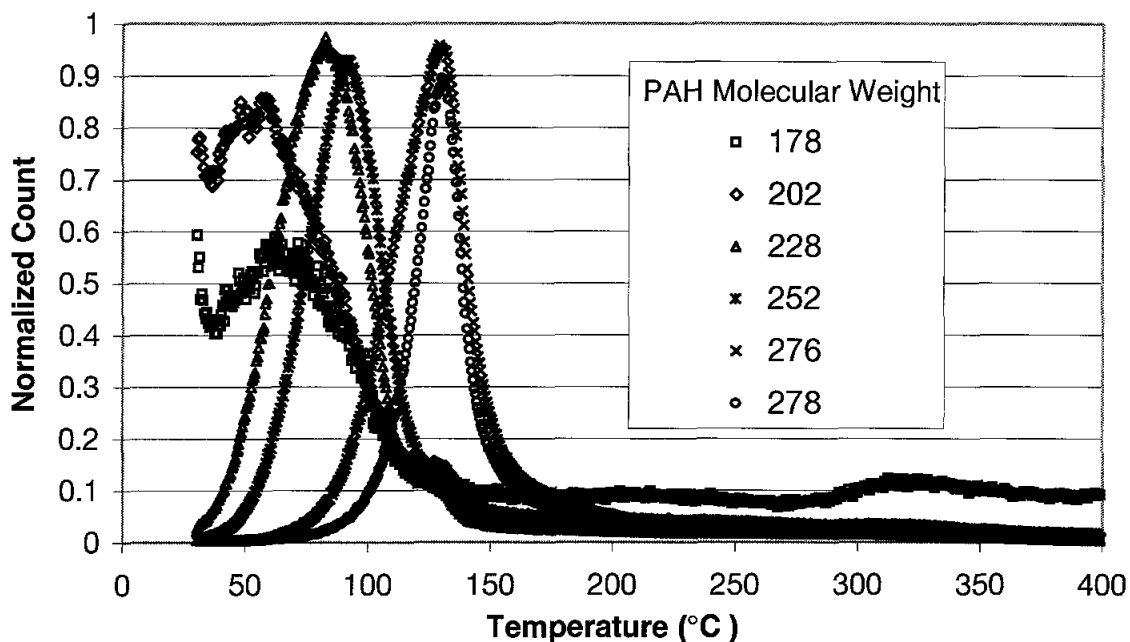


Figure 6. Thermal program desorption mass spectrometry profile for a mixture of sixteen PAHs spiked onto glass beads.

TPD peak response for solid PAHs from vapor pressure estimation. The tendency of a solid, unadsorbed chemical to transfer into a gaseous environmental phase is determined by its vapor pressure. For most organic compounds, whether liquid or solid, the vapor pressure increases rapidly with temperature. At the boiling point, the equilibrium vapor pressure equals the ambient pressure and the compound is rapidly converted to the gaseous form. In the ion volume of the MS, the ambient pressure was on the order of 10^{-7} atm. Thus, knowledge of how the vapor pressure of PAHs changes with temperature may provide an indication of the temperature at which the maximum rate of PAH release may be observed in a TPD experiment comprising solid PAHs.

The vapor pressure of an organic liquid can be estimated theoretically from Equation 1 which is derived from the Clausius-Claperyon equation (12, 13).

$$\ln P^{\circ} = 19 \left(1 - \frac{T_b}{T} \right) + 8.5 \left(\ln \frac{T_b}{T} \right) \quad (\text{atm}) \quad (1)$$

where P° is the vapor pressure of the compound [atm], T_b is the boiling point of the compound [K] at 1 atm, and T is the temperature [K] for which the vapor pressure is being estimated. Below the melting point of a compound, Equation 1 yields the vapor pressure of the subcooled liquid denoted as $P^{\circ}(L)$. An approximate relationship between the solid vapor pressure $P^{\circ}(s)$ and $P^{\circ}(L)$ is given by Prausnitz (14):

$$\ln \frac{P^{\circ}(s)}{P^{\circ}(L)} = - \frac{\Delta S_{\text{melt}}(T_m)}{R} \left(\frac{T_m}{T} - 1 \right) \quad (2)$$

where $\Delta S_{\text{melt}}(T_m)$ [J/mol-K] is the entropy of fusion at the melting point and R is the gas constant. Using Equations 1 and 2, the vapor pressure of an organic compound from its solid or liquid state can be estimated from entropy of fusion, melting point, and boiling point. The relevant thermodynamic data of eight representative PAHs were obtained from the NIST database (<http://webbook.nist.gov/chemistry/>) and Mackay et al. (15).

The predicted vapor pressures of the eight representative PAH compounds are plotted in Figure 7. Measured values of vapor pressures for naphthalene, fluorene, and phenanthrene obtained from CRC (16) are shown also in Figure 7 for confirmation of the model prediction for some of these compounds. It is seen that the predicted vapor pressures match closely with the experimentally measured values. The nominal pressure in the MS according to operating specifications was 10^{-7} atm. During the TPD experiments, the pressure indicated by the ion gauge was approximately 1.4×10^{-7} to 2.2×10^{-7} atm. Thus, during a TPD run with PAHs spiked in the sample vial, the vapor pressure of the PAHs would rise with increase in temperature, showing an increased flux of PAHs in the ion volume. The maximum flux was observed near the temperature for which the vapor pressure of the PAH matched the system pressure. As the mass of the PAHs is depleted in the sample vial due to volatilization losses, the PAH flux into the ion volume decreases as the temperature is increased further.

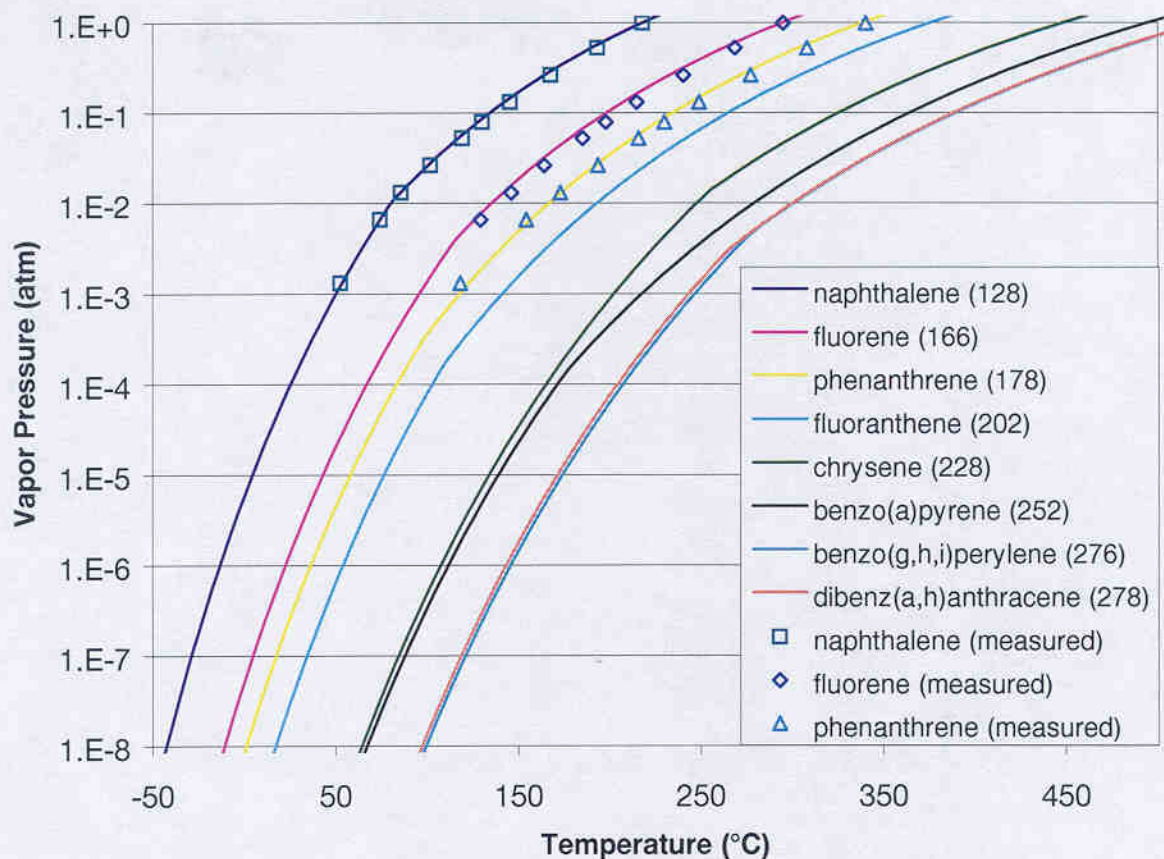


Figure 7. Change in vapor pressure with temperature for eight representative PAHs.

Data in Table 2 compares the observed peak temperature for individual PAHs and PAH homologs in a mixture spiked into sample vial and on glass beads with the estimated temperature at which the vapor pressure of the PAHs equals the pressure within the TPD instrument. The estimated peak temperatures for naphthalene, fluorene, and phenanthrene are lower than the starting temperature of the TPD experiment. Desorption peaks for naphthalene and fluorene were not observed in the TPD experiments where the sample vial or glass beads were spiked with sixteen PAH compounds. These two volatile compounds were probably lost before the start of the TPD run. For phenanthrene and fluoranthene, the latter part of the TPD desorption peak was observed as shown in Figures 4-6. The peak temperatures of desorption of the remaining four listed PAHs for the spiked sample vial and the glass beads are in the range of the temperatures for which the estimated vapor pressure equals the nominal pressure of 10^{-7} atm. Thus the release of PAHs deposited on glass

surfaces is similar to what is expected from a pure solid PAH based on estimate of vapor pressure increase with temperature. The pure solid-like desorption behavior for PAHs deposited on these glass surfaces is expected due to the relatively low surface area and binding affinity for PAHs on glass.

Table 2. Temperature data for PAHs. Melting points and boiling points, estimated temperature at which vapor pressure = 10^{-7} atm, and observed peak desorption temperature (T_p) for individual PAHs and PAH homolog spiked either to the sample vial or glass beads.

PAH compound or homolog	Melting point (°C)	Boiling Point (°C)	VP= 10^{-7} atm (°C)	T_p , spiked vial, single PAH (°C)	T_p , spiked vial, 16 PAH mix (°C)	T_p , glass beads, 16 PAH mix (°C)
naphthalene (128)	81	218	-29	NA	NA	NA
fluorene (166)	116	295	5	NA	NA	NA
phenanthrene (178)	99	339	18	NA	NA	NA
fluoranthene (202)	110	375	34	33	41	49
chrysene (228)	255	448	85	102	94	81
benzo(a)pyrene (252)	177	495	88	106	111	92
benzo(g,h,i)perylene (276)	277	525	121	130	136	130
dibenz(a,h)anthracene (278)	266	524	119	143	148	131

TPD-MS response of PAHs sorbed on geologic materials. PAHs were spiked on a sand, kaolin, alumina, and coal to study how the binding of PAHs on geologic materials affect thermal desorption. A polymeric resin XAD-4 and pulverized activated carbon were studied as surrogates for polymeric organic matter and soot carbon respectively that may be found in soils and sediments. Three TPD profiles of PAH molecular weight 252 spiked on sand (60 ppm) and the average response is shown in Figure 8 to illustrate the reproducibility of the desorption response of PAHs from these natural materials. The average peak temperature (T_p) for the three runs is 108°C. There is little difference in the peak temperature between replicates of 1/8 filled sample vials for molecular weight 252 on spiked sand or for the other molecular weights (data not shown). There was difference in the absolute peak height of the TPD response between replicates. This was probably a result of nonuniform spiking of

individual sand grains, which resulted in heterogeneity of PAH concentrations at the sample milligram scale.

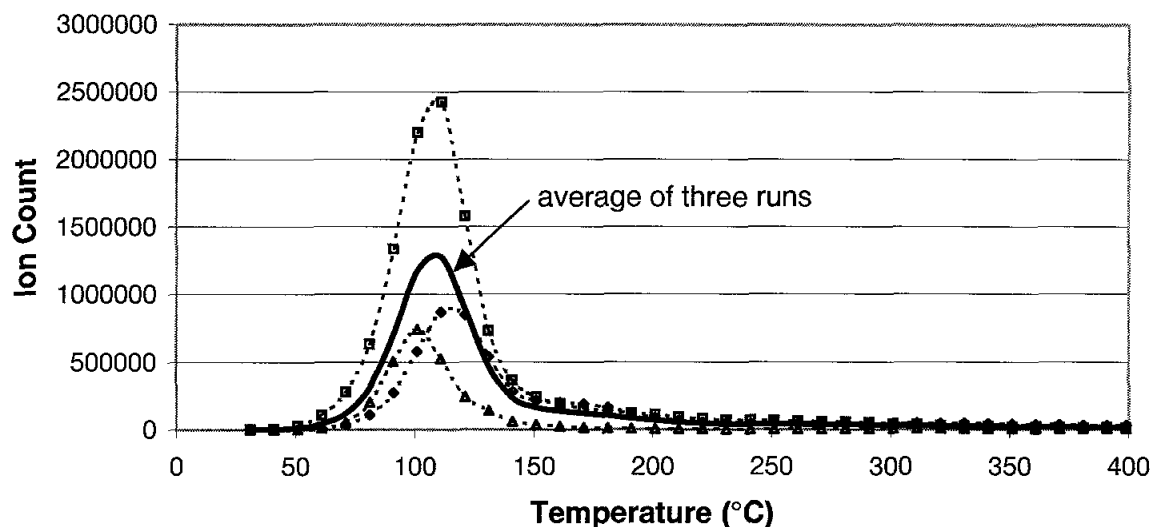


Figure 8. Three thermal program desorption mass spectrometry runs and average response for PAH homolog 252 (benzo(a)pyrene, benzo(b)fluoranthene, and benzo(k)fluoranthene) spiked onto sand at 20 ppm.

The solid surfaces exhibited a similar trend for TPD response in regard to the relationship of peak temperature and PAH molecular weight. As shown in Figure 9, increase in peak temperature was associated with an increase in PAH molecular weight. PAH molecular weight 276 and 278 are not sufficiently different in boiling point to exhibit markedly different peak temperatures. The sample vial with individual PAHs and the sample vial with the sixteen PAH mixture, and glass beads and sand spiked with the sixteen PAH mixture, all exhibit very similar trends and similar peak temperatures, as shown in Figure 9. The sample vial with individual PAHs spiked had 100 ng PAH for each TPD run, while the sample vial spiked with sixteen PAHs had 500 ng each for a total of 8000 ng of PAHs for each single TPD run. These differences in PAH mass concentrations did not result in differences in peak temperature responses.

To visually compare the TPD response from the various solid surfaces studied; the data were normalized by dividing by the total area under the peak of the TPD response curve (for Figures 10, 11, and 12), which corresponds to the total PAH mass desorbed from the

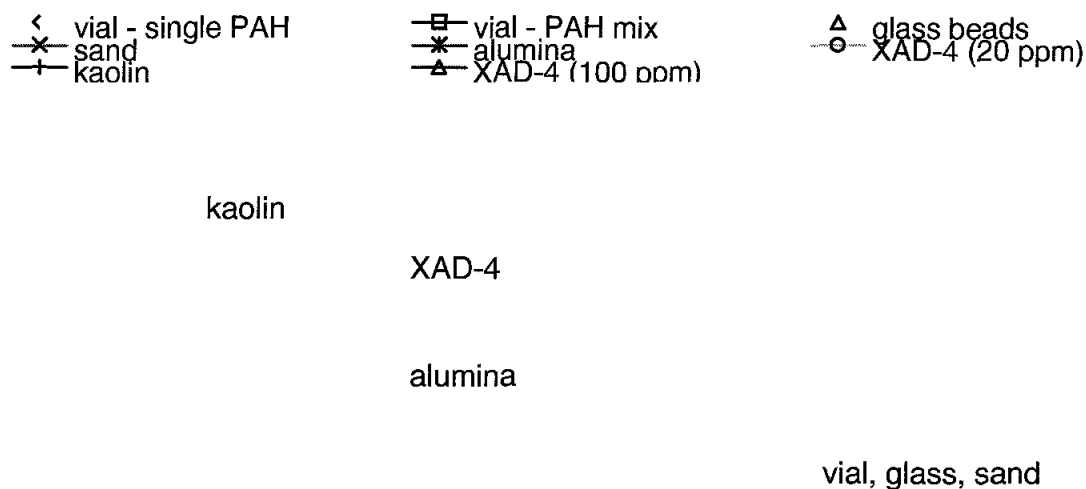


Figure 9. Peak desorption temperatures for PAHs spiked onto different solid surfaces, which illustrates the change in peak temperature for release of PAHs from different solids.

solid. For the spiked and aged coal and pulverized activated carbon, desorption was not complete within the 400 °C temperature limit and peak temperatures could not be assessed. These samples showed the beginning of an apparent peak near the upper temperature limit of 400°C, but since these peaks are not complete, they could not be scaled and are not shown. Figure 10 compares the normalized TPD response for PAH molecular weight 228 for the solid surfaces showing complete peaks of desorption. The peak temperature of PAH release for sand is similar to that seen for the glass beads and the spiked sample vial. The remaining three substrates: alumina, XAD-4, and kaolin show increasing peak temperatures. For molecular weight 228, the peak desorption temperature for sand is 90 °C compared to 161 °C for alumina, 265 °C for XAD-4 and 338 °C for kaolin. The higher peak temperatures for some of the solid surfaces is probably due to the greater solid surface area allowing greater interaction with the solid substrate, thus lowering vapor pressure and retarding the release of the PAHs.

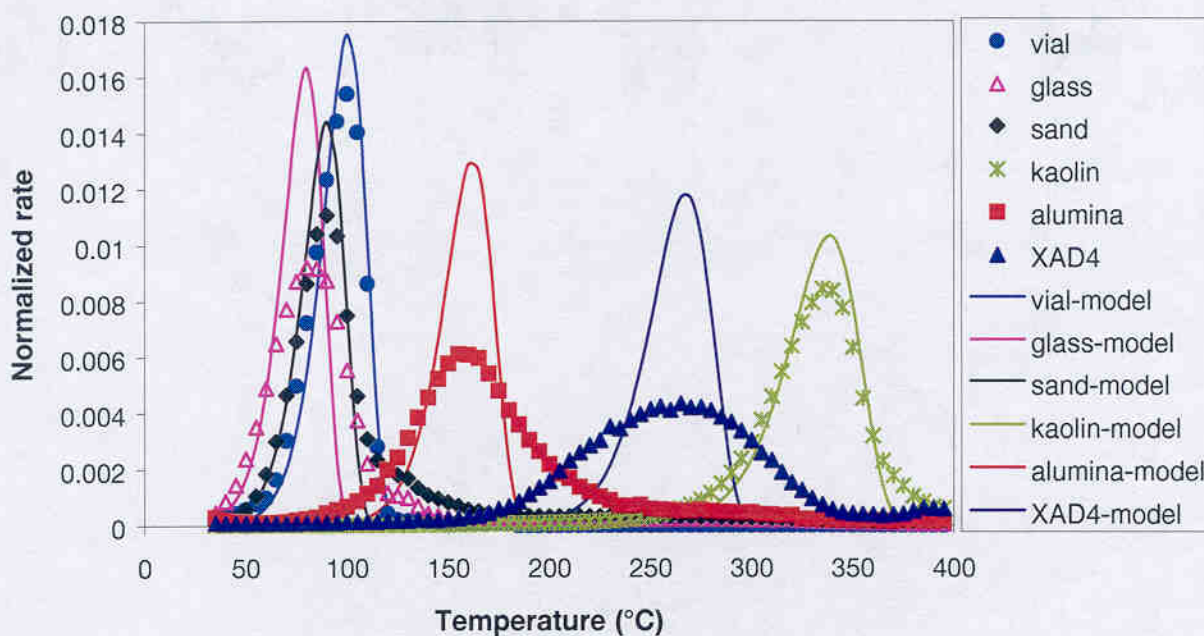


Figure 10. Thermal program desorption mass spectrometry response for MW 228 (benzo(a)anthracene and chrysene) showing release from different solid surfaces and comparison with a model based on parameter estimates using the peak temperature method and assuming $\nu = 10^{13} \text{ sec}^{-1}$.

Modeling release of PAHs during TPD. The desorption of PAHs and other hydrophobic organic compounds from solids can be modeled as a first order rate process as in Equation 3.

$$\frac{dC}{dt} = -kC \quad (3)$$

where, C is the concentration of the PAHs present in the solid, k is the rate constant, and t is time. An Arrhenius equation is typically used to describe the change in the rate constant, with temperature as shown in Equation 4.

$$k = \nu e^{-E/RT} \quad (4)$$

where E is the desorption activation energy (J/mol), ν is the preexponential factor (sec^{-1}), and R is the universal gas constant (J/mol-K). Equation 5 is obtained by combining Equations 3 and 4 and replacing dt with dT , assuming a constant heating rate β (K/sec).

$$\frac{dC}{dT} = -\frac{\nu}{\beta} C e^{-E/RT} \quad (5)$$

The form of this equation is similar to expressions used to describe the effect of temperature increase on release of sorbate materials from surfaces. The thermal desorption of compounds from a solid surface is often described in the surface science field by a similar Arrhenius expression known as the Polanyi-Wigner equation:

$$\frac{d\theta}{dT} = -\nu(\theta) \theta^n e^{-E(\theta)/RT} \quad (6)$$

where θ is the adsorbate coverage (unitless), n is the order of the desorption process, and for which both ν and E can be functions of adsorbate coverage. The Polanyi-Wigner equation expressed in simplified terms results in Equation 5 when the order of the reaction is 1, the heating rate is constant, the terms ν and E are assumed to be coverage independent, and coverage corresponds to concentration. Equation 5 and several modified versions of it have been used extensively in the surface science literature to describe the desorption of gases sorbed on metal surfaces and catalysts (4, 5, 17). Three methods used traditionally in the surface science field to fit the two parameters E and ν in equation 5 to measured TPD data were evaluated in this work. A fourth method to fit Equation 5 to the measured TPD data was based on a nonlinear curve fitting technique. These four methods are described below.

1) *Peak temperature method (18)*. In this method, equation 5 is differentiated to obtain a relationship of E with the peak temperature of desorption for concentration-independent desorption parameters:

$$\frac{E}{RT_p^2} = \frac{\nu}{\beta} e^{-E/RT_p} \quad (7)$$

where T_p is the peak temperature of desorption, and β is the heating rate in K/sec. Equation 7 is an implicit function of E and needs to be solved by iteration. A major shortcoming of this method however is that a value of ν has to be assumed to estimate E . Values of ν used in the surface science applications vary widely, anywhere between 10^{10} and 10^{20} sec^{-1} (19). De Jong and Niemantsverdriet (17) suggest a typical value of 10^{13} sec^{-1} .

2) *Chan-Aris-Weinberg method* (20). This method utilizes both the peak temperature and peak width at half or three quarters of the maximum intensity to estimate the two parameters of the Polanyi-Wigner model. The equations used to estimate the parameters from the peak temperature and peak width at half height are:

$$E = RT_p [-1 + (\gamma^{-2} + 5.832\gamma)^{0.5}] \quad (8)$$

$$\nu = \frac{E\beta}{RT_p^2} e^{E/RT_p} \quad (9)$$

Where, γ is the ratio of peak temperature (K) and peak width at half height. Using this method, both E and ν can be estimated independently.

3) *Leading edge method* (21). This method uses the initial part of the TPD curve where it is assumed that the change in surface concentration is small and, therefore, concentration remains constant. This simplifies Equation 5 and a plot of $\ln(dC/dT)$ vs $1/T$ yields a slope of $-E/R$ and an intercept of $\ln(\nu/\beta)$. A shortcoming of this method is that it uses the leading edge of the thermal desorption spectrum, where the desorption rate is small and therefore the accuracy of measurement is low.

4) *Nonlinear curve fitting*. In this method, the two parameters E and ν in Equation 5 are fitted using a nonlinear curve fitting routine by minimizing the sum of squared errors between the model and the measured TPD data. The TPD data obtained in ion counts versus temperature are first normalized by dividing by the total area under the TPD curve, which corresponds to total release. The TPD curves then are replotted as normalized rate versus

temperature prior to nonlinear curve fitting. The model shown in Equation 5 was solved with an initial normalized concentration of 1 at the beginning of the TPD run. A generalized reduced gradient nonlinear optimization code (Microsoft Excel 97 solver) was used to minimize the sum of squared errors between the model and the data.

Results of model fitting to TPD data. Interpretation of the data by the peak temperature method required an assumption of the parameter ν . An average ν value of 10^{13} sec^{-1} suggested by De Jong and Niemantsverdriet (17) was used, as well as the higher value of 10^{14} sec^{-1} and the lower value 10^{12} sec^{-1} for comparison. The value of E for these three values of ν were estimated by solving Equation 7 iteratively and the results for PAH molecular weight 228 are shown in Table 3. Figure 10 compares the model prediction of TPD response for PAH molecular weight 228 for six solid surfaces for an assumed value of $\nu = 10^{13} \text{ sec}^{-1}$. As may be expected, the fitted model simulation using the parameter values estimated from the peak temperature method match the peak temperatures of the TPD response well, as shown in Figure 10 for an assumed value of $\nu = 10^{13}$. However, the peak shapes are not predicted well, as only the peak temperature information from the TPD response is used in the data analysis. As seen in Table 3, the estimated values of E

Table 3. Estimated values of E using the peak temperature method (Eq. 7) for three values of ν . Units are kJ/mol for E and s^{-1} for ν , for PAH homolog 228.

Solid	T_p (K) (MW 228)	$\nu = 10^{12}$	$\nu = 10^{13}$	$\nu = 10^{14}$
		E	E	E
sample vial	375	100	106	113
glass-beads	354	94	100	107
sand	363	96	103	110
Al_2O_3	434	116	124	132
XAD-4	538	145	155	166
kaolin	611	164	176	187

increase by approximately 15% as the value of ν is increased from 10^{12} to 10^{14} for each solid material. It is clear that without an independent measure of ν , unique values of the two parameters cannot be estimated by this method. This is illustrated in Figure 11 where the model simulation using the three estimated values of E for the three assumed values of ν are compared with the TPD data for desorption of molecular weight 228 from alumina. For all three cases, the peak temperature matches closely with the observed data, however, the values of the parameters are quite different.

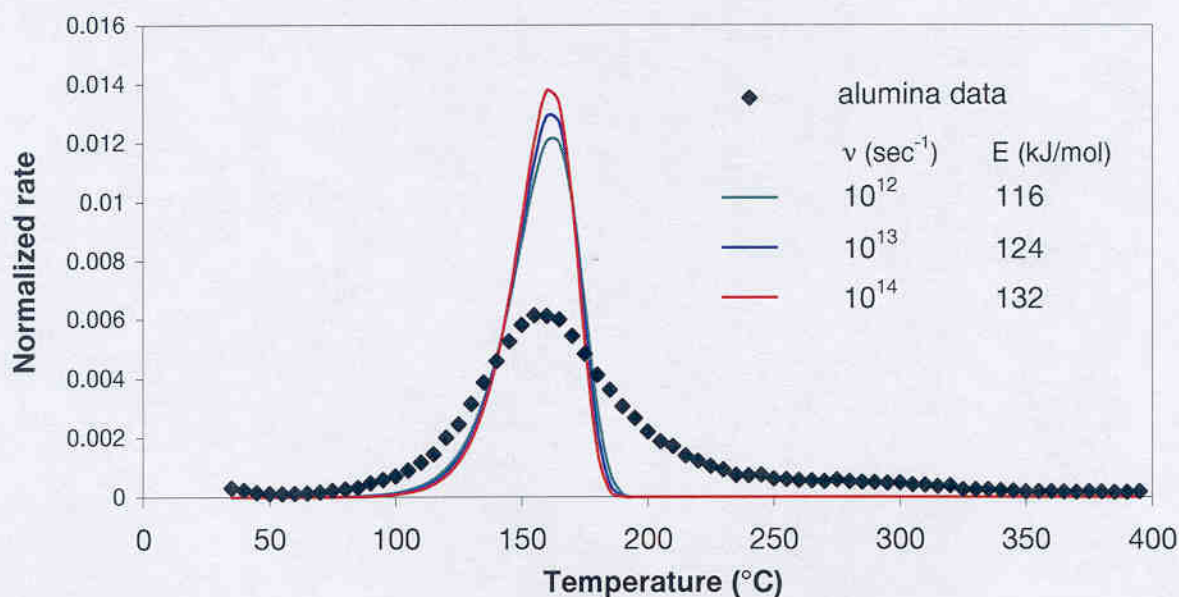


Figure 11. Comparison of model fit using the peak temperature method for three assumed values of preexponential factor ν and corresponding activation energy E for desorption of PAH molecular weight 228 (benzo(a)anthracene and chrysene) from alumina.

The estimated values of E and ν using the other three fitting methods are shown in Table 4 for PAH homolog 228. The estimation method based on peak temperature and width (method 2) provides parameter values that are small for both E and ν compared to those estimated by the other three methods. A possible reason for the very different values of the parameters estimated using method 2 is the high sensitivity to the peak width value in the estimation. One reason that the width of the TPD response may be greater than what is expected from a single compound is that PAHs measured in this research comprise two or

more PAH compounds per homolog. As seen in Equations 8 and 9, a smaller value of the ratio of peak temperature to peak width results in the estimation of a smaller value of E and ν . Therefore, the parameter estimation method using the peak width may not be appropriate for this case. Historically, this method has been used for the thermal programmed desorption of simple organics from smooth metal surfaces (22).

Table 4. Estimated values of E and ν using Chan-Aris-Winberg, leading edge, and nonlinear curve fitting techniques for PAH molecular weight 228 desorption. Units are kJ/mol for E and s^{-1} for ν .

Solid	Chan-Aris-Winberg		Leading Edge		Nonlinear Fit	
	E	ν	E	ν	E	ν
sample vial	23	5.39	100	1.55E+12	94	2.00E+11
glass-beads	17	0.87	82	1.46E+10	56	1.50E+06
sand	22	5.59	117	1.31E+15	76	7.80E+08
Al ₂ O ₃	20	0.63	58	3.08E+04	53	1.10E+04
XAD-4	20	0.13	72	4.38E+04	53	4.10E+02
kaolin	39	4.67	103	2.19E+06	137	4.20E+09

The nonlinear curve fitting technique provided the best fit to the entire dataset among the four methods tested as demonstrated in Figure 12. This method provided a good fit of not just the peak temperature but also the shape of the entire TPD curves.

An inherent problem with all these data reduction methods lies in fact that there is a high degree of correlation between the parameters to be estimated. Correlation between the two parameters E and ν in Equation 5 makes it difficult to estimate an unique set of parameter values by fitting TPD data. Thus, several sets of these parameter values may provide a reasonable description of the measured TPD response. This is illustrated below by analyzing the error space of the parameter fitting.

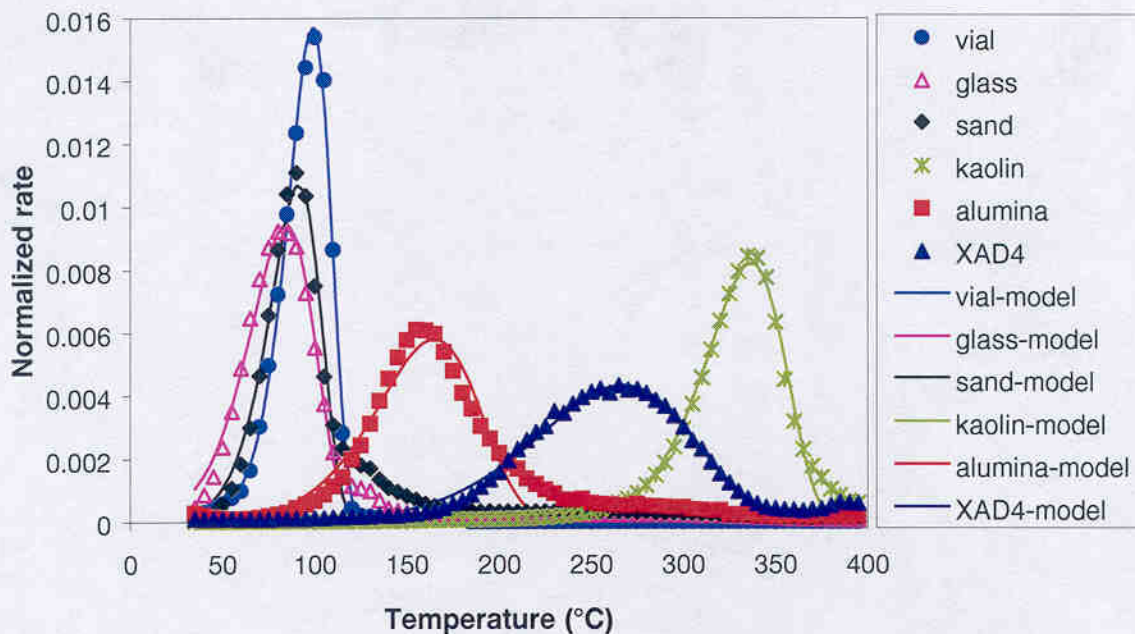


Figure 12. Fitted model to thermal program desorption mass spectrometry data for PAH MW 228 (benzo(a)anthracene and chrysene) for various solids using the nonlinear curve fitting technique.

Parameter estimation and error analysis from nonlinear curve fitting. A sensitivity analysis was performed to investigate the problem associated with estimating unique parameters by fitting the model in Equation 5 to the TPD data. TPD data for PAH molecular weight 228 on XAD-4 was used to perform the sensitivity analysis. For a range of assumed values of the parameter ν/β [K^{-1}] spanning four orders of magnitude, the value of E was varied to span a range across the value that provided a minimum of the sum of squared errors. The sum of squared error values are plotted as a function of ν/β and E as shown in Figure 13. The error surface forms a long, narrow valley with several minimum values as illustrated. Since the two parameters were correlated, several sets of values of ν/β and E provide a good fit and a minimum value of sum of squared errors. These sets of possible parameter values fall in a straight line in the ν/β - E plane. The high correlation between the two model parameters makes their estimation difficult from the TPD data alone and results in the large variability in the parameter values estimated by the different methods.

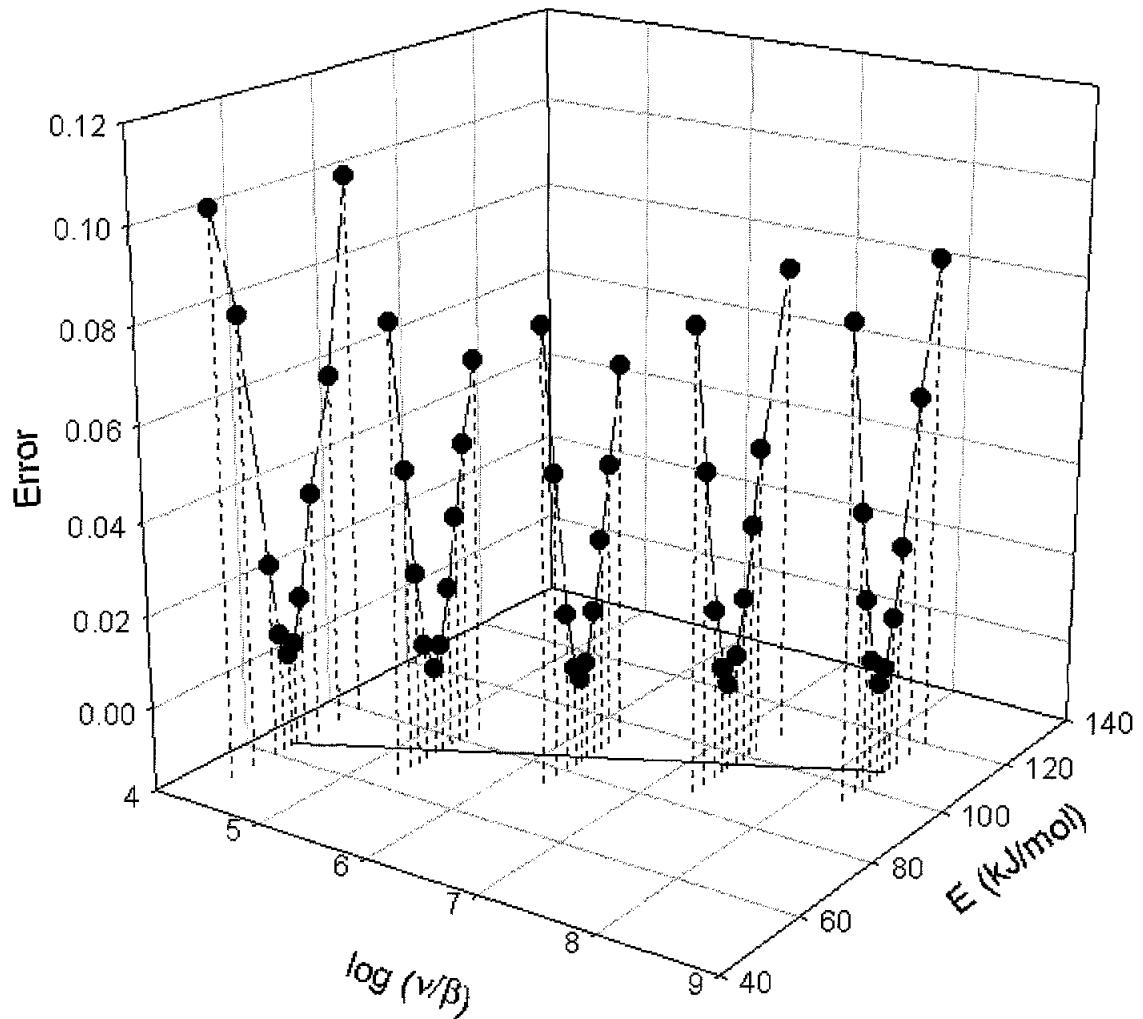


Figure 13. Error surface plot showing a long valley illustrating the difficulty in obtaining a unique set of parameters to describe the thermal program desorption mass spectrometry for release of PAH MW 228 (benzo(a)anthracene and chrysene) from XAD 4.

Interpretation of estimated parameters. One way to interpret the results of the TPD analysis of the different solid surfaces and the fitted parameter values is to use Equation 5 and estimate the relative values of the desorption rate constants at ambient temperatures. This provides a method to use the estimated parameter values to compare the expected rates of desorption of PAHs at ambient temperatures for the different solid surfaces studied. We compare the desorption rate constants relative to the estimated desorption rate constants for the solid PAHs in the sample vial as shown in Equation 10.

$$\frac{k}{k_{sv}} = \frac{v}{v_{sv}} e^{(E_{sv} - E)/R \cdot 298} \quad (10)$$

Where the subscript *sv* stands for the parameter values for the desorption of PAHs from the sample vial. Using the parameter values obtained from the peak temperature, leading edge, and nonlinear fitting techniques, rate constant ratios estimated at 25 °C are shown in Table 5.

Table 5. Comparison of relative desorption rate constants (k/k_{sv}) estimated for 25°C and different solids.

	Peak Temp	Leading Edge	Nonlinear
<i>sample vial</i>	1.00E+00	1.00E+00	1.00E+00
<i>glass</i>	1.25E+01	1.19E+01	2.68E+01
<i>sand</i>	3.96E+00	8.14E-01	5.85E+00
<i>Al₂O₃</i>	9.50E-04	4.60E-01	8.16E-01
<i>XAD-4</i>	2.61E-09	2.56E-03	3.57E-02
<i>kaolin</i>	7.47E-13	4.26E-07	5.02E-10

The estimated values are different for the three parameter estimation techniques due to the non-uniqueness of the estimated parameter values but, nevertheless, indicate similar trends. The relative desorption rate constants for the solid surfaces: kaolin, aluminum oxide, and XAD-4 are estimated to be several orders of magnitude smaller than the desorption rate constant for solid PAHs. Thus, although PAHs are desorbed easily from these solid surfaces during a TPD experiment, the desorption rates are predicted to be very small at ambient temperatures due to the large activation energies involved. Among the inorganic surfaces studied, sand shows minimum PAH binding with desorption rate constants similar to solid PAHs in a sample vial. Both kaolin and aluminum oxide show higher binding compared to sand due to surface interaction and the much larger surface areas in these powdery materials. However, the estimated desorption rate for PAHs on kaolin is several orders of magnitude smaller than for XAD-4 which is not expected based on the known stronger binding of PAHs to hydrophobic organic surfaces and the spiking procedures that allowed some solvent penetration. The estimated kinetic parameter values based on TPD results alone may not be realistic due to the problem of parameter correlation described earlier.

This technique of using TPD results to estimate relative desorption rate constants provides a method to compare the relative strength of PAH binding to different solid

surfaces, and these data may give an indication of reduced PAH availability when sorbed to these surfaces. We conclude, however, that estimates of the desorption rate constants at ambient temperatures, or apparent binding activation energies, are not feasible from TPD analysis alone due to the problem associated with determining a unique set of parameters in a two-parameter desorption model. Thus, for assessment of binding activation energies for sorbed PAHs, and the effect of temperature on PAH release from solids, an independent measurement of the desorption rate at a fixed temperature is required in combination with thermal programmed desorption. This is the focus of a subsequent investigation.

Acknowledgement

This work was sponsored by the Strategic Environmental Research and Development Program (SERDP) and the U.S. Army Engineer Research Development Center (ERDC).

References

1. Ghosh, U., Gillette, J.S., Luthy, R.G., Zare, R.N. *Environ. Sci. Technol.* **2000**, 34, 1729-1736.
2. Karapanagiota, H.K.; Kleinedam, S.; Sabatini, D.A.; Grathwohl, P.; Ligouis, B. *Environ. Sci. Technol.* **2000**, 34, 406-414.
3. Luthy, R.G.; Aiken, G.R.; Brusseau, M.L.; Cunningham, S.D.; Gschwend, P.M.; Pignatello, J.J.; Reinhard, M.; Traina, S.J.; Weber, W.J., Jr.; Westall, J.C. *Environ. Sci. Technol.* **1997**, 31, 3341-3347.
4. King, D.A. *Surface Science.* **1975**, 47, 384-402.
5. Falconer, J.L., Madix, R.J. *Surface Science.* **1975**, 48, 393-405.
6. Keys, B.R., Silcox, G.D. *Environ. Sci. Technol.* **1994**, 28, 840-849.
7. Yun, Y.; Meuzelaar H.L.C. *Energy & Fuels.* **1991**, 5, 22-29.
8. Tesconi, M. Yalkowski, S.H. *J. of Pharmaceutical Science*, **1998**, 87, 1512-1520
9. Oja, V., Suuberg, E.M. *Anal. Chem.* **1997**, 69, 4619-4626.
10. Farrell, J., Grassian, D., Jones, M. *Environ. Sci. Technol.* **1999**, 33, 1237-1243.
11. Robbat, A., Jr.; Liu, T.; Abraham, B.M. *Anal. Chem.* **1992**, 64, 358-364.
12. Schwarzenbach, R.P., P.M. Gschwend, D.M. Imboden. *Environmental Organic Chemistry.* John Wiley and Sons. NY. **1993**.
13. Mackay, D., A. Bobra, D.W. Chan, W.Y. Shiu. *Environ. Sci. Technol.* **1982**, 16, 645-649.
14. Prausnitz, J.M. *Molecular Thermodynamics of Fluid-Phase Equilibria*, Prentice Hall, Englewood Cliffs, NJ, **1969**.

15. Mackay, D., W.Y. Shiu, K.C. Ma. Illustrated Handbook of physical-chemical properties and environmental fate for organic chemicals. Lewis Publishers, Chelsea, MI. **1992**.
16. CRC Handbook of Chemistry and Physics. R.C. Weast, ed. CRC Press, FL. **1985**.
17. de Jong, A.M.; Niemantsverdriet, J.W. *Surface Science*. **1990**, 233, 355-365.
18. Redhead, P.A. *Vacuum*, 12, 203, 1962.
19. Rudzinski, W., Steele, W.A., Zarablich, G. Equilibria and Dynamics of Gas Adsorption on Heterogeneous Solid Surfaces. Elsevier Press, **1997**.
20. Chan, C.M.; Aris, R.; Weinberg, W.H. *Appl. Surf. Sci.* **1978**, 1, 360.
21. Habenschaden, E.; Kuppers, J. *Surface Science*. **1984**, 138, L147-L150.
22. Masel, R. I., Principles of Adsorption and Reaction on Solid Surfaces. John Wiley & Sons, Inc. **1996**.

Section 5

Kinetics and Thermodynamics of PAH Desorption From Sediment Particles*

Abstract

Milwaukee Harbor dredged sediment contains two primary classes of particles for size ranges < 2mm: a lighter-density coal and wood derived fraction with 62% of total PAHs and a heavier-density sand, silt, and clay fraction containing the remaining 38% of the PAHs. Room temperature desorption kinetic studies were conducted with Tenax beads as PAH extractants to measure the desorption rates of PAHs from the different sediment fractions. PAH desorption kinetic studies on separated sediment fractions revealed slow desorption rates for the coal particles and fast desorption rates for the clay/silt particles. The effect of temperature on PAH release was measured by thermal program desorption to investigate the desorption activation energies for PAHs on the different sediment particle classes. Three activated diffusion-based models and an activated first order rate model were used to describe the thermal desorption of PAHs. PAH binding with the coal-derived particles was found to be associated with much higher activation energy, i.e., in the range of 112-135 kJ/mol, compared to PAHs bound to the clay and silt material, i.e., in the range of 30-41 kJ/mol. Among the desorption models tested, the spherical diffusion model with initial PAH concentration on the outer regions appeared to describe adequately the PAH desorption from coal-derived particles. This PAH distribution pattern on coal-derived particles agreed with prior measurement of PAH locations at the sub-particle scale. These studies reveal that heterogeneous particle types in sediment exhibit much different amounts and binding of PAHs. We suggest that this provides a more complete picture of PAH mobility and bioavailability in sediments.

*Upal Ghosh¹, Jeffrey W. Talley², Richard G. Luthy¹

¹Department of Civil and Environmental Engineering, Stanford University, Stanford, CA 94305-4020

²Environmental Laboratory, U.S. Army Engineer Research and Development Center, Vicksburg, MS 39180

Introduction

The release of soil- or sediment-bound hydrophobic organic compounds (HOCs), including polycyclic aromatic hydrocarbons (PAHs), from the solid to the aqueous phase typically results in an initial period of rapid release, followed by a period in which little or no loss of contaminant from the solid can be detected (1-3). Numerous researchers have suggested that the diminishment in the progression of release of organic contaminants from sediments results from contaminant desorption limitations. Natural soils and sediments are highly heterogeneous media exhibiting particle-scale differences in both surface properties, such as surface binding energies, and physical characteristics such as shape, size, organic matter content, and porosity leading to several possible physicochemical mechanisms that could account for HOC sorption and slow desorption (4). It has been hypothesized that two likely causes of slow desorption are: i) high activation energy of sorptive interactions, and ii) mass transfer limitations (5). Several kinetic models based on these two basic mechanisms have been proposed, which include first order, multiple first order, Langmuir type second order kinetics, and various diffusion rate laws (6-7).

Direct measurement of PAH contaminant location on sediments at the microscale has not been possible until recently (8). Many prior studies have investigated organic compound desorption kinetic or equilibrium results from bulk sediments and used such data to infer possible desorption mechanisms. Hence, past methods that employed macroscopic techniques for assessing sorption and sequestration of HOCs, like PAHs, on geosorbents do not provide information about where toxic contaminants are located, how they are associated, nor what fundamental mechanisms govern HOC sorption. These deficiencies point to the need for improved understanding of PAH-geosorbent interactions and sequestration processes at the particle and sub-particle level, and the effect of such processes on bioavailability and toxicity of PAHs in geosorbents (4, 9). Additionally, the understanding that the nature of PAH association with sediment particles can result in much lower availability can improve decision making for setting sediment quality criteria, defining cleanup goals, selecting appropriate treatment technologies, and helping to set priorities among environmental problems.

A physical mechanism that may explain slow desorption is slow diffusion which may occur either through an organic matter matrix or through and along the walls of intraparticle pores, possibly with a hydrophobic wall coating. Organic-matter diffusion models with shallow penetration depths on the order of sub-micron to tens of nanometers have been proposed (6, 10-11). Many intraparticle diffusion-based models (12-15) assume a particle-scale pore diffusion process, although direct physical evidence is lacking on typical depths of penetration for contaminants in field sediments. In a previous study (8) we reported the first microscale observations of PAH distribution within the interior of sediment particles, which showed that the majority of the PAHs in dredged Milwaukee Harbor sediment were present in the near surface regions ($< 5\mu\text{m}$) of coal-derived particles. These observations suggest that slow desorption in the study sediment was related to sorption in coal-derived polymeric organic matter, and possibly associated with shallow diffusional distances compared to the particle scale.

In our earlier work (8) we showed that Milwaukee Harbor dredged sediment particles comprised two principal classes of particles in each size range: 1) a lighter-density coal and wood derived fraction (contributing 5% of the sediment weight and 62% of total PAHs) and 2) a heavier-density sand, silt, and clay fraction (contributing 95% of the sediment weight and 38% of total PAHs). Desorption kinetic studies were carried out at room temperature using the separated sediment components to investigate the nature of the PAH sorption process in the two primary sediment particle types. These studies provide information on the relative contribution of sediment particle types to the fast and slow desorption of PAHs. We report in this paper results of the effect of temperature on desorption as measured by thermal program desorption mass spectrometry (TPD-MS). To investigate the thermodynamics of the sorption process on different sediment particle types, four desorption models were tested to describe the process of PAH release from the sediment particles. The experimental data and model fitting allowed the estimation of the desorption activation energy for the different sediment components revealing information about the PAH sorption mechanism for the different particle types in the sediment.

Model Development and Parameter Estimation

Four models were developed to describe the process of thermal programmed desorption (TPD) of PAHs from sediment particles. An activated first order rate model and three activated diffusion-based models with different diffusional geometries were evaluated to describe the thermal desorption of PAHs from sediment particles.

First order model.

A first order desorption model to describe PAH loss from sediment particles is described in Equation 1.

$$\frac{dC}{dt} = -kC \quad 1.$$

where, C is the concentration of PAH in the particle at any time t , and k is the first order rate constant. During thermal program desorption, the increase in k with temperature can be described by an Arrhenius function shown in Equation 2.

$$k = k_o e^{\frac{-E_a}{RT}} \quad 2.$$

where, k_o is a preexponential factor, and E_a is the activation energy (kJ/mol), R is the universal gas constant, and T is temperature in K. The value of k_o can be expressed as a function of a fixed temperature desorption rate constant and substituted in Equation 2 as shown in Equation 3.

$$k = k_{25C} e^{\frac{E_a}{R} \left(\frac{1}{298} - \frac{1}{T} \right)} \quad 3.$$

where, k_{25C} is the desorption rate constant measured at 25°C. Substituting Equation 3 in 1, Equation 4 is obtained which describes the loss of PAH from a particle as a function of temperature where the two unknown parameters are k_{25C} and E_a .

$$\frac{dC}{dt} = -C k_{25C} e^{\frac{E_a}{R} \left(\frac{1}{298} - \frac{1}{T} \right)} \quad 4.$$

It has been shown earlier (16) that the two parameters k_{25C} and E_a are highly correlated and unique values of both cannot be estimated simultaneously from a single set of TPD data. Therefore, an independent measure of one of the parameters is necessary. This is

possible through desorption kinetics tests conducted at a fixed temperature to estimate k_{25C} . Once k_{25C} is known, the desorption activation energy can be estimated by fitting Equation 4 to thermal program desorption data.

Diffusion-based models.

Geosorbent organic matter is considered to have a macromolecular structure, and slow diffusion through macromolecular organic matter is often considered similar to polymer diffusion (17-18). Mechanistically, polymer sorption is very different from surface adsorption on metals, and is understood to proceed through a sequence of two steps: the creation of a hole in the polymeric matrix (an endothermic process) and the accommodation of a solute molecule in that hole (an exothermic process). The overall sorption process is exothermic. The sorption of HOCs to organic polymers is a thermodynamically favored process as the entropy of sorption is highly positive due to the disappearance of the structured water molecules surrounding the dissolved HOC and the increased disorder in the polymer mesh (18-19). Sorption of PAHs on coal particles is expected to resemble polymer sorption due to the physical structure of coal, which is described as a porous macromolecular gel (20). In addition, there is evidence to suggest specific binding of PAH molecules to aromatic structures present in coals. Nuclear magnetic resonance studies on interactions between PAHs and coals have revealed that PAHs penetrate within the coal matrix and interact with the coal matrix through associative bonding such as π - π electrodynamic interactions (21). Such molecular interactions between a PAH molecule and the aromatic rings with a coal polymer can enhance the sorptive binding of a PAH molecule.

The diffusion of HOCs through a polymer matrix is controlled by the frequency of the molecular "jumps" from one hole to another. The temperature dependence of diffusion is governed by the activation energy that is required to make such jumps. Since these jumps require space within the polymer matrix, the activation energy will depend on intra- and inter-chain forces in the polymer structure (18-19). Therefore, the diffusion coefficient of HOCs through polymers can be expressed by an Arrhenius function as in Equation 5 [Cussler, 1995] (17).

$$D = D_0 \exp\left(\frac{-E_a}{RT}\right) \quad 5.$$

where:

D = diffusion coefficient through organic matter (cm²/s)

D_0 = preexponential factor (cm²/s)

E_a = activation energy for diffusion in polymer (kJ/mol)

R = universal gas constant (kJ/mol-K)

Conceptually, the preexponential factor D_0 is related to the number of holes in which the solute molecule can be accommodated, which depends on polymer density and solute size. The activation energy of diffusion depends on the ease with which the solute can move from one hole to another. Thus for a given polymer-solute system, the rate of diffusion is controlled by these thermodynamic factors and estimates of both D_0 and E_a are required to predict D . For a constant value of D_0 in Equation 5, the value of D decreases with increasing value of activation energy. This may give the erroneous notion that a solid-sorbate system with higher activation energy will result always in slower diffusion at any temperature. Rather, because the value of D_0 may vary widely for different materials, the overall response of D with temperature depends on the values of D_0 and E_a .

The value of the preexponential factor D_0 in Equation 5 cannot be determined directly. If the value of D is known at one temperature (T_0) we can estimate the preexponential factor and use it to predict the diffusivity at any other temperature as shown in Equation 6. In this fashion, the value of D_0 estimated from the value of D_{T_0} becomes a function of E_a for the system. Thus, for larger values of E_a , the estimated value of D_0 also will be larger for a given D_{T_0} value and the resulting function for D would be positively dependent on E_a for values of temperature greater than T_0 as shown in Equation 8. The value of D at room temperature can be estimated from desorption kinetic studies at constant temperature where conditions are maintained for mass transfer limitation in the solid phase.

$$D_{T_0} = D_0 e^{\left(\frac{-E_a}{RT_0}\right)} \quad 6.$$

$$D = \frac{D_{T_0}}{e^{\left(\frac{-E_a}{RT}\right)}} e^{\left(\frac{-E_a}{RT_0}\right)} \quad 7.$$

$$D = D_{T_0} e^{\frac{E_a}{R} \left(\frac{1}{T_0} - \frac{1}{T} \right)} \quad 8.$$

It is instructive to note how the change in D with temperature responds to different E values for a given value of D at room temperature. Equation 6 was solved for values of E_a ranging from 0 to 120 kJ/mole and a plot of D/D_{T_0} versus temperature appears in Figure 1. For an unactivated process with $E_a = 0$, D/D_{T_0} remains constant and does not change with increasing temperature. However, with increasing value of E_a , D/D_{T_0} becomes increasingly sensitive to temperature. Typical values of E_a for diffusion of organic molecules through polymeric material are in the range of 50-120 kJ/mole (18, 23). For this range of values of E_a , it can be seen from Figure 1 that the value of D/D_{T_0} increases by six to twelve orders of magnitude as the temperature is increased from room temperature to 400 °C. For smaller values of E_a , the increase in D/D_{T_0} with temperature is significantly smaller.

Three diffusion geometries were modeled:

1. Diffusion from a sheet with uniform initial PAH concentration: This model conceptualizes desorption from a thin layer of organic matter coating on inert mineral surfaces with diffusion occurring from the exposed planar surface. Direct evidence of such desorption regime was reported in an earlier study (8) where infrared microspectroscopic work revealed the existence of organic matter coatings with PAHs on silica particles in the sediment. Diffusion of PAHs from a planar source can be described by a one-dimensional diffusion equation as shown below.

$$\frac{dC}{dt} = D \frac{\partial^2 C}{\partial x^2} \quad 9.$$

An analytical solution to describe the mass remaining in a plane sheet with one surface exposed to an infinite sink is available (24).

$$\frac{M_t}{M_o} = \frac{8}{\pi^2} \sum_{n=0}^{\infty} \frac{1}{(2n+1)^2} \exp\left\{-\frac{D}{a^2} (2n+1)^2 \pi^2 t\right\} \quad 10.$$

where:

M_t = PAH remaining in the plane sheet at time t

M_o = initial PAH mass in the plane sheet

D/a^2 = diffusional rate ($1/t$)

The diffusive rate can be envisioned as the diffusivity divided by the diffusional distance.

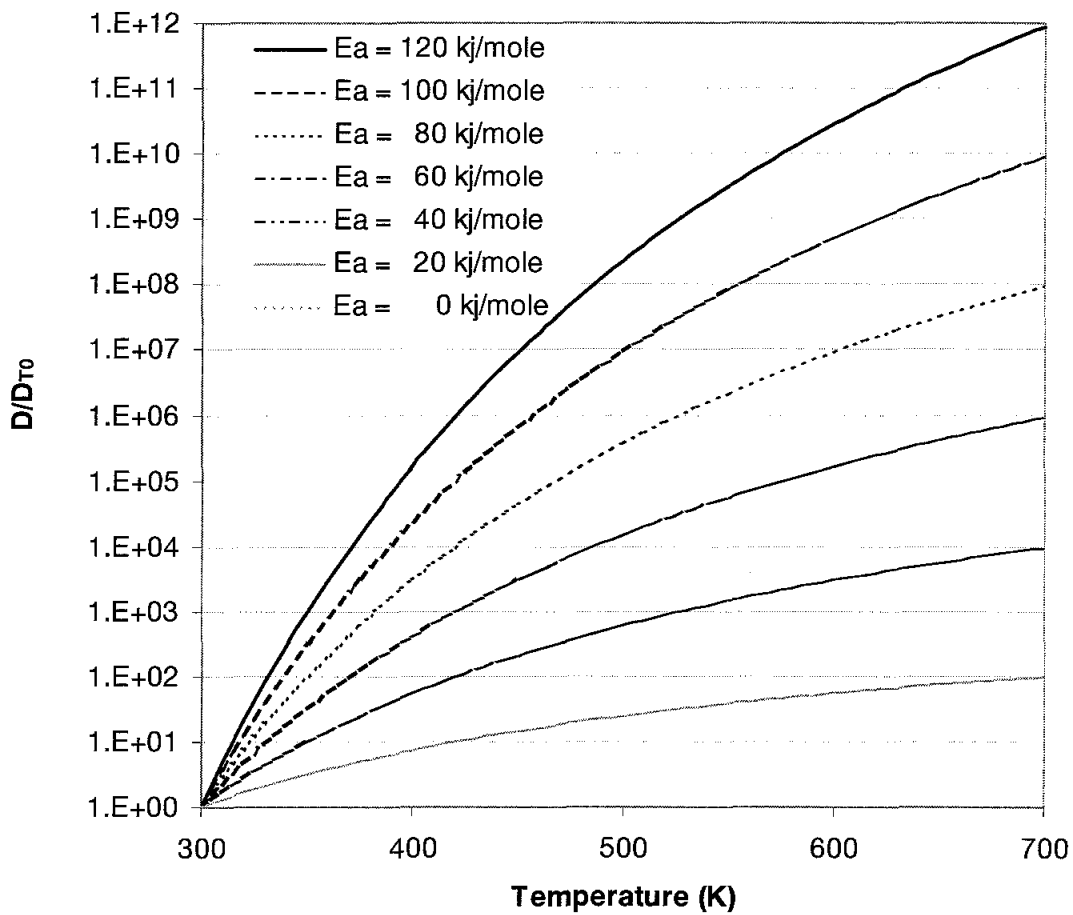


Figure 1. Effect of desorption activation energy (E_a) on change in diffusivity with temperature.

During thermal program desorption the value of D/a^2 changes with temperature as in equation 8. The diffusional distance parameter a can be assumed to remain constant. The

value of D_{T_0} in Equation 8 is estimated from a room temperature desorption kinetics study. For a changing value of D/a^2 , Equation 9 can be solved for small incremental time steps during which the value of D/a^2 remains sufficiently constant. This approximation can be improved with a more rigorous numerical integration procedure.

2. Fully penetrated spherical particles with uniform initial PAH concentration: The most commonly used diffusion model assumes a spherical geometry as in equation 11.

$$\frac{dC}{dt} = D \left(\frac{\partial^2 C}{\partial r^2} + \frac{2}{r} \frac{\partial C}{\partial r} \right) \quad 11.$$

Where, r is the radius of a spherical particle. An analytical solution for equation 11 has been provided by Crank (24) under the condition of uniform initial concentration within the sphere, and is shown in Equation 12.

$$\frac{M_t}{M_o} = \frac{6}{\pi^2} \sum_{n=1}^{\infty} \frac{1}{n^2} e^{\left(\frac{-Dn^2\pi^2 t}{a^2} \right)} \quad 12.$$

Where:

- C = concentration of diffusing substrate in solid particle
- R = radius of spherical solid particle
- M_t = mass of substrate in particle at time t
- M_o = mass of substrate in particle at time 0
- D = effective diffusivity of substrate in particle
- a = particle radius

The lumped diffusional rate parameter D/a^2 determines the rate of release of a diffusing substrate from the solid phase in this polymeric organic matter model. As in the previous model, the value of D/a^2 changes with temperature as described in Equation 5, and a is constant.

3. Spherical particles with PAHs located on the outer regions of sorbent particles: This model assumes PAH sorption on outer regions of a polymeric material such as coal in sediments. In an earlier study (8) we have shown that PAHs on coal derived particles in Milwaukee Harbor dredged sediment are located on the near surface ($< 5 \mu\text{m}$) region. Therefore a fully penetrated spherical geometry for diffusion, which is commonly invoked, may not be appropriate for describing the desorption of PAHs from such sediment coal particles. Modeling of contaminant diffusion from geosorbents with non-uniform initial concentrations has not been done in the past due to the lack of direct evidence of penetration depth of contaminants within geosorbent particles, and difficulty in describing the initial concentration profile existing within the geosorbent particle. Also, convenient analytical solutions are not available and a rigorous numerical treatment is required.

A finite difference solution scheme was adopted to solve the diffusion equation in spherical coordinates with central difference in space (500 nodes) and weighted average in time. The numerical model was coded in Visual Fortran (Digital Equipment Corporation) and run on a 266 MHz IBM compatible personal computer. The model was first run in the absorption mode to form the initial concentration profile for the desorption phase. This was followed by running the model in a constant temperature desorption mode to simulate the room temperature desorption studies. Other model runs simulated the temperature program desorption mode where the temperature of desorption increased at $10^\circ\text{C}/\text{min}$ following the temperature ramp rate of the TPD experiments. The following initial and boundary conditions were used:

Absorption phase: Initial condition: $C=0$ for all r at $t=0$
 $C=C_0$ at $r=R$ for $t > 0$
Boundary condition: $dC/dt = 0$ at $r=0$

Desorption phase: Initial condition: C profile created during absorption phase
Boundary condition: $C=0$ at $r=R$ for $t > 0$
 $dC/dt = 0$ at $r=0$ for all t

For the non-uniform spherical diffusion model, the room temperature diffusivity value was obtained by trial and error. Here, the model was run in the absorption mode for 30 year simulation time (assuming an average field aging time of 30 years) with an assumed value of diffusivity, then the model was run in the room temperature desorption mode for 100 days. The value of room temperature diffusivity was estimated by fitting the model desorption profile with the room temperature desorption data.

Materials and Methods

The sediment used in this study was obtained from the Milwaukee Harbor Confined Disposal Facility (CDF) operated by the Milwaukee Harbor Port Authority. These sediments originated from the Milwaukee Harbor during the process of dredging to maintain waterway navigability. Dredged sediment environmental issues include the potential for release of contaminants from such CDF sites and closure requirements (25) and the feasibility of composting biotreatment to reduce PAH concentrations and convert the dredged sediment to material suitable for offsite beneficial uses (26). The sediment was composed primarily of silt and clays (61% by weight < 63 μm), sand (24% by weight 63 μm - 1000 μm), and carbonaceous matter derived from coal and wood (5% by weight). The total PAH concentration in the sediment was 90 mg/kg, the majority of which (62%) was found in the coal-derived fraction (8).

Particle Separation.

Wet sieving was performed to separate the sediment into four size fractions (>1000 μm , 1000-250 μm , 250-63 μm , and <63 μm). The larger size fractions (>63 μm) were composed primarily of sandy grains, coal-derived particles, and woody material. It was possible to wash off the lighter fractions (coal and wood) from the heavier sand by swirling with water in a beaker and draining off the entrained lighter particles. This process was repeated several times until most of the lighter material was removed. Materials in the fine fraction (<63 μm) were density separated using a cesium chloride solution having a specific gravity of 1.8. Five grams of wet sediment and 40 ml of cesium chloride solution were centrifuged at 2000 rpm for 10 minutes in 50 ml glass centrifuge tubes. The fine coal and wood particles floated to the top and were decanted off and collected in filter paper and

washed with water several times. The heavy clay and silt were similarly washed several times to remove cesium chloride. Each of these size and density separated fractions were then analyzed for PAHs.

PAH analysis by gas chromatography-flame ionization detection (GC-FID).

PAH extraction from whole sediment was performed by three successive ultrasonic extractions (15 seconds on and 15 seconds off pulsing for a total of 3 minutes) with a 50:50 mixture of hexane and acetone following EPA method 3550B. The extracts were combined and cleaned using a silica gel column as outlined in EPA method 3630C. A Hewlett Packard gas chromatograph (Model 6890) with a fused silica capillary column (HP-5, 30 m x 0.25 mm I.D.) and a flame ionization detector was used for analysis based on EPA method 8100 for PAHs. A standard EPA mixture of 16 PAH compounds obtained from Ultra Scientific was used for calibration.

PAH desorption study.

PAH desorption kinetic studies were conducted using the original sediment and separated fractions. Desorption tests followed procedures used previously (19, 27). Contaminated sediment (2.0 g) and Tenax beads (0.5g, 40-60 mesh, Suppelco, Bellefonte, PA) were added to a 15 ml glass vial containing 10 ml of water and continuously mixed in a rotator. Mercuric chloride (1.0 mg) was added to the mixture to prevent any biological growth. These studies were conducted in duplicate. At sampling times, the Tenax beads were harvested by allowing the sediment to settle and the Tenax beads to float up. The Tenax beads were scooped out of the test tube and fresh Tenax beads were added. PAHs were extracted from the Tenax beads by agitating the beads in 10 ml of hexane and acetone (50:50 mixture) for 12 hours and repeating twice. The extracts were then combined and concentrated, cleaned using silica gel, and analyzed by GC-FID.

Thermal program desorption study.

A gas chromatograph quadrupole mass spectrometer (GCQ-MS) with a direct insertion probe (DIP) manufactured by Thermoquest was used for thermal program desorption (TPD) measurements. The sample is inserted into the mass spectrometer in a 1

mm diameter glass vial inserted in the probe. The temperature of the probe containing the sample glass vial is then increased according to a predetermined temperature ramp. The volatilized compounds are then ionized and selectively filtered in the quadrupole for the mass ions to be detected in the mass spectrometer. The high sensitivity of the GCQ enables single-grain analyses. A detailed description of the TPD instrument and use for PAH measurement on solids is presented elsewhere (16).

Results and Discussion

Measurement of desorption rates at room temperature.

Unseparated Milwaukee sediment was subjected to desorption experiments with successive Tenax additions as the PAH extractant to study the overall desorption behavior of the PAHs in the sediment. Similar desorption experiments were performed with the lighter coal and wood fraction (63-250 μm) and the clay/silt fraction (< 63 μm) from which the lighter particles had been removed by density separation.

The results of these desorption experiments for sixteen total EPA priority pollutant PAHs from Milwaukee Harbor dredged sediments have been presented earlier (8). In this paper, detailed analysis and modeling results are presented for a representative PAH molecular weight 202 (MW202) from the EPA mixture, which comprises fluoranthene and pyrene. The aqueous desorption results for MW202 from the whole sediment and separated coal particles and silt/clay particles are shown in Figure 2. This test shows that approximately 46% of MW202 were released quickly and approximately 54% were strongly bound. The PAHs associated with the coal fraction appear to be bound very strongly, as only about 10% of the PAHs in this fraction were released in one hundred days. The data suggest that the majority of the PAHs associated with this coal fraction may not be bioavailable for degradation nor exhibit a highly toxic response. In contrast, desorption data from the heavier clay/silt fraction indicate a higher availability with nearly 90% of the initial PAHs in this fraction readily desorbing in one month, and more than 98% in 100 days. The desorption rates of the other PAHs exhibited a pattern similar to that for MW202.

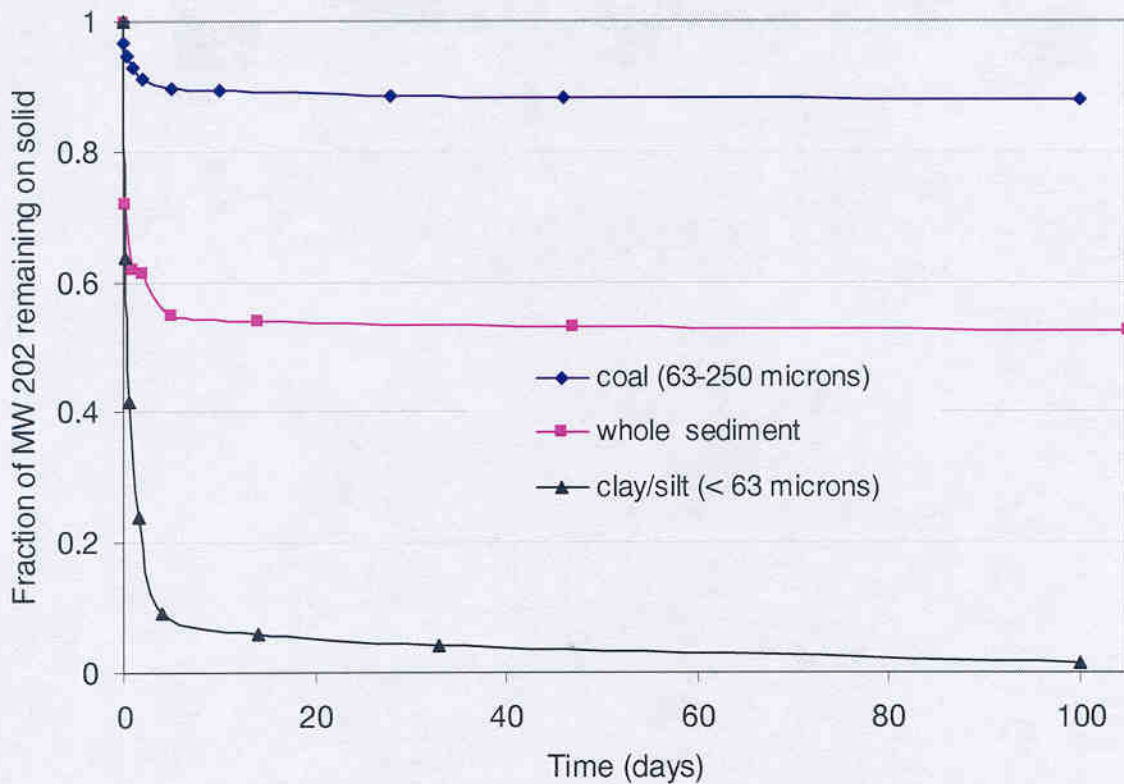


Figure 2. Desorption of fluoranthene and pyrene (MW 202) from Milwaukee Harbor sediment showing faster desorption from the heavy clay/silt fraction compared to the light coal/wood fraction.

A phenomenological two compartment model comprising both fast and slow desorbing PAH compartments in sediment describes the desorption kinetics observed in Figure 3.

$$\frac{C}{C_o} = fe^{-k_f t} + (1-f)e^{-k_s t} \quad 13.$$

- Where:
- C = PAH concentration in sediment
 - C_o = initial PAH concentration in sediment
 - f = fraction of fast desorbing pool in sediment
 - k_f = first-order rate constant for fast component
 - k_s = first-order rate constant for slow component

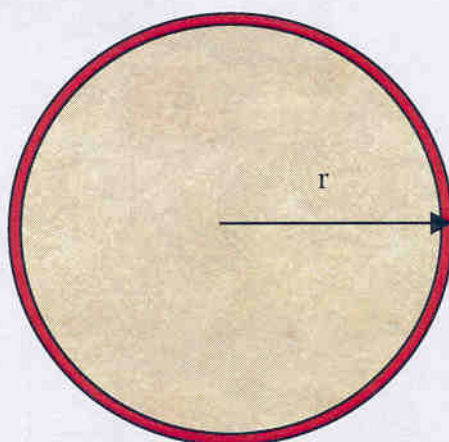


Figure 3. Schematic cross-section of model coal particle showing PAHs on the outer regions of the particle.

Similar two compartment models have been used previously to model the desorption of hydrophobic organic compounds from sediments (19, 28). The model was fitted to the normalized PAH desorption data to estimate the room temperature desorption rate constants. A nonlinear curve fitting routine based on the Marquardt-Lavenberg algorithm was used to fit the nonlinear model to the measured data on PAH desorption. The least-squares routine produced estimates for the model parameters. Three parameters were estimated for each set of desorption data: the first-order desorption coefficients for fast and slow pools (k_f and k_s), and the fast pool PAH fraction (f). The fraction of PAHs in the slow desorbing pool was calculated as $(1-f)$. The estimated parameters for PAH molecular weight 202 desorption from the silt/clay fraction ($<63 \mu\text{m}$) and the coal-derived ($63\text{-}250 \mu\text{m}$) sediment fraction are presented in Table 1.

It was suggested in early work on chromatography (29) that first-order mass transfer could be used to approximate diffusion. An approximate correlation between a first order rate constant and diffusion coefficient shown in Equation 14 has been proposed (30-31).

$$k = 15(D_e/a^2) \quad 14.$$

Where,

k = first order rate constant

D_e = effective diffusivity

a = diffusional distance

Values of D/a^2 calculated from the values of k_f and k_s are shown in Table 1. Since the desorption kinetics experiments were conducted at room temperature (25°C), these values of D/a^2 can now be used for D_{T_0} in Equation 8 to model the change in diffusivity with rise in temperature.

Table 1. Parameters f , k_f , and k_s estimated from PAH molecular weight 202 desorption data of coal and wood derived fraction and silt/clay fraction of sediment shown in Figure 2.

Particle type	f (fast fraction)	k_f (day ⁻¹)	k_s (day ⁻¹)	$[D/a^2]_f$ (min ⁻¹)	$[D/a^2]_s$ (min ⁻¹)
coal-derived (63-250 μm)	0.09	1.8	0.0003	8.3E-5	2.3E-8
silt/clay (<63 μm)	0.94	0.9	0.005	4.2E-5	2.3E-7

Thermal program desorption results and interpretation.

Thermal program desorption experiments were conducted using coal-derived (63-250 μm) and silt/clay (<63 μm) sediment fractions to investigate the thermodynamics of the PAH desorption process from different sediment particle types. In each experiment approximately 1-2 mg sample was placed in a TPD glass vial and inserted into the TPD-MS. A temperature ramp of 10°C/min was used from a starting temperature of 30°C, and the test was run to a maximum temperature of 400°C. The MS signal was collected in a selective ion-monitoring (SIM) mode with a sampling frequency of approximately 80/min resulting in nearly 3000 datapoints for each run. The data were reduced by averaging every 5 consecutive values, which also resulted in eliminating data noise. Figure 4a shows a smoothed TPD response obtained by such processing for PAH mass numbers 178 (phenanthrene and anthracene), 202 (fluoranthene and pyrene), 228 (chrysene and benzo(a)anthracene), and 252

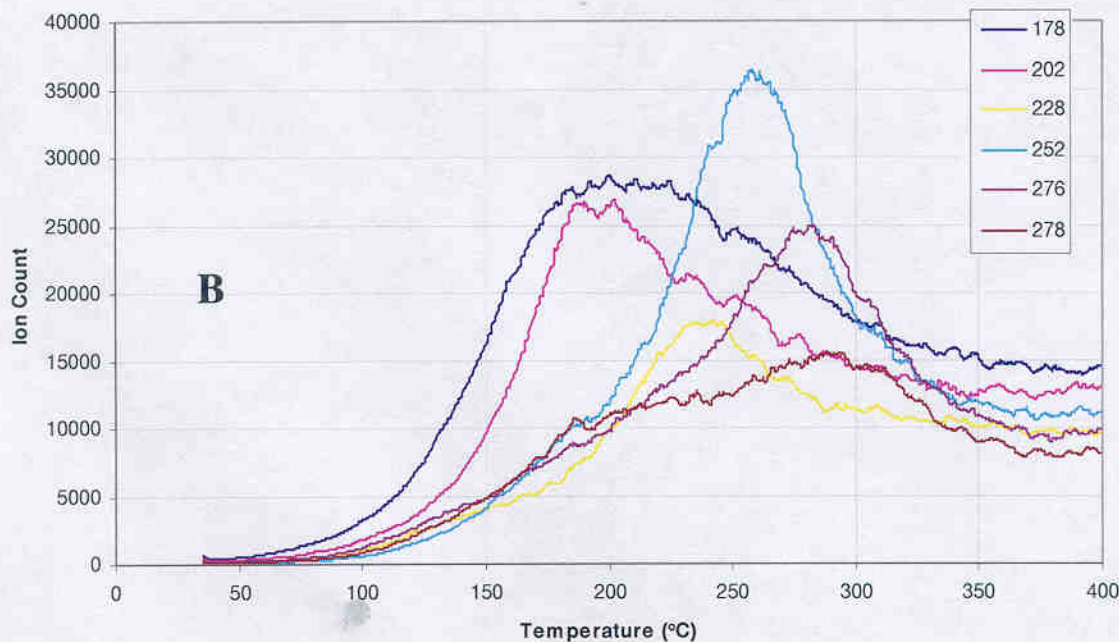
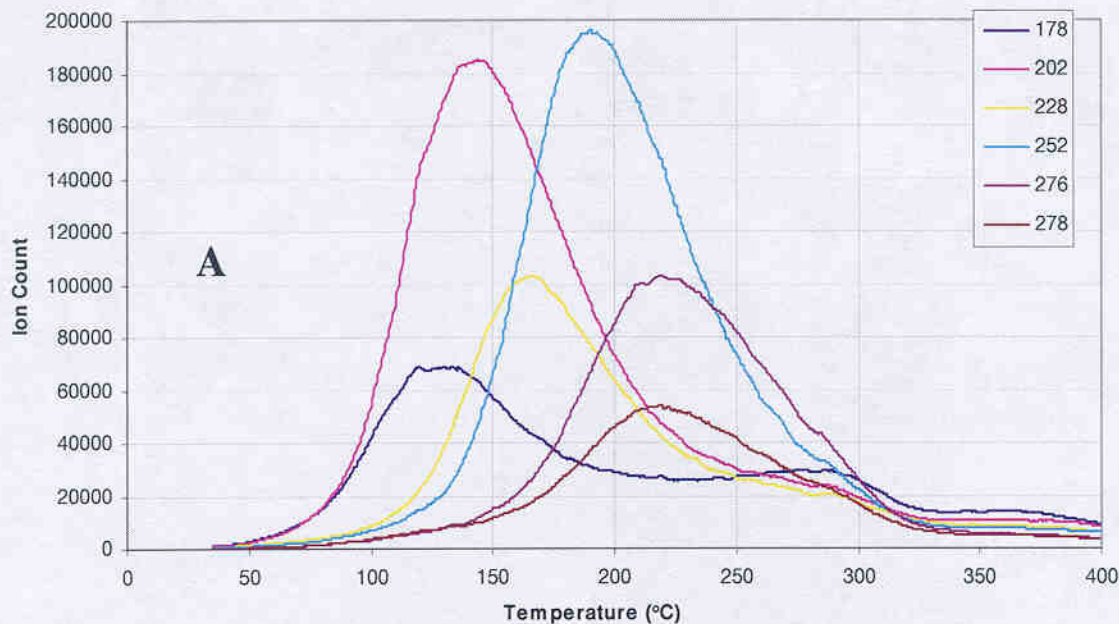


Figure 4. TPD response of PAH mass numbers 178 (phenanthrene and anthracene), 202 (fluoranthene and pyrene), 228 (chrysene and benzo(a)anthracene), 252 (benzo(b)fluoranthene, benzo(k)fluoranthene, and benzo(a)pyrene), and 278 (dibenzo(a,h)anthracene, benzo(g,h,i)perylene) for (a) coal particles (63-250 μm) and (b) silt/clay particles (<63 μm) from Milwaukee Harbor sediment. Data presented are averages of three replicate TPD runs.

(benzo(b)fluoranthene, benzo(k)fluoranthene, and benzo(a)pyrene) for coal particles (63-250 μm) from Milwaukee Harbor sediment. The area under each curve represents the total mass of the compound released over the time period of desorption.

The TPD response of the same PAHs for sediment silt/clay fraction is shown in Figure 4b. There are two major differences in the TPD responses from coal-derived and silt/clay particles as shown in Figures 4a and 4b. Firstly, the TPD signal response for coal-derived particles is nearly one order of magnitude higher compared to that of the silt/clay particles. This difference is due to the much higher concentration of PAHs present in the coal-derived particles in the sediment as measured by extraction and analysis (8). Secondly, the peak temperatures of TPD response for silt/clay particles are approximately 70°C higher than for the corresponding peaks for coal-derived particles. The difference in peak temperatures for the two particle types is investigated further through TPD model simulations. For both types of particles, the TPD response does not reach a zero value in the tailing edge of the peak. This is more pronounced for the silt/clay particles for which the overall TPD response is small. Two possible causes for this behavior are: increasing TPD-MS baseline with increasing temperature, and beginning of pyrolysis of organic matter at temperatures above 350°C.

Results of TPD model simulations.

The nature of the desorption process for PAHs from the different sediment particle types was investigated by applying the four desorption models to fit the TPD-MS data. These models were: 1) first order desorption, 2) desorption from a thin layer of organic matter with uniform initial concentration, 3) desorption from a spherical particle with uniform initial concentration, and 4) desorption from a spherical particle with a nonuniform initial concentration. The fourth model, which is more appropriate to describe polymer diffusion through coal-type particles, was not applied to the silt/clay material. All four models used an Arrhenius relationship to describe the effect of temperature on desorption rate or diffusivity as shown in Equations 2 and 6.

Silt/clay particles. The first three desorption models were used to describe the TPD results of silt/clay particles. The room temperature desorption rate or diffusive rate estimated from the aqueous desorption study (Table 1) was used to fix one of the two parameters in the model. The predominant rate fraction (fast fraction for silt/clay, and slow fraction for coal-derived) that described the desorption rate of >90% of PAHs in the solid phase was used for the desorption model. The activation energy parameter was fitted by trial and error to obtain a desorption peak temperature matching the measured TPD peak. The result of model fitting to TPD response from silt/clay particles is shown in Figure 5. For ease in comparison, TPD

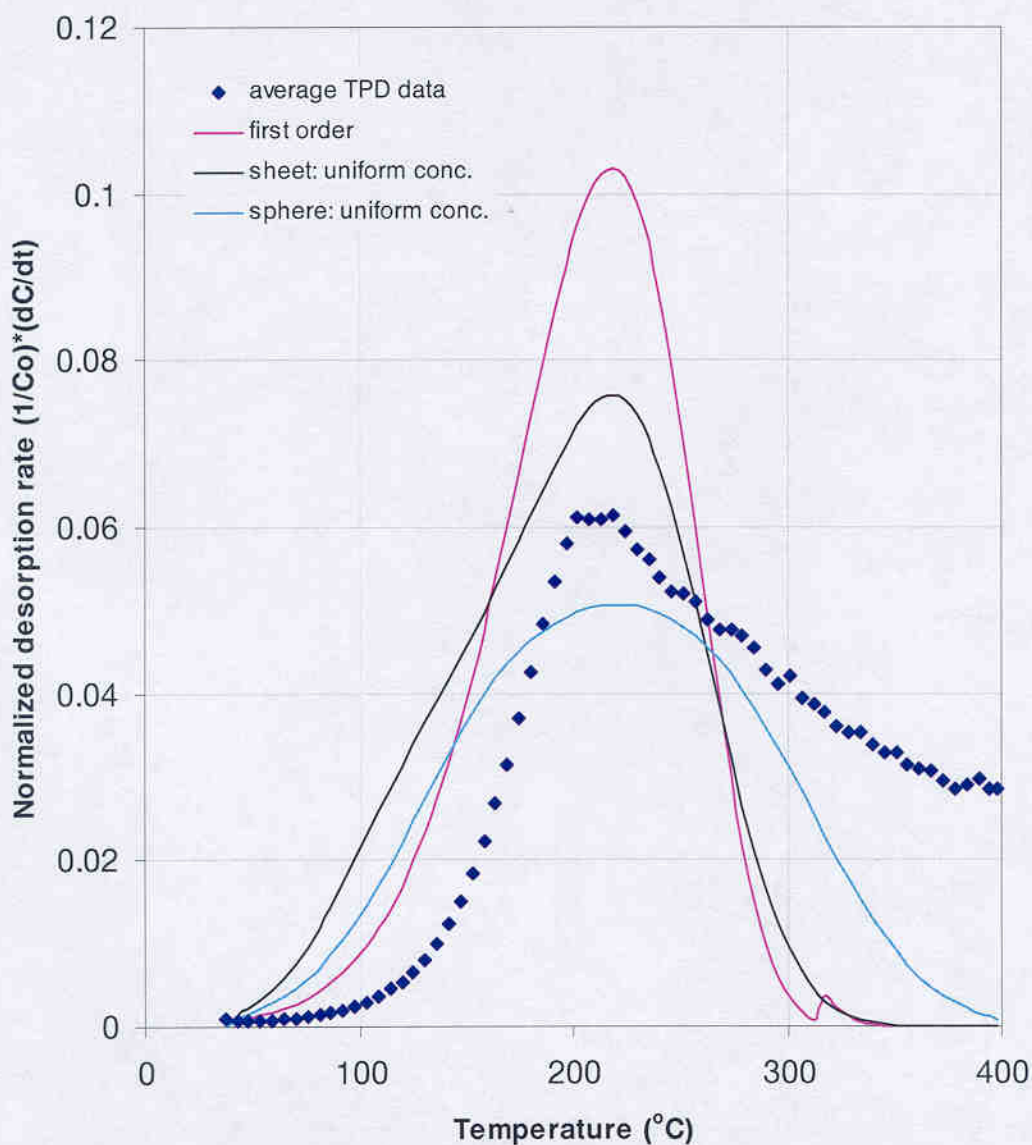


Figure 5. TPD-MS signal for PAH molecular weight 202 (fluoranthene and pyrene) and prediction based on activated first order and two activated diffusion models.

data and model simulations are presented as normalized desorption rates obtained by dividing desorption rates by initial PAH concentrations, which is the same as the total area under the desorption rate curve with time units in the x-axis. All three models provide a reasonable simulation of the peak temperature with estimated activation energy values ranging from 30-41 kJ/mol. Such low values of desorption activation energy are expected for sorption of PAHs on mineral surfaces and humic matter coated surfaces. However, the shapes of the simulated TPD response differ and do not match well with the data. One reason for the difference is the distorted nature of the TPD data for silt/clay particles, which may be due in part to the relatively low signal, and possible pyrolysis of natural organic matter on clay.

Table 2. Fitted values of desorption activation energies for silt/clay and coal-derived particles in the sediment.

	silt/clay (kJ/mol)	coal-derived (kJ/mol)
First order	41	135
Sheet diffusion	35	119
spherical diffusion: uniform	30	116
spherical diffusion: non-uniform		112

Coal-derived particles. The results of fitting the four desorption models to the TPD-MS data for coal-derived particles are shown in Figure 6. All four desorption kinetics models provided high activation energy values ranging between 112-135 kJ/mole. Such high activation energies are expected for PAH sorption on polymeric organic matter such as coal. Carroll et al. (11) reported an activation energy of 193 kJ/mol for the desorption of PCBs from condensed soil organic matter. Thus, based on all four model fits to fixed temperature desorption data and TPD-MS data, desorption of PAH MW202 from silt/clay particles is associated with low activation energies (30-41 kJ/mol) compared to coal-derived particles which are associated with high activation energies (110-135 kJ/mol).

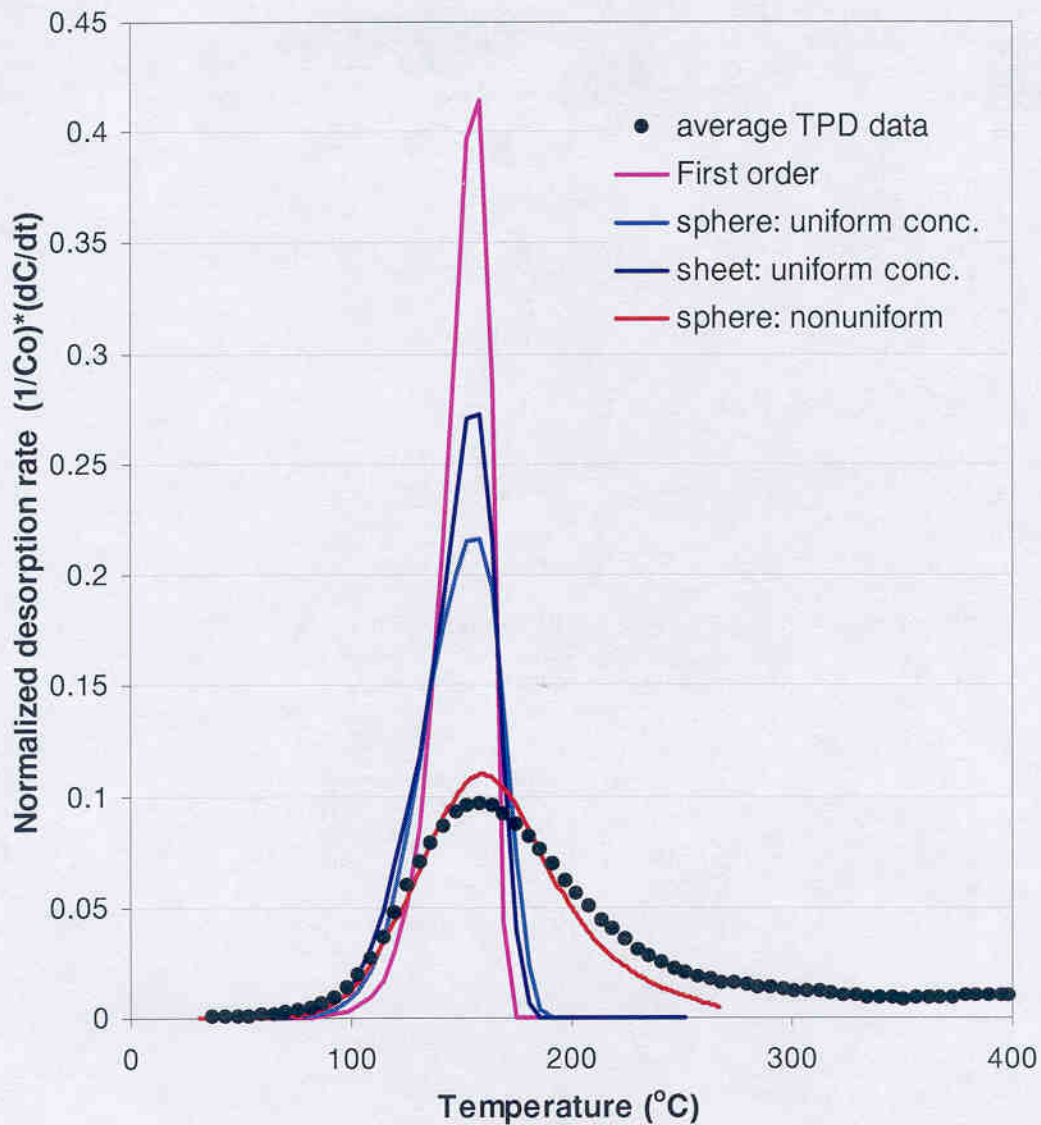


Figure 6. TPD-MS signal for PAH molecular weight 202 (fluoranthene and pyrene) and prediction based on activated first order model and three activated diffusion models.

All four desorption models appeared to fit the observed peak temperature of the TPD profile for coal-derived particles reasonably well, giving similar values of activation energies. However, there were major differences in the desorption rate profile. The first three models simulated a very narrow peak with a sharp tailing edge of the TPD response. In contrast, the measured TPD data showed a much wider peak with a slowly reducing tail. Only the spherical diffusion model with a nonuniform initial PAH concentration appeared to

simulate the shape of TPD-MS profile well. The nonuniform initial concentration profile for this model was created based on a simulated absorption process whereby the outer regions of the spherical particle sorbed high concentrations of PAHs as shown in Figure 7 such that at room temperature, the desorption rate matches the room temperature desorption data. During room temperature desorption tests only a small fraction of the sorbed PAHs are released over a desorption time of 100 days. Based on the simulated results, the depth of penetration of PAHs in the coal particles is in the order of 3-4 microns which is a small fraction of the particle radius. This observation agrees with our earlier direct measurement of internal PAH profile of coal-derived particles from Milwaukee harbor sediments where we concluded that the PAHs were located within the outer 0-5 micron layer of coal-derived particles (8).

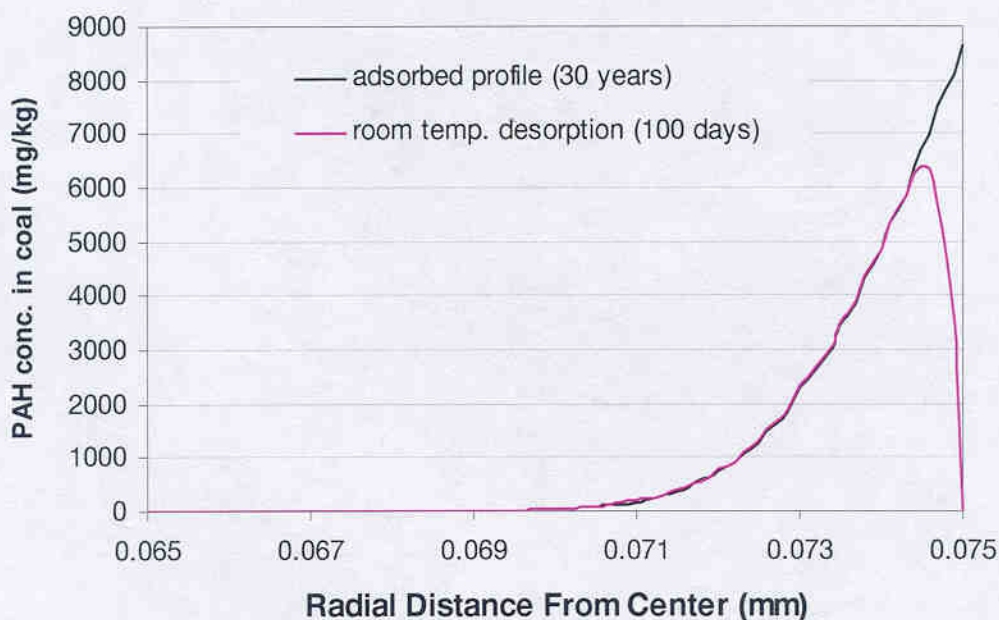


Figure 7. Simulated PAH molecular weight 202 concentration profile within a coal particle before and after 100-day aqueous desorption experiment.

The modeling revealed that during the TPD process, PAHs that had accumulated on the outer regions of the spherical particle also diffuse increasingly towards the interior because the diffusivity increases by several orders of magnitude with the increase in temperature. This effect is illustrated in Figure 8 which shows the predicted internal PAH concentration profile during a TPD experiment. As the temperature is increased, PAHs in the outer layers of the spherical particle are desorbed out. However, PAHs in the inner layers

continue to diffuse inwards due to the negative concentration gradient toward the interior of the particle as well. This results in a slowdown of the overall release of PAHs out of the particle, and produces the distinctively broader TPD peak and slow release tail of the TPD simulation. Thus, among the four models tested, it appears that the desorption of PAHs from sediment coal-derived particles is best described by a diffusion model wherein the initial concentration of PAHs is localized within the outer few micron layers of a sorbent particle.

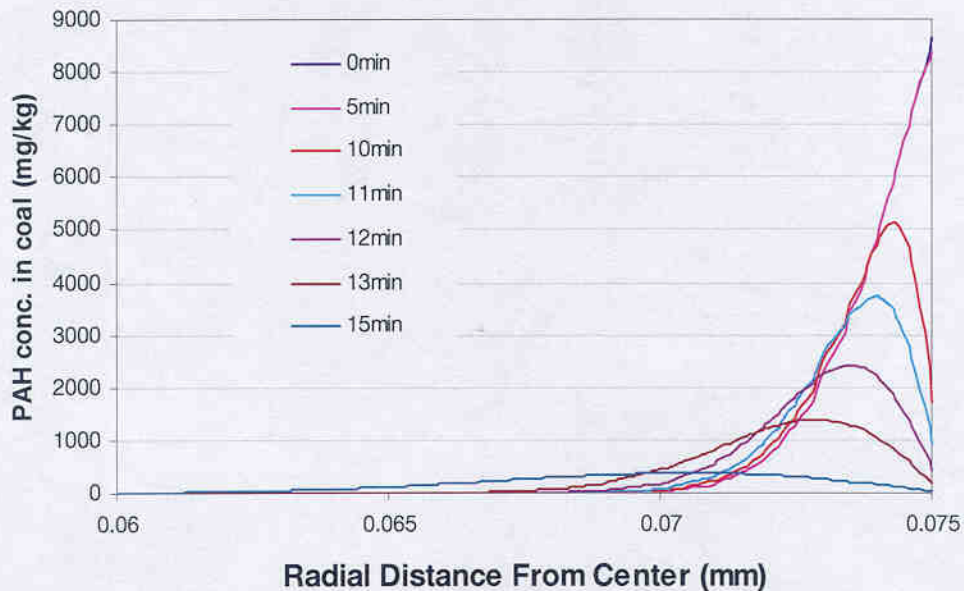


Figure 8. Simulated PAH molecular weight 202 concentration profile within a coal particle during a thermal program desorption experiment showing inward diffusion of PAHs.

We have demonstrated for Milwaukee Harbor sediment that PAHs associated with silt/clay particles desorb faster at room temperature and are characterized by low desorption activation energies; whereas PAHs associated with coal-derived material desorb at a much slower rate at room temperature and are characterized by high desorption activation energies. During TPD experiments, PAHs from coal-derived particles are released faster compared to PAHs on silt/clay particles. This is due to the high desorption activation energy, resulting in the diffusivity of PAHs in coal-derived particles increasing much faster with temperature than for PAHs sorbed on silt/clay particles. This analysis explains why PAHs sorbed on the outer regions of sediment coal-derived particles may be much less available for desorption.

The high activation energy required for desorption makes PAHs on coal-derived material strongly bound and unavailable at ambient temperatures. PAHs associated with media having large activation energies may comprise the unavailable PAH fraction in these sediments, and these PAHs may pose less risk than PAHs in clay and silt fractions for which the activation energy for desorption is much less.

Acknowledgements

We acknowledge funding and technical support for this research from the U.S. Army Engineer Research Development Center (ERDC), and the Department of Defense through the Strategic Environmental Research and Development Program. We would like to thank Samuel Tucker and John S. Furey for their assistance with thermal program desorption measurements.

Literature Cited

- (1) Guerin, W. F.; Boyd, S. A. *Appl. and Environ. Microbiol* **1997**, *58*, 1504-1512.
- (2) Alexander, M. *Environ. Sci. Technol.* **1995**, *29*, 2713-2717.
- (3) Loehr, R. C.; Webster, M. T. *J. of hazardous materials* **1996**, *50*, 105-128.
- (4) Luthy, R. G.; Aiken, G. R.; Brusseau, M. L.; Cunningham, S. D.; Gschwend, P. M.; Pignatello, J. J.; Reinhard, M.; Traina, S.; Jr., W. J. W.; Westall, J. C. *Environ. Sci. Technol* **1997**, *31*, 3341-3347.
- (5) Pignatello, J. J.; Xing, B. *Environ. Sci. Technol.* **1996**, *30*, 1-11.
- (6) Brusseau, M. L.; Rao, P. S. C. *Crit Rev Environ Control* **1989**, *19*, 33-99.
- (7) Weber, W. J. J.; McGinley, P. M.; Katz, L. E. *Water Research* **1991**, *25*, 499-528.
- (8) Ghosh, U.; Luthy, R. G.; Gillette, J. S.; Zare, R. N. *Environ Sci Technol* **2000**, *34*, 1729-1736.
- (9) NRC *Contaminated Sediments in Ports and Waterways, Cleanup Strategies and Technologies*; National Research Council: Washington DC, 1997a.
- (10) Pignatello, J. J.; Ferrandino, F. J.; Huang, L. Q. *Environ. Sci. Technol.* **1993**, *27*, 1263-1271.
- (11) Carroll, K. M.; Harkness, M. R.; Bracco, A. A.; Balcarel, R. R. *Environ. Sci. Technol.* **1994**, *28*, 253-258.

- (12) Ball, W. P.; Roberts, P. V. *Environ Sci Technol* **1991**, *25*, 1237-1249.
- (13) Pedit, J. A.; Miller, C. T. *Environ Sci Technol* **1995**, *29*, 1766-1772.
- (14) Wu, S.; Gschwend, P. M. *Water Resources Research* **1988**, *24*, 1373-1383.
- (15) Gong, Y.; Depinto, J. V. *Water Research* **1988**, *32*, 2518-2532.
- (16) Talley, J. W.; Ghosh, U.; Tucker, S. G.; Furey, J. S.; Luthy, R. G. *Submitted to Environ Sci Technol*. **2000**.
- (17) Cussler, E. L. *Diffusion Mass Transfer in Fluid Systems*; Cambridge University Press: New York, 1995.
- (18) TenHulscher, T. E. M.; Cornelissen, G. *Chemosphere* **1996**, *32*, 609-626.
- (19) Cornelissen, G.; Van Noort, P. C. M.; Govers, A. J. *Environ. Toxicol. Chem.* **1997**, *16*, 1351-1357.
- (20) Gorbaty, M. L. *Fuel* **1994**, *73*, 1819-1828.
- (21) Sakurovs, R. *Energy & Fuels* **1998**, *12*, 631-636.
- (22) Pilorz, K.; Bjorklund, E.; Bowadt, S.; Mathiasson, L.; Hawthorne, S. *Environ Sci Technol* **1999**, *33*, 2204-2212.
- (23) Cornelissen, G.; Van Noort, P. C. M.; Govers, H. A. J. *Environmental Science and Technology* **1998**, *32*, 3124-3131.
- (24) Crank, J. *The Mathematics of Diffusion*; Oxford Science Publisher: Oxford, 1975.
- (25) Bowman, D. W.; Brannon, J. M.; Batterman, S. A. *Proceedings of the 11th US Army Corps of Engineers Waterways Experiment Station Seminar*, 1996.
- (26) Bowman, D. W.; U.S. Army Engineer District: Detroit, 1999.
- (27) Pignatello, J. J. *Environ. Toxicol. Chem.* **1990**, *9*, 1107-1126.
- (28) Ghosh, U.; Weber, A. S.; Jensen, J. N.; Smith, J. R. *J. of Soil Contamination* **1999**, *8*, 593-613.
- (29) Glueckauf, E.; Coates, J. I. *Journal of Chemical Society* **1947**, *II*, 1315-1321.
- (30) Young, D. F.; Ball, W. P. *Water Resources Research* **1995**, *31*, 2181-2192.
- (31) Brusseau, M. L.; Jessup, R. E.; Rao, P. S. C. *Environ Sci Technol* **1991**, *25*, 134-142.

SECTION 6

Succession of Phenotypic, Genotypic and Metabolic Community Characteristics During Bioslurry Treatment of PAH-Contaminated Sediments*

Abstract

This work applied microbial ecology techniques to assess the capability of indigenous microorganisms to degrade polycyclic aromatic hydrocarbons (PAHs) in dredged harbor sediment. Dredged materials from the Milwaukee Confined Disposal Facility (CFD) were collected and homogenized to provide sufficient sample for four month bioslurry treatment testing and for PAH analyses on whole sediment. Microbial ecology testing used polar lipid fatty acid (PLFA) analyses, DNA procedures, and radiolabel microcosm studies.

Chemical analyses indicated that total PAH concentrations declined by 52% as a result of the bioslurry treatment, with individual PAHs showing reductions as great as 75% (i.e., acenaphthene and fluorene). Mineralization rates for each of the PAHs examined were greatest at times one month and two months, corresponding to the greatest biomass levels and the introduction of nutrients. The observed rates of ^{14}C -PAH mineralization in the microcosm tests generally increased in the order of benzo(a)pyrene < chrysene < pyrene < phenanthrene.

The PLFA characterization identified the level of biomass present in the sediment and general information about the microbial community structure. Ester-linked phospholipid fatty acid analysis revealed a 3-fold increase in microbial biomass and a shifting microbial community structure with the observed decrease in total PAH concentration. The DNA analysis was utilized to target the presence of select genes known to be present during active PAH degradation. Nucleic acid analyses revealed that copies of genes encoding PAH-degrading enzymes (extradiol dioxygenases, hydroxylases and meta-cleavage enzymes)

*David B. Ringelberg¹, Jeffrey W. Talley¹, Edward J. Perkins¹, Samuel G. Tucker¹, Richard G. Luthy², Edward J. Bouwer³, Herbert L. Fredrickson¹

¹Environmental Laboratory, U.S. Army Engineer Research and Development Center, Vicksburg, MS 39180

²Department of Civil and Environmental Engineering, Stanford University, Stanford, CA 94305-4020

³Department of Geography and Environmental Engineering, Johns Hopkins University, Baltimore, MD 21218

increased by as much as four orders of magnitude during the bioslurry treatment with the shift in gene copy numbers correlating with shifts in microbial community structure and PAH reduction.

The significant findings of this work were that changes in PAH levels during bioslurry treatment were related to fluctuation in total microbial community biomass, changes in potential rates of ^{14}C -PAH mineralization, dynamics of PLFA-defined microbial taxa, and changes in genetic catabolic potential. This correlation suggests phenotype and genetic potentials of the extant microbiota can be used as biomarkers to assess the intrinsic biodegradative potential of the sediment. Currently, laboratory studies are routinely performed to provide this information. The combination of microbial techniques reported here could minimize the future need for extensive laboratory treatability studies resulting in more timely and cost-effective treatment assessment

Introduction

Polycyclic aromatic hydrocarbons (PAHs) are frequently encountered pollutants in nature, and are often associated with the sediments found in navigation channels. Since navigation channels require continual maintenance through dredging, handling of contaminated materials is an often-occurring problem. It is estimated that approximately 10% of these dredged materials are impacted with organic and inorganic contaminants (1). Current treatment technologies do not allow for the economical disposal and treatment of sediments for their reuse as reclaimed soil. Bioremediation may fulfill this need (2), but in order for bioremediation to work efficiently and successfully we need to learn about the interaction between microbial community and biodegradation.

Microbiological processes may reduce hydrocarbon concentrations in sediments to levels that no longer pose an unacceptable risk to the environment or human health (3). PAHs naturally occur in the environment resulting in ample opportunity for prokaryotes to develop the catabolic enzyme systems necessary to use PAHs as carbon and energy sources. The microbial biodegradation of 2- and 3- ring PAHs has been extensively reviewed (4-7). More recently, a variety of microorganisms have been isolated and shown to use PAHs with up to 4 rings as the sole source of carbon and energy (8). Although individual species of bacteria and bacterial consortia have been shown to metabolize PAHs in culture, identifying

such a potential in a community of microorganisms *in situ* is often far less apparent. Biodegrading organisms may or may not be the predominant species, which directly affects an ability to identify and quantify their presence. In addition, the physicochemical properties of the immediate environment can have a major influence on microbial physiology as well as contaminant bioavailability.

Contaminants can affect an indigenous microbial population resulting in an alteration in microbial community structure and/or function (9). To fully identify the nature of a contaminant's impact on an extant microbiota, a polyphasic approach that combines phenotypic and genotypic measurements is necessary. In 1998, Langworthy et al. (10) identified a phenotypic and genotypic adaptation within a freshwater sedimentary microbial community to elevated levels of PAHs. By combining the ester-linked polar lipid fatty acid analysis (PLFA) with the nucleic acid analyses, they were able to characterize shifts in the *in situ* microbial community structure as a result of PAH exposure and quantify a higher frequency of degradative gene expression in the more highly contaminated materials.

The analysis of ester-linked phospholipid fatty acids (PLFA) and their use in defining microbial community shifts in subsurface environments has a 20-year history (11). This quantitative technique, which examines cell membrane constituents, provides an estimate of the 'viable' microbial biomass (assuming rapid degradation of intact phospholipids upon cell death) as well as a 'fingerprint' of the *in situ* microbial community structure (12). Changes in individual PLFA and PLFA patterns can be measured over time and the effect of contaminant exposure on community composition quantified (13).

However, shifts in microbial community composition can also be induced by changes in other environmental factors such as temperature, pH, moisture content, nutrient levels, etc. One way to minimize misinterpretation of *in situ* microbial community shifts (by PLFA) is to tie these shifts to the production of genes related to the biodegradation of the target contaminants. This can be accomplished by use of a multiplex polymerase chain reaction (PCR) approach designed to determine the multiple numbers of biodegradative gene copies present in a single sample. Gene sequences are typically selected for their relationship to a particular biodegradation pathway or toward a general assessment of multiple biodegradative pathways. The identification of a gene sequence in a DNA extract does not, however,

indicate that the gene is being actively expressed. As Langworthy et al. (10) have demonstrated, the polyphasic approach toward the characterization of an extant microbiota can be exploited to assess the intrinsic biodegradation potential of contaminated media.

In this work we used PLFA and DNA analyses to track microbial community biomass and gene presence over time from untreated and biotreated PAH-contaminated sediments. Biotreatment of sixteen EPA priority pollutant PAHs was measured through CG/MS analyses from a combination of radiolabeled microcosm and bioslurry tests. The reduction in PAH levels was correlated with fluctuation in total microbial community biomass, changes in potential rates of ^{14}C -PAH mineralization, dynamics of PLFA-defined microbial taxa, and changes in genetic catabolic potential.

Materials and Methods

Study material

The sediment used in this study was obtained from the Jones Island Confined Disposal Facility (CDF) (commonly known as the Milwaukee CDF) operated by the Milwaukee Harbor Port Authority. It is a 44-acre CDF located in the South Milwaukee Harbor. The CDF was constructed in 1975 and has a maximum thickness of 10 meters. It serves as a disposal facility for maintenance-dredged materials unsuitable for open-lake disposal (14). These sediments originated from the Milwaukee Harbor and Port Washington Harbor, located 25 miles north of Milwaukee. These sediments originated from the Milwaukee harbor during the process of dredging to maintain waterway navigability. The sediment was mixed, sieved using a 2 mm sieve, and stored in 55-gallon drums at 4°C before use in bioslurry studies.

Bioslurry Reactors

The bioslurry reactor study consisted of six reactors operated for four months. Two reactors were controls (anaerobic and poisoned), and four reactors were active (aerobic) reactors. Each bioreactor received 5309 grams (wet weight) of dredged material. The Milwaukee CDF dredged material was 56.5% sediment (by weight) and 43.5% water. Each reactor had 1.5 liters of sediment (30% by volume) and 3.5 liters (70% by volume) of a modified Stanier's Basal Media (15). The media did not contain any carbon source. Each reactor contained two impellers mounted to a shaft to aid in mixing. The bottom impeller

was a 3.8" A-310 Impeller with 5/16" bore from Lightnin (part # 809411PSP). This impeller was positioned about an inch from the bottom of the reactor. The top impeller was similar in design and was mounted about three inches above the lower impeller. Each reactor had three diffuser stones in the bottom that bubbled either argon (control reactors) or air (aerobic reactors). The gas was fed from compressed gas cylinders and passed through double charcoal filters before entering the bioreactors. The reactors were continuously stirred at 350 revolutions per minute (rpm). Each reactor was allowed to mix overnight before conducting initial sampling. All of the reactors were vented to a fume hood.

The anaerobic reactors were poisoned with sodium azide and mercuric chloride. Each reactor was dosed with 500 ppm of both compounds. Initial biomass analyses indicated the poisoning was not effective in killing the microbial community for longer than a few days. Thus another 500 ppm of both compounds was added 18 days into the experiment. The microbial community was able to rebound within the week, so an additional 1000 ppm of each compound was added to each anaerobic reactor. Finally a few days later, and every three weeks afterward, an additional 750 ppm of each compound was used. This successfully attenuated the microorganisms and maintained that attenuation for the anaerobic controls.

The reactors were tested for sterility at each sampling event and several times during the first month by streaking the slurry onto a nutrient agar plate. Four plates were streaked. There was a control with nothing on the plate, two plates streaked, one for each anaerobic control reactor, and a plate streaked with sediment from an aerobic reactor. Each plate was incubated at 30.0°C and checked at 24, 48, and 72 hours. No growth after 72 hours was a positive indication of successfully killed microorganisms.

The bioreactors were tested on a regular daily schedule for pH, dissolved oxygen, oxidation-reduction potential, and temperature. Bioslurry water was collected initially every two days for nitrate and phosphate analysis. After the initial 4-week period, nitrate and phosphate measurements were recorded weekly. Carbon: nitrogen: phosphorus ratios were maintained at 100:10:1. The carbon content was based on the sediment TOC. TOC at the beginning of the study ranged from 4,000 to 38,000 mg/kg for the active reactors. Dissolved oxygen was maintained in the range of 8 to 9 mg/L for the aerobic reactors and 0 mg/L for the control anaerobic reactors. pH was maintained at or near neutral conditions, pH \approx 7.0.

Phosphate was added from a stock solution (1M Na₂HPO₄ and 1M KH₂PO₄, 200 mL total volume) to the active reactors 4 weeks into the study and every 2 to 3 weeks thereafter to minimize the possibility of nutrient limitation. Sediment was initially analyzed for PAH concentrations. Once the reactors were loaded and operated for 18 hours (T_{0.025} month), they were sampled for PLFA and DNA analyses. Thereafter the reactors were sampled once a month for a total of 4 months (T₁ to T₄). Approximately 22 g (wet weight) of slurry material was captured at each sampling event for microbiological studies. Sub-samples were removed and placed into sterile screw-top containers for centrifugation at 5000g for 12min. PAH, radiometric, and biochemical assays were then performed on the palletized material.

Contaminant Chemistry

An initial study was performed to compare the efficiency of Soxhlet extraction (EPA Method 3540), Accelerated Solvent Extraction (EPA Method 3454A) and Super Critical Fluid Extraction (EPA Method 3561). This study utilized ten different untreated Milwaukee Harbor sediment samples for extraction and GC/MS analyses. These tests were performed in triplicate. Based upon this initial evaluation, it was determined that Soxhlet extraction provided the best reliability. Initial PAH concentrations (T_i) were determined by analysis of four replicates from the sieved and mixed 55-gallon drum. Samples from each bioslurry reactor were collected at T_{0.025}, T₁, T₂, T₃, and T₄ months. These samples underwent Soxhlet extraction and GC/MS analyses for determination of PAH concentrations according to EPA method 3540.

Radio-respirometry

Two grams (wet weight) of slurry material were placed into 15 ml teflon-lined screw cap test tubes to which was added 2.7 mL of Stanier's Basal media and a tracer amount of the ¹⁴C-labeled substrate. Triplicate microcosms were spiked with 20,000 DPM of phenanthrene-9-¹⁴C (>95%) at a specific activity of 46.9 mCi/mmole (Sigma Chemical Co, St Louis, MO), pyrene-4,5,9,10-¹⁴C (>95%) at a specific activity of 58.7 mCi/mmole (Sigma Chemical Co, St Louis, MO), chrysene-5,6,11,12-¹⁴C (98%) at a specific activity of 47.4 mCi/mmole (ChemSyn Laboratories, Lenexa, KA), benzo[a]pyrene-7-¹⁴C (>95%) at a specific activity of 16.2 mCi/mmole (Sigma Chemical Co, St Louis, MO) or acetic acid-1,2-¹⁴C (>95%) at a specific activity of 116 mCi/mmole (ICN Pharmaceuticals, Inc., Costa Mesa,

CA). A modified version of the method described by Fulthorpe et al. (16) was then used to assess microbial activity.

Glass fiber filters (Whatman, Maidstone, UK), 10 mm diameter, saturated in 1M barium hydroxide and placed into the caps of screw top test tubes, were used to trap evolved $^{14}\text{CO}_2$. Test tubes were incubated at room temperature on a tube roller inclined at 45° and rotated at 10 rpm. Filters were collected and replaced once a day for the first week and 3 times a week for the remainder of incubation. Tube headspace was purged with filtered air (0.2 μm nylon filter, Waters, Maidstone, UK) at each sampling period. Filters were placed into 15 ml of scintillation cocktail (Ultima Gold, Packard Instruments Co., Downers Grove, IL) and counted with a top count microplate scintillation counter (Packard Instrument Co., Downers Grove, IL). Filters were counted twice, and counts were corrected for background and counting efficiency using the external standard method described by the manufacturer. Activity was then expressed, as a ratio with that of labeled PAH initially added.

Ester-Linked Polar Lipid Fatty Acid (PLFA) Analyses

Polar lipid fatty acid analysis has been detailed elsewhere (11). Briefly, 2 g wet weight of slurry material was extracted for 3 hours at room temperature in 6 ml of a mixture of dichloromethane:methanol:water (1:2:0.8, v:v:v). The total lipid extractant was then partitioned against water and taken to dryness under N_2 . Amino-propyl solid phase extraction columns (Supelco, Bellefonte, PA) were used to separate the total lipid into neutral, glyco- and polar lipid fractions (17). Phospholipid fatty acid methyl esters (from the polar lipid fraction) were prepared for gas chromatography/mass spectrometry (GC/MS) by mild alkaline methanolic transesterification. The resulting phospholipid fatty acid methyl esters were dissolved in hexane containing methyl nonadecanoate ($50 \text{ pmol } \mu\text{L}^{-1}$) as an internal standard and analyzed using a gas chromatograph equipped with a 50m x 0.25mm (ID) DB-1 capillary column (0.1 μm film thickness, J&W Scientific, Folsom, CA) and a flame ionization detector. Peak identities were confirmed using a gas chromatograph-mass selective detector (Hewlett Packard GC6890-5973 MSD) with electron impact ionization at 70eV. Areas under the peaks were converted to concentrations, summed and then normalized to the gram weight extracted for biomass determinations. For community comparisons, the percent contribution of each peak was calculated and then normalized using an arcsine transformation.

DNA isolation from bioslurry reactors

Total DNA was isolated from triplicate 500 mg slurry samples using a mini bead beater system as described (18), and purified using Fast DNA SPIN Kit as described by the vendor (FastPrep7 Instrument FP120; BIO 101, Vista, CA). Total DNA was suspended in 50 ul of Molecular Biology Grade H₂O (Five prime-Three prime, WI) and stored at -20 °C for further analysis.

Primers and targets used in multiplex PCR

Details on the multiplex PCR assay and primers used are being published elsewhere (19). Briefly, the primers target the following genes: 1. Toluene dioxygenase (*todC1*) from *Pseudomonas putida* F1 (forward primer todC1F: GCGAGATAGAAGCGCTCTTG, reverse primer todC1R: GTATTGATACCTGGGAGGAAG with an expected product size of 924 bp; (20). 2. Toluene-4-monooxygenase (*tmoA*) from *P. mendocina* KR1 (forward primer tmoAF: GCTATGTTACCGAAGAGCAGC, reverse primer tmoAR: GGAATAGATCCCAGTACCAGG with an expected product size of 900 bp; (20). 3. Alkane hydroxylase (*alkB*) from *Pseudomonas oleovorans* TF4-1L (forward primer alkB-f: TGGCCGGCTACTCCGATGATCGGAATCTGG, reverse primer alkB-r: CGCGTGGTGATCCGAGTGCCGCTGAAGGTG with an expected product size of 869 bp ; (21). 4. Biphenyl dioxygenases (forward primer bph-f: TGCAGCTACCACGGCTGGGCCTA, reverse primer bph-r2: GCNGCRAAYTTCCARTTRCANGG with an expected product size of 295bp; (19). 5. Catechol 2,3-oxygenase (*xylE*) from *Pseudomonas putida* mt-2 pWW0 (forward primer c2303f: CAAGGCCACGACGTGGCNTT, reverse primer c2303r:CGGTTACCGGACGGGTCGAAGAAGT with an expected product size of 202 bp; (19) and 6. Naphthalene dioxygenase and 2-nitrotoluene dioxygenase (*ntdAc*) from *Pseudomonas* sp. JS42 (forward primer 2NT-F: TTTGTGTGCGGYTACCACGGNTGGGG, reverse primer 2NT-R: TCTCACCTACAAAGTTTTCCGCAAARSCTTCCAGTT with an expected product size of 321 bp; (19).

Multiplex PCR reaction conditions

Each sub-sample was analyzed by multiplex PCR in four dilutions (1/1, 1/10, 1/100, 1/1000). Five µl of each dilution was then added to each PCR reaction, so that the initial sample represents DNA from 5 mg of sediment.

PCR reactions were composed of: 50 mM KCl, 10 mM Tris-HCL (pH 8.3), 2.5 mM MgCl₂, 5% dimethylsulfoxide, 500 mg ml⁻¹ bovine serum albumin, 200 μM of each deoxynucleoside triphosphate, 8 picomoles of each primer, 0.8 U of AmpliTaq Gold DNA polymerase (PE Biosystems, Foster City, CA) and 5 μl bioslurry DNA extract for a final reaction volume of 20 μl. PCR reactions were amplified in 200 μl thin walled tubes using a PTC-200 thermal cycler (M J Research, Watertown MA). The thermal profile for amplification was 15 minutes denaturation at 95 °C followed by 35 cycles of 20 sec denaturation at 94 °C, one minute annealing at 60 °C, and four minutes of extension at 72 °C. PCRs were finished by 10 minutes of extension at 72 °C.

Twenty μl PCR reactions were precipitated with 5 μl 10M ammonium acetate and 75 μl of ethanol. DNA was recovered by centrifugation at 14000 x g in a micro-centrifuge. DNA pellets were washed with 70% ethanol to remove residual salts. Pellets were then re-suspended into 2 μl of SYBR Green I loading dye, which contained 17 mg ml⁻¹ Blue Dextran (Sigma Chemical Co., St. Louis, MO), 8 mM EDTA and a 1/1000 dilution of SYBR Green I (Molecular Probes, Beaverton OR). Molecular weights of the PCR products were estimated by comparison to the Genescan 2500 ROX size standard (PE Biosystems, Foster City, CA), which was stained in SYBR Green I loading dye. DNA was analyzed on a 5% Long Ranger Hydrolink nondenaturing gel (FMC BioProducts, Rockland, ME) using an ABI 377 automated DNA sequencer (PE Biosystems, Foster City, CA). 12 cm long and 0.4mm thick gels and running conditions were performed using standard ABI protocols (PE Biosystems, Foster City, CA).

Determination of minimum detectable gene copy number

A band was scored as either present or absent at each size (bp length) and dilution (1-1/10,000). Each target gene had a specific-bp length range. A band was scored as being significant if at least 2 of the 3 PCR amplifications of replicate sub-samples showed the band. For each band, the point of dilution to extinction was determined. For example, if a band was diluted so no product was visible in dilutions greater than 1/100, the band was assigned a score of 100. This was derived from the fact that at least 100 copies of the target must be present for detection at a dilution of 1/100. If no band was visible at the 1/1 dilution, the sample was scored a 0. If no band was visible at the 1/10 dilution, the sample was scored a 1.

If no band was apparent at a dilution greater than 1/10, the sample was scored a 10. It was assumed that the slurry samples would have similar effects upon gene detection limits. Therefore, the minimum detectable gene copy number was determined to be equal to the maximum dilution factor at which the gene was detected in two or more replicates per μl of sample DNA extract times the total μl of slurry DNA extract per gram of sample slurry.

Statistical Analyses

Differences between treatments were assessed with a Tukey's honest significant difference test. Correlations between contaminant and PLFA percentages and gene copy numbers were evaluated using Spearman rank order and canonical correlation analyses. Relationships among variables within a data set were examined by hierarchical cluster analysis (Wards method). All examinations were performed with the Statistica software package, version 5.0 (Statsoft, Inc., Tulsa, OK).

Results

Extractable PAH

Total extractable PAH concentrations decreased 17% in the control reactors from an average T_i month concentration of $115 \pm 5.7 \text{ mg kg}^{-1}$ to $95 \pm 3.8 \text{ mg kg}^{-1}$ at T_4 , with the greatest reductions occurring in MW 124-143 (55%), MW 252 (27%) and MW 272-278 (28%). Reductions occurred in MW 154-178 and MW 202-228, but to a lesser degree. Previous work by Johnson et al. (22) on the same sediment using the same reactors under anaerobic conditions reported similar results. Johnson estimated that a 30% disappearance in the two-ring compounds (naphthalene and 2-methylnaphthalene) was due to volatilization, but that much of the other reductions were due to bioremediation (22). The initial difficulty in killing the microorganisms in the control reactors may have accounted for the small reductions in PAHs in the control reactors.

The active reactors showed a net loss in total extractable PAH of approximately 52%. PAH concentrations decreased from the T_i average of $115 \pm 5.7 \text{ mg kg}^{-1}$ to $56 \pm 3.8 \text{ mg kg}^{-1}$ at $T=4$ month (Figure 1). The decline in total PAH was statistically significant at an alpha of 0.05. The greatest loss of 67%, occurred in the 154-178 MW compounds (acenaphthene, fluorene, phenanthrene, and anthracene), followed by 52% loss in the 202-228 MW compounds (fluoranthene, pyrene, chrysene and benzo[a]anthracene), 48% loss in the 252

MW compounds (benzo(b)fluoranthene, benzo(k)fluoranthene, and benzo(a)pyrene), 26% loss in the 276-278 MW compounds (benzo(g,h,i)perylene, indeno(1,2,3-c,d)pyrene, and dibenzo(a,h)anthracene, (Table 1).

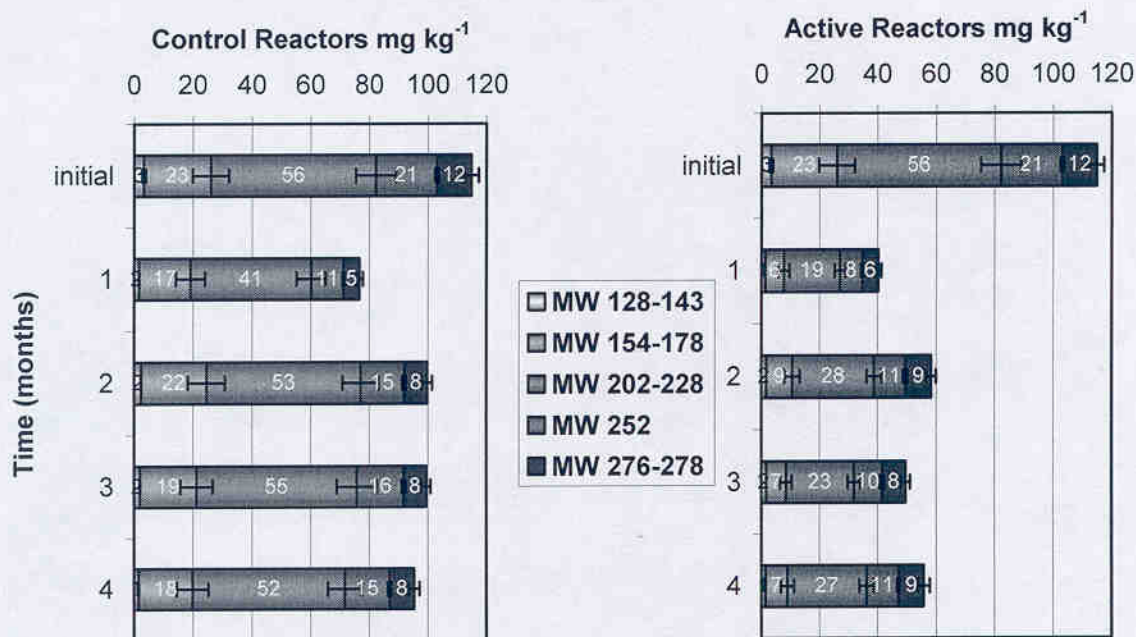


Figure 1. Average PAH concentrations in control (n=2) and active (n=3) bioslurry reactors categorized by molecular weight (MW) as follows: MW 128 (Naph), MW154-178 (AceNaph, Fluor, Phen and Anth), MW 202-228 (Pyr, Fluoranth, Chry and B(a)A), MW 252 (B(b)F, B(k)F and B(a)P) and MW 276 (Indeno, and B(g,h,I)P). PAH abbreviations are defined in Table 2. Error bars indicate ± 1 standard deviation.

Table 1. Average loss or gain (as a percentage of T_i) in extractable PAH from continuously stirred bioreactors.

	Reactor			
	Control		Active	
	% loss	(p) ¹	% loss	(p) ¹
MW 128-143	55	(.000)	55	(.000)
MW 154-178	19	(.000)	67	(.000)
MW 202-228	8	(.422)	52	(.000)
MW 252	27	(.000)	48	(.000)
MW 276-278	28	(.003)	26	(.002)
Total	17	(.002)	52	(.000)

¹ p-value ($\alpha = .05$) calculated using a Tukey HSD post hoc analysis of a one-way ANOVA

Microbial Biomass and Community Composition (PLFA)

Microbial biomass in the control reactors was always less than that in the active reactors (Figure 2). Active reactor biomass was significantly greater (LSD test at $\alpha = 0.10$) than that measured in the control reactors at 1 month through 3 months of the incubation period. Microbial biomass in the active reactors also indicated a dynamic community, showing changes as a result of the nutrient addition. Yet, poisoning suppressed the community responsible for PAH degradation as shown by the dendrogram (Figure 3) of higher cluster analyses.

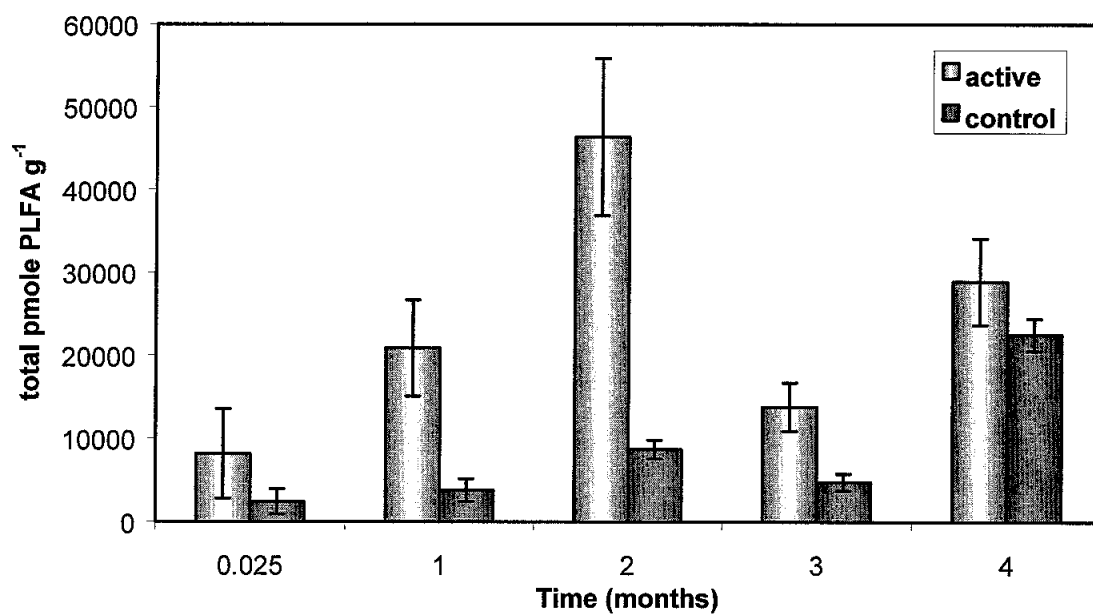


Figure 2. PLFA concentrations (pmole PLFA g⁻¹ sediment) in control and active bioslurry reactor sediments recovered monthly over a four month incubation period. Nutrients (1M Na₂HPO₄ and 1M KH₂PO₄) were added between the 1st and 2nd months of incubation at ~6 weeks. Error bars indicate ± 1 standard deviation.

Although biomass in the control reactors increased through four months of the study, hierarchical cluster analysis showed the microbial community composition of the control reactors to be very different from that of the active reactors at each time sampled (Figure 3A). Within treatment (active and control) differences in microbial community structure were also identifiable. Cluster groups were apparent for each time point sampled (T₁ month to T₄ months) within the active treatment. T_{0.025} month active reactors clustered with T_{0.025} month control reactors. Time points T₂ months, T₃ months and T₄ months from the control

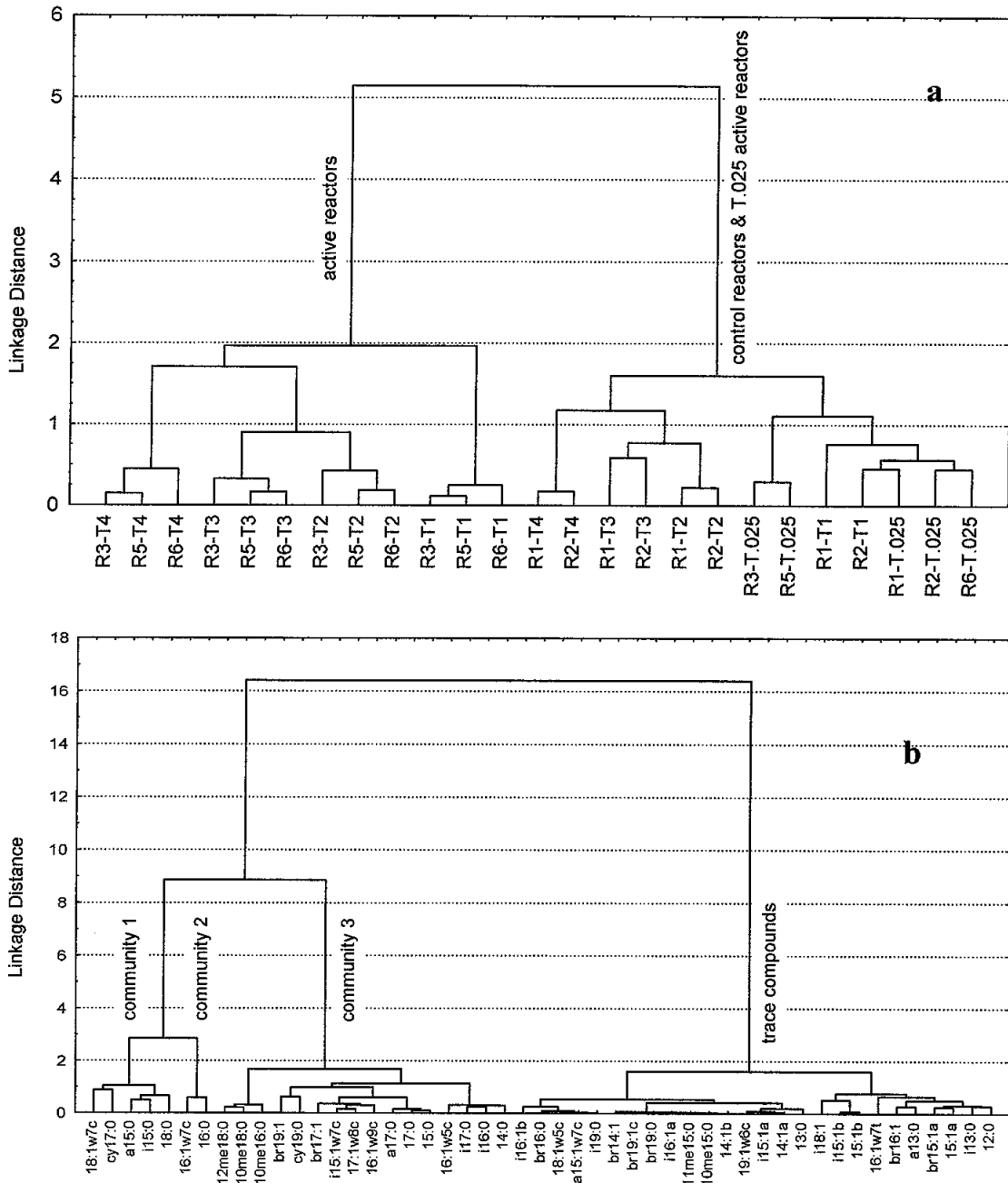


Figure 3. Dendrogram illustrations of the results of hierarchical cluster analyses of arcsine square root transformed PLFA mole percentages identified in control and active bioslurry reactor sediments. Panel A illustrates results when the algorithm (Ward's method) was run against variables (samples) and panel B when run against cases (PLFA from the active reactors only). Active reactor samples in Panel A are indicated by the prefixes R₃, R₅ and R₆ and control reactors by the prefixes R₁ and R₂. Samples taken at one month time intervals are indicated by the suffix T₁ to T₄. The T_{0.025} suffix indicates an initial analysis. The robustness of the identified clusters in both panels was verified by K-means analysis. Community types 1 to 3 are defined by a linkage distance of 2.0 or less.

reactors were distinguishable from the earlier time points. This result corresponds with the observed increase in biomass in these reactors, indicating that the poisoning was not 100% effective.

The data matrix used to generate the dendrogram provided in Figure 3a was transposed and used to indicate which PLFA co-varied across the active reactor samples. A k-means clustering algorithm was then used to define three discrete microbial communities (i.e., four PLFA cluster groups) (Figure 3b). Community 1 was comprised of 18:0, i15:0, a15:0, and cy17:0, which are indicative of both Gram-positive and Gram-negative bacteria. Community 2 included the PLFA 16:0, 16:1w7c, and 18:1w7c which are indicative of Gram-negative bacteria. Community 3 included 14:0, 15:0, 17:0, i16:0, i17:0, a17:0, 16:1w5c, 16:1w9c, 17:1w8c, cy19:0, i15:1w7c, i18:1, br17:1, br19:1, n16:1w7t, 10me16:0, 10me18:0, 10me18:0 and 12me18:0, which are indicative of Gram-positive and Gram-negative bacteria as well as actinomycetes and some fungi. The final cluster group comprised a number of trace compounds, the sum total of which never exceeded 6%. Biomass contributions from the three defined communities are illustrated in Figure 4. Community 1 remained relatively unchanged throughout the study period (a mixed community of Gram-positive and Gram-negative bacteria), community 2 showed a slight decline in relative abundance (a Gram-negative community) whereas community 3 showed a general increase (another mixed community also showing the presence of actinomycete PLFA biomarkers).

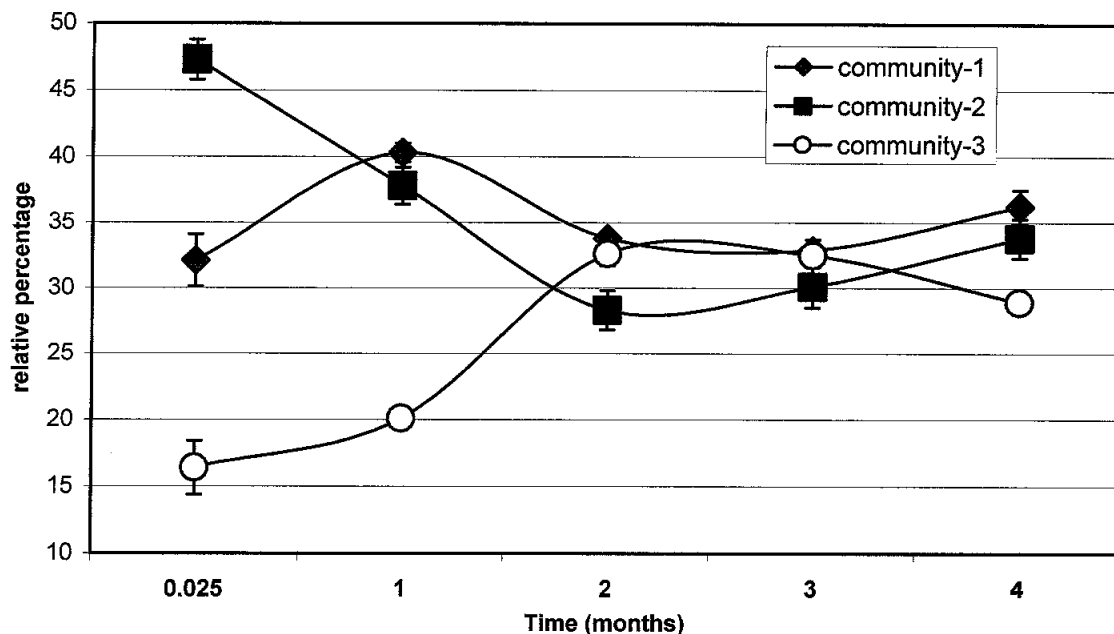


Figure 4. Average distribution of the community types defined in Figure 3 within the active bioslurry reactors throughout the four month incubation period. The relative percentage of each community type is derived from the sum total of the individual PLFA that make up the community.

Although polyunsaturated PLFA were detected, their contribution to the overall community dynamics in the active reactors was minimal (Table 2). Linoleic acid (18:2w6) was the predominant dienoic acid detected and eicosapentanoic acid (20:5w3) the predominant polyunsaturated fatty acid detected. Both of these acids are synthesized by a number of eukaryotes.

Table 2. Average mole percentages of individual polyunsaturated PLFA detected in the active bioslurry reactors.

PLFA	RT ¹	T _{0.025}	T ₁	T ₂	T ₃	T ₄
n16:2	18.83	0±0	0±0	0.3±0.1	0.1±0.1	0±0
n18:2	24.06	0±0	0±0	0.4±0.1	0.4±0.1	0±0
n18:2	24.19	0±0	0±0	0.3±0.1	0±0	0±0
n18:2w6	24.44	3.6±0.6	1.8±0.3	2.4±0.1	2.0±0.1	1.2±0.0
n20:4w6c	28.73	0±0	0±0	0.4±0.1	0.3±0.0	0±0
n20:5w3	28.87	1.1±1.1	0.4±0.3	0.2±0.0	0.5±0.1	0.6±0.2
n20:2w3	29.88	0±0	0±0	0.4±0.1	0±0	0±0
Total		4.76±1.6	2.2±0.1	4.3±0.5	3.2±0.2	1.8±0.2

¹ retention time in minutes

Mineralization Potentials (Radiorespirometry)

Potential rates of ^{14}C -PAH mineralization in the sediment slurries generally increased in the order of benzo(a)pyrene < chrysene < pyrene < phenanthrene (Figure 5). For T_4 months, chrysene mineralization rate exceeded that of pyrene. Mineralization rates for each of the PAHs examined were greatest at times T_1 month and T_2 months (Table 3), corresponding to the greatest biomass levels and the introduction of nutrients. Mineralization rates for phenanthrene, pyrene and chrysene never reached background levels over the 4-month incubation period. However, benzo(a)pyrene mineralization rates barely exceeded background levels. The low level of benzo(a)pyrene mineralization may have resulted from its toxicity to the microorganisms, its hydrophobicity, its tight binding to soil organic matter, and/or the lack of microorganisms with the metabolic pathways required for catabolism of

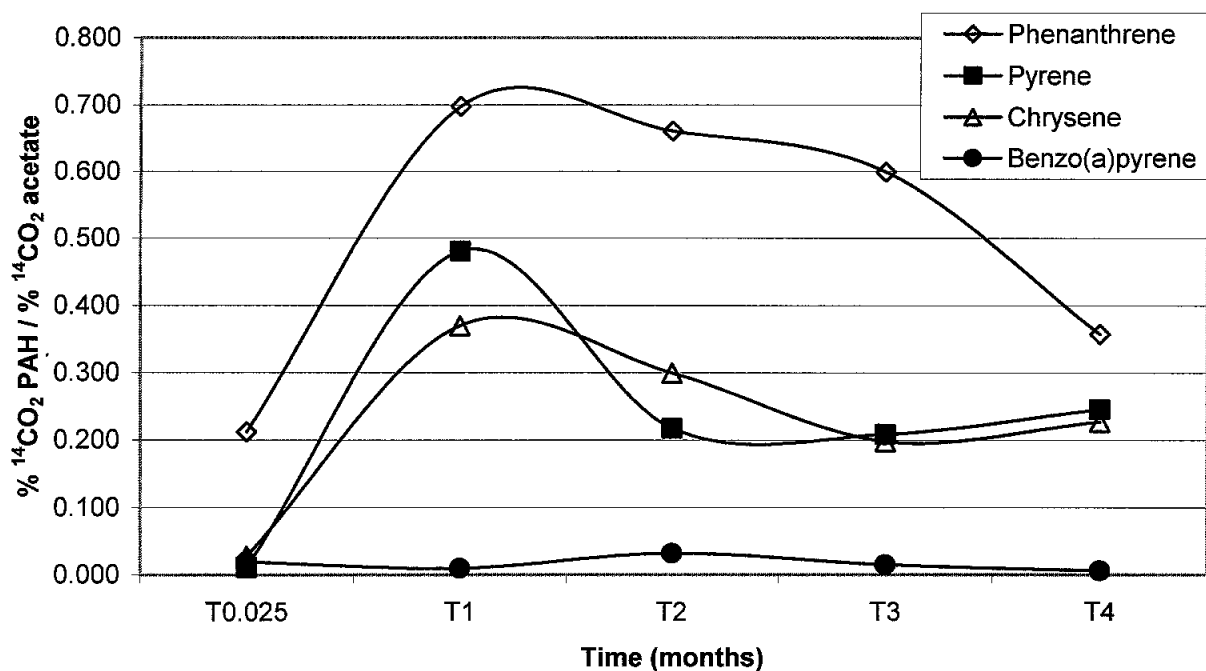


Figure 5. Mineralization of added radio-labeled ^{14}C -phenanthrene, ^{14}C -pyrene, ^{14}C -chrysene and ^{14}C -benzo[a]pyrene in respirometry microcosms amended with active bioslurry reactor sediments initially and at each of the four time points sampled. Mineralization extents (or cumulative percentage, relative to the spike of radio-label added) for the added PAH compounds were normalized to the mineralization extent recorded for added ^{14}C -acetate to account for fluctuations in microbial biomass over the time course.

organics comprised of multiple aromatic rings. Since total microbial biomass fluctuated over the incubation period, PAH mineralization rates were normalized to independent measures of ^{14}C -acetate mineralization (a Krebs' cycle intermediate) as shown in Figure 5.

Table 3. Average mineralization rates for ^{14}C labeled acetate, phenanthrene, pyrene, chrysene and benzo(a)pyrene in the active slurry reactors.

SUBSTRATE	TIME (MONTHS)				
	0.025	1	2	3	4
ACETATE	5.5±0.16	6.2±1.27	5.3±0.04	5.8±0.71	4.5±0.71
PHENANTHRENE	1.2±0.54	5.7±0.14	3.5±0.43	3.5±0.39	1.6±0.28
PYRENE	0.1±0.04	3.0±1.66	1.2±0.67	0.8±0.17	1.1±0.42
CHRYSENE	0.2±0.05	2.3±0.44	1.2±0.12	1.2±0.17	1.0±0.33
BENZO(A)PYRENE	0.1±0.03	0.1±0.04	0.1±0.04	0.1±0.04	0.0±0.02

¹ Values represent cumulative $^{14}\text{CO}_2$ represented as a percentage of the total ^{14}C -substrate added divided by 5 days of incubation

Genetic Catabolic Potential

Genes encoding enzymes associated with aromatic degradation – naphthalene dioxygenase, biphenyl dioxygenase, catechol 2,3-dioxygenase, toluene monooxygenase, and alkane hydroxylase - were present in the original soil in copy numbers below the detection limit of the assay (<1 gene copy per gram). Copy numbers for each of the genes assayed for increased to the maximum detectable number (10,000 copies) within the first and second months of incubation. To identify trends in the data, the log was taken of the total number of gene copies detected in each of the three active slurry reactors and plotted against the time sampled (Figure 6). Data below the 1 gene copy detection limit was plotted at 0.01. Three of the catabolic genes assayed, naphthalene dioxygenase, biphenyl dioxygenase and catechol 2,3-dioxygenase remained at the maximum detectable level for the duration of the study. The increase in copies of these genes corresponds with the increase in microbial biomass and phenanthrene, fluorene, and chrysene mineralization rates. In contrast, toluene monooxygenase and alkane hydroxylase decreased in gene copy numbers to below detectable limits after three and four months of incubation, respectively. Since the reactors were operated in batch mode, the reduction in gene copy numbers could not have been a result of washout, but rather a result of biological activity.

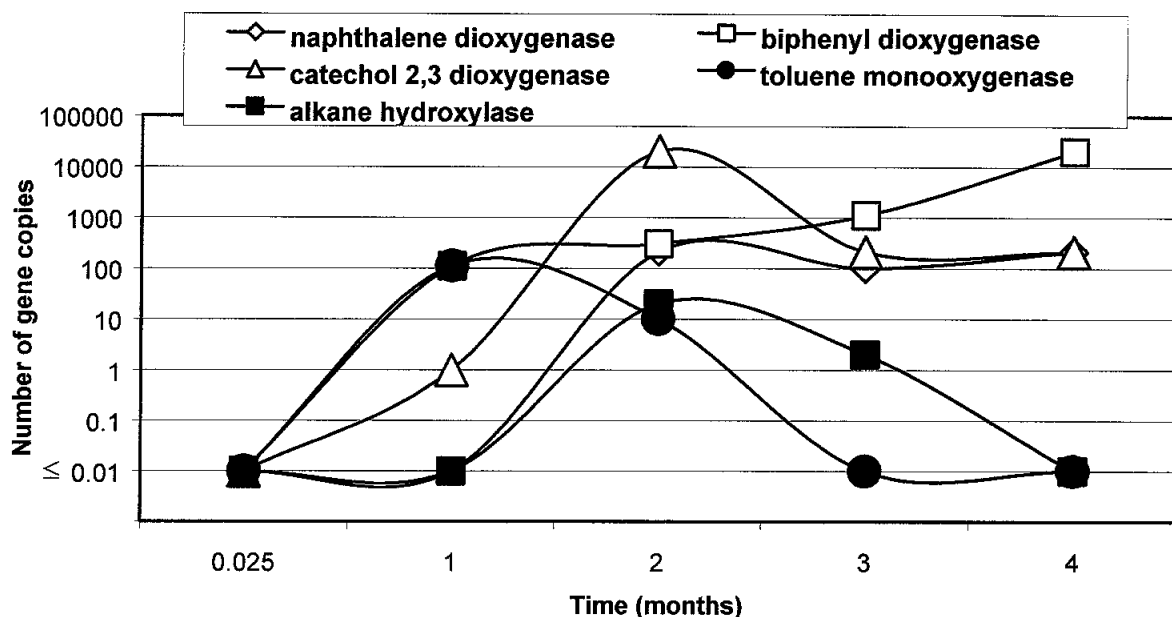


Figure 6. The total number of gene copies (plotted logarithmically over time) of specific enzymes involved in PAH biodegradation as identified by multiplex PCR analysis of active bioslurry reactor sediments. Two categories of enzymes were represented: (1) class I carboxylated proteins (toluene monooxygenase and alkane hydroxylase) and intra- and extradiol aromatic cleavage dioxygenases (naphthalene dioxygenase, biphenyl dioxygenase and catechol-2,3,4-dioxygenase). The time course spanned a four-month period with each point (T_1 to T_4) indicating one month.

Correlations Among Microbial Parameters

Spearman's rank order coefficients were used to correlate PLFA k-means defined microbial communities (Type 1 to Type 3 as a relative percentage) to the log of the total number of gene copies detected in the three active reactors at each sampling period (Table 4). Biphenyl dioxygenase was positively correlated to community 1 (mixed community of Gram-positive and Gram-negative bacteria). Catechol-2,3-dioxygenase and alkane hydroxylase were positively correlated with community 3 (a mixed community including actinomycete PLFA biomarkers). Community 2 (comprised only of 16:0 and 16:1w7c) and the trace components did not positively correlate with any of the catabolic genes measured.

Table 4. Significant ($p < 0.05$) correlations resulting from the comparison of PLFA group (k-means defined) mole percentages and numbers of gene copies in the active reactors ($n=3$) across all time points.

Spearman Rank Order, R					
	Naphthalene dioxygenase	Biphenyl dioxygenase	Catechol-2,3-dioxygenase	Toluene monooxygenase	Alkane hydroxylase
Community 1 ¹				0.65	
Community 2	-0.54	-0.65	-0.94		-0.64
Community 3	0.68	0.67	0.90		0.75
Trace compounds			0.63		

¹ PLFA describing each community type are provided in the text

Correlations Between Microbial Parameters and PAH Profiles

Correlation analyses were used to determine significant relationships between microbial biochemical characteristics and PAH chemical characteristics. PLFA and PAH concentrations were expressed as relative percentages (of the respective total identified) and compared by canonical and Spearman rank order correlation analyses. A high (r^2 of 0.999) canonical correlation coefficient indicated that individual PAH and PLFA concentrations co-varied throughout the bioslurry time course. Spearman rank order analysis indicated a number of significant relationships between individual PAH and PLFA percentages (Table 5). Only those PLFA and PAH that showed a significant correlation ($p < 0.05$) are listed and only negative correlations (i.e. as PLFA percentage increases, PAH percentage decreases) are highlighted. The PLFA showing a significant negative correlation with the three ring PAHs (MW 154 to 178) include 15:0, 17:0, 18:0, i17:0, 16:1w9c, 16:1w5c, br17:1, 10me16:0, and 12me18:0, the same fatty acids (except for 18:0) that defined community 3 illustrated in figure 3b except for 18:0. Those PLFA used to define community 2 (16:0, 16:1w7c, and 18:1w7c) showed significant negative correlations with only the 5 and 6 ring (MW 252 to 278) PAH moieties. Community 1 PLFA (cy17:0, a15:0, and i15:0) showed significant negative correlations with both 3 and 4 ring PAH moieties.

Table 5. Significant ($p < 0.05$) correlations resulting from the comparison of PLFA and PAH relative percentages taken from active reactors ($n=3$) over a 4 month incubation period.

Spearman Rank Order, R

PAH ¹	Naph	AceNaph	Fluor	Phen	Anth	Pyr	Fluoranth	Chry	B(a)A	B(b)F	B(k)F	B(a)P	Indeno	B(g,h,i)P	Dibenzo
# of rings	2	3	3	3	3	4	4	4	4	5	5	5	6	6	5
mw ²	128	152	166	178	178	202	202	228	228	252	252	252	276	276	278
(PLFA) ³															
n14:0	-0.65														-0.64
n15:0															
n16:0										-0.59					-0.74
n17:0		-0.66	-0.60	-0.55	-0.53										
n18:0		-0.58		-0.51					0.59						
i15:0					-0.74							0.60			
a15:0							0.60	0.62							
i16:0															
i17:0		-0.64	-0.66	-0.61	-0.64										
a17:0	-0.59						0.63		0.64						
n16:1w9c		-0.58	-0.59	-0.61	-0.66	-0.76				0.71			0.58	0.63	0.58
n16:1w7c		0.90	0.87	0.79	0.82	0.69		0.60				-0.69	-0.71	-0.55	
n16:1w7t		0.63	0.52					0.83					-0.53		
n16:1w5c		-0.65	-0.64	-0.66	-0.65	-0.66							0.68	0.63	
n17:1w8c	0.67														0.55
cy17:0	0.78						-0.68		-0.51						0.62
n18:1w7c		0.56	0.54		0.51				-0.52						
cy19:0	0.66						-0.55			0.68					0.77
i15:1w7c	0.56							-0.54		0.49					0.61
br17:1		-0.82	-0.84	-0.86	-0.84	-0.86				0.73		0.69	0.77	0.75	0.57
i18:1										0.64	-0.58				0.70
br19:1	0.56									0.68					0.75
n10me16:0		-0.87	-0.83	-0.80	-0.76	-0.64						0.55	0.78	0.67	
n10me18:0		-0.60				-0.54		-0.60					0.53		
n12me18:0		-0.70	-0.61	-0.64	-0.70	-0.68		-0.74					0.66	0.60	

¹ polycyclic aromatic hydrocarbons: Naph (naphthalene), AceNaph (acenaphthylene), Fluor (fluorene), Phen (phenanthrene), Anth (anthracene), Pyr (pyrene), Fluoranth (fluoranthene), Chry (chrysene), B(a)A (benzo[a]anthracene), B(b)F (benzo[b]fluoranthene), B(k)F (benzo[k]fluoranthene), B(a)P (benzo[a]pyrene), Indeno (indeno[1,2,3-c,d]pyrene), B(g,h,i)P (benzo[g,h,i]perylene, Dibenzo (dibenzo[a,h]anthracene)

² molecular weight

³ phospholipid fatty acid

The above described relationships, between PAH percentages and the relative abundance of the defined PLFA community types, are illustrated in Figure 7. Three ring PAH moieties declined in relative abundance as the PLFA describing community type 3 increased, whereas PLFA describing community type 2 decreased in relative abundance as

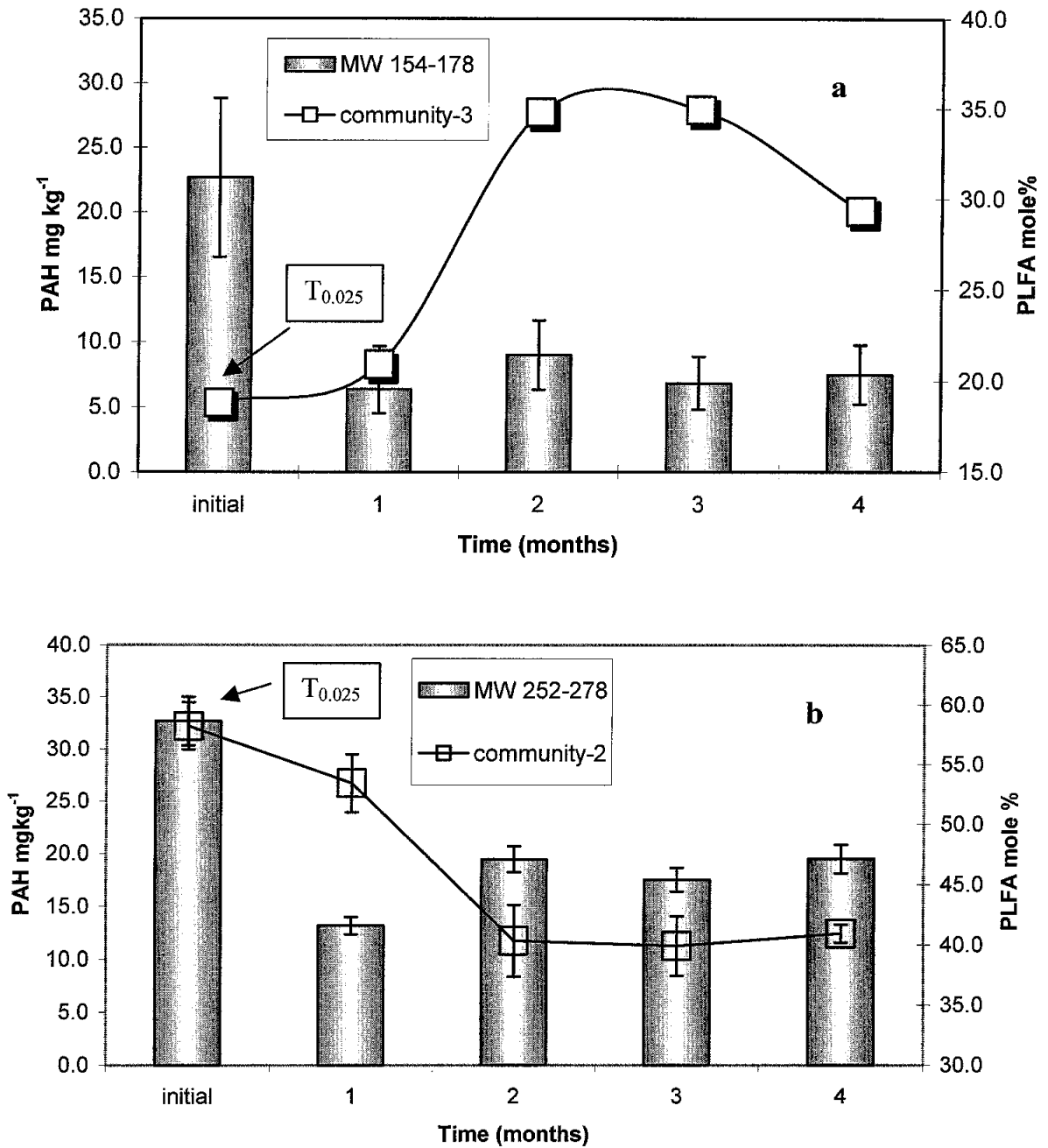


Figure 7. A comparison of K-means defined community types (PLFA cluster groups) and specific PAH subsets (expressed as a % of the total) defined by molecular weight (MW). Panel A illustrates a comparison of community type 3 (see Figure 3) with PAHs of molecular weight 154 to 178 (see Table 4). Panel B illustrates a comparison of community type 2 (see Figure 4) with PAHs of molecular weight 252-278 (see table 4). Error bars indicate ± 1 standard deviation.

PAH relative abundance increased. These results imply that the 3 and 4 ring PAH moieties may serve as a carbon and energy source for one subset of the microbial community (i.e., one containing PLFA indicative of Gram-positive and Gram-negative bacteria as well as actinomycetes and some fungi, which produce dioxygenase catabolic enzymes). In contrast, the 5 and 6 ring PAH moieties in the molecular weight range of 252 – 278, may be toxic to another subset of the microbial community (i.e., one containing PLFA indicative of Gram-negative bacteria, which showed no correlation to any of the catabolic genes assayed for).

Discussion

PAH levels and microbial community characteristics were monitored in replicate for five 5 L bioreactors (2 controls and 3 active) comprising continuously mixed sediment slurry system for four months (23). We realized a net reduction in extractable levels of PAH molecular weight classes from MW 128 to 278. Factors that control the bioavailability of hydrophobic contaminants (24) in sediments after prolonged exposure simultaneously affect the ability of the contaminant to cause toxicity and be accessible to microbial catabolic enzymes. The microbial community in the bioslurry reactors remained remarkably dynamic throughout the 4-month slurry period. This was inadvertently demonstrated by our inability to kill the microbial community in the attenuated controls even after repeated additions of effective poisoning agents.

The active reactors were supplemented with N and P but no carbon energy source. The resident microbiota were able to use the carbon and energy sources liberated from the slurried soil to increase their biomass five fold during the first two months. Because the reactors were operated as a closed, batch system, the decrease in biomass after T₂ months must have been the result of biological mechanisms (i.e., competition and predation). Microbial growth and changes in community composition were driven by carbon and energy sources liberated from the slurried sediment. As PAHs became bioavailable, carbon and energy sources were provided as well as a negative selective pressure in the form of toxic inhibitors.

The dynamic nature of the microbial populations within the active reactors was captured and catalogued as successions in PLFA-defined microbial communities, changes in

potential rates of ^{14}C -PAH mineralization, and dramatic fluxes in copy numbers of catabolic genes.

By synthesizing results obtained by independent analytical methods we were able to show significant relationships among changes in contaminant chemistry, microbial community structure and microbial function. Throughout the study, rates of phenanthrene mineralization exceeded mineralization rates for pyrene and chrysene (both 4 ring PAH moieties) (Figure 5). We also observed a substantial number of significant negative correlations between the 3 ring PAH moieties (MWs 154 to 178) and specific PLFA (Table 5). Those PLFA that correlated with the loss in the 3 ring PAHs also co-varied and defined a unique community type, identified as community 3 (see Figure 3). This community increased in relative abundance throughout the four months (Figure 4). The increase in relative abundance of this community correlated significantly with an increase in gene copy numbers for naphthalene dioxygenase, biphenyl dioxygenase and catechol-2,3-dioxygenase (Table 4). Thus, the biodegradation of three ring PAH moieties (the potential for which was confirmed by radiorespirometry) was identified in terms of an affect on *in situ* microbial community structure, which in turn was directly related to the *in situ* occurrence of genes encoding for catabolic enzymes.

The relationships between PAH and PLFA can be further interpreted, however, since most PLFA are distributed across multiple genera, ambiguous interpretations often result in the analysis of fatty acid patterns from whole communities. It must be assumed that the PLFA highlighted in Table 5 are shared by a number of different groups of bacteria. For example, i17:0, a PLFA that correlated significantly with the loss of fluorene, phenanthrene and anthracene, is common to species of *Arthrobacter*, *Streptomyces* and *Rhodococcus*. Species of *Rhodococcus* are also known to synthesize 10me16:0 and 10me18:0, PLFA biomarkers that are often associated with actinomycetes (25). Species of *Alcaligenes* and *Pseudomonas* are known to be capable of mineralizing fluoranthene and both genera show an abundance of cyclopropyl fatty acids in the phospholipid bilayer (26). As a result, based on the PLFA analysis alone, it can only be inferred that a taxa of bacteria known to synthesize a particular PLFA are present in the sample. Bearing this in mind, it can be inferred from Table 1 that the three ring PAHs were being degraded by *Rhodococcus*, actinomycetes and possibly Gram-positive taxa (i.e., *Arthrobacter* and *Bacillus* species) and four ring PAHs by

Alcaligenes and *Pseudomonas* species. Microorganisms that synthesize 16:0 and 16:1w7c are defined as community 2 (Figure 7).

Although it is unlikely that the PAHs served as the sole source of carbon and energy for the extant biota in the slurry reactors, the above discussion indicates that the availability of these compounds had a marked effect on the microbiology of the system. Values related to PAH mineralization, PAH loss, and microbial growth further the argument. For example, phenanthrene loss between $T_{0.025}$ and T_1 was approximately 4 mg/kg. This loss occurred over a 30 day period. At $T_{0.025}$, phenanthrene mineralization was occurring at a rate of 2%/day whereas at T_1 the mineralization rate had increased to 5%. Taking the average mineralization rate of 3.5%/day and multiplying this value by the total amount of PAH lost over the 30 day incubation period yields a value of 4.2 mg/kg of phenanthrene. Thus an estimated amount of phenanthrene the extant microbiota was capable of mineralizing over the 30 day period corresponds with the realized amount of phenanthrene lost in the same time period.

Microbial biomass also increased between $T_{0.025}$ and T_1 . An increase of 2,782 pmole of PLFA/g, corresponding to approximately 5.6×10^6 cells/g (assuming 1 pmole of PLFA is equivalent to 2×10^4 bacterial cells) (27) was recorded. Boonchan et al. (28) showed a bacterial consortia isolated from a creosote-contaminated soil to increase (using MPN enumeration) by 10^4 cells over a 20-day period in which pyrene, at 0.25mg/mL, was supplied as the sole source of carbon in a basal salts medium. Although the magnitude of the cell number increase was two orders of magnitude greater in our bioslurry reactors, it must be noted that the organisms in the bioslurries were exposed to PAH mixtures and not a single moiety. In their study, Boonchan et al. (28) found only a 10^2 increase in bacterial biomass as a result of benzo(a)pyrene exposure, two orders of magnitude less than that observed with pyrene. It is very likely that carbon sources other than the PAH contamination contributed to microbial growth and metabolism in our active bioslurry reactors. However, the measured effect on microbial community composition and activity suggest a strong biodegradation component within the system.

In summary, qualitative and quantitative changes in the extractable PAHs and the phenotype and genetic potentials of the extant microbiota were evaluated. Correlations between extractable PAHs and microbial community dynamics were determined and related

to microbial community succession and PAH biodegradation. Intrinsic biodegradative potential of dredged sediment was derived from the polyphasic characterization of the *in situ* microbial ecology. Radiochemical, PLFA, and nucleic acid methods enabled changes in extractable PAH levels to be correlated with fluctuation in total microbial community biomass, changes in potential rates of ^{14}C -PAH mineralization, dynamics of PLFA-defined microbial taxa, and changes in genetic catabolic potential.

The significant findings of this work were that the biodegradation potential of the Milwaukee CDF sediment was determined by correlating the microbial community structure (through PLFA analyses) to gene presence (using DNA analyses) to PAH loss (by chemical analyses). This is the first time where the application of in-situ biomarkers has been used to define the capability of PAH-degraders in real sediment systems. This approach provides direct nonbiased measurements to define in-situ biodegradation potential, which can be related to kinetic rates. Currently, laboratory studies are routinely performed to provide this information. The combination of microbial techniques reported here could minimize the future need for extensive laboratory treatability studies, resulting in more timely and cost-effective treatment assessment. However, additional work is needed on other sediments and soils before phenotype and genetic potentials of the extant microbiota can be used as biomarkers to assess the absolute intrinsic biodegradative potential. Further definition of DNA analyses to determine whether the genes present are from dead or live cells is required. Continued research is needed to expand beyond potential capability (DNA analyses) to expressed capability (RNA analyses). Overall, this work provides a new and useful approach to assess the potential bioavailability and treatability of PAHs in dredged sediments.

Acknowledgements

This study was funded by the Strategic Environmental Research and Development Program (SERDP) and the U.S. Army Engineer Research and Development Center (ERDC). We especially thank Ms. Deborah Felt of the Biotechnology Research Group, Environmental Laboratory (ERDC) for providing support and technical collaboration, which made this research possible. Additionally, we acknowledge Dr. Steven L. Larson and the Environmental Chemistry Branch (ECB), also at the Environmental Laboratory, ERDC for their analytical and technical support. We thank the SERDP staff and Technical Advisory Committee (TAC) for their helpful comments and suggestions during this research.

Literature Cited

1. Winfield, L.E., and Lee, C.R. Dredged material characterization tests for beneficial use suitability. DOER Technical Notes Collection (TN DOER-C2), U.S. Army Engineer Research Development Center, Vicksburg, MS., **1999**.
2. Myers, T.E., and Bowman, D.W. "Bioremediation of PAH-contaminated dredged material at the Jones Island CDF: Materials, equipment, and initial operations," DOER Technical Notes Collection (TN DOER-C5), U.S. Army Research Engineer Development Center, Vicksburg, MS., **1999**.
3. Nalkes, D. V.; Linz, D. G; eds. *Environmentally Acceptable Endpoints in Soil*. Annapolis, MD: American Academy of Environmental Engineers, **1997**.
4. Atlas, R. M. Microbial degradation of petroleum hydrocarbons: an environmental perspective. *Microbiol. Rev.* **1981**, 45:180-209.
5. Cerniglia, C. E. Microbial metabolism of polycyclic aromatic hydrocarbons. *Adv. Appl. Microbiol.* **1984**, 30:31-71.
6. Cerniglia, C. E. Biodegradation of polycyclic aromatic hydrocarbons. *Biodegradation*. **1992**, 3:351-368.
7. Gibson, D. I., and V. Subrahmanian. Microbial degradation of aromatic hydrocarbons, p. 181-252. In D. T. Gibson (ed.), *Microbial degradation of organic compounds*. Marcel Dekker, Inc., New York, N.Y. **1984**.
8. Sutherland, J.B., F. Raffi, A.A. Khan, and C.E. Cerniglia. Mechanisms of polycyclic aromatic hydrocarbon degradation. In: *Microbial Transformation and Degradation of Toxic Organic Chemicals* (L.Y. Young and C.E. Cerniglia, eds) Wiley-Liss, Inc., Ny, NY, **1995**, 269-306.
9. Madsen, E.L. Methods for determining biodegradability. In: *Manual of Environmental Microbiology* (C.J. Hurst, G.R. Knudsen, M.J. McInerney, L.D. Stetzenbach and M.V. Walter, eds.) p709-20. ASM Press, Washington, D.C. **1997**.
10. Langworthy, D.E., R.D. Stapleton, G.S. Sayler, and R.H. Findlay. Genotypic and phenotypic responses of a riverine microbial community to polycyclic aromatic hydrocarbon contamination. *Appl. Environ. Microbiol.* **1998**, 64:3422-3428.

11. White, D.C. and D.B. Ringelberg. Signature lipid biomarker analysis. In: Techniques in microbial ecology (R.S. Burlage, R. Atlas, D. Stahl, G. Geesey, and G. Sayler, eds.), Oxford University Press, Inc. New York. P. **1998**, 255-272.
12. White, D.C., H.C. Pinkart, and D.B. Ringelberg. Biomass measurements: Biochemical approaches. In: Manual of Environmental Microbiology, 1st edition (C.H. Hurst, G. Knudsen, M. McInerney, L.D. Stezenbach and M. Walter, eds.) Amer. Soci. For Microbiol. Press, Washington, DC, **1996**, 99-101.
13. Smith, G.A., J.S. Nickels, B.D. Kerger, J.D. Davis, S.P. Collins, J.T. Wilson, J.F. McNabb and D.C. White. Quantitative characterization of microbial biomass and community structure in subsurface material: A prokaryotic consortium responsive to organic contamination. *Canad. J. Microbiol.* **1986**, 32:104-111.
14. Bowman, D.W., Brannon, J.M., and Batterman, S.A. "Evaluation of Polychlorinated Biphenyl and Polycyclic Aromatic Hydrocarbon Concentrations in Two Great Lakes Dredged Material Disposal Facilities," Water Quality 96 Proceedings of the 11th Seminar, 26 February – 01 March 1996, Seattle, Washington, Miscellaneous Paper W-96-1, July **1996**.
15. American Type Culture Collection, "ATCC Culture Medium 1127 Stanier's basal medium," www.atcc.org, **2000**.
16. Fulthorpe, R.S., Rhodes, A.N., and Tiedje, J.M. Pristine soils mineralize 3-chlorobenzoate and 2,4-dichlorophenoacetate via different microbial populations. *App. Environ. Microbiol.* **1996**, 62:1159-1166.
17. Pinkart, H.C., Devereux, R. & Chapman, P.J. Rapid separation of microbial lipids using solid phase extraction columns. *J. Microbiol. Meth.* **1998**. 34:9-15.
18. Borneman, J., Skroch, P.W., O'Sullivan, K.M., Palus, J.A., Rumjanek, N.G., Jansen, J.L., Nienhuis, J., and Triplett, E.W. Molecular diversity of an agricultural soil in Wisconsin. *Appl. Environ. Microbiol.* **1996**, 62:1935-43.
19. Perkins, E. Multiplex PCR approach for estimating in situ explosives biodegradation potentials, *J. Microbiol. Met.* (In Preparation).

20. Zylstra, G., Wackett, L., and Gibson, D. Trichloroethylene degradation by *Escherichia coli* containing *Pseudomonas putida* F1 toluene oxygenase genes. *Appl. Environ. Microbiol.* **1989**, 62:316-22.
21. Kock, M., Oldenhuis, R., Van der Linden, M. Raatjes, P., Vanlelyveld, P., Kingma, J., and Witholt, B. The *Pseudomonas oleovorans* alkane hydroxylase gene. Sequence and expression. *J. Biol. Chem.* **1989**, 264:5435-41.
22. Johnson, Kraig. Anaerobic Biodegradation of Polycyclic Aromatic Hydrocarbons in Dredged Material, Ph.D. Dissertation, Department of Civil and Environmental Engineering, University of Utah, **2000**.
23. Talley, J, Tucker, S., Furey, J., Ghosh, U., and Luthy. R.G. Availability and Bioslurry Treatment of PAHs in Contaminated Dredged Materials. *Environ. Sci. Technol.* (In Draft).
24. Luthy, R., Aiken, G., Brusseau, M., Cunningham, S., Gschwend, P., Pignatello, J., Reinhard, M., Traina, S., Weber, W., Jr., and Westall, J. Sequestration of Hydrophobic Organic Compounds by Geosorbents. *Environ. Sci. Technol.* **1997**, 31:3341-3347.
25. Kroppenstadt, RM. Fatty acids and menaquinone analysis of actinomycetes and related organisms. p 174-199. In: M. Goodfellow and D.E. Minnikin (eds) Chemical methods in bacterial systematics. Academic Press, London. **1985**.
26. Lechivalier, M.P. Lipids in bacterial taxonomy-a taxonomist's view. *Crit. Rev. Microbiol.* **1977**, 5:109-210.
27. Balkwill, DL, Leach FR, Wilson JT, McNabb JF, White DC. Equivalence of microbial biomass measures based on membrane lipid and cell wall components, adenosine triphosphate, and direct counts in subsurface sediments. *Microb Ecol.* **1988**, 16:73-84.
28. Boonchan, S., M. L. Britz, and G. A. Stanley. Degradation and mineralization of high-molecular-weight Polycyclic aromatic hydrocarbons by defined fungal-bacterial co-cultures. *Appl. Environ. Microbiol.* **2000**, 66:1007-1019.

Section 7

Availability and Bioslurry Treatment of PAHs in Contaminated Dredged Materials*

Abstract

The purpose of this study was to apply various investigative technologies to assess the locations and associations of PAHs in dredged harbor sediment, and to use this information to infer the availability of PAHs in the sediment and interpret the results of bioslurry treatment and earthworm bioassay testing. This investigation explores geochemical processes controlling PAH sequestration using physical, physicochemical, chemical, and biological techniques to examine the distributions, associations, and sequestration energies affecting the bioavailability and bioaccumulation of PAHs in dredged Milwaukee Harbor sediments. Aqueous desorption and thermal program desorption mass spectrometry (TPD-MS) experiments were performed to evaluate PAH release and apparent sequestration energies. These data were used to correlate PAH associations with different forms of sorbent organic matter that are believed to play a significant role in the sequestration and bioavailability of PAHs on geosorbents. Bioslurry treatment tests provided samples for physicochemical, bioassay, and microbial testing. The combined results were used to develop a conceptual framework for the assessment and understanding of the bioavailability of PAHs in contaminated dredged materials.

The significant findings of this work were: the identification of two principle particle classes for PAHs: clay/silt and coal-derived; that PAHs were found preferentially on coal-derived particles; that clay/silt particles released PAHs more readily than coal-derived particles; that bioslurry treatment reduced PAHs on the clay/silt fraction but not the coal-derived fraction; that PAH reduction in clay/silt fractions resulted in significant reduction in earthworm PAH accumulation; and that PAH sorption on coal-derived particles were associated with high binding energies. The benefits of this work include: improved assessment of toxicity and risk for contaminants in sediments; improved assessment for the

*Jeffrey W. Talley¹, Samuel G. Tucker¹, John S. Furey¹, Richard G. Luthy², Upal Ghosh²

¹Environmental Laboratory, U.S. Army Engineer Research and Development Center, Vicksburg, MS 39180

²Department of Civil and Environmental Engineering, Stanford University, Stanford, CA 94305-4020

potential success of biotreatment; improved understanding of contaminant availability; improved decision making regarding the treatment of PAH-impacted sediments; and reduced treatment costs and greater likelihood for reuse of dredged sediments.

Introduction

Over three hundred million cubic yards of sediment are dredged from United States ports, harbors, and waterways each year to maintain and improve the nation's navigation system for commercial, national defense, and recreational purposes. It is estimated that approximately 10% of these dredged materials are impacted with organic and inorganic contaminants (1). Contaminated dredged materials are generally discharged into confined disposal facilities (CDFs). CDFs are diked areas used to contain dredged materials. Many CDFs are filled or reaching their design capacity and the diminishing capacity for contaminated dredged material disposal is a significant concern. Various physical, chemical, and biological treatments in engineered systems are being considered to extend the life of CDFs by producing clean material for reuse as fill or soil. However current treatment technologies have many problems, and conservative estimates of the technical and economic feasibility of these technologies suggest that any realistic solutions are many years in the future for contaminated materials currently placed in CDFs. What is needed is a bridging technology that supports the economics of disposal in CDFs, eliminates adverse contaminant impacts, and converts dredged material to material suitable for reuse as reclaimed soil. Bioremediation has emerged as a serious candidate for consideration to fulfill these needs.

The reuse of dredged materials as reclaimed soil will extend the operational life of CDFs while benefiting the environment through reclamation of topsoil and fill material. However, dredged harbor sediments contaminated with PAHs face very stringent cleanup standards prior to reuse. The reuse of contaminant-impacted dredged material is restricted to terrestrial application; therefore, it generally must meet either state soil or solid waste clean-up criteria. This is a serious impediment for reuse of dredged materials. In Wisconsin, for example, the use of contaminated dredged material for topsoil is governed by the State of Wisconsin suggested generic soil cleanup levels (2). If the contaminated dredged material is reused as fill material, it falls under Wisconsin's regulation for the beneficial use of industrial

byproducts (3). For non-industrial (topsoil) or residential (fill material) use certain PAH contaminants such as benzo(a)pyrene and dibenzo(a,h)anthracene must be cleaned up to as low as 8.8 parts per billion [ppb] (2,4). These levels are practically unachievable using bioreclamation technologies. Thus, relatively low-cost, natural cleanup processes like composting may not meet cleanup standards. These low-level cleanup standards assume that the PAHs are readily available and may result in environmental exposure. There is a growing awareness among both practitioners and regulators that soil and dredged material cleanup levels should be more site-specific, as determined by actual contaminant availability and risk. However, adequate tools to evaluate and understand contaminant availability in dredged materials are lacking; thus, conservative, low-level cleanup standards are invoked. Consequently, cleanup is driven by total contaminant mass removal rather than what should be cleaned up to be environmentally protective.

Microbiological processes may reduce hydrocarbon concentrations in sediments to levels that no longer pose an unacceptable risk to the environment or human health (5). However, hydrocarbons that remain in treated sediments still might not meet stringent regulatory levels, even if such levels represent site specific, environmentally acceptable endpoints. There is a great need to understand contaminant-sediment interactions and their effect on bioavailability and toxicity of sediments (6). This is especially true for polycyclic aromatic hydrocarbons (PAHs). The adherence and slow release of PAHs from soils or sediments, i.e., geosorbents, is an obstacle to remediation (7, 8) and is challenging concepts about cleanup standards and risks (9). This is particularly the case for biological treatment of PAHs where one of the most important of the site-specific factors is the availability of the compounds held within solids and how this affects treatment rates and acceptable toxicological endpoints.

Bioremediation of PAH contaminated sediments often results in high residual concentrations that do not satisfy the minimum standards for reuse as soil (10). In general it is believed that these high residual concentrations are caused by the limited bioavailability of PAHs. Biotreatment efficiencies and endpoints are unpredictable for sediment bioremediation. Hence, microbial treatability studies at the bench or pilot level have been

used to determine the efficiency of bioremediation technologies. These studies use microbiological conversion efficiency to provide an overall assessment of the bioavailability. Alternative physicochemical tests have been and are being developed to assess contaminant availability and the potential feasibility of biological treatment. Such tests are usually based on the determination of readily-available PAHs as measured by release into the water phase. These tests may involve desorption of PAHs with uptake of dissolved PAHs onto a solid sorbent (11-13); or transport of dissolved PAHs across a semipermeable membrane followed by entrapment in a hydrophobic solvent phase (12). Thermal program desorption may be useful in conjunction with aqueous desorption tests (14).

The purpose of this study was to apply various investigative technologies to assess the locations and associations of PAHs in dredged harbor sediment, and to use this information to infer the availability of PAHs in the sediment and interpret the results of bioslurry treatment and earthworm bioassay testing.

Milwaukee Confined Disposal Facility (CDF)

The sediment used in this study was obtained from the Jones Island Confined Disposal Facility (CDF) (commonly known as the Milwaukee CDF) operated by the Milwaukee Harbor Port Authority. Shown in Figure 1 is the 44-acre CDF located in the South Milwaukee Harbor. The CDF was constructed in 1975 and has a maximum thickness of 10 meters. It serves as a disposal facility for maintenance-dredged materials unsuitable for open-lake disposal. These sediments originated from the Milwaukee Harbor and Port Washington Harbor, located 25 miles north of Milwaukee. The design capacity is 1.2 million cubic meters (MCM) or 1.6 million cubic yards (MCY). Historically, dredging activities deposit 19,000 to 73,000 CM (25,000 to 95,000 CY) of sediment per year into the CDF. The majority of the CDF was filled via hydraulic dredging and consisted of consolidated, fine-grained material. The CDF was reaching its fill capacity in 1999 (15).

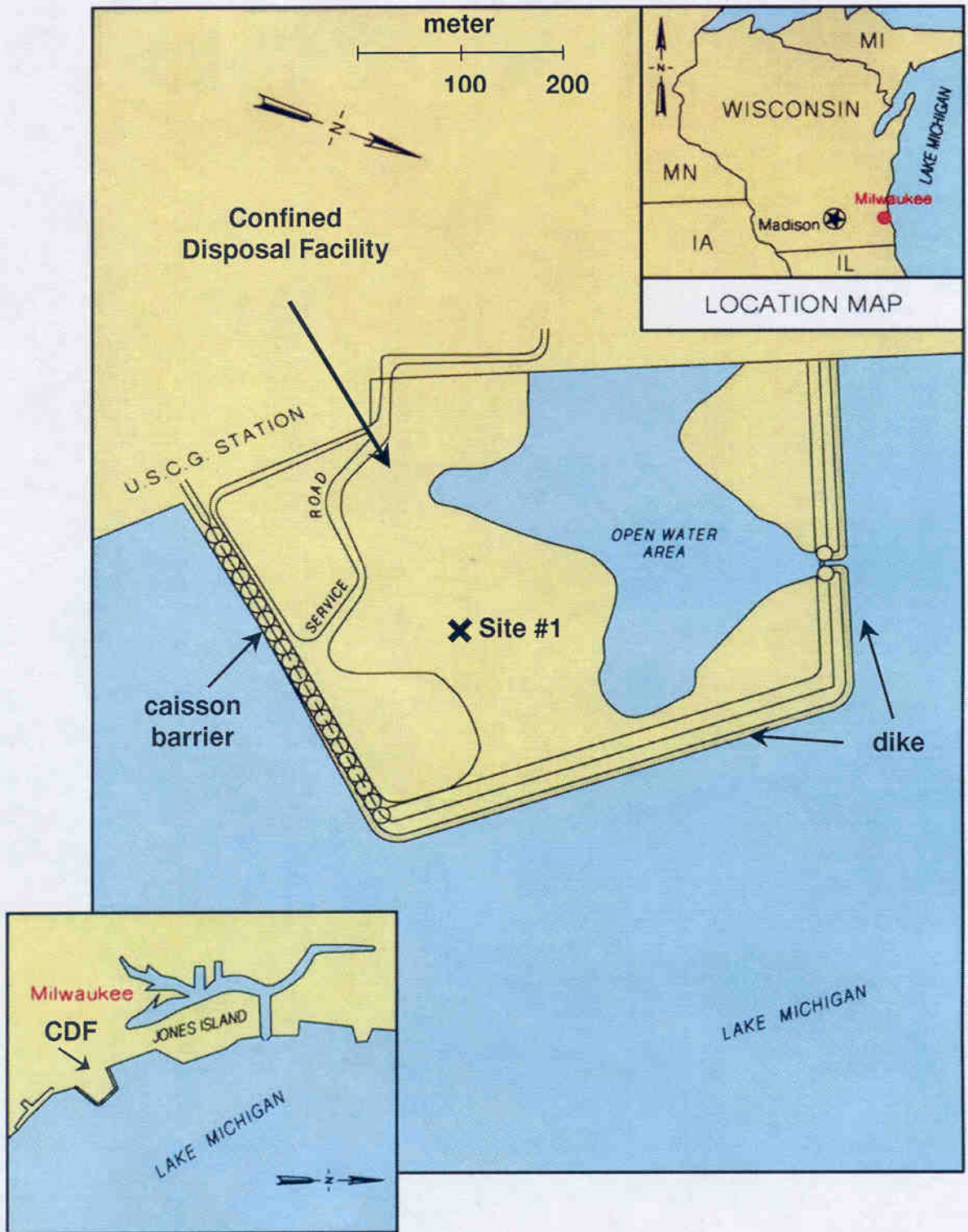


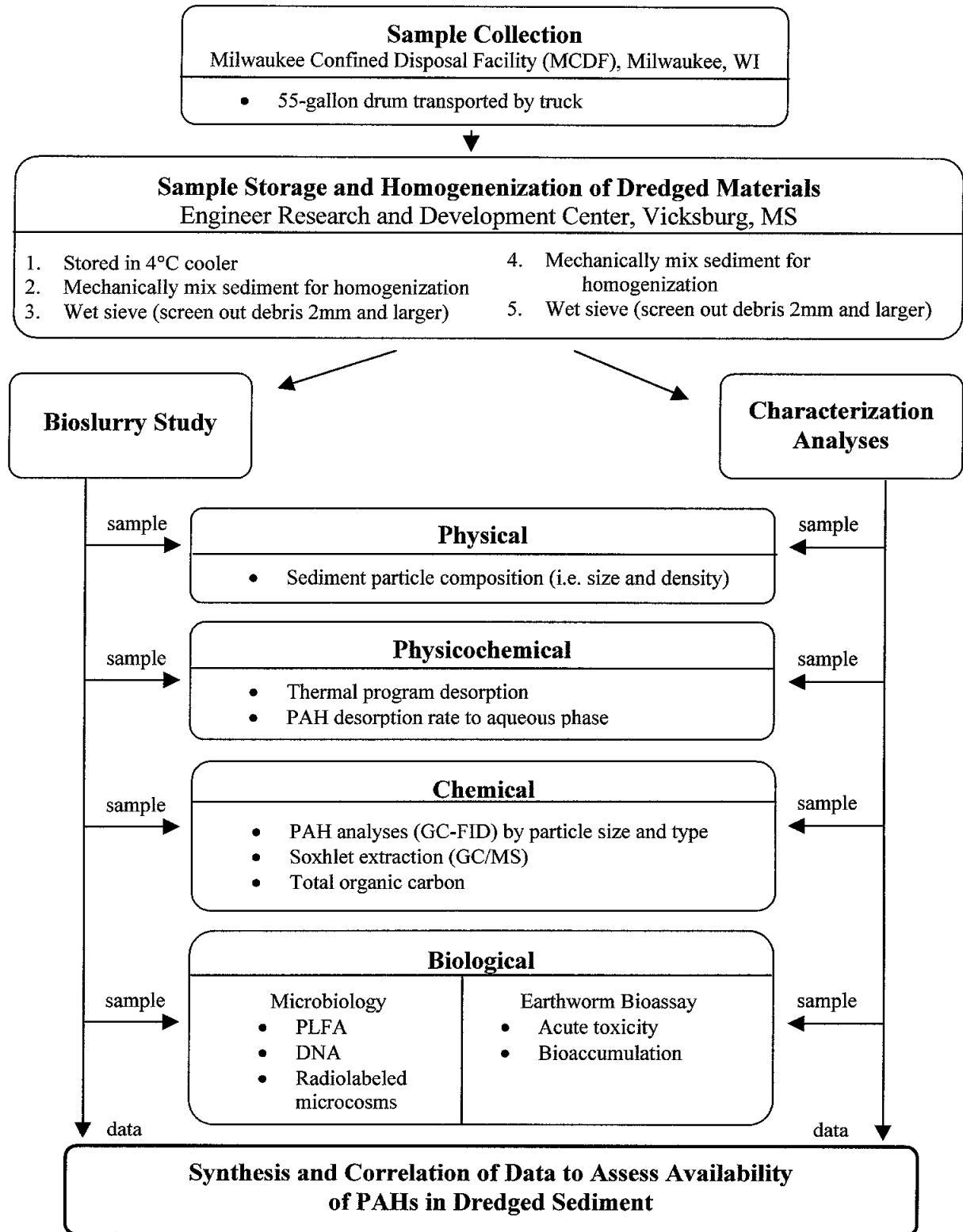
Figure 1. Site map of Milwaukee Confined Disposal Facility and sample site. The sample was collected at a depth of four meters. The maximum depth of dredged material was ten meters.

CDF closure studies show that the organic contaminant concentrations in CDFs tend to be reduced in the upper vadoze zone while concentrations in the saturated zone remain constant (8). PAH analyses of six borings from the Milwaukee CDF indicate a similar pattern. Contamination levels for total PAHs were 50 mg/kg (ppm) near the surface (within 2 meters), 275 ppm at 5 meters, and 100 ppm at 7 meters (15). Samples for this work were collected from Site #1 in October of 1996. A backhoe was used to dig the sampling pit. At a depth of 3.5 meters, water filled up the bottom of the pit. Gas bubbled up through this water for the entire 24 hours the pit was open. Layers of marsh grass and other organic material embedded in the CDF were also discovered. The sample was collected at a depth of four meters. The dredged material was grayish-black in color and clay-like. The recorded temperature, oxidation-reduction potential (ORP), and pH at the sampling depth were 13 degrees C, -50 mv (Eh), and 6.7 respectively. Sufficient material was collected to fill a 55-gallon drum. The drum was sealed on site and shipped by truck to the Environmental Laboratory, U.S. Army Engineer Research and Development Center. The drum was stored at 4 °C.

Experimental Design

The experimental design used in this investigation is outlined in Figure 2. Dredged materials from the CDF were collected and homogenized to provide sufficient sample for bioslurry treatment testing and for PAH analyses on various size and density fractions. These samples were characterized using chemical, physicochemical, physical, and biological analyses. Chemical analyses included sediment PAH analysis by soxhlet extraction with GC/MS and PAH analyses using GC-FID for determination of PAH distribution by particle size and type. Physicochemical analyses included room temperature Tenax bead aqueous desorption experiments and thermal program desorption (TPD) studies. Physical analyses included identification of sediment particle composition by size and density. The dredged material underwent four months of bioslurry reactor treatment. This biotreated-dredged material was then analyzed using the chemical, physicochemical, physical, and biological analyses. Biological analyses integrated microbiology and earthworm bioassays for pre- and post-bioslurry treated sediment. Microbial ecology testing used polar lipid fatty acid (PLFA) and DNA procedures and radiolabel microcosm studies. Earthworm bioassays studied the

Figure 2 Experimental Design



acute toxicity effects and the bioaccumulation results from untreated and biotreated PAH-impacted dredged materials. Overall, the results were used to synthesize and correlate data to assess the availability of PAHs in dredged sediments.

Homogenization of Dredged Materials

The 55-gallon drum sediment sample was removed from the 4 °C cooler and homogenized through mechanical mixing. The sediment was shoveled into an unlined aluminum trough and mixed using a heavy duty industrial Lightning Mixer supported by a hoist. The mixer was lifted up and down during the process to ensure all dredged material was mixed. This was done continuously for 6 hours in ambient air at room temperature. The homogenized material was placed back into the 55-gallon drum and awaited separation of particle types by wet sieving.

Wet sieving was used to screen the sediment and to determine the particle size distribution. The sediment was scooped out of the drum at about 1 kg at a time. The sediment was placed onto a 2 mm sieve, and then wet sieved. Sievings were collected in a 5-gallon bucket and were poured into a 55-gallon drum until filled with sieved sediment and water. All objects above the 2 mm limit were discarded. The drum containing the wet sieved dredged material was allowed to settle for one month. Then the surface water layer was pumped out of the barrel using a peristaltic pump. The water was sampled and centrifuged to see if there was any evidence of significant amounts of suspended sediments. After confirmation that the water was relatively free of suspended solids, the remaining surface water was pumped off the settled sediment. The sediment was again re-homogenized prior to sampling and loading the bioslurry reactors.

Bioslurry Reactor System

The bioslurry reactor system shown in Figure 3 consisted of six reactors. Reactors 1 and 2 were controls (anaerobic and poisoned). Reactors 3 through 6 were active (aerobic) reactors. Each bioreactor received 5309 grams (wet weight) of dredged material. The Milwaukee CDF dredged material was 56.5% sediment (by weight) and 43.5% water. Each reactor had 1.5 liters of sediment (30% by volume) and 3.5 liters (70% by volume) of a

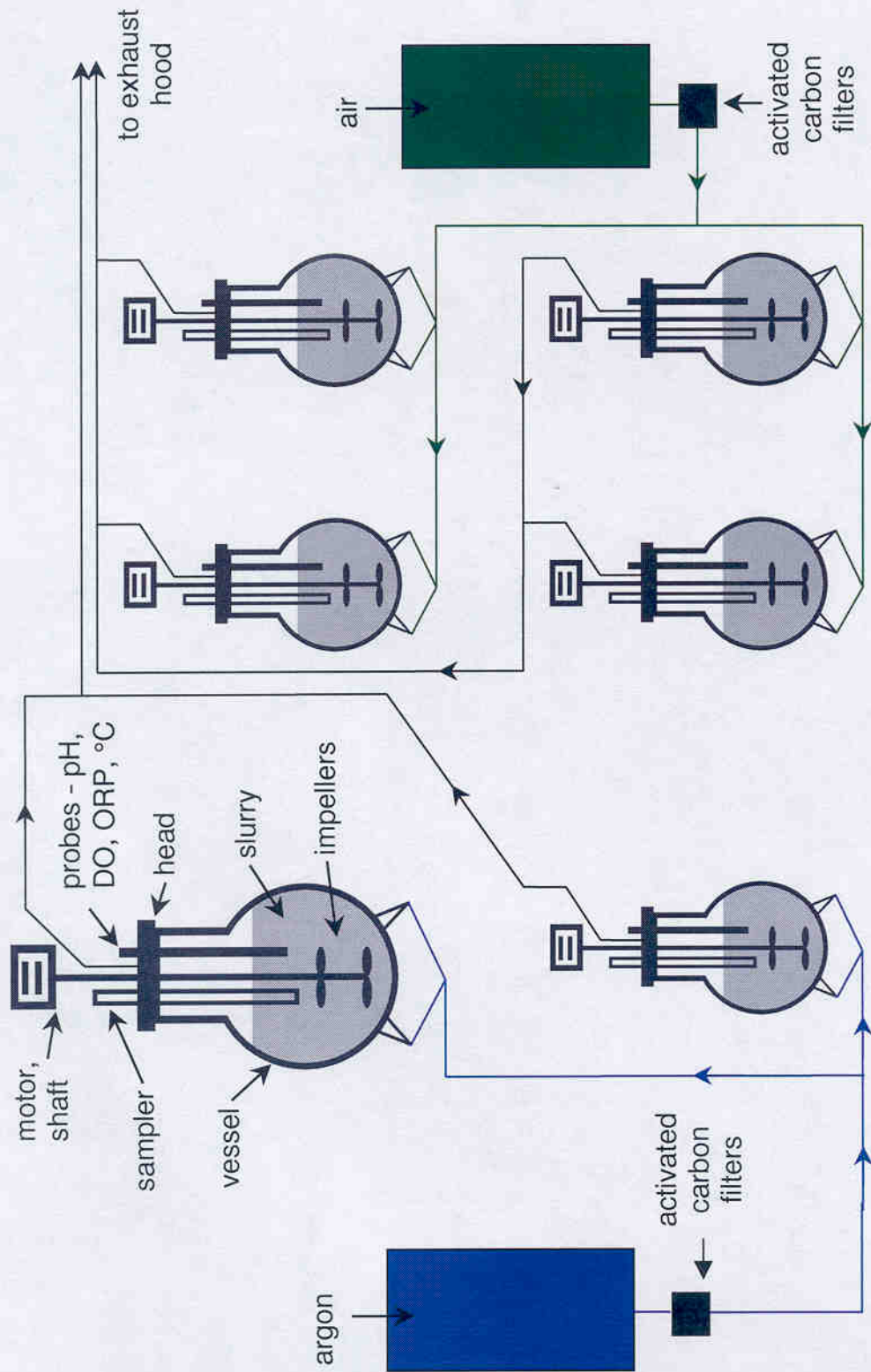


Figure 3. Schematic of the bioreactor system using 5 L bioslurry reactor vessels. The slurry in each reactor is 30% (by volume) solids and 70% Stanier's basal medium.

modified Stanier's Basal Media (16). The media did not contain any carbon source. Each reactor contained two impellers mounted to a shaft to aid in mixing. The bottom impeller was a 3.8" A-310 Impeller with 5/16" bore from Lightnin (part # 809411PSP). This impeller was positioned about an inch from the bottom of the reactor. The top impeller was similar in design and was mounted about three inches above the lower impeller. Each reactor had three diffuser stones in the bottom that bubbled either argon (control reactors) or air (aerobic reactors). The gas was fed from compressed gas cylinders and passed through double charcoal filters before entering the bioreactors. The reactors were continuously stirred at 350 revolutions per minute (rpm). Each reactor was allowed to mix overnight before conducting initial sampling. All of the reactors were vented to a fume hood.

The anaerobic reactors were poisoned with sodium azide and mercuric chloride. Each reactor was dosed with 500 ppm of both compounds. Initial biomass analyses indicated the poisoning was not effective in killing the microbial community for longer than a few days. Thus another 500 ppm of both compounds was added 18 days into the experiment. The microbial community was able to rebound within the week, so an additional 1000 ppm of each compound was added to each anaerobic reactor. Finally a few days later, and every three weeks afterward, an additional 750 ppm of each compound was used. This successfully killed the microorganisms and maintained sterile anaerobic controls.

The anaerobic control reactors were tested for sterility at each sampling event and several times during the first month by streaking the slurry onto a nutrient agar plate. Four plates were streaked. There was a control with nothing on the plate, two plates streaked, one for each anaerobic reactor, with the anaerobic reactor sediment, and a plate streaked with sediment from an aerobic reactor. Each plate was incubated at 30.0°C and checked at 24, 48, and 72 hours. No growth after 72 hours was a positive indication of successfully killed microorganisms.

The bioreactors were tested on a regular daily schedule for pH, dissolved oxygen, oxidation-reduction potential, and temperature. Bioslurry water was sampled initially every two days for nitrate and phosphate analysis. After the initial 4-week period, nitrate and

phosphate measurements were recorded weekly. Carbon: nitrogen: phosphorus ratios were maintained at 100:10:1. The carbon content was based on the sediment TOC. TOC at the beginning of the study ranged from 4,000 to 38,000 mg/kg for the active reactors. Dissolved oxygen was maintained in the range of 8 to 9 mg/L for the aerobic reactors and at 0 mg/L for the control anaerobic reactors. pH was maintained at or near neutral conditions, pH \approx 7.0.

Each month a preset amount of sediment was sampled using a 50 ml pipette. Before the sampling of the sediment, the motor and gas flow to each reactor was shut off. Bioslurry reactors were allowed to settle for one hour. The tops of the reactors were then removed and the sample would be drawn up using the pipette. Samples were collected from 5 different locations and at three different depths (top, middle and bottom) within each reactor. The collected slurry was placed in sterile screw-top containers. These containers were placed in a centrifuge and the supernatant separated from the sediment. The sediment was then placed in a pan lined with sterile aluminum foil and mixed thoroughly with a sterile spatula. The sediment was then weighed and placed into sample vials. All sampling tools were autoclaved prior to use ensuring sterilization of all equipment. Table 1 shows the sampling

Table 1. Sampling events for each bioreactor by analyses type and sample size (grams)

	02-Apr-99 T ₁	02-May-99 T ₁	02-Jun-99 T ₂	02-Jul-99 T ₃	02-Aug-99 T _F
Physical					
Particle size distribution	1	1			1
PAH distribution by size	200				500
Total organic carbon	15				15
Physicochemical					
TPD	6	6	6	6	6
PAH desorption rate to aqueous phase	4	4	4	4	4
Chemical					
Soxhlet extraction	100	100	100	100	100
Biological					
PLFA	6	6	6	6	6
DNA	1.5	1.5	1.5	1.5	1.5
<i>Microcosm</i>					
Aerobic	18	18	18	18	18
Anaerobic	6	6	6	6	6
<i>Toxicity (dry weight)</i>					
Bioaccumulation	500				500
Acute toxicity	200				
Freeze					
	15	15	15	15	15

events for the bioslurry reactors categorized by the type of analyses and size of sample.

Characterization Analyses of Dredged Materials

Physical Analysis

The whole sediment was separated into four size fractions ($>1000\ \mu\text{m}$, $1000\text{-}250\ \mu\text{m}$, $250\text{-}63\ \mu\text{m}$, and $<63\ \mu\text{m}$) for purposes of determining if PAH presence and availability differ within the sediment. The larger size fractions ($>63\ \mu\text{m}$) were composed primarily of sandy grains, coal derived particles, and woody material. Each of these size-separated fractions was then placed into cold storage. It was possible to wash off the lighter fractions (coal and wood) from the heavier sand by swirling with water in a beaker and draining off the entrained lighter particles. Materials in the fine fraction ($<63\ \mu\text{m}$) were density separated using cesium chloride solution having a specific gravity of 1.8 (17). Five grams of wet sediment and 40 ml of cesium chloride solution were centrifuged at 200 rpm for 10 minutes in 50 ml glass centrifuge tubes. The fine coal and wood particles floated to the top and were decanted off and collected in filter paper and washed with tap water several times. The heavy clay and silt were similarly washed several times to remove cesium chloride. Each of these density-separated fractions was placed into cold storage. Total organic carbon (TOC) analysis was also performed on each reactor after 18 hours ($T_{0.025}$ month) of operation and at the conclusion (T_{final} or T_f months) of the study.

Physicochemical Analyses

Room temperature desorption kinetic studies were conducted to evaluate the mass transfer of the PAHs from the whole and separated fractions of sediment to Tenax beads (17). Desorption tests followed procedures used previously by Pignatello et al. (18) and Cornelissen et al. (19). Contaminated sediment (2.0 g) and Tenax beads (0.5g, 40-60 mesh, Suppelco, PA) were added to a 15 ml glass vial containing 10 ml of water and continuously mixed in a rotator. Mercuric chloride (1.0 mg) was added to the mixture to prevent any biological growth. These studies were conducted in duplicate. At sampling times, the Tenax beads were harvested by allowing the sediment to settle and the Tenax beads to float up. The Tenax beads were removed from the glass vials and fresh Tenax beads were added. PAHs

were extracted from the Tenax beads by agitating the beads in 10 ml of hexane and acetone (50:50 mixture) for 12 hours and repeating twice. The extracts were then combined and concentrated, cleaned using silica gel, and analyzed by GC-FID.

A gas chromatograph quadrupole mass spectrometer (GCQ-MS) with a direct insertion probe (DIP) manufactured by Thermoquest was used for thermal program desorption (TPD) measurements. These tests were used to evaluate semi-quantitatively the binding energy, as interpreted from TPD rate responses, for PAHs from untreated and bioslurry treated sediment. TPD tests followed procedures outlined by Talley et al. (14) that showed the release of PAHs is dependent both on PAH molecular weight and the character of the sorbent material. Samples of whole sediment and separated fractions at milligram level were inserted into the mass spectrometer in a 1 mm diameter glass vial inserted in the probe. The temperature of the probe containing the sample glass vial was then increased 10°C per minute. Each TPD run began at 30°C and continued until the probe reached 400°C. As the probe heated up, the volatilized compounds were ionized and selectively filtered in the quadrupole. The mass ions signal would then be detected in the mass spectrometer. The high sensitivity of the GCQ enables analyses down to the particle-level.

Chemical Analyses

An initial comparison study was performed comparing the efficiency of Soxhlet extraction (EPA Method 3540), Accelerated Solvent Extraction (EPA Method 3454A) and Super Critical Fluid Extraction (EPA Method 3561). This study utilized ten different untreated Milwaukee Harbor sediment samples for extraction and GC/MS analyses. These tests were performed in triplicate. Based upon this initial evaluation, it was determined that Soxhlet extraction provided the best reliability. Initial PAH concentrations (T_i) were determined by four replicates from the sieved and mixed 55-gallon drum. After the bioslurry reactors were loaded, samples were collected each month (T_1 , T_2 , T_3 , and T_4) from each reactor. These samples underwent Soxhlet extraction and GS/MS analyses for determination of PAH concentrations according to EPA method 3540. CG-FID was used for PAH analyses on whole sediment and size fractions to determine PAH distribution by particle size and

density (17). This procedure followed EPA method 3550B with ultrasonic extractions and silica gel cleanup following EPA method 3630C.

Biological Analyses

Once the reactors were loaded and operated for 18 hours ($T_{0.025}$ month), they were sampled for PLFA and DNA analyses. Thereafter the reactors were sampled once a month for a total of 4 months (T_1 to T_4). The biological analyses consisted of microbial analyses and earthworm bioassays. The microbial analyses included radiolabeled microcosm studies, PLFA characterization, and DNA analysis. The microcosm studies used radiolabeled phenanthrene, pyrene, chrysene, and benzo(a)pyrene compounds to determine if PAH-degrading microorganisms were present in the sediment. The PLFA characterization identified the level of biomass present in the sediment and general information about the microbial community structure. The DNA analysis was utilized to target the presence of select genes known to be present during active PAH degradation. Earthworm bioassays evaluated the adverse effects of the PAH associated with the sediment to earthworms (*Eisenia fetida*). Both acute toxicity and bioaccumulation tests were performed. The acute toxicity was a 14-day exposure test that measured the survivability of the earthworms. The bioaccumulation test was a 28-day test that measured PAH uptake within earthworm tissue.

Microbial Analyses

For the radiolabel microcosm study, aerobic systems were evaluated for acetate, phenanthrene, pyrene, chrysene, and benzo(a)pyrene mineralization. Anaerobic systems were tested for acetate and phenanthrene mineralization. Microcosm studies were conducted on sediment collected from each bioslurry reactor at $T_{0.025}$ through T_f months. One gram (wet weight) of slurry material was placed into 15 ml teflon-lined screw cap test tubes to which was added 2.7 mL of the modified Stanier's Basal media (16) and a tracer amount of the ^{14}C -labeled substrate. Triplicate microcosms were spiked with 20,000 DPM of phenanthrene-9- ^{14}C (>95%) at a specific activity of 46.9 mCi/mmol (Sigma Chemical Co, St Louis, MO), pyrene-4,5,9,10- ^{14}C (>95%) at a specific activity of 58.7 mCi/mmol (Sigma Chemical Co, St Louis, MO), chrysene-5,6,11,12- ^{14}C (98%) at a specific activity of 47.4 mCi/mmol (ChemSyn Laboratories, Lenexa, KA), benzo[a]pyrene-7- ^{14}C (>95%) at a

specific activity of 16.2 mCi/mmole (Sigma Chemical Co, St Louis, MO) or acetic acid-1,2-¹⁴C (>95%) at a specific activity of 116 mCi/mmole (ICN Pharmaceuticals, Inc., Costa Mesa, CA). A modified version of the method described by Fulthorpe et al. (20) was then used to assess microbial activity.

Glass fiber filters (Whatman, Maidstone, UK), 10 mm diameter, saturated in 1M barium hydroxide were placed into the caps of screw top test tubes to trap evolved ¹⁴CO₂. Test tubes were incubated at room temperature on a tube roller inclined at 45° and continuously rotated at 10 rpm. Filters were collected and replaced once a day for the first week and 3 times a week for the remainder of the four-week incubation. Tube headspace was purged with filtered air (0.2 µm nylon filter, Waters, Maidstone, UK) at each sampling period. Filters were placed in 15 ml of scintillation cocktail (Ultima Gold, Packard Instruments Co., Downers Grove, IL) and counted with a top count microplate scintillation counter (Packard Instrument Co., Downers Grove, IL). Filters were counted twice, and counts were corrected for background and counting efficiency using the external standard method described by the manufacturer. Activity was then expressed as a ratio of labeled PAH initially added.

Polar lipid fatty acid analyses (PLFA) was performed as described by White and Ringelberg (21). Briefly, 2 g-wet weight of slurry material was extracted for 3 hours at room temperature in 6 ml of a mixture of dichloromethane:methanol:water (1:2:0.8, v:v:v). The total lipid extractant was then partitioned against water and taken to dryness under N₂. Amino-propyl solid phase extraction columns (Supelco, Bellefonte, PA) were used to separate the total lipid into neutral, glyco- and polar lipid fractions (22). Phospholipid fatty acid methyl esters (from the polar lipid fraction) were prepared for gas chromatography/mass spectrometry (GC/MS) by mild alkaline methanolic transesterification. The resulting phospholipid fatty acid methyl esters were dissolved in hexane containing methyl nonadecanoate (50 pmol g⁻¹) as an internal standard and analyzed using a gas chromatograph equipped with a 50m x 0.25mm (ID) DB-1 capillary column (0.1 µm film thickness) (J&W Scientific, Folsom, CA) and a flame ionization detector. Peak identities were confirmed using a gas chromatograph-mass selective detector (Hewlett Packard GC6890-5973 MSD)

with electron impact ionization at 70eV. Areas under the peaks were converted to concentrations, summed and then normalized to the gram weight extracted for biomass determinations. For community comparisons, the percent contribution of each peak was calculated and then normalized using an arcsine transformation.

Total DNA was isolated from triplicate 500 mg slurry samples using a mini bead beater system as described Borneman et al. (23), and purified using FastDNA SPIN Kit as described by the vendor (FastPrep7 Instrument FP120; BIO 101, Vista, CA). Total DNA was suspended in 50 ul of Molecular Biology Grade H₂O (Five prime-Three prime, WI) and stored at -20 °C for further analysis.

Earthworm Bioassays

Earthworm bioassays experiments provide information on the potential of organisms to respond to and accumulate soil-associated contaminants. In as much as dredged sediment for the Milwaukee CDF was disposed on land and any reuse of dredged sediment would involve terrestrial application, earthworm bioassays were determined to be most appropriate for toxicity endpoints. The effects of chemicals on earthworms, field test methods, laboratory tests, chemical uptake and metabolism, and the use of these organisms as indicators of environmental pollution have been well documented (24-25).

Earthworm survival 14-day tests were conducted to estimate the acute toxicity of the PAHs to the earthworms as described by the EPA (26-27). Earthworms were exposed in a static system of the untreated (T_i) PAH-contaminated sediment mixed with artificial soil. Ten concentrations of sediment (100%, 75%, 50%, 25%, 12.5%, 6.25%, 3.125%, 1.56%, 0.78%, and 0%) were used where the amount of contaminated sediment was cut in half at each dilution. The percent concentration refers to the amount of contaminated sediment present in the test. The 100% concentration was the undiluted PAH-contaminated sediment with out any artificial soil. The 50% concentration was 50% contaminated sediment and 50% artificial soil. The 0% concentration was 0% contaminated sediment and 100% artificial soil, which served as the control for the tests. Test jars of each concentration were prepared in triplicate. Each jar contained 100 grams (dry weight) of test sediment. The

sediment was homogenized before and after the addition of the artificial soil. After mixing, the test sediment was hydrated to 75% of water holding capacity with deionized water. Ten earthworms were placed into each jar. Earthworms were placed on the surface of the test sediment. Jars were capped and secured. The tests were conducted at room temperature (25°C). Test results were based on the survival of the earthworms.

Earthworm bioaccumulation tests followed a modified ASTM method E 1676-97 (28) where 500 grams of sediment was collected from each reactor. After the sample was homogenized, three test containers were filled with 160 grams each. Sixteen earthworms were added to each test container. The control was the use of a manufactured soil containing peat moss, sand, and kaolinite. The sediment and manufactured soil were hydrated to 75% of water holding capacity. The test containers were then covered with cotton muslin cloth to allow the passage of air, but not allow escape of the earthworm. The test containers were stored in a humidity-controlled room for 28 days. The test containers were periodically checked for moisture and food addition. A few flakes of powder oatmeal were added to the surface of each test container. This would attract the earthworms to the surface resulting in greater earthworm mobility and activity. At the end of the 28 days the earthworms were rinsed with dechlorinated water and placed in scintillation vials lined with filter paper. The worms remained in the vials (2 per vial) for 1 day in order to allow them to clean out their gullet. The worms were then placed in a -70°C freezer. On the day of chemical analysis, the worms were removed from the freezer and freeze dried in a lyophilizer. The lyophilizer produces a dry earthworm powdery material which then undergoes Soxhlet extraction (EPA Method 3540) and analysis on the GC/MS. Bioaccumulation tests were performed on untreated ($T_{0.025}$ month) and biotreated (T_f months) sediment.

Results and Discussion

Distribution and Availability of PAHs Before Bioslurry Treatment

Total PAHs were 115 ± 5.7 mg/kg (ppm) based on the average value for all bioslurries. Individual PAHs for the initial sampling event (T_i) are shown in Figure 4. Four PAH compounds (naphthalene, 2-methylnaphthalene, acenaphthene, acenaphthylene,

dibenzo(a,h)anthracene, and fluorene) were all 2.3 mg/kg or below. There were four PAH compounds (phenanthrene, fluoranthene, pyrene, and chrysene) that had concentrations above 9.8 mg/kg with fluoranthene having the highest concentration at 21.8 mg/kg. Benzo(a)pyrene concentrations exceeded 7 mg/kg. Of the sixteen PAH compounds, ten of them exceeded either the Wisconsin suggested generic soil cleanup levels (2) or the solid waste cleanup levels for the beneficial use of industrial byproducts (3, 4), as shown in Table 2.

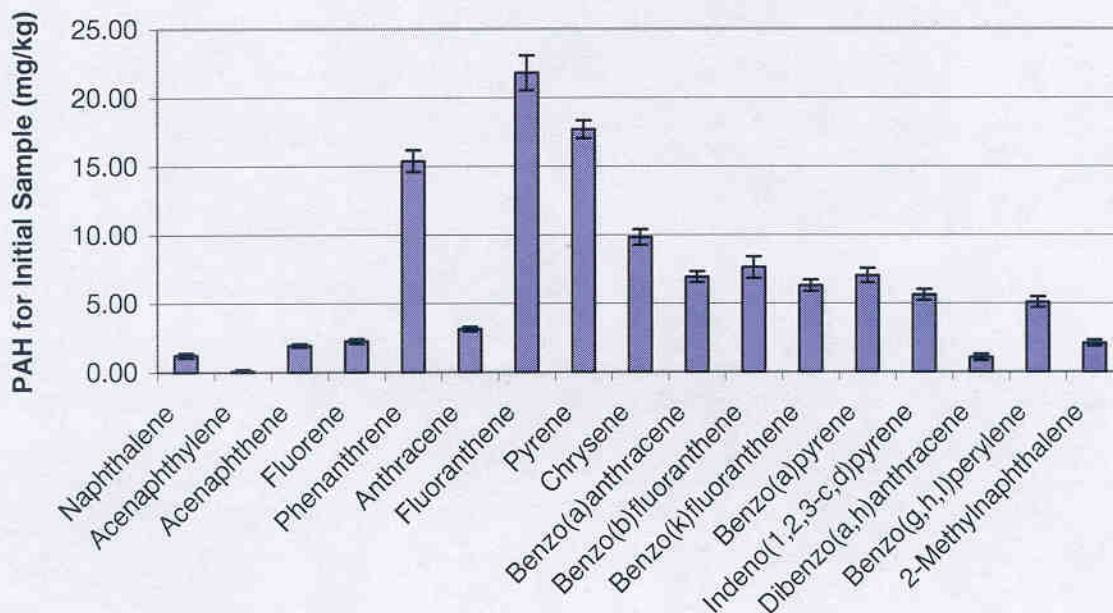


Figure 4. PAH distribution in sediment prior to bioslurry treatment. Error bars indicate ± 1 SD.

The mass and PAH distribution in the different sediment fractions are shown in Figure 5. The heavy sediment fraction in the sediment, which includes clays, silt, and sand, constituted 95% of the sediment by weight. The light fraction and debris constituted the remaining 5% of the sediment weight. However, the distribution of the PAHs in the sediment is predominately in the lighter density fraction. The lighter coal/wood-derived material and debris contains 62% of the PAHs. Only 38% of the total PAHs are associated with the heavy sediment fraction (clays and silt).

Table 2. Comparison of PAH Concentrations (mg/kg) in Untreated (T_i) Milwaukee CDF Sediment to Wisconsin Required Cleanup Levels (mg/kg) for Reuse of Dredged Material

Compound	Concentration	Wisconsin Generic Soil Cleanup Levels			Wisconsin Solid Waste Cleanup Levels	
		GW Pathway	Non-Industrial	Industrial	Unrestricted	Restricted
Naphthalene*	1.2	0.4	20	110	600	6000
2-Methyl-naphthalene	2.1	20	600	40000	NA	NA
Acenaphthylene	0.1	0.7	18	360	8.8	88
Acenaphthene	1.9	38	900	60000	900	9000
Fluorene	2.3	100	600	40000	600	6000
Phenanthrene*	15.4	1.8	18	390	0.88	8.8
Anthracene	3.1	3000	5000	300000	5000	50000
Fluoranthene	21.8	500	600	40000	600	6000
Pyrene	17.7	8700	500	30000	500	5000
Chrysene	9.8	37	8.8	390	8.8	88
Benzo(a)anthracene*	6.9	17	0.088	3.9	0.088	0.88
Benzo(b)fluoranthrene*	7.6	360	0.088	3.9	0.088	0.88
Benzo(k)fluoranthrene*	6.3	870	0.88	39	0.88	8.8
Benzo(a)pyrene*	7.0	48	0.0088	0.39	0.0088	0.08
Indeno(1,2,3-C,D)pyrene*	5.6	680	0.088	3.9	0.088	0.88
Dibenzo(a,h)anthracene*	1.1	38	0.0088	0.39	0.0088	0.088
Benzo(g,h,l)perylene*	5.1	6800	1.8	39	0.88	8.8

*Denotes PAHs that exceed at least one of the cleanup levels required for reuse of dredged materials. Generic soil cleanup levels are for reuse as topsoil or near-surface soil. Non-industrial and industrial soil cleanup levels are based on direct contact pathways. GW pathway cleanup levels assume reuse will be in areas where the material will come into contact with groundwater. Restricted solid waste cleanup levels are limit the reuse to capped, roadfill or non-residential applications. Unrestricted solid waste cleanup levels are based on unrestricted reuse as fill material.

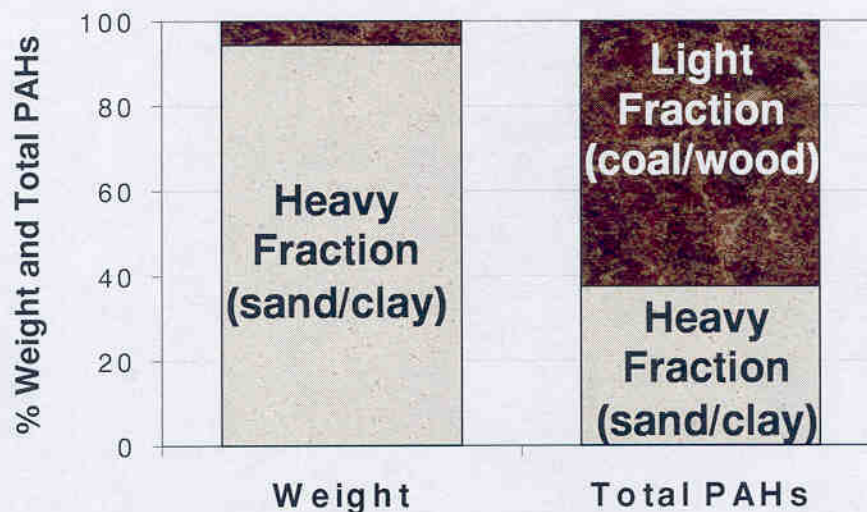


Figure 5. Sediment weight and PAH distribution. The light density sediment fraction accounts for only 5% of the sediment weight but more than 60% of the PAHs.

Figures 6 a-c show the initial PAH concentrations based on sediment size fractions and densities. The heavy, <63 μ m size fraction is comprised of clays and silt and is the most abundant component in the sediment at about 60% by weight. Figure 6b shows the clays/silt (<63 μ m heavy) contributing nearly all the PAHs for the heavy sediment fractions. Thus, 5% of the sediment, the coal/wood-derived material and debris, contains more than three-fifths of the total PAHs. Figure 6c shows the PAH concentration by dry mass within each fraction. The light fractions have two orders of magnitude higher PAH concentration than the heavier fractions.

Desorption kinetic studies were conducted with the whole sediment and separated fractions to investigate the availability of PAHs. Results of these 100-day desorption kinetic tests are shown in Figure 7 (17). The desorption study with whole sediment shows that approximately 40% of the PAHs were released quickly and approximately 60% were strongly bound. Thus, approximately 40% of the PAHs in the whole sediment may constitute the available fraction. The PAHs associated with the light coal and wood fractions appear to be bound very strongly, as only about 8% of the PAHs in this fraction were released in 100 days. This test suggest that the majority of the PAHs associated with this coal and wood fraction may not be bioavailable for degradation nor exhibit a highly toxic response. In contrast, desorption data from the heavier clay/silt fraction indicate a higher availability with nearly 80% of the PAHs in this fraction readily desorbing in 100 days. This suggests that the majority of the PAHs in this size fraction may be bioavailable.

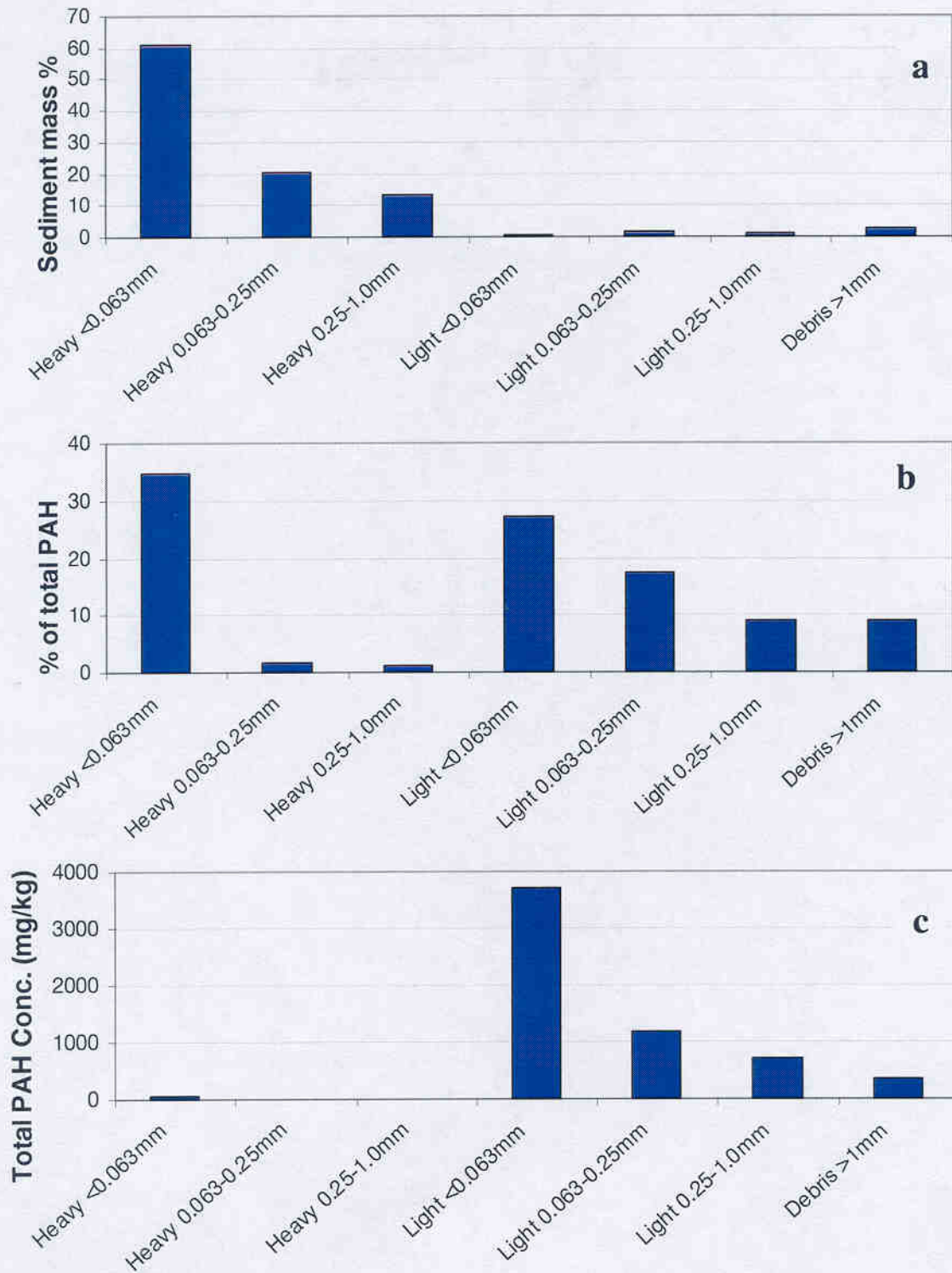


Figure 6. (a) Mass distribution of sediment by size and density fractions. (b) Total PAH distribution in sediment by size and density fractions. (c) PAH concentration in sediment fractions by size and density (17).

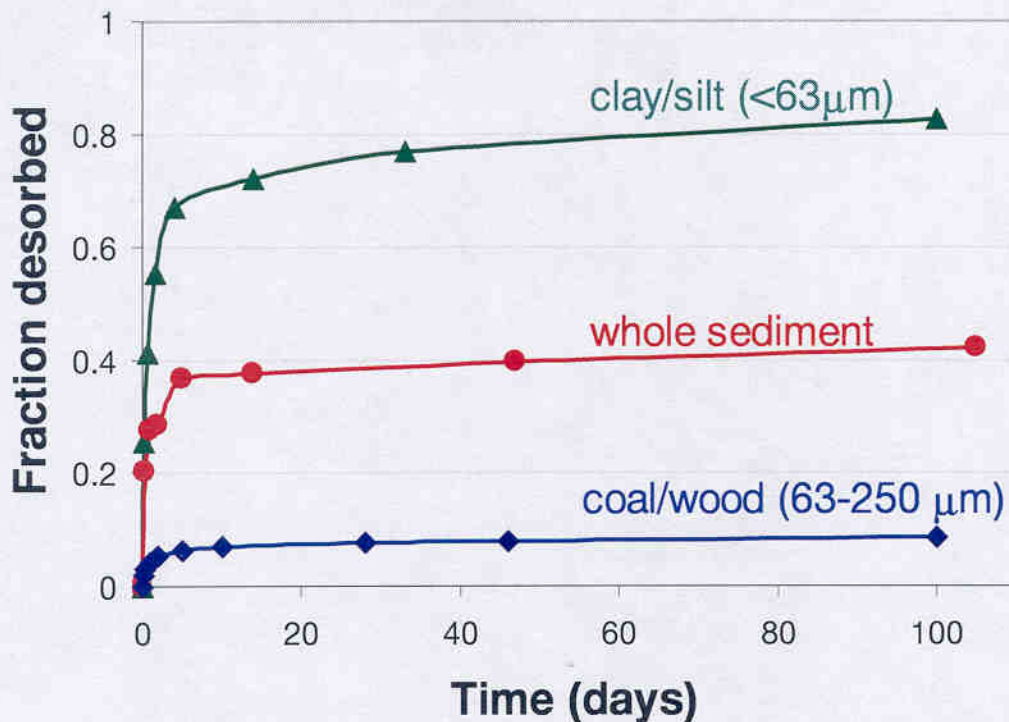


Figure 7. Desorption of total PAHs from Milwaukee Harbor sediment showing faster desorption from the heavy clay/silt fraction compared to the light coal/wood fraction (17).

Biodegradation Capability of Indigenous Microorganisms

Radiolabeled microcosm studies were performed to determine if the Milwaukee CDF sediment had indigenous microorganisms capable of degrading PAHs. Radiolabeled CO_2 was captured from each microcosm to track the mineralization of spiked radiolabeled phenanthrene, pyrene, chrysene, and benzo(a)pyrene. Mineralization rates for each of the PAHs examined were greatest at times T_1 month and T_2 months, corresponding to the greatest biomass levels and the introduction of nutrients. The observed rates of ^{14}C -PAH mineralization in the microcosm tests increased in the order of benzo(a)pyrene < chrysene < pyrene < phenanthrene. Mineralization rates for phenanthrene, pyrene and chrysene were above background levels over the 4-month bioslurry study, as illustrated for phenanthrene (Figure 8a) and chrysene (Figure 8b). Benzo(a)pyrene mineralization rates barely exceeded background levels indicating uncertainty regarding the ability of microorganisms to degrade

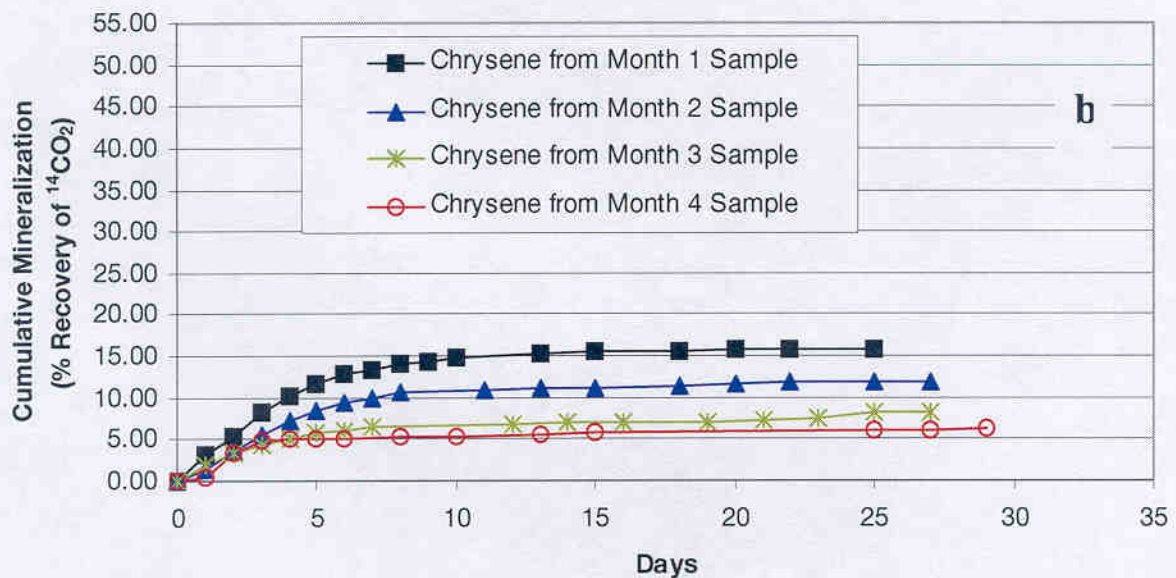
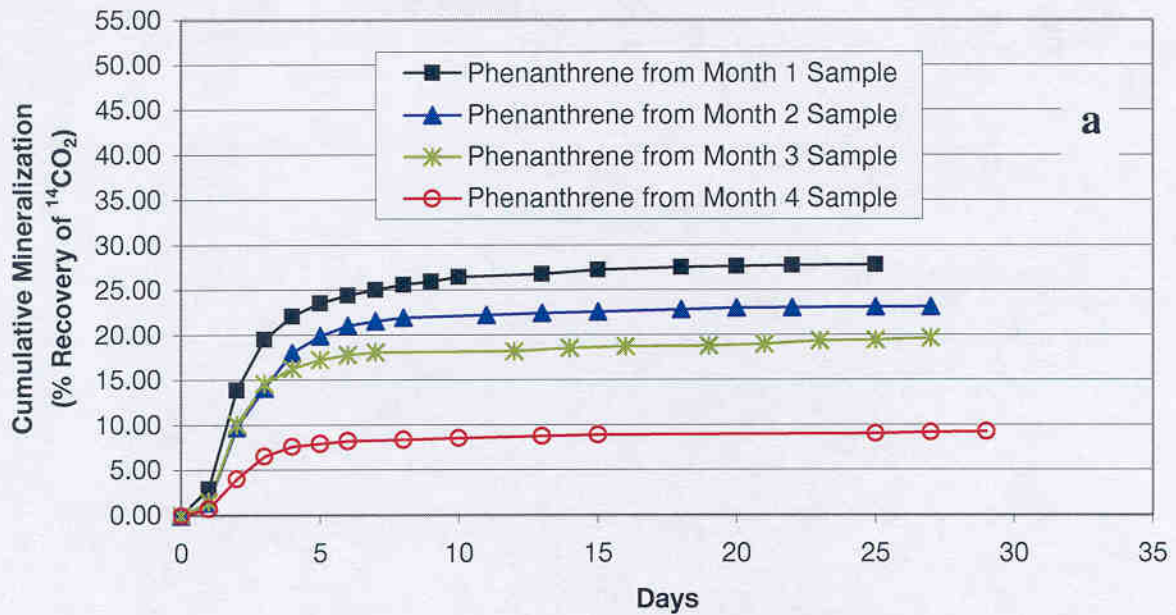


Figure 8. Sampling during each month of the study provided sediment for radiolabeled studies. The figures show (a) cumulative mineralization of ¹⁴C phenanthrene in microcosms of active treatment bioslurries (b) cumulative mineralization of ¹⁴C chrysene in microcosms of active treatment bioslurries. These data show viable PAH-degrading organisms were present in the bioreactors.

benzo(a)pyrene. The results from these microcosm tests demonstrate that viable PAH-degrading organisms were present in the sediment with activity being expressed with addition of oxygen and nutrients.

PLFA analyses revealed that microbial biomass was relatively low in the control reactors averaging less than 8000 total pmole PLFA g^{-1} through T_3 months. At T_4 months, the biomass increased to over 20,000 total pmole PLFA g^{-1} indicating that the poisoned controls had lost their effectiveness in the last month of the study. Biomass in the active reactors ranged from slightly less than 10,000 total pmole PLFA g^{-1} at $T_{0.025}$ month to almost 50,000 total pmole PLFA g^{-1} at T_2 months. At T_3 months, the biomass dropped to less than 15,000 total pmole PLFA g^{-1} , but had increased to almost 30,000 total pmole PLFA g^{-1} by T_4 months indicating the microbial biomass in the active reactors were a dynamic community. Initial biomass increase correlated well with total PAH reduction in the aerobic reactor system (29). The microbial community primarily responsible for this was Gram-positive, Gram-negative bacteria, actinomycetes, and some fungi (29). This community showed a large increase in biomass over the first two months as the total PAH concentration showed a concomitant decrease in concentration. Breakdown by molecular weight shows a strong correlation between 2- and 3-ring PAH reduction (29). This data is supporting evidence of a microbial link to the PAH degradation and that the aerobic reactors contained viable PAH-degrading microorganisms.

The DNA analyses with the sediment at $T_{0.025}$ month showed gene encoding enzymes associated with aromatic degradation (naphthalene dioxygenase, biphenyl dioxygenase, catechol 2,3-dioxygenase, toluene monooxygenase, and alkane hydroxylase) were present in copy numbers below the detection limit of the assay (<1 gene copy per gram). By the first and second month of bioslurry treatment the copy numbers for each of the genes assayed increased to the maximum detectable number - 10,000 copies g^{-1} . This correlates strongly to the microbial biomass increase and to the decrease in PAH concentrations (29). The increase in the copies of these genes and increase in microbial biomass is consistent with observed mineralization response for phenanthrene, pyrene, and chrysene detected in the microcosm studies.

Reduction of PAHs by Bioslurry Treatment

Bioslurry treatment was conducted for four months. All of the bioslurry reactors were maintained throughout the study, except reactor 4, which cracked after two months. However, since no significant change in PAH concentrations occurred between 2 and 4 months of treatment, the T_2 month data for reactor 4 was included in the overall average for T_f . As explained in Chapter IV, total PAH concentrations in the control reactors decreased 17%, indicating partial bioremediation and volatilization. Averaged concentrations of total and individual PAHs from all active reactors for the initial sample (before biotreatment), month two, and month four (after biotreatment) are shown in Figure 9.

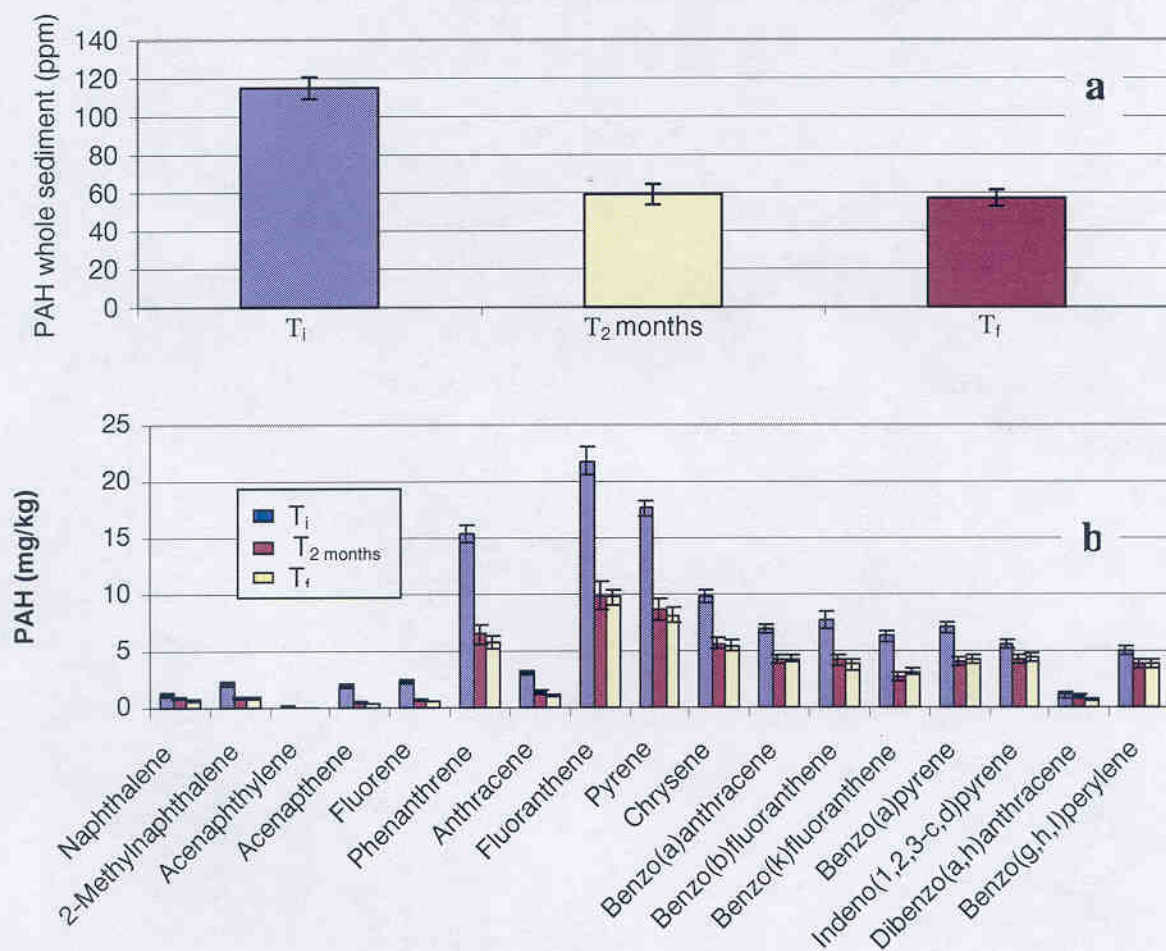


Figure 9. These figures show the bioslurry treatment results (a) total PAH concentrations for initial sample, 2nd, and 4th month; (b) individual PAH concentrations for initial PAH concentration, 2nd, and 4th month. There was a 49% reduction of total PAHs by month 2 and a 50% reduction by month four. Error bars indicate ± 1 SD.

The PAH data in Figure 9 are an average of the active bioslurry reactors. These active reactors showed a net loss in total extractable PAH of approximately 50% over the four-month study. PAH concentrations decreased from a T_i average of 115 ± 5.7 mg/kg to 57 ± 4.4 mg/kg at T_f (Figure 9a). The decline in total PAH was statistically significant at an alpha of 0.05 ($p=0.0000115$). All PAH compounds, as seen in Figure 9b, showed a decrease in concentration. The greatest loss of 64% ($p=0.00823$) occurred for the 128-178 MW compounds (naphthalene, 2-methylnaphthalene, acenaphthylene, acenaphthene, fluorene, phenanthrene, and anthracene), followed by 51% ($p=0.000142$) loss in the 202-228 MW compounds (pyrene, fluoranthene, chrysene and benzo[a]anthracene). The higher molecular weight compounds were reduced by a 38% ($p=0.0000479$) decrease in the 252-278 MW compounds (benzo(b)fluoranthene, benzo(k)fluoranthene, benzo(a)pyrene, benzo(g,h,i)perylene, indeno(1,2,3-c,d)pyrene, dibenzo(a,h)anthracene).

Samples were also collected from the bioslurry reactors to assess PAH degradation by particle size and type. PAH reductions by size fraction are shown in Figure 10. A marked distinction between the availability of PAHs on heavy and light fractions was observed. PAH degradation was achieved mainly by the $<63\mu\text{m}$ heavy and the >1 mm debris fractions, which both exhibited slightly over a 75% reduction over the 4-month bioslurry treatment. The coal/wood material in $<63\mu\text{m}$ to 1 mm size fractions had no reduction of PAH concentrations. The debris fraction may have undergone attrition. Thus, it cannot be inferred that the apparent reduction in the PAHs in the debris size fraction was due to biodegradation.

The data in Figure 10 suggest that the PAHs on the $<63\mu\text{m}$ heavy (clay silt) fractions are largely available and the PAHs on light $<63\mu\text{m}$ to 1 mm size fractions are not. The lack of change of PAHs in the $<63\mu\text{m}$ to 1 mm size fraction clearly indicates that the PAHs on the light fraction were not bioavailable. In Figure 11 the individual PAH concentrations are shown for the $<63\mu\text{m}$ heavy fraction before and after biotreatment. The $<63\mu\text{m}$ clay/silt fraction showed reduction in concentration for every PAH compound tested for in the study. The greatest percent reduction ($>85\%$) was achieved by fluoranthene and pyrene.

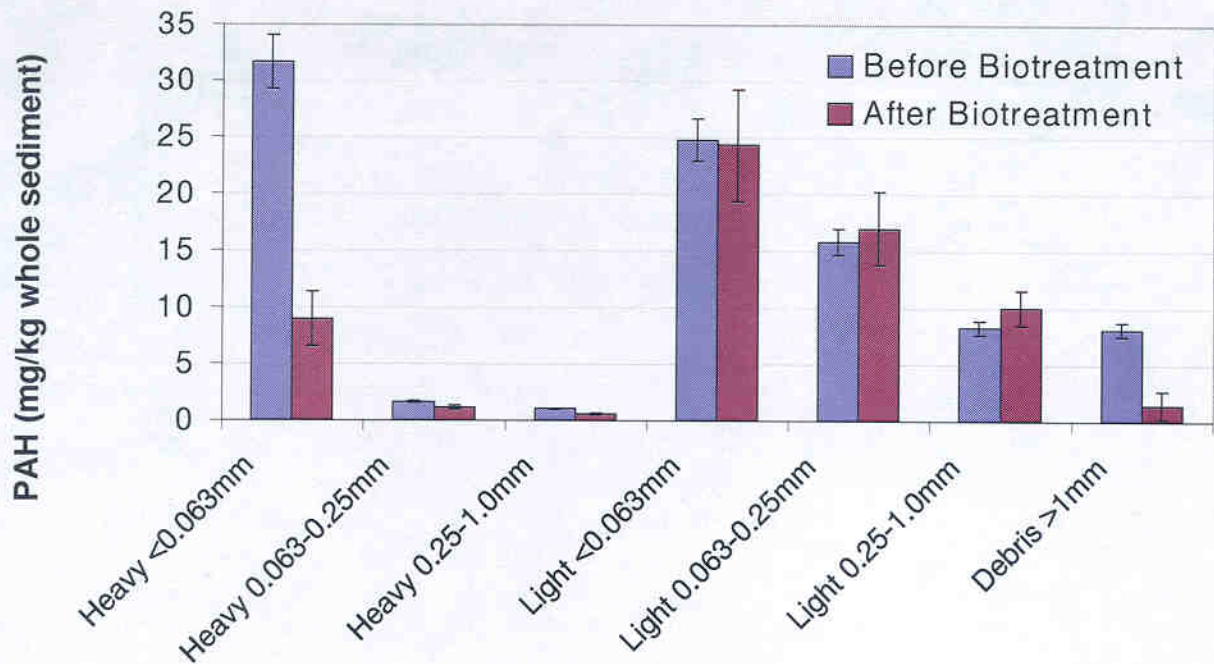


Figure 10. PAH reduction in sediment fractions before and after bioslurry treatment for four months. These values are based on the percentage of PAH concentration for each fraction (Figure 6b) for a total PAH concentration of 90 mg/kg as measured by GC-FID. Error bars indicate ± 1 SD.

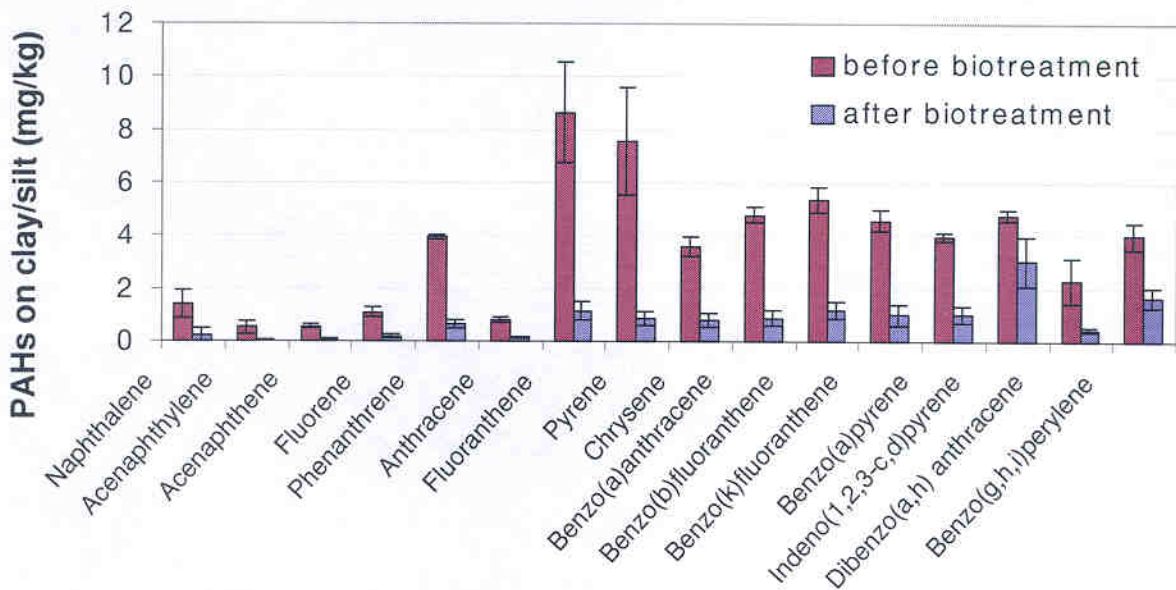


Figure 11. PAH concentrations for the Milwaukee CDF clay/silt fraction before and after bioslurry treatment. Error bars indicate ± 1 SD.

Earthworm Toxicity and Bioaccumulation

Earthworm acute toxicity tests were performed at T_i . The results from these tests showed a 100% survival rate indicating that the PAHs present initially in the sediment were not toxic to induce death. It is unclear if this is due to PAH concentration below earthworm toxicity thresholds or if the PAHs were limited in their availability due to strong binding. Since no acute toxicity existed, no post bioslurry toxicity test was conducted.

Earthworm bioaccumulation tests were performed on sediment before ($T_{0.025}$ month) and after (T_4 months) bioslurry treatment. The results for individual PAHs are shown in Figure 12. These data comprised an average of the results from 192 earthworms exposed to sediment before treatment and 144 earthworms exposed to sediment after four months of bioslurry treatment. Each reactor had triplicate earthworm subsamples (16 earthworms per subsample) for extraction and analyses. The uptake of total PAHs in earthworm tissue from the untreated sediment was 8.1 mg/kg. Earthworm uptake after bioslurry treatment was reduced to 2.0 mg/kg. This represents a 75% reduction in total PAH uptake. There were 7 PAHs (naphthalene, 2-methylnaphthalene, acenaphthene, fluorene, fluoranthene, pyrene, and benzo(b)fluoranthene) with concentration reductions over 80%. All PAHs had a reduction of over 56% in the earthworm tissue.

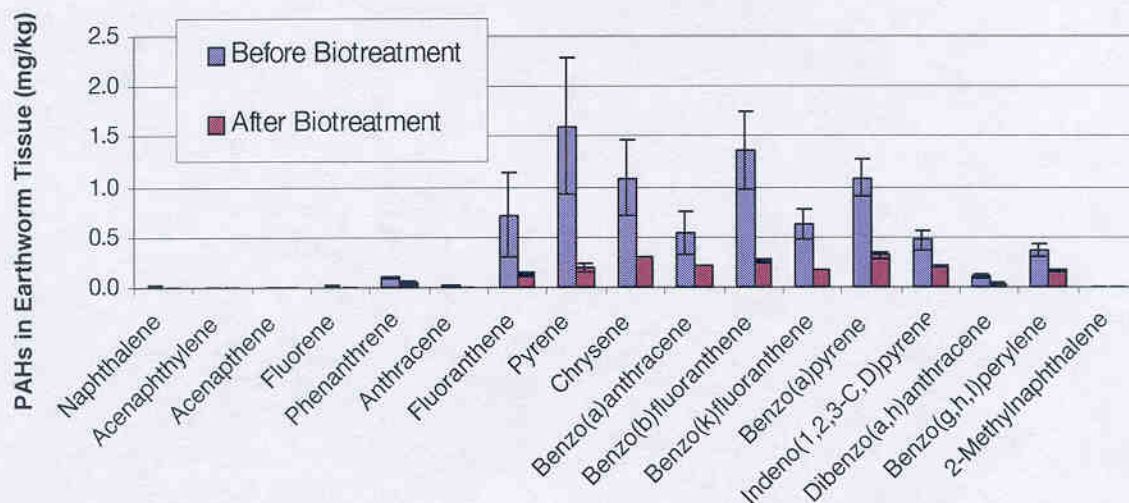


Figure 12. Measurement of the bioaccumulation of PAHs by earthworms (*Eisenia fetida*) from Milwaukee CDF sediment before and after biotreatment. Error bars indicate ± 1 SD.

When comparing Figures 11 and 12, a similar trend is found. Both the clay/silt fraction (Figure 11) and earthworm uptake (Figure 12) decreased 75%. Further examination reveals that there appears to be a strong correlation between the individual PAHs biodegraded and those reduced in earthworm tissue uptake. This observation suggests that only the PAHs in the clay/silt fraction comprise the readily available fraction to both microorganisms and earthworms.

Thermal Programmed Desorption Response of PAHs

TPD tests were used to examine semi-quantitatively the apparent PAH binding energy, as interpreted from TPD rate responses, for Milwaukee CDF sediment before (T_1) and after (T_2) bioslurry treatment. TPD rate responses for PAH MW 202, 252 and 276 from the <0.063 mm light, <0.063 mm heavy, and the 0.063 – 0.25 mm light size fractions were evaluated. The data presented is an average of three TPD runs for each density and size fraction. The individual runs, which make up the averages, have been smoothed using Excel's 10-point moving average option. To visually compare the TPD response rate from the different MW and sediment size fractions studied, the data were normalized by dividing by the total area under the TPD response curve (for Figures 13a and 14), which corresponds to the total PAH mass desorbed from the solid.

Figure 13a shows that there was no significant difference in peak temperatures for the T_1 and reactor 4 T_2 month data for MW 202, 252, and 276, <0.063 mm light fraction. However, thermograms shift to the right with an increase in molecular weight indicating that higher molecular weight PAHs have higher binding energy. Figure 13b shows the TPD results for the <0.063 mm heavy fraction. Distinct peaks are observed for the untreated samples with thermograms shifting to the right for increasing MW. However, the reactor 4 T_2 month data became very broad and shallow. Peak temperatures remain similar to the T_1 month data for MW 252 and 276 but MW 202 shifted right approximately 50°C. This phenomenon was observed consistently when lower molecular weight PAHs (MW<202) were present in low concentrations. A total of nine runs were made (three are averaged for Figure 13b), each giving a low ion count response. The ion counts for reactor 4 T_2 month (12,000-20,000) were 20% of the ion counts at T_1 month (70,000 to 90,000) indicating that

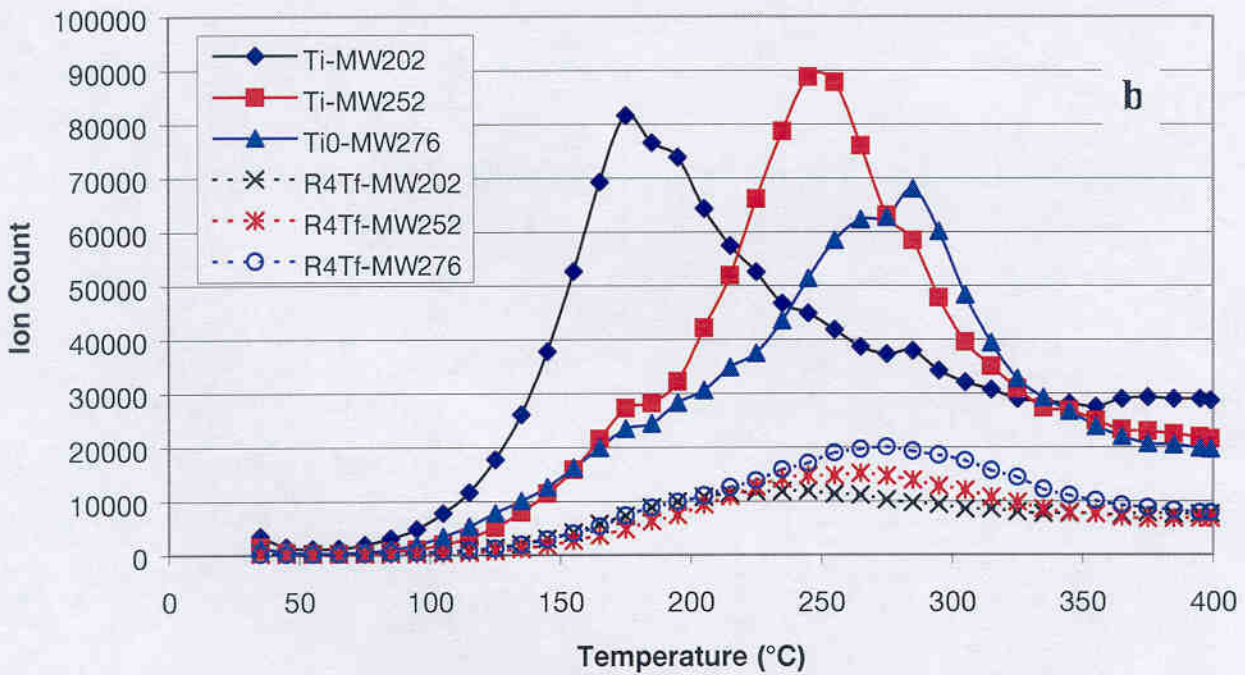
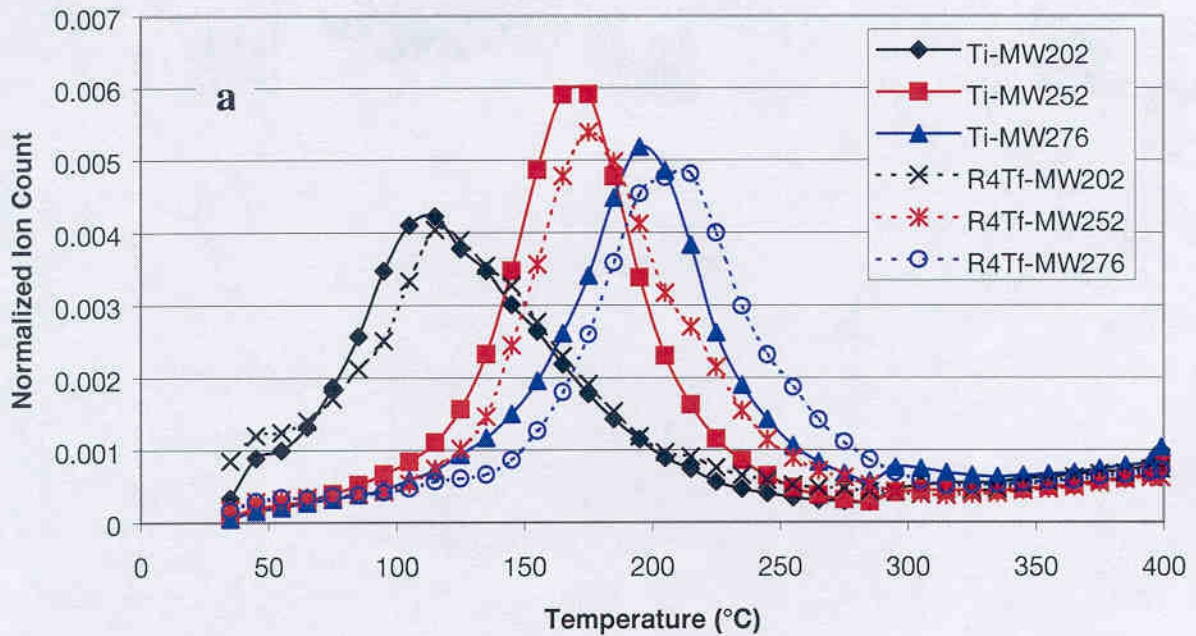


Figure 13. A comparison of Thermal Program Desorption rate response for Milwaukee CDF sediment at initial sampling (T_i) and after 2 months bioslurry treatment (T_2) in reactor 4. The figures show data for PAH homolog 202, 252, and 276 at T_i and T_2 for a 1/8 filled crucible containing size fraction (a) $<.063\text{ mm}$ light and (b) $<.063\text{ mm}$ heavy.

they may be more in the baseline response making clearly defined peaks more difficult to see. This could be related to the difficulty in particle separation or reflect the biodegradation of the PAHs from the <0.063 mm heavy fraction. The heavy fraction PAHs are released at higher temperatures than the light fraction PAH. These data trends are consistent with TPD results reported in Chapter III.

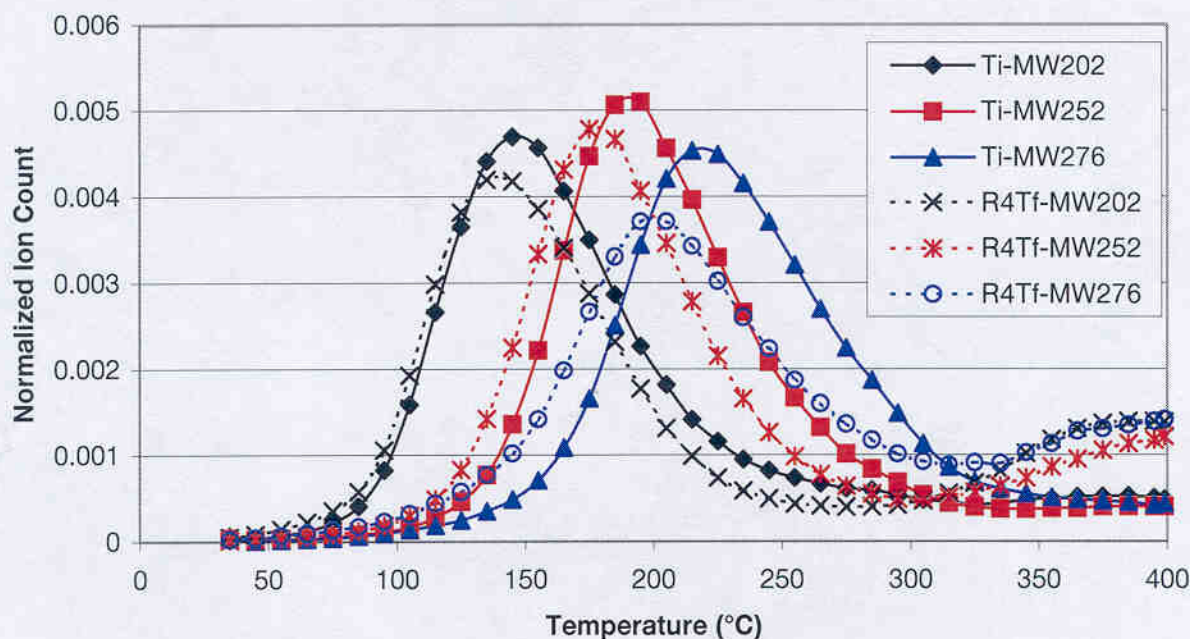


Figure 14. Thermal Program Desorption rate response for Milwaukee CDF sediment at initial sampling (T_i) and after 2 months bioslurry treatment (T_2) for reactor 4. The figure shows data for PAH homolog 202, 252, and 276 at T_0 and T_2 for a 1/8 filled crucible containing size fraction 0.063 - 0.25 mm light.

As explained in Chapter III, the light fraction exhibits higher apparent desorption activation energies than the heavy (clay/silt) fraction. Ghosh et al. (30) described this phenomenon as being attributed to activated diffusion. At room temperatures, the PAHs associated with the heavy fraction (clays/silts) desorb faster than the light (coal/wood) fraction. The PAHs sorbed on the heavy fractions are characterized by much lower binding activation energies, and thus the release is much less temperature dependent. In contrast, as the light (coal/wood) fraction sample is heated in the TPD probe the release of PAHs is very temperature dependent owing to the large desorption activation energy. It is envisioned that this behavior is due to the coal-like structure becoming less rigid and polymeric. The heavy

fraction (clay/silts) organic matter structure does not significantly change with elevated temperatures as that for the coal-like material.

Figure 14 presents similar data as Figure 13a, but for a larger size light fraction (0.063 – 0.25 mm). Like Figures 13a, there is little difference between the peak temperatures of T_1 and reactor 4 T_2 data. However, the peak temperatures are slightly higher (10 to 20°C) than those of the <.063 mm light fraction. One explanation could be that the larger size fraction requires more time to respond to the elevated temperatures thus activated diffusion is delayed. Since the larger size fraction has lower PAHs and surface area, this too could have an effect.

The overall conclusion from the results presented in Figures 13 and 14 is that the bioslurry treatment did not change significantly the character of the sorbent with respect to binding the PAHs.

Summary

We show in this work that the PAHs associated with the fine clay/silt fraction are potentially the PAH contaminants of greatest concern. PAHs associated with coal-like materials are much less available and potentially much less of a concern for protection of the environment, even though the PAHs in this fraction comprises the majority of the PAHs in the sediment. Thus decisions about dredged sediment quality criteria and treatment and material reuse should focus in the PAH associated with the clay/silt fraction.

As the requirements for dredging continue and disposal options become more restrictive, improved assessment of toxicity and risk for contaminants in dredged materials in CDFs is needed. Existing CDFs must find ways to improve decision-making regarding the treatment of PAHs-impacted sediments. The investigative approach presented in this work provides better understanding of contaminant availability and thereby improve the assessment for the potential success of technologies such as biotreatment. By recognizing that both labile and residual fractions of contamination exist, it may be possible to allow the

use of less costly treatments while increasing the likelihood for the reuse of already dredged and deposited sediment.

Acknowledgements

This study was funded by the Strategic Environmental Research and Development Program (SERDP) and the U.S. Army Engineer Research and Development Center (ERDC). We especially thank Ms. Deborah Felt of the Biotechnology Research Group and Mr. David B. Ringleberg, Dr. Edward J. Perkins, and Dr. Herbert L. Fredrickson of the Microbial Ecology Research Group, Environmental Laboratory (ERDC) for providing microbial ecology support and technical collaboration, which made this research possible. Additionally, we acknowledge Dr. Steven L. Larson and the Environmental Chemistry Branch (ECB), also at the Environmental Laboratory, ERDC for their analytical and technical support. We thank the SERDP Technical Advisory Committee (TAC), staff and our Project Shepherd for their helpful comments and suggestions during this research.

Literature Cited

1. Winfield, L.E., and Lee, C.R. "Dredged material characterization tests for beneficial use suitability," DOER Technical Notes Collection (TN DOER-C2), U.S. Army Engineer Research Development Center, Vicksburg, MS., **1999**.
2. Wisconsin Department of Natural Resources, "Soil Cleanup Levels for Polycyclic Aromatic Hydrocarbons (PAHs) Interim Guidance," Publication RR-519-97, April **1997**.
3. Wisconsin Department of Natural Resources, "Guidance For the Beneficial Use of Industrial Byproducts," CH. NR 538, Wis. Adm. Code, April **1998**.
4. Myers, T.E., and Bowman, D.W. "Bioremediation of PAH-contaminated dredged material at the Jones Island CDF: Materials, equipment, and initial operations," DOER Technical Notes Collection (TN DOER-C5), U.S. Army Research Engineer Development Center, Vicksburg, MS., **1999**.
5. Nalkes, D. V.; Linz, D. G; eds. *Environmentally Acceptable Endpoints in Soil*. Annapolis, MD: American Academy of Environmental Engineers, **1997**.

6. NRC, *Contaminated Sediments in Ports and Waterways, Cleanup Strategies and Technologies*, National Research Council Report, National Academy Press, Washington D.C., **1997**.
7. NRC, *Alternatives for Groundwater Cleanup*, National Research Council Report, National Academy Press, Washington, D.C., **1994**.
8. Moore, J.N.; Brook, E.J.; Johns, C.; "Grain Size Partitioning of Metals in Contaminated Coarse-Grained River Flood Plain Sediment", *Environmental Geology and Water Science*, **1989**, 14(2): 107-115.
9. Alexander, M. *Environ. Sci. Technol.* **1995**, 29, 2713-2717.
10. Myers, T. E., and Williford, C.W. "Concepts and technologies for bioremediation in Confined Disposal Facilities," DOER Technical Notes Collection (ERDC TN-DOER-C11), U.S. Army Engineer Research Development Center, Vicksburg, MS., **2000**.
11. Cornelissen, G.; Riggerink, H.; Ferdinandy, M.M.A.; van Noort, P.C.M. *Environ. Sci. Technol.* **1998**, 32, 966-970.
12. MacRae, J.D.; Hall, K.J. *Environ. Sci. Technol.* **1998**, 32, 3809-3815.
13. Tang, J.; Robertson, B.K.; Alexander, M. *Environ. Sci. Technol.* **1999**, 33, 4346-4351.
14. Talley, J.W., Ghosh, U., Tucker, S.G., Furey, J.S., Luthy, R.G. "Thermal Programmed Desorption of PAHs From Mineral and Organic Surfaces," *Environ. Sci. Technol.* Submitted, **2000**.
15. Bowman, D.W., Brannon, J.M., and Batterman, S.A. "Evaluation of Polychlorinated Biphenyl and Polycyclic Aromatic Hydrocarbon Concentrations in Two Great Lakes Dredged Material Disposal Facilities," Water Quality 96 Proceedings of the 11th Seminar, 26 February – 01 March 1996, Seattle, Washington, Miscellaneous Paper W-96-1, July **1996**.
16. American Type Culture Collection, "ATCC Culture Medium 1127 Stanier's basal medium," www.atcc.org, **2000**.
17. Ghosh et al., 2000 ES&T 34, 1729-36.
18. Pignatello, J.J., *Environ. Toxicol. Chem.*, **1990**, 9, 1107-1126.
19. Cornelissen, G., Van Noort, P.C.M. and Grover, A.J., *Environ. Toxicol. Chem.*, **1997**, 16, 1351-1357.

20. Fulthorpe, R.S., Rhodes, A.N., and Tiedje, J.M. Pristine soils mineralize 3-chlorobenzoate and 2,4-dichlorophenoacetate via different microbial populations. *App. Environ. Microbiol.* **1996**, 62:1159-1166.
21. White, D.C. and Ringleberg, D.B. "Signature lipid biomarker analysis." In: *Techniques in Microbial Ecology*, Oxford University Press, Inc. New York, **1998**, 255-272.
22. Pinkart, H.C., Devereux, R. & Chapman, P.J. Rapid separation of microbial lipids using solid phase extraction columns. *J. Microbiol. Meth.* **1998**. 34:9-15.
23. Borenorneman, J., Skroch, P.W., O'Sullivan, K.M., Palus, J.A., Rumjanek, N.G., Jansen, J.L., Nienhuis, J., and Triplett, E.W. "Molecular Diversity of an Agricultural Soil in Wisconsin," *Applied and Environmental Microbiology*, 1996, 62, 1935-43.
24. Tang, J., Carroquino, M.J., Robertson, B.K., Alexander, M., *Environ. Sci. Technol.* **1998**, 32, 3586-3590.
25. Tang, J., Robertson, B.K., Alexander, M., *Environ. Sci. Technol.* **1999**, 33, 4346-4351.
26. EPA, *Ecological Effects Test Guidelines*, OPPTS 850.6200 Earthworm Subchronic Toxicity Test, EPA712-C-96-167, April **1996**.
27. EPA, *Protocols for Short Term Toxicity Screening of Hazardous Waste Sites*, EPA/600/3088/029, February **1989**.
28. ASTM, "Standard Guide for Conducting Laboratory Soil Toxicity or Bioaccumulation Test With the Lumbricid Earthworm *Eisenia foetida*," E 1676-97, February **1998**.
29. Ringelberg, D., Talley, J.W., Perkins, E., Tucker, S., Luthy, R.G., and Bower, E. "Succession of Phenotypic, Genotypic and Metabolic Community Characteristics During Treatment of PAH-Contaminated Sediment," *Applied and Environmental Microbiology* (In Draft).
30. Ghosh, U., Talley, J.W., Luthy, R.G., "Kinetics and Thermodynamics of PAH Desorption from Sediment Particles," *Environ. Sci. Technol.* (In Draft).

Section 8

Summary and Conclusions

The purpose of this work was to apply new techniques to assess the locations, distribution and associations of polycyclic aromatic hydrocarbons (PAHs) in dredged harbor sediment. This investigation explored the processes controlling PAH sequestration using physical, physicochemical, chemical, and biological analyses. One 55-gallon drum of dredged material from the Milwaukee confined disposal facility (MCDF) was collected and transported to the Environmental Laboratory, U.S. Army Engineer Research and Development Center (ERDC). The dredged material was homogenized and samples collected for bioslurry treatment testing and for PAH analyses on various size and density fractions.

Direct Observation of PAHs at the Sub-Particle Scale

Microprobe two-step laser desorption ionization mass spectroscopy (μL^2 MS) was used to identify and characterize PAHs found on laboratory and aged field samples. The data showed lateral variation in the extent of sorption at the sub-particle scale, which indicates that sorption phenomena are heterogeneous at the sub-particle dimensions.

Microscale Location, Characterization, and Association of PAHs

Microprobe two-step laser desorption laser ionization mass spectroscopy was used for PAH measurements, infrared microspectroscopy was used for organic carbon measurements, and scanning electron microscopy with wavelength dispersive X-ray spectroscopy was used for elemental microanalysis. PAH concentrations on coal- and wood-derived particles were found to be several orders of magnitude higher than on silica particles in the Milwaukee Harbor sediment samples. A cryomicrotome sectioning procedure was employed for particle cross-sectional investigations and it was found that most PAHs are concentrated on external surface regions indicating near surface sorption mechanisms.

Physical Analyses

Physical analyses involved separating the whole sediment into four size fractions (>1000 μm , 1000-250 μm , 250-63 μm , and <63 μm) for purposes of determining if PAH presence and availability differ within the sediment. These size fractions (except >1000 μm) were further separated out by density resulting in heavy (clay/silt) and light (coal/wood) density fractions. The heavy sediment fraction in the sediment, which includes clays, silt, and sand, constituted 95% of the sediment by weight. The light sediment fraction comprising coal-derived material and debris constituted the remaining 5% of the sediment weight.

Chemical Analyses

Chemical analyses included sediment PAH analysis by soxhlet extraction with GC/MS and PAH analyses using GC-FID for determination of PAH distribution by particle size and type. Total PAHs in the whole sediment before bioslurry treatment were 115 mg/kg; however, concentrations for the lighter, coal-derived material in the sediment ranged from slightly less than 1000 mg/kg (1000-250 μm) to almost 4000 mg/kg (<63 μm). PAHs in the heavy fractions were primarily limited to the <63 μm size fraction with concentrations at 35 mg/kg. More than 60% of the PAHs were in the light fractions, principally associated with coal-derived material.

Bioslurry Treatment

The bioslurry reactor studies consisted of six reactors and were operated for four months. Two active bioslurry reactors were controls (anaerobic and poisoned) and the remaining were active, (aerobic) bioslurry reactors. Each reactor had 1.5 liters of sediment (30% by volume) and 3.5 liters (70% by volume) of a modified Stanier's Basal Media with no added carbon source. Chemical analyses after bioslurry treatment indicated that total PAH concentrations declined by 50%, with some individual PAHs showing reductions greater than 65% (i.e., anthracene, fluorene, and acenaphthene). A marked distinction was observed between the biodegradation of PAHs on the heavy and light sediment fractions. PAH degradation was mainly achieved in the <63 μm clay/silt fractions, which exhibited slightly over 75% reduction over the 4-month bioslurry treatment. The coal/wood material in the <63 μm to 1 mm size fractions showed no reduction of PAH concentrations. This

marked difference in PAH biodegradation between the clay/silt and coal-derived sediment fractions was shown to result from substantially different availabilities of the PAHs on these materials.

Physicochemical Analyses

Physicochemical analyses included room temperature Tenax bead aqueous desorption experiments and thermal program desorption (TPD) studies. Room temperature desorption kinetic studies using Tenax beads as PAH extractants were conducted to measure the physical availability of PAHs from the different sediment fractions. The intermediate size fraction of the light coal-derived particles (0.063-25 μm) and the heavy silt and clay fractions (<0.063 μm) were used for the desorption kinetic tests. PAH desorption kinetic studies on these separated fractions revealed a relatively low availability of PAHs from the coal-derived (light) fraction and a high availability from the clay/silt (heavy) fraction. As concluded from the TPD studies described below, PAHs associated with clays and silts desorbed faster at room temperatures and are characterized by low binding activation energies, whereas PAHs associated with coal-derived material desorbed at a much slower rate and are characterized by high binding activation energies.

Thermal Programmed Desorption

The initial TPD effort investigated the release of PAHs from solid surfaces and sediment particles using thermal desorption mass spectrometry. An experimental protocol was developed to obtain real-time PAH desorption data through use of a TPD probe that places the sample directly in the ion volume of a mass spectrometer then gradually heats the sample at a predetermined rate. Thermal desorption profiles of milligram-size samples were analyzed in order to explore the release of PAHs from mineral and organic surfaces and to compare the release of PAHs with increasing molecular weight. This showed that the release of PAHs is dependent both on PAH molecular weight and the character of the sorbent material.

TPD tests were then used to examine semi-quantitatively the apparent PAH binding activation energies, as interpreted from TPD rate responses, for Milwaukee CDF sediment

before and after bioslurry treatment. TPD rate responses for PAH MW 202, 252 and 276 from the <0.063 mm light, <0.063 mm heavy, and the 0.063 – 0.25 mm light size fractions were evaluated. PAH thermograms from both density fractions shifted to the right with increasing molecular weight indicating that higher molecular weight PAHs have higher binding energy. Peak temperatures for pre- and post-bioslurry treatment also remain similar, with the exception that the biotreated heavy fraction was low in ion count indicating a loss of PAHs. The fact that peak temperatures did not change for the lighter, coal-derived particles from the bioslurry treatment shows that biotreatment did not change the character of the sorbent.

TPD-MS measurements showed that PAHs on the heavy fraction sediment particles were released at higher temperatures than PAHs on the light fraction sediment particles PAHs. This phenomenon is attributed to lack of significant activated diffusion processes for this size fraction. At room temperatures, the PAHs associated with the heavy fraction (clays/silts) desorb faster than the light (coal-derived) fraction. The PAHs sorbed on the heavy fractions are characterized by much lower binding activation energies, and thus the release is much less temperature dependent. In contrast, as the light (coal-derived) fraction sample is heated in the TPD probe the release of PAHs is very temperature dependent owing to the large desorption activation energies. It is envisioned that this behavior is due to the coal-like structure becoming less rigid and polymeric with increasing temperature. The heavy fraction (clay/silts) organic matter structure does not significantly change with elevated temperatures as that for the coal-like material. The overall conclusion from the results is that the bioslurry treatment did not change significantly the character of the sorbent with respect to binding the PAHs, and that the bioavailability of the PAHs is described by two markedly different responses owing to differences in binding activation energies.

Biological Analyses

The biological analyses consisted of microbial analyses and earthworm bioassays. The microbial analyses included radiolabeled microcosm studies, polar lipid fatty acid analyses (PLFA) characterization, and DNA analysis. The microcosm studies used radiolabeled PAHs to confirm that PAH-degrading microorganisms were present in the

sediment. Mineralization rates for each of the PAHs examined were greatest at times T₁ month and T₂ month, corresponding to the greatest biomass levels and the introduction of nutrients.

The PLFA characterization identified the level of biomass present in the sediment and provided general information about the microbial community structure. The DNA analysis was utilized to target the presence of select genes known to be present during active PAH degradation. Ester-linked phospholipid fatty acid analysis revealed a significant increase in microbial biomass and a shifting microbial community structure with the observed decrease in total PAH concentration. Nucleic acid analyses revealed that copies of genes encoding PAH-degrading enzymes (extradiol dioxygenases, hydroxylases and meta-cleavage enzymes) increased by as much as four orders of magnitude during the bioslurry treatment with the shift in gene copy numbers correlating with shifts in microbial community structure and PAH reduction.

Earthworm Bioassays

Earthworm bioassays evaluated the adverse effects of the PAHs associated with the sediment to earthworms (*Eisenia fetida*). Both acute toxicity and bioaccumulation tests were performed. The acute toxicity was a 14-day exposure test that measured the survivability of the earthworms. The bioaccumulation test was a 28-day test that measured PAH uptake within earthworm tissue. Earthworm acute toxicity tests with Milwaukee Harbor dredged sediment showed a 100% survival rate indicating that the PAHs present initially in the sediment were not toxic to induce death. It is unclear if this is due to PAH concentration below earthworm toxicity thresholds or if the PAHs were limited in their availability due to strong binding.

Earthworm bioaccumulation tests were performed on sediment before and after bioslurry treatment. These data comprised an average of the results from 192 earthworms exposed to sediment before treatment and 144 earthworms exposed to triplicate sediment samples after four months of bioslurry treatment. The uptake of total PAHs in earthworm tissue from the untreated sediment was 8.1 mg/kg. Earthworm uptake after bioslurry

treatment was reduced to 2.0 mg/kg. This represents a 75% reduction in total PAH uptake. There were seven PAHs (naphthalene, 2-methylnaphthalene, acenaphthene, fluorene, fluoranthene, pyrene, and benzo(b)fluoranthene) with concentration reductions over 80%. Both the PAH content in the clay/silt fraction and the bioaccumulation of PAHs by earthworms decreased 75% as a result of bioslurry treatment. Since there was no reduction of PAHs on the coal-derived particle fractions, there is a strong correlation between the individual PAHs biodegraded on the clay/silt fraction and those reduced in earthworm tissue uptake. This observation suggests that only the PAHs in the clay/silt fraction comprise the readily available fraction to both microorganisms and earthworms.

Significant Findings

The significant findings of this work are: the release of PAHs is dependent both on PAH molecular weight and the character of the sediment sorbent material; most PAHs are concentrated on external surface regions indicating near surface sorption mechanisms; two principal sediment particle classes dominated the distribution and release of PAHs; clay/silt and coal-derived; PAHs were found preferentially on coal-derived particles; clay/silt particles released PAHs more readily than coal-derived particles; bioslurry treatment reduced PAHs on the clay/silt fraction but not the coal-derived fraction; PAH reduction in clay/silt fractions by biotreatment resulted in significant reduction in earthworm PAH bioaccumulation; PAHs on coal-derived particles were associated with high binding activation energies; and changes in the phenotype and genetic potentials of the extant microbiota can be used to assess intrinsic biodegradative potential.

Benefits

The benefits of this work include: improved assessment of toxicity and risk for PAH contaminants in sediments by use of particle-scale techniques to assess PAH distribution and behavior; improved assessment for the potential success of biotreatment through understanding of factors contributing to the available and unavailable PAH fractions; improved decision making regarding sediment quality criteria for PAHs and the biotreatment of PAH-impacted sediments; and reduced treatment costs and greater likelihood for reuse of

dredged sediments through knowledge of the underlying processes affecting PAH locations, availability, treatability, and toxicity.

This work shows that the PAHs associated with the fine clay/silt fraction are potentially the PAH contaminants of greatest concern. PAHs associated with coal-like materials are much less available and potentially much less of a concern for protection of the environment, even though the PAHs in this fraction comprise the majority of the PAHs in the sediment. Thus, decisions about dredged sediment quality criteria, and sediment treatment and material reuse, should focus on the PAHs associated with the clay/silt fraction, not on total PAHs in bulk sediment.

As the requirements for dredging continue and disposal options become more restrictive, improved assessment of toxicity and risk for contaminants in dredged materials in CDFs is needed. Existing CDFs must find ways to improve decision-making regarding the treatment of PAH-impacted sediments. The investigative approach presented in this work provides better understanding of contaminant availability and thereby improves the assessment for the potential success of technologies such as biotreatment. By demonstrating that both available and unavailable fractions of PAH contamination exist in sediment, and showing the connection to sediment treatment and toxicity, it may be possible to allow the use of less costly sediment treatments while increasing the likelihood for the reuse of already dredged and deposited sediment.

Limitations and Future Work

Direct inserted probe TPD-MS is not ready as a stand-alone tool for the assessment of the availability and treatability of PAHs in sediments. Numerous limitations still exist which prevent application beyond the research and development arena. Small sample size heterogeneity, fluctuating TPD responses for varying materials and low-molecular weight compounds, and difficulties in data reduction all contribute to the need for more work. More fundamental TPD research needs to be done on well-defined substrates. Using more homogenous substrates, varying PAH concentrations, and varying temperature ramps could increase our understanding of release mechanisms. This knowledge could improve our

ability to properly model and assess PAH sequestration mechanisms from TPD responses. TPD-MS/MS capabilities could be utilized to further examine the structural effects and differences of binding for PAHs with the same molecular weight. These results could then be compared to various sub-sample physical and geochemical characteristics, PAH location and distribution, and PAH treatment and toxicological effects, which together could further define the issues of risk and exposure for residual and less mobile PAHs.

The overall approach presented in this work should be extended to other sediments and soils to determine if similar observations and conclusions can be made. Other contaminants, such as TNT and PCBs, should be examined. These compounds are tightly bound in soils and sediments and may have availability and treatability characteristics similar to PAHs. The knowledge that PAHs in the Milwaukee CDF sediments were preferentially bound to coal-derived particles, suggests that such materials may be used beneficially to in-situ stabilize the labile and mobile fraction of PAHs. Sediment dredging in conjunction with particle separation should explore large-scale, selective separation techniques to process the PAH-laden light sediment fraction. Future remediation strategies should target the heavy, fine-grained, sediment fraction, which represents the available and treatable PAHs.

APPENDICES

Appendix A

Measurements of Microbial Activity on Sediment Particle Surfaces and Correlation with Distribution of Sorbed PAHs

Summary

An in situ PCR technique has been partially developed to detect the presence of bacteria on soil particle surfaces that carry naphthalene dioxygenase genes related to the *nah A* dioxygenase gene in *Pseudomonas putida* NCIB 9816. This is the first application of in situ PCR to the observation of bacteria attached to surfaces. The success of the technique depends in large part on the preparation of the soil/sediment particles. A workable procedure has been developed to circumvent problems with the permeabilization process and the inhibition of PCR caused by the presence of soil particles. PCR was performed on single sand grains and amplicons could be detected using PCR primers for 16s RNA and *nah A* genes. Success with in situ PCR has not been obtained to date. As a model system, we have examined attached PAH-degrading microbial communities in contaminated soils where degradation activities have been enhanced by treatments with bulking agents, fertilizer, and an organism that produces a biosurfactant. Samples of these soils were tested in our procedure for fixing the attached cells and making them permeable to PCR reagents. Attached cells, as shown by acridine staining, remained fully intact during the process and should be amenable to PCR detection.

Work to develop a green fluorescent protein (GFP) sensor for PAH degradation activity has been marginally successful, and we are nearing the point where we may have a workable biosensor for phenanthrene on soil particle surfaces. We underestimated the complexity of developing this system. We can now, however, express our GFP construct (expression controlled by phenanthrene) in a suitable host and show that it is effected by phenanthrene. Unfortunately, expression is very faint and further work is proceeding to make the system amenable to use directly in soil.

Background

The objective of this project has been to develop methods for monitoring the activities of individual bacteria or clusters of bacteria on the surface of contaminated soil or sediment particles and to relate this activity to the presence of sorbed PAHs that might be serving as a growth substrates for the bacteria. Efforts this year continue to develop in situ PCR methods for bacteria attached to soil particle surfaces and to develop a biosensor for phenanthrene degradation based on controlled expression of green fluorescent protein (GFP) as the reporter system.

In situ PCR is a relatively new technique that is based on the idea that the reagents for a PCR reaction can be infused directly into fixed and permeablized cells where they will function to produce amplicons of a particular gene sequence. If the amplicons are then detected using a fluorescently-labeled nucleic acid probe, cells will, in essence, appear green in an epifluorescence microscope. In situ PCR has been used commonly with tissue culture studies but has only recently been demonstrated for bacteria. To date, procedures for the detection of four genes have been developed. These are the dioxygenase genes for naphthalene, *nah A* (Hodsen et al., 1995), and toluene, *todC1* (Chen et al., 1999), the nitrogen fixation gene, *nifH* (Hodsen et al., 1995), and the 16S rRNA sequences of lignin degrading bacteria (Chen et al., 1997).

A summary of the in situ PCR technique is provided to aid in understanding the process. The sequence of bases of a particular gene must be known. In our case, we used the A subunit of the naphthalene dioxygenase gene (*nah A*) in *Pseudomonas putida* strain NCIB 9816 which has been sequenced by Yang et al., (1996). In last year's report, we selected two short sequences (primer design) that would amplify the *nah A* gene by PCR. Oligonucleotides complementary to these sequences were synthesized and used as PCR primers. The primers are infused into permeablized cells (cell walls made porous) where they hybridize to their complementary region in the cell's DNA; that is the sequences selected to define the *nah A* gene. DNA polymerase is added to the cells along with appropriate nucleoside triphosphate bases. The polymerase fills in the space between the primers with bases using the cell's DNA as a template. The resulting synthesized piece is the amplicon of the *nah A* gene. The cells are then heated to 90°C which causes the DNA to denature and release the amplicon from the DNA. When the cells were cooled to 50°C, the DNA reanneals and the primers stick again their complementary region in the cell's DNA. This allows the polymerase to make another amplicon. Repeating the heating and cooling cycle many times (70 in our case), produces many amplicons. A nucleic acid probe, carrying a fluorescent chromophore, is then added to the cells. The probe is a short oligonucleotide (30 bases) that is commercially synthesized with a sequence that is exactly complementary to a 30 base sequence in the middle of the amplicon. The probe will therefore hybridize only with the amplicon. If there is no amplicon present the probe will be washed out of the cells. Since the probe carries a chromophore that fluoresces green, only cells containing the amplicon-probe will appear green under an epifluorescence microscope. Green cells mean that they contain a *nah A* gene very similar to that in NCIB 9816; that is, the PCR primers find complementary regions in the cells DNA to hybridize to and thus commence PCR. These are not

necessarily NCIB cells, but other cells carrying a very similar *nah A* gene. The *nah A* gene is known to be wide spread in the environment, especially in PAH-contaminated soils (Sayler and Layton, 1990). We associate the *nah A* gene with the ability to degrade naphthalene and phenanthrene. Thus, in situ PCR, in this case, reveals the presence of cells with the capability to degrade PAHs. It does not determine if the cells are degrading PAHs (i.e., expression). Expression will be the next step after having established that the capability exists.

In Situ PCR Protocol

Using the method described above and following the work of Chen et al, 1995, 1997) we have found that the in situ PCR procedure is very sensitive to the permeabilization step. The permeabilizing step requires fixing the cells with para-formaldehyde, followed by a desiccation step with ethanol, and finally a lysozyme treatment to partially breakdown the cell walls and allow the PCR reagents to diffuse inside. Too much lysozyme totally disintegrates the cells and leaves nothing to visualize. We have optimized this procedure, after considerable trial and error, using staining of cells with acridine orange and a special DNA stain, YoPro. If cells are permeabilized appropriately, they are left intact with their DNA. Acridine orange and YoPro stain cells by interaction with DNA, producing green fluorescence under an epifluorescence microscope. If the cells have been damaged by the permeabilization process (DNA leaks out), and much less fluoresce occurs. The objective was to visualize mostly green cells on soil particle surfaces that had been treated with the permeabilization process. Green cells mean the DNA is present and PCR can then be performed. The procedure outlined below gives green cells on particle surfaces.

In addition, we have been using a different form of PCR to check our soil preparations. This involves universal PCR primers for sequences in the 16sRNA genes that are common to all bacteria. Thus, DNA from any bacteria associated with the soil particles can be amplified and the technique can be used to detect any interferences in the PCR process.

The procedure for preparing soil particles and attached microorganisms for PCR is as follows. Small 1g samples of Popile soil were suspended in phosphate buffered saline (PBS). Popile soil was used because it is contaminated with PAHs and it is one of the soils that has a reasonable number of live bacteria attached to surface of silica sand particles. Sand grains are the optimal size particles to work with because they are Large enough for laser probe analysis of PAHs on the particle surface. The presence of bacteria on these sand grains, however, is highly variable. Smaller particles (clays, aggregates, small sand grains), which are generally where most of the bacteria are located, can also be used for chemical analysis using a technique described below.

The soil suspension was vigorously mixed (not vortexed) and the heavy particles allowed to settle for a few seconds. The fines that remained suspended were decanted off

and saved. Fresh PBS was added and the process repeated. After approximately 10-15 washes, very few fines remained that could be decanted off. Microscopic examination showed that the heavy particles were primary large sand grains with a light yellowish-brown coating on most particles. The sand grains can be easily pick (with forceps) by hand and placed in a drop of PBS on a microscope slide. By repicking the sand grain several times and washing it in fresh PBS, a collection of "pure" sand grains can be obtained. Microscope examination shows they are generally of free unattached bacteria. However, in continued handling of the sand grains, bacteria tend to sluff off the surface. This hand picking process also allows only sand grains with a yellow to black coating "dirty" sand grains) to be collected.

The fines (pooled from the washing of the big particles), if allowed to settle for a longer time, will have heavier particles settling out. We refer to these as the "heavy fines". The heavy fines can be further washed to remove the light fines, the latter being discarded. The heavy fines consist of very small sand grains, some of which are dark brown and some of which have bacteria on their surfaces. These particles can also be hand picked, but it is harder to eliminate background cells and light fines.

Sand grains were then resuspended in fresh cold (4°C) para-formaldehyde solution (4% in PBS) to fix the attached cells and incubated for 90 minutes in an ice bath. The sand was then rinsed three times with PBS by resuspension and decanting. Bacteria on the sand particle surfaces were dehydrated by successively resuspending and decanting the sand particles in 50%, 70%, 85%, and 98% ethanol. The final prep was left slightly moist and stored 4°C. Cells remained intact in this state for considerable periods and thus a large sample could be prepared and repeatedly subsampled. Attached cells were then permeabilized by treatment with lysozyme solution (0.5 µg/ml in EDTA/TRIS buffer with 0.01U/µl RNase) was for 15 minutes and washed 3 times with PBS. These cells had to be used for in situ PCR or staining within 24 hours.

Following fixing, sand grains were individually picked for staining or PCR. The initial use of microchambers for the PCR reaction proved inefficient and instead, PCR was performed in small Eppendorf tubes. This change came about following work conducted in Dr. Robert Hodson's laboratory. We now know that any more than 2-3 "dirty" sand grains in a reaction mixture (50 µl, working volume) inhibits the PCR reaction as monitored using the 16sRNA primers. This procedure involved an initial step in the PCR sequence to heat the soil particles to 95°C for 10 minutes, thus releasing DNA into solution where amplification occurs. A positive control was also used in which standard template DNA was added to the reaction mixture. The template produces a specific 528 base pair amplicon that can be recognized by gel electrophoresis. If this amplicon is not produced, the PCR process, in general, is not working. PCR is known to be easily inhibited by the presence of soil organic matter and this seems to be reflected by its sensitivity to the sand grains. Inhibition is often due to effects on Mg^{++} concentrations or adsorption of the reactants, especially the DNA, on to the particle surfaces. We have spent considerable time optimizing the conditions for PCR in the presence of sand grains. The best conditions in the presence of **one** sand grain were 4 mM Mg^{++} , 20 mM dNTP's, 50 pmol of each primer, 7 units of polymerase, and 2.5%

DMSO. Figure 1 shows typical results. Most importantly, an amplicon was produced in the absence of template which shows that bacteria on the sand particle had DNA that could be amplified by the 16sRNA primers. Permeablization of the cells on the sand grains reduced that amount of the 16sRNA amplicon produced, but it was nonetheless, detected.

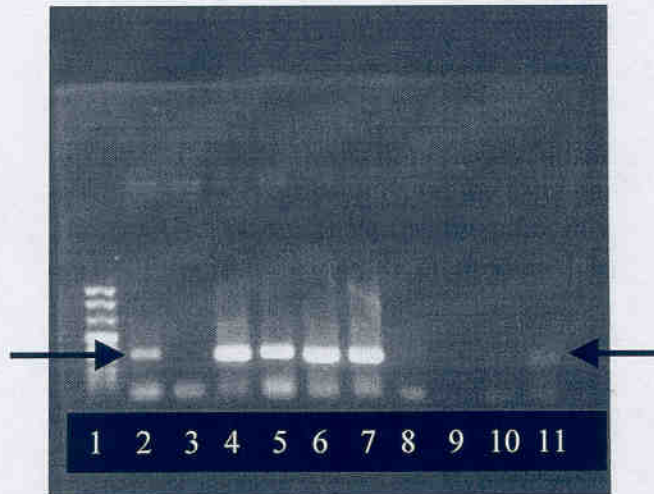


Figure 1. Gel electrophoresis of PCR products (arrow) produced from added DNA (template) and DNA extracted from sand grains. Lane 1; 500 bp ladder, lane 2; PA 64 DNA alone: lanes 3-7 are PA 64 DNA, two sand particles and increasing concentrations of Mg^{++} from 1.5 mM to 6.5 mM; lanes 8-11 are no added DNA and two sand grains using the same titration with Mg^{++} .

The experiments were repeated with the *nah* primers for the *nah A* gene of NCIB; positions 653 to 674 and position 758 to 1779. These are referred to as the 396 and 397 primers. Their sequences are 396 *nah A* 5' AAG CTT CGC TAT GAA CAT TC and 397 *nah A* 3' GGT ACC GCT TCG TTA TTA GAC TTA. By using the initial heating step to release DNA from the soil particles (2 dirty sand particles), an amplicon corresponding to the *nah* region (702 base pairs) was detected, both in the presence of template (NCIB DNA) and in the absence. In the latter case, this suggests that there are cells associated with the sand grains that have DNA sequences homologous to the *nah A* gene.

We have performed similar studies with the heavy fines and gotten similar results. The heavy fines must be diluted to approximately 10^5 particles per ml to avoid inhibition of the PCR reaction.

Previous studies with the use fluorescently labeled nucleoside triphosphate bases in the PCR reaction produced nonspecific binding of the bases and the production of false positives (i.e., the observation of green cells on particle surfaces may not have been due to in situ PCR). We have tried many different variations of the procedure described by Hodson et al. (1995), but with little success. Based on the work of Dr. Chen and Dr. Hobson (Chen et al., 1999), we switch to the fluorescently labeled nucleoside probe approach outlined above. This can be used for either 16s RNA or *nah A* gene amplicons. We have had a probe synthesized that is specific for the *nah A* gene amplicon produced by our PCR primers. It has the following sequence;

5' CY3- CTC GCT GGC AAT GCG GCG CTA CCA CCT GAA -3'.

CY3 is the chromophore synthesized into the probe. It will emit orange-red fluorescence with yellow light excitation.

Following a PCR reaction, the sand particles must be examined microscopically. This is best done by decanting off most of the liquid and then transferring the particles to a glass slide with a Pasteur pipette. The particles are picked with a forceps and placed on two sided sticky tape on a second slide. Once the liquid evaporates, the particles stick to the tape. A drop of water is added back to the slide to hold a cover slip and the particle is observed under oil immersion 600x epifluorescence. The cover slips keeps immersion oil off the particles. The tape can be scored with a razor blade to provide reference lines locating the particle. Since with sand grains there is only one to two particles to observe, location is not difficult. This procedure now allows us to work with individual sand particles and to focus on specific sites on a particle where attached cells are found and where microchemistry can be performed. Heavy fines can also be attached to the sticky tape. This allows one to scan over the particles with the desorption laser. Hopefully particles, rather than the particle surfaces, with associated PAHs will be detected and these can be collocated with the insitu PCR.

Examination of Attached Bacterial Cells in Popile Soil

As we indicated above, it was important to demonstrate that we could visualize bacterial cells on a soil particle surface following the cell permeablization procedure. Staining cells with acridine orange or YoPro dye served this purpose because, if this was not possible, in situ PC would also not work. DNA specific dyes will stain all cells, whereas in situ PCR will presumably stain only cells containing the *nah A* gene sequence. Samples of Popile soil from different treatments were therefore run through the fixing and permeablization procedure described above. Attached cells could indeed be observed on sand particle surfaces following fixing with para-formaldehyde and ethanol and permeablization with lysozyme. Thus these cells should be readily amenable to in situ PCR.

In the process, we have discovered that Popile soils treated with dried blood fertilizer and a biosurfactant producing microorganism, strain PA 64, have sand particles covered with attached bacteria. These bacteria are clearly in patches on the sand particle

surfaces and often associated with the edges of crevices and depressions. The soil samples from which these particles were obtained showed considerable degradation of PAHs after 11 months incubation. Sand particles taken from Popile soils that were not treated with the fertilizer and the biosurfactant producer show much less colonization of the surfaces.

Establishing a permanent record of the cells visualized on the surfaces of the sand particle surfaces is tricky. First, the fluorescence is quickly bleached when observed under the epifluorescence microscope. This will be as true for the nucleic acid probe with the attached chromophore, as it is with the staining. Thus images have to be taken quickly. Second, the depth of field in working with a sand grain is large, even at 200x magnification, which is the lowest power in which bacteria are visible. Examples of are shown in Figure 2. In some cases, one can scan up the side of a crevice where bacteria are located, but images must be take quickly before they fade. It is clear however, that patches of bacteria on the sand particle surfaces can be observed at a lower magnification and this will allow us to identify morphological features of the particle. This will give an orientation reference for performing the microchemistry in the same area where the bacteria are located.

Green Fluorescent Protein Expression

Now that we have constructed the proper plasmid containing the green fluorescent protein (GFP) gene coupled to the promoter for the phenanthrene degradation pathway (*pnahP*-GFP; see last year's report), it was necessary to move this plasmid into a phenanthrene degrading strain and get it to express the GFP gene. The principle organisms that we have used are *Pseudomonas putida* stains NCIB 9816 and KBM1. The most direct method for moving *pnahP*-GFP into NCIB was to use electroporation but this has not been successful despite trying many different electroporation conditions. The *nahP*-GFP fragment has been successfully cloned into other broad host range plasmids, pK240 and pRK415 in *E. coli*, but electroporation of the resulting DNA produced only one transformant. That transformant that turned out to be a slow growing culture that weakly produced green color when grown in the presence of salicylate, the inducer of the *nah* genes in NCIB and KBM1. This culture was lost before the presence of the *nahP*-GFP could be verified.

We then began to develop a conjugal mating process that might successfully move the plasmid into NCIB, KBM1, or other strains. This work has been done by Joanne Jones-Meehan and the time she has given to this study is greatly appreciated.

We have used several broad host range plasmids containing GFP constructs in experiments to try to mark *Pseudomonas putida* strain NCIB 9816-4, *P. putida* strain KBM1 and *Acinetobacter calcoaceticus* strain RAG-1. Our strategy was to put the GFP construct either on an antibiotic resistance plasmid in a PAH-degrader or, preferably, insert the GFP construct into the chromosome so that antibiotic selection would not be required to maintain GFP expression. For insertion of GFP into the chromosome, we

used a suicide vector pLBT with a Tn10 transposon and we used a Tn5::gfp transposon. We have performed plate mating conjugation experiments with GFP-tagged conjugative plasmids. The plasmids we have used are:

- 1.) pKT230::GFP (Km^r); we constructed the GFP plasmid from EcoR1 digest of pKT230, which is a 11.9 kb mobilizable broad host range plasmid that has been previously moved into *E. coli*, *Pseudomonas* and *Acinetobacter* as referenced in Bagdasarin et al. (1981).
- 2.) pmut2; a pKEN plasmid carrying a bright mutant of GFP (Cormack et al. 1996).
- 3.) pSMC2; a pmut2 plasmid containing GFP and 1.8kb stabilizing fragment from pUC181.8; stable in the absence of antibiotic selection (Bloemberg et al., 1997).
- 4.) PLOFpttkm; a plasmid carrying Km^r and a construct in which IPTG induces transposition of Tn10 which acts as a suicide vector to the donor. (Herrero et al., 1990).
- 5.) pLBT (ATCC 87711); plasmid containing Ap^r Km^r and a construction pLOFKmGFP which is pLOFpttkm, a promoterless *lacZ* gene in the Tn10 transposon along with GFP - when this transposon jumps from the suicide plasmid vector to either the chromosome or plasmid in recipient cell it will express GFP only if the transposon has inserted into an active gene (Albertson et al., 1996).
- 6.) pUTmini-Tn5GFP (ATCC 87454); a Ap^r Tc^r plasmid with a promoterless Tn5 transposon linked with GFP. When this transposon jumps from the suicide plasmid vector it will express GFP only if the transposon has inserted into an active gene (Stretton et al. 1996).

We have been able to introduce pKT230::gfp into *Pseudomonas putida* NCIB 9816-4 and *Acinetobacter calcoaceticus* RAG-1, and obtained expression. However, the expression of GFP was very faint. None the less, it is responsive to phenanthrene and salicylic acid. Under a fluorescent microscope, the bacteria glowed faintly but not enough to give adequate detection when the GFP-tagged bacteria were added to soil particles from the creosote-contaminated Southern Maryland Wood Treatment or to Popile soil.

References

Albertson et al. 1996 FEMS Microbiol. Lett. **140**:287-294.

Bagdasarin et al. 1981. Gene **16**:237-247.

Bloemberg et al. 1997. Appl. Environ. Microbiol. **63**:4543-4551

Chen, F., J.M. Gonzalez, W.A. Dustman, M.A. Moran, and R.E. Hodson. 1997. In situ transcription, an approach to characterize genetic diversity and activities of prokaryotes. *Appl. Environ. Microbiol.* 63:4907-4913.

Chen, F., W.A. Dustman and R.E. Hodson. 1999. Microscopic detection of the toluene dioxygenase gene and its expression inside bacterial cells in seawater using prokaryotic in situ PCR. *Hydrobiologia.* 401:131-138.

Cormack et al. 1996. *Gene* 173:33-38.

Herrero et al. 1990. *J. Bacteriol.* 172:6557-6567.

Hodson, R.E., W.A. Dustman, R.A. Garg, and M.A. Moran. 1995. In situ PCR for visualization of microscale distribution of specific genes and gene products in prokaryotic communities. *Appl. Environ. Microbiol.* 61:4074-4082.

Sayler, G.S., and A.C. Layton. 1990. Environmental application of nucleic acid hybridization. *Ann. Rev. Microbiol.* 44:625-648.

Stretton et al. 1996. *Appl. Environ. Microbiol.* 64:2554-2559.

Tani, K., K. Kurokawa, and M. Nasu. 1998. Development of a direct in situ PCR method for detection of specific bacteria in natural environments. *Appl. Environ. Microbiol.* 65:1536-1540.

Yang, Y, R.F. Chen, and M. P. Shiaris. 1994. Metabolism of Naphthalene, Fluorene, and Phenanthrene: Preliminary Characterization of a Cloned Gene Cluster from *Pseudomonas putida* NCIB 9816. *J. Bacteriol.* 176(8):2158-2164.

APPENDIX B

Data Reduction Methods and Techniques

The direct probe TPD MS data presented in this paper were reduced with unique programs to enable further analyses. These programs are provided here with explanation and motivation of their use. A flow chart illustrating the handling of the data is shown in the Figure A1. The final output is a set of ASCII numeric data in a convenient universal spreadsheet format.

The raw data produced by the Thermoquest GCQ hardware with the Xcalibur data acquisition software has the "raw" extension (*.raw) denoting their proprietary binary data format. The Xcalibur suite of GC software provides powerful analytical capabilities, but like all such software is designed primarily for the analysis of chromatographic data. The direct probe TPD research does not involve chromatography as with a column, and the shapes and locations of TPD peaks are not describable with GC concepts.

The extensive numerical analysis of the TPD data involves curve fitting and TPD model parameter estimation, which is not possible with the Xcalibur software nor other commercially available software. In fact, although there are commercially available packages from other companies which can convert various kinds of MS and GC data formats, none was available which can convert the *.raw format. Thus, unique programs perform the conversion and reduce the data.

Each of the raw data files represents a single TPD run of a single sample, as described in the paper. The raw data of interest consists primarily of a time series of sets of mass spectra, with the time stamp of each set being the time of recording in decimal minutes from the start of the run. The full-scan spectra recorded the intensities for all the ion masses detected, with the masses recorded as decimal amu. Actually for MS the ion masses are really m/z , and the correct SI units are daltons per electronic charge.

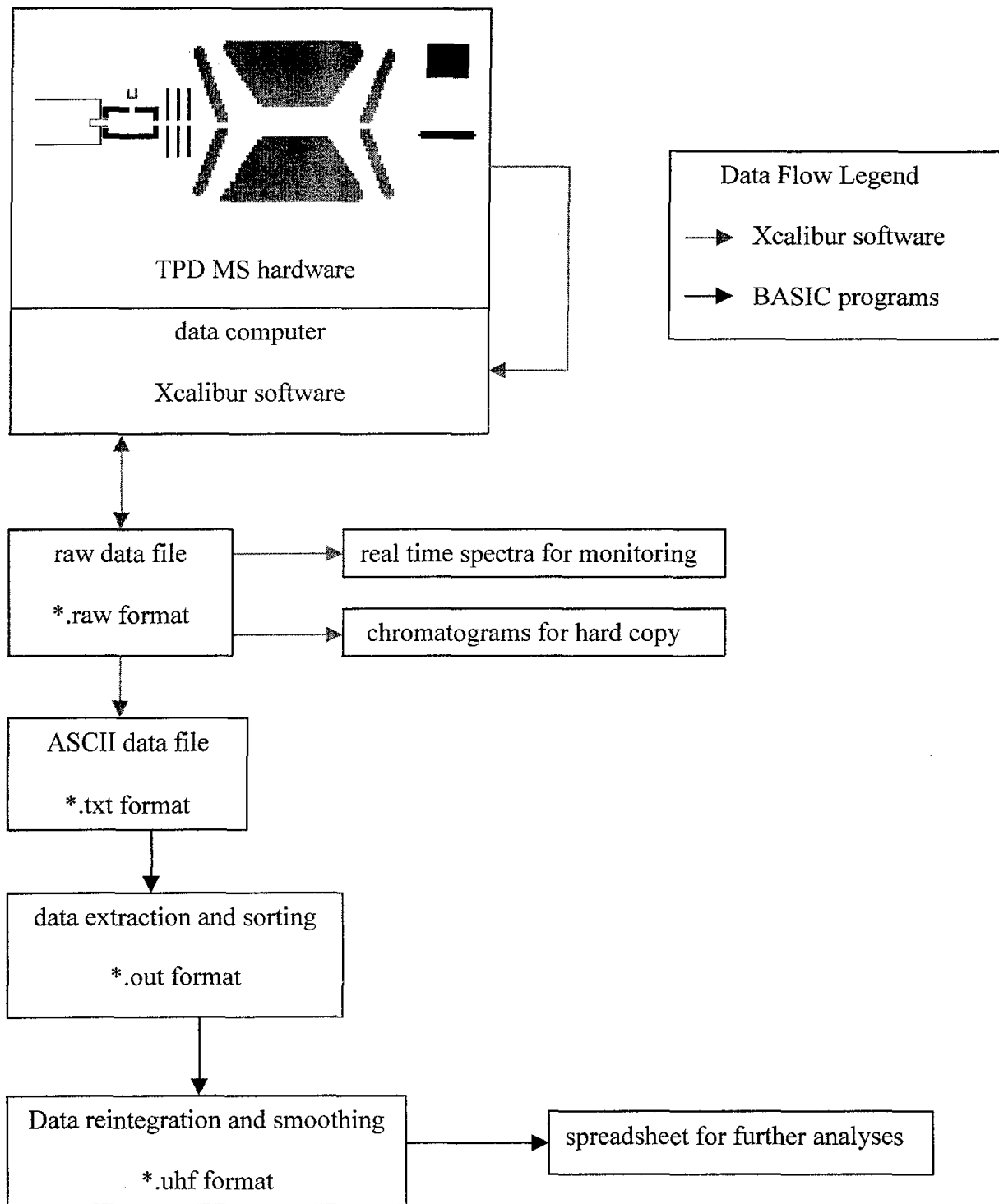


Figure A1. Data Reduction Flow Chart

Many of the ion masses of not of interest for TPD of PAHs. They can be informative of background contamination or indicative of interferences, but are not used further in TPD analysis. There is also other information in the raw data files that is not of interest for further numerical analyses, such as operators' names and other such information. The data of interest must be selected from the other data.

The data reduction programs were written in two parts, one to extract and sort the data of interest from the other data in the raw files, and one to reduce the data of interest to a more convenient form. The data extraction part takes the longest to run, even after using the Xcalibur software to convert the files to an ASCII readable format. The first program extracts the information at each time for selected ion masses, which are the molecular weights (m/z) of the PAH contaminants of concern, rounding each to a standard unit mass width. Other ion masses selected for further analyses enable additional monitoring of the quality of the runs.

The first program implementing the first part is called XCAL-OUT.BAS written in standard BASIC. It can be used compiled, or uncompiled as with Microsoft QBASIC. A hard copy of this program follows. Some of the lines overflow onto new lines to fit this page format, but otherwise it should run as written. A few remarks in single quotes have been inserted to help ensure explanations of operation.

XCAL-OUT.BAS

'This program is written in standard BASIC for maximal portability.'

'This program converts mass spectra from the uniquely formatted Xcalibur data to a standard ASCII numeric spreadsheet format, in order to enable further analyses.'

'The standard format is a type of the universal histogram format, otherwise known as the columnar x many y format, or multivariable times series.'

'The data of interest are the intensities of selected ion masses (m/z) at each time as recorded by the GCQ instrument.'

DIM SHARED intensities(1 TO 12) AS DOUBLE

DIM SHARED masses(1 TO 12) AS DOUBLE

'The first six selected masses are the molecular weights (m/z) of the PAH contaminants of concern for further analyses.'

'The other masses are additionally monitored for reference. Technically the mass units are not amu but daltons per electronic charge.'

masses(1) = 178: masses(2) = 202: masses(3) = 228: masses(4) = 252: masses(5) = 276:

masses(6) = 278:

masses(7) = 128: masses(8) = 152: masses(9) = 153: masses(10) = 154: masses(11) = 165:

masses(12) = 166:

'This program is set up to batch process a variable list of files. The list is manually edited in this version, with no graphical user interface.'

'The *.txt files are in the format produced by the Xcalibur software. The *.out files are used as an intermediate step for convenience, because of the length of time it takes to run.'

'First open the correct files. The dummy variable "filen" is a counter.'

ON ERROR GOTO endit

FOR filen = 1 TO 7

IF filen = 1 THEN

OPEN "060301.txt" FOR INPUT AS #1

OPEN "060301.out" FOR OUTPUT AS #2

END IF

IF filen = 2 THEN

OPEN "060302.txt" FOR INPUT AS #1

OPEN "060302.out" FOR OUTPUT AS #2

END IF

```
IF filen = 3 THEN
OPEN "060303.txt" FOR INPUT AS #1
OPEN "060303.out" FOR OUTPUT AS #2
END IF
IF filen = 4 THEN
OPEN "060304.txt" FOR INPUT AS #1
OPEN "060304.out" FOR OUTPUT AS #2
END IF
IF filen = 5 THEN
OPEN "060305.txt" FOR INPUT AS #1
OPEN "060305.out" FOR OUTPUT AS #2
END IF
IF filen = 6 THEN
OPEN "060401.txt" FOR INPUT AS #1
OPEN "060401.out" FOR OUTPUT AS #2
END IF
IF filen = 7 THEN
OPEN "060402.txt" FOR INPUT AS #1
OPEN "060402.out" FOR OUTPUT AS #2
END IF
```

'What follows next is working through the data file format, sorting, and disregarding irrelevant entries.'

```
FOR n = 1 TO 4
LINE INPUT #1, a$
NEXT n
```

```
LINE INPUT #1, a$
b$ = RIGHT$(a$, LEN(a$) - 12)
n = 1
```

```
DO UNTIL MID$(b$, n, 1) = ","
n = n + 1
LOOP
firstscan = VAL(LEFT$(b$, n - 1))
b$ = RIGHT$(a$, LEN(a$) - 12 - n - 12)
n = 1
DO UNTIL MID$(b$, n, 1) = ","
n = n + 1
LOOP
lastscan = VAL(LEFT$(b$, n - 1))
```

```
FOR n = 1 TO 14
LINE INPUT #1, a$
NEXT n
```

```
FOR s = firstscan TO lastscan
```

```
FOR n = 1 TO 4
LINE INPUT #1, a$
NEXT n
LINE INPUT #1, a$
b$ = RIGHT$(a$, LEN(a$) - 12)
n = 1
DO UNTIL MID$(b$, n, 1) = ","
n = n + 1
LOOP
time = VAL(LEFT$(b$, n - 1))
LINE INPUT #1, a$
b$ = RIGHT$(a$, LEN(a$) - 14)
n = 1
DO UNTIL MID$(b$, n, 1) = ","
```

```

n = n + 1
LOOP
numreadings = VAL(LEFT$(b$, n - 1))
FOR n = 1 TO 10
LINE INPUT #1, a$
NEXT n

FOR n = 1 TO 12
intensities(n) = 0
NEXT n
FOR nr = 1 TO numreadings
LINE INPUT #1, a$
LINE INPUT #1, a$
b$ = RIGHT$(a$, LEN(a$) - 21 - LEN(STR$(nr)))
n = 1
DO UNTIL MID$(b$, n, 1) = ","
n = n + 1
LOOP
temp_intensity = VAL(LEFT$(b$, n - 1))
b$ = RIGHT$(a$, LEN(a$) - 21 - LEN(STR$(nr)) - n - 16)
mass = VAL(b$)

```

'The *.out files have an entry for each time recorded of the sum of intensities within a single mass unit width centered on each of the selected masses.'

```

FOR n = 1 TO 12
IF CINT(mass) = masses(n) THEN
intensities(n) = intensities(n) + temp_intensity
END IF
NEXT n
LINE INPUT #1, a$

```

```
NEXT nr,
```

'Finally the data is printed single space delimited.'

```
PRINT #2, time;
```

```
FOR n = 1 TO 12
```

```
PRINT #2, " ", intensities(n);
```

```
NEXT n
```

```
WRITE #2,
```

```
NEXT s
```

```
CLOSE #1
```

```
CLOSE #2
```

```
NEXT filen
```

```
endit:
```

```
END
```

The second program OUT-UHF.BAS implements the second data reduction part. It changes the *.out format produced by the first program into a universal histogram format with *.uhf extension. It runs much faster than the first program despite performing more manipulations, so it is convenient to use larger processing batches. Part of the problem when working with the data files is the varying of the acquisition times. The time between records averaged near one second as set up by the acquisition method. But this interval varies a bit, making the numbers and times of records variable, even though the standard protocol was always the same; 10 °C/min from 30 °C to 400 °C.

Direct comparison between data files or other manipulations such as subtraction is greatly enhanced if the all the data have equal times. Additionally, the raw data has some unimportant jitter noise which smooths away. A five-point smoothing algorithm at exactly uniform 0.05 minute (0.5 °C) intervals was chosen as the smallest useful implementation.

Larger intervals could have been used, especially for the wider peaks, but it was necessary to be sure to capture any possible very narrow peaks. A hard copy of this program follows.

OUT-UHF.BAS

'This program is written in standard BASIC for maximal portability.'

'This program performs an equiinterval reintegration and smoothing of data in the *.out format, producing a standard ASCII numeric spreadsheet format.'

'The uniform length and uniform spacing of times helps enable further analyses. In this program all real numbers have double precision but are printed in the final output to single precision using the CSNG function.'

DIM y(-2 TO 2, 1 TO 12) AS DOUBLE

DIM t(-2 TO 2) AS DOUBLE

'For each output time the smoothing is done by a weighted average over the five nearest input times.'

'The selected time intervals are uniformly spaced .05# time units (minutes) for a selected uniform length of time.'

delttime# = .05#

firstime# = .05#

lastime# = 36.95#

'This program is set up to batch process a variable list of files. The list is manually edited in this version, with no graphical user interface.'

'The *.uhf format is a type of universal histogram format, otherwise known as the columnar x many y format, or multivariable time series.'

'First open the correct files. The dummy variable "filen" is a counter.'

```
ON ERROR GOTO endit
FOR filen = 1 TO 7
IF filen = 1 THEN
OPEN "060301.out" FOR INPUT AS #1
OPEN "060301.uhf" FOR OUTPUT AS #2
END IF
IF filen = 2 THEN
OPEN "060302.out" FOR INPUT AS #1
OPEN "060302.uhf" FOR OUTPUT AS #2
END IF
IF filen = 3 THEN
OPEN "060303.out" FOR INPUT AS #1
OPEN "060303.uhf" FOR OUTPUT AS #2
END IF
IF filen = 4 THEN
OPEN "060304.out" FOR INPUT AS #1
OPEN "060304.uhf" FOR OUTPUT AS #2
END IF
IF filen = 5 THEN
OPEN "060305.out" FOR INPUT AS #1
OPEN "060305.uhf" FOR OUTPUT AS #2
END IF
IF filen = 6 THEN
OPEN "060401.out" FOR INPUT AS #1
OPEN "060401.uhf" FOR OUTPUT AS #2
END IF
IF filen = 7 THEN
OPEN "060402.out" FOR INPUT AS #1
OPEN "060402.uhf" FOR OUTPUT AS #2
```

END IF

'Initializing smoothing and printing the initial data.'

timen# = firstime#

FOR n = -2 TO 2

INPUT #1, t(n), y(n, 1), y(n, 2), y(n, 3), y(n, 4), y(n, 5), y(n, 6), y(n, 7), y(n, 8), y(n, 9), y(n, 10), y(n, 11), y(n, 12)

NEXT n

n = -2

DO WHILE t(n) < timen#

n = n + 1

LOOP

PRINT #2, CSNG(timen#);

m = 7

yy# = y(n, m)

PRINT #2, " ", CSNG(yy#);

yy# = 0#

FOR m = 8 TO 10

yy# = yy# + y(n, m)

NEXT m

PRINT #2, " ", CSNG(yy#);

yy# = 0#

FOR m = 11 TO 12

yy# = yy# + y(n, m)

NEXT m

PRINT #2, " ", CSNG(yy#);

```
FOR m = 1 TO 6
yy# = y(n, m)
PRINT #2, " ", CSNG(yy#);
NEXT m
```

```
WRITE #2,
timen# = timen# + deltime#
```

'Reintegrating, smoothing, and printing the rest of the data.'

```
DO UNTIL timen# > 36.95#
FOR n = -2 TO 1
t(n) = t(n + 1)
FOR m = 1 TO 12
y(n, m) = y(n + 1, m)
NEXT m
NEXT n
n = 2
INPUT #1, t(n), y(n, 1), y(n, 2), y(n, 3), y(n, 4), y(n, 5), y(n, 6), y(n, 7), y(n, 8), y(n, 9), y(n,
10), y(n, 11), y(n, 12)
IF t(0) > timen# THEN
PRINT #2, CSNG(timen#);
```

```
m = 7
yy# = (y(-2, m) + 2# * y(-1, m) + 2# * y(0, m) + 2# * y(1, m) + y(2, m)) / 8#
PRINT #2, " ", CSNG(yy#);
```

```
yy# = 0#
FOR m = 8 TO 10
yy# = yy# + (y(-2, m) + 2# * y(-1, m) + 2# * y(0, m) + 2# * y(1, m) + y(2, m)) / 8#
NEXT m
```

```

PRINT #2, " ", CSNG(yy#);

yy# = 0#
FOR m = 11 TO 12
yy# = yy# + (y(-2, m) + 2# * y(-1, m) + 2# * y(0, m) + 2# * y(1, m) + y(2, m)) / 8#
NEXT m
PRINT #2, " ", CSNG(yy#);

FOR m = 1 TO 6
yy# = (y(-2, m) + 2# * y(-1, m) + 2# * y(0, m) + 2# * y(1, m) + y(2, m)) / 8#
PRINT #2, " ", CSNG(yy#);
NEXT m

WRITE #2,
timen# = timen# + deltime#
END IF
LOOP

CLOSE #1
CLOSE #2
NEXT filen
endit:
END

```

The universal histogram format with the *.uhf extension is directly importable in spreadsheet programs such as Microsoft Excel. In the spreadsheet files given in other data appendices additional relevant information was recorded for each data file, such as the sample information. For these files the times are in the first column, starting at 0.05 minute going up to 36.95 minutes. The intensities for each of the selected ion masses are in the other columns as labeled. These data are given as indexed in the subsequent data appendices.

APPENDIX C

Data Files included in this appendix are:

Folder - *Figure 3*

File – *Figure 3 Support Data.xls*

File – *Figure 3.xls*

Folder - *Figure 4*

File – *Figure 4 Support Data.xls*

File – *Figure 4.xls*

Folder - *Figure 5*

File – *Figure 5 Support Data.xls*

File – *Figure 5.xls*

Folder - *Figure 6*

File – *Figure 6 Support Data.xls*

File – *Figure 6.xls*

Folder - *Figure 7*

File – *Figure 7 Support Data.xls*

File – *Figure 7.xls*

Folder - *Figure 8*

File – *Figure 8 Support Data.xls*

File – *Figure 8.xls*

Folder - *Figure 9*

File – *Figure 9.xls*

Folder – *Support Data*

File – *Alumina.xls*

File – *Glass beads.xls*

File – *Individual PAH in Crucible.xls*

File – *Kaolin.xls*

File – *Mixed PAHs in Crucible.xls*

File – *Sand.xls*

File – *XAD 4 100ppm.xls*

File – *XAD 4 20ppm.xls*

Folder - *Figure 10*

File – *Figure 10 Support Data.xls*

File – *Figure 10.xls*

Folder - *Figure 11*

File – *Figure 11 Support Data.xls*

File – *Figure 11.xls*

Folder - *Figure 12*

File – *Figure 12 Support Data.xls*

File – *Figure 12.xls*

Figure 13 and support data were generated by Dr. Upal Ghosh, Stanford University

Folder - *Table 2*

File – *Table 2.xls*

Folder – *Support Data*

File – *Glass beads.xls*

File – *Individual PAH in Crucible.xls*

File – *Mixed PAHs in Crucible.xls*

Folder - *Table 3*

File – *Table 3 Support Data.xls*

File – *Table 3.xls*

Folder - *Table 4*

File – *Table 4 Support Data.xls*

File – *Table 4.xls*

Folder - *Table 5*

File – *Table 5 Support Data.xls*

File – *Table 5.xls*

APPENDIX D

Data Files included in this appendix are:

Folder - *Figure 4*

File – *Figure 4 Support Data.xls*

File – *Figure 4a.xls*

File – *Figure 4b.xls*

Figures 1-3, 5-8, Table 1-2, and support data were generated by Dr. Upal Ghosh, Stanford University

APPENDIX E

Data Files included in this appendix are:

Folder - *Figure 1*

File – *Figure 1 Support Data.xls*

File – *Figure 1a.xls*

File – *Figure 1b.xls*

Folder - *Figure 2*

File – *Figure 2 Support Data.xls*

File – *Figure 2.xls*

Folder – *Figure 5*

File – *Figure 5.xls*

Folder – *Support Data*

File – *T0 Microcosm Data.xls*

File – *T1 Microcosm Data.xls*

File – *T2 Microcosm Data.xls*

File – *T3 Microcosm Data.xls*

File – *T4 Microcosm Data.xls*

Folder - *Figure 7*

File – *Figure 7 Support Data.xls*

File – *Figure 7a.xls*

File – *Figure 7b.xls*

Folder - *Table 1*

File – *Table 1 Support Data.xls*

File – *Table 1.xls*

Folder - *Table 3*

File – *Table 3.xls*

Folder – *Support Data*

File – *T0 Microcosm Data.xls*

File – *T1 Microcosm Data.xls*

File – *T2 Microcosm Data.xls*

File – *T3 Microcosm Data.xls*

File – *T4 Microcosm Data.xls*

Figures 3, 4, 6 and Tables 2, 4, 5 and support data were generated by Mr. David Ringelberg, Environmental Laboratory, U.S. Army Engineer Research and Development Center

APPENDIX F

Data Files included in this appendix are:

Folder - *Figure 4*

File – *Figure 4 Support Data.xls*

File – *Figure 4.xls*

Folder - *Figure 8*

File – *Figure 8a.xls*

File – *Figure 8b.xls*

Folder – *Support Data*

File – *T0 Microcosm Data.xls*

File – *T1 Microcosm Data.xls*

File – *T2 Microcosm Data.xls*

File – *T3 Microcosm Data.xls*

File – *T4 Microcosm Data.xls*

Folder - *Figure 9*

File – *Figure 9 Support Data.xls*

File – *Figure 9a.xls*

File – *Figure 9b.xls*

Folder - *Figure 12*

File – *Figure 12 Support Data.xls*

File – *Figure 12.xls*

Folder – *Figure 13*

Folder – *Figure 13a*

File – *Figure 13a Support Data.xls*

File – *Figure 13a.xls*

Folder – *Figure 13b*

File – *Figure 13b Support Data.xls*

File – *Figure 13b.xls*

Folder - *Figure 14*

File – *Figure 14 Support Data.xls*

File – *Figure 14.xls*

Figures 5-7, 10-11 and support data were generated by Dr. Upal Ghosh, Stanford University